Maynooth University
National University of Ireland Maynooth

Wave Projections from North Atlantic to the Irish Coast

A dissertation submitted for the degree of
Doctor of Philosophy

By:

Ashly Kalayil Uthaman

Under the supervision of:

Dr. Gerard McCarthy

Dr. André Düsterhus

Dr. Tomasz Dabrowski

ICARUS, Department of Geography
National University of Ireland Maynooth
Ollscoil na hÉireann, Má Nuad

October 2025

This thesis is dedicated to my parents, Tankamani & Uthaman, my brother, Arun and my husband, Nikhil, whose love and encouragement has guided me throughout this journey.

Declaration

I hereby declare that I have produced this manuscript without the prohibited assistance of any third parties and without making use of aids other than those specified.

The thesis work was conducted from November 2021 to October 2025 under the supervision of Dr. Gerard McCarthy and Dr. André Düsterhus in the Department of Geography, ICARUS, National University of Ireland Maynooth and Dr. Tomasz Dabrowski in the Marine Institute, Galway.

Ashly Kalayil Uthaman

Maynooth, Ireland,

October 2025.

Sponsor

This work (Grant-Aid Agreement No: MI/CS/20/111) is carried out with the support of the Marine Institute and funded under the Marine Research Programme by the Government of Ireland.

Collaborations

Dr. Gerard McCarthy: As my supervisor, supervised and collaborated on the work of all chapters.

Dr. André Düsterhus: As my supervisor, supervised and collaborated on the work of all chapters.

Dr. Tomasz Dabrowski: As my supervisor, supervised and collaborated on the work of all chapters.

Publications

The chapters contained in this thesis have been either published or submitted to peer-reviewed journals. Chapter 4 has been submitted to the journal *Journal Of Geophysical Research: Oceans* and is currently under review.

Submitted articles (under review):

- Uthaman, A. K., Dabrowski, T., McCarthy, G. D., & Düsterhus, A. (2025). Wave Projections for the Northeast Atlantic using High Resolution Surrogate winds. Under review in the journal *Journal Of Geophysical Research: Oceans*. *arXiv* preprint: 10.22541/essoar.174231789.91051332/v1.

Contents

Abstract

Shaped by distant storms and local winds, the waves reaching Ireland's coast do not only carry energy, but also reflect the changing patterns of the climate – with growing impacts on coasts

This idea is central to this thesis. As climate changes, ocean waves around Ireland will also change. These shifts affect both the offshore conditions and wave behaviour near the coast, including how far they run up onshore. Understanding these changes is crucial not only for protecting vulnerable coasts but also for supporting sectors such as offshore renewable energy and coastal planning. To investigate the evolving wave climate and its coastal impacts, a multi-scale approach is applied. The study integrates large-scale atmospheric processes with regional wave simulations and coastal-scale impact assessments. Statistical and numerical methods are combined to link oceanic variability in the North Atlantic to coastal responses around Ireland. A detailed analysis using lagged cross-correlation to swell period data estimates swell travel times and identifies source regions, forming the basis for selecting the North Atlantic domain for wave simulations. A nested WAM-SWAN modelling system, driven by surrogate wind fields generated for the winds from the MPI-ESM model together with sea ice and sea level inputs, captures the spatial distribution and projected changes in wave heights. To translate these offshore wave conditions into coastal impacts, a one-dimensional model is developed to simulate wave run-up for a selected site in Galway Bay. The results reveal that the projected changes in wind fields, storm activity, and sea level will continue shaping waves near the Irish coast. The findings demonstrate that Ireland's coastal hazards cannot be assessed in isolation from the broader North Atlantic system or without considering local influences, underscoring the need for multi-scale approaches for managing future coastal risks around Ireland.

Acknowledgements

First and foremost, I would like to express my heartfelt gratitude to my supervisors Dr. André Düsterhus, Dr. Gerard McCarthy and Dr. Tomasz Dabrowski, for their invaluable guidance, encouragement, and unwavering support throughout my PhD journey. Each of you played a unique and important role in shaping me as a researcher. I am deeply grateful for the freedom you gave me to share my ideas and for always listening with patience and understanding. Your positivity and appreciation on small achievements helped me gain confidence during challenging times and played a key role in bringing me to where I am today. Thank you all for sharing your knowledge and for being wonderful mentors.

A special thanks to André for being an exceptional teacher. I sincerely appreciate your patience in answering all my questions, no matter how small, for explaining things repeatedly when I had difficulties understanding, and for helping me fix even the tiniest bugs in my code. From the day I was selected, you helped me with everything from the initial paperwork and settling in Ireland to guiding me with care through every stage of my PhD. Even after you moved from Ireland, you never made me feel that supervising from a distance was tiring or frustrating. You always made time to listen to my presentations, helped me improve my communication skills, and encouraged me to speak with confidence. Beyond academic guidance, you taught me to stay strong and optimistic and gave me courage whenever I faced challenges.

I am thankful to Gerard for the warm welcome to the ICARUS Ocean team. Your positivity and kind words motivated me during moments of self-doubt. I am especially grateful for the opportunities you provided such as joining research cruises which broadened my perspective and enriched my experience in oceanographic data collection.

I thank Tomasz for your continuous support and encouragement. You were always approachable and ready to help, even over emails, and I truly appreciate how you connected me with members of your team whenever I needed extra help.

This work would not have been possible without the support of the Marine Institute. I sincerely thank them for providing the financial and other resources that made this research possible.

I am grateful to Dr. Mikhail Dobrynin, Dr. Sebastian Brune, and Kieran Lyons for their insightful discussions and valuable input, which greatly contributed to the progress of my work. A special thanks to Sebastian for setting me up on the HPC Levante system in Hamburg, and to the DKRZ Helpdesk for promptly resolving technical issue during the initial stages. I also thank the Danish Meteorological Institute in Denmark for the welcoming atmosphere during my research visit. This opportunity helped me understand the practical applications of scientific research.

I would also like to extend my thanks to my ICARUS Ocean team. Special thanks to Catherine for helping me with everything, from research and university-related tasks to my endless small questions, since the day I joined. I am thankful to Guillaume for your patience, understanding, and for always listening to my dramatic stories. My sincere thanks to Kirsty for checking in on me and motivating me whenever I needed it; you stood beside me like a sister during the final phase of my PhD. I also appreciate Sam and Emmanuel for your advice and encouragement, and Patrick and Sam Diabate for your kindness and support. I am grateful to all of you for celebrating even my smallest successes, which gave me the encouragement to keep moving.

Next I thank the ICARUS family for creating a friendly and cheerful atmosphere. The fun, jokes, and laughter were a welcome relief during rough times. I would especially like to thank Corinne for all your help with project-related and administrative matters, and for being a wonderful listener and advisor beyond work. I am also grateful to Nannan for your thoughtful advice and for always bringing laughter and lightness to my stressful days.

My sincere thanks to Prof. Mary Gilmartin for the support you provided at the beginning of my journey. The confidence you gave me during those early stages formed a strong foundation for my growth, and your kind approach encouraged me to believe in myself and in my own voice. I also acknowledge Prof. Rowan Fealy for his valuable input, motivation, and timely guidance during the annual meetings.

I thank Michelle, Neasa, Sandra, Sudipto, and Yangyao, as well as everyone in the Department of Geography, for being such wonderful and friendly colleagues.

I would also like to thank all my teachers who have guided and inspired me throughout my academic journey. A special thanks to Kiran A S and Dr. Jayakumar Sheelam for teaching me the basics of numerical modelling, which laid the groundwork for my

research in this field.
I thank George, Jesbin, Jubin, and Neeraj, for helping me clear doubts related to the models and for giving me the support, and motivation to keep going always.
My heartfelt thanks go to my friends, who have been my greatest source of strength. I am grateful to Alex, Meenu, Rao, Reshmitha, and Vishnu for your continuous support and frequent check-ins. Even from afar, you made me feel cared for and connected. A special thanks to Meenu and Reshmitha, who have been with me since childhood, celebrating small victories and constantly motivating me. I also thank Ander, Elia, Mengqi and Mudita for your constant support, and the many comforting chats that made tough days lighter. Special thanks to Arathy for taking such good care of me, especially during my final year.
I am forever grateful to my family for being my foundation. Thank you to my father, Uthaman, for believing in the importance of a girl's education–it is because of you that I am here today and to my mother, Thankamani, who taught me the basics, you were my first teacher. I thank my brother, Arun, for teaching me how to dream and for always believing that I could achieve this, and my sister-in-law, Swathy, for being so understanding and supportive during my difficult days. I am also thankful to my parents-in-law, Sathy and Soman, for your constant support and prayers.
Finally, my deepest gratitude goes to my husband, Nikhil, who joined me in this journey, trusted me completely, and waited patiently while I was chasing my dream. Thank you for being my constant support, strength, and companion in every step of this path.

List of Figures

List of Tables

Acronyms

BREAK	Wave Breaking source term
BSBT	Backward Space Backward Time (propagation scheme)
CMIP6	Coupled Model Intercomparison Project Phase 6
CFL	Courant-Friedrichs-Lewy
EA	East Atlantic Pattern
EA/WR	East Atlantic-Western Russian
ECMWF	European Centre for Medium-Range Weather Forecasts
EMODnet	European Marine Observation and Data Network
ENSO	El Niño-Southern Oscillation
ETNA	Extra Tropical North Atlantic
GCC	Galway City Council
GEBCO	General Bathymetric Chart of the Oceans
GEN3	Third Generation mode
GEV	Generalised Extreme Value
GSI	Geological Survey of Ireland
INFOMAR	Integrated Mapping for the Sustainable Development of Ireland's Marine Resources
IPHYS	Input Physics parameterisation scheme
ISNL	Depth Scaling of Nonlinear wave-wave Interactions
JONSWAP	Joint North Sea Wave Observation Project
MPI-ESM	Max-Planck Institute of Earth System Modelling
mpts	mean period of total swell
NA	North Atlantic
NAO	North Atlantic Oscillation
NCC	Normalised Cross-Correlation

NSWE	Non-linear Shallow Water Equation
NEA	Northeast Atlantic
OpenFOAM	Open Field Operation And Manipulation
OPW	Office of Public Works
PHILL	Phillips Source Function
POT	Peak Over Threshold
QUAD	Quadruplet wave-wave interactions
RCP	Representative Concentration Pathways
SCAND	Scandinavian Pattern
SLR	Sea Level Rise
SWAN	Simulating WAves Nearshore
SWAN0.025	SWAN with 0.025°
SWARM-1D	Shallow WAter WAve Run-up Model in 1-Dimension
SWASH	Simulating WAves till SHore.
TNA	Tropical North Atlantic
WAM	WAve Model
WAM1.0NA	WAM with 1° for North Atlantic
WAM0.5NEA	WAM with 0.5° for Northeast Atlantic
WESTH	Nonlinear Saturation-based Whitecapping combined with wind input
WRF	Weather Researching and Forecasting model
WW3	WaveWatch-III
XBeach	eXtreme Beach behaviour

CHAPTER 1

Introduction

This chapter outlines the motivation for studying wave dynamics around Ireland. It then highlights the scientific gaps in understanding the role of swells, the projected changes in wave heights under future climate conditions, and their combined impact on the coast alongside with sea level rise. Building on this context, the chapter introduces the objectives of the thesis and methodological approaches adopted to address these objectives.. Finally, it presents the key research questions that guide the studies presented in the following chapters.

1.1 Motivation

Ocean waves are a fascinating and complex phenomenon, forming an essential part of Earth's climate system. They play a critical role in shaping coastlines, supporting marine ecosystems, and influencing a range of human activities, including shipping, coastal infrastructure, and renewable energy (Bento et al., 2018; Gallagher et al., 2016c; Ardhuin et al., 2007). Understanding wave dynamics is particularly important for an island nation like Ireland, which lies on the eastern edge of the North Atlantic (NA) Ocean and is directly exposed to high-energy waves from the NA basin (Tiron et al., 2015). This exposure makes the Irish coast especially vulnerable to coastal hazards like erosion, overtopping, and coastal flooding. Moreover, with over 50% of Ireland's population residing within a 15 km radius of coastline (Devoy, 2009) – compared to the global average of around 38% residing in coastal zones (Seibert et al., 2020) – the potential impacts of these hazards are both socially and economically significant.

A wide range of factors influence coastal hazards including human activity, wave conditions, sea level, long-term atmospheric forcing, shoreline configuration and geological constraints, nearshore and beach conditions (Borzi et al., 2025). These storms are one of the most significant drivers of coastal erosion in Ireland (Kandrot et al., 2016). During the exceptionally stormy winter of 2013/2014, the Irish coastline was impacted by a sequence of large storms. The cumulative effects of strong winds, tidal surges, and low pressure systems caused widespread coastal erosion and infrastructure damage exceeding €110 million, particularly along the south and west coasts (Kandrot et al., 2016).

The destructive influence of storms are further amplified when combined with extreme waves and high sea levels. For Ireland's major coastal cities such as Galway, Cork, and Dublin, storm surges coupled with high-energy waves pose an increasing risk of flooding and overtopping (Murphy et al., 2023). These risks are amplified on the west coast of Ireland due to the influence of remotely generated swells travelling across the NA (Bricheno et al., 2023; O'Brien et al., 2013; Devoy, 2009), where extreme wave events are observed repeatedly. For example, waves exceeding height of 20 m have been recorded off the west coast, including a 20.4 m wave at one of the Irish observational buoys (M4) in 2011, a 25 m wave at the Kinsale Energy gas platform in 2014, 26.1 m wave during Storm Ophelia in 2018 and a record-breaking 30.96 m wave during Storm Jake in 2016 (O'Brien et al., 2018).

While extreme events capture attention, Ireland's wave climate is continuously shaped by the persistent influence of NA swells (Gaughan and Fitzgerald, 2020; Fusco et al., 2010). Long-period waves, generated by distant storm systems across the Atlantic basin, travel thousands of kilometres to reach Irish shores and constitute a significant portion of the annual wave energy (Shanahan and Fitzgerald, 2025; Nic Guidhir et al., 2022; Gaughan and Fitzgerald, 2020; Gallagher et al., 2014). Unlike locally generated storm waves, swells arrive year-round and play a crucial role in everyday coastal processes, sediment transport, and the baseline wave conditions (Guisado-Pintado and Jackson, 2019). Understanding where these waves originate and their impact on the Irish coast is a crucial step in building a complete picture of wave-driven hazards in the region.

Waves also shape long-term coastal evolution. Wave characteristics influence the development of spits and barriers (Forbes et al., 1991; Orford and Carter, 1982). This is particularly relevant in Ireland, where southwest facing coastal barriers are mainly shaped by waves generated by Atlantic westerly depressions and southwest swell component that influences beach orientation (Devoy, 2009). Recent IPCC projections indicate that while overall storm frequency in the NA may decrease or remain stable, the inten-

sity of extreme storms are expected to increase, with the most severe events becoming significantly more powerful (Lopez et al., 2024; Seneviratne et al., 2021). Regional model projections for Irish waters suggest storm intensity may increase by approximately 15% between 2021–2060 (McGrath et al., 2005). As extreme storm events intensify, the wave energy reaching Irish coasts are expected to increase correspondingly. Such changes, combined with projected sea level rise, represent a serious threat to beaches through enhanced flooding, erosion, and morphological adjustment (Allan et al., 2023).

Sea level rise in Ireland has accelerated in recent decades, reaching rates of 7 mm/year between 1997 and 2016 (Shoari Nejad et al., 2022). In the long term, sea level is projected to rise in Ireland (up to 0.31 m at the end of the 21^{st} century; McGrath et al., 2008; Olbert et al., 2012). This further amplifies the impact of wave driven hazards on soft sediment shorelines and low-lying coastal zones (Vousdoukas et al., 2017).

One of the physical mechanisms through which offshore wave conditions translate into actual coastal impact is wave run-up: the process that determines how far waves travel up the beach face (Van der Meer, 2017; Brocchini and Baldock, 2008). Run-up is a critical parameter for the design of coastal engineering structures and for the management of hydrodynamic and morphodynamic hazards (Dodet et al., 2018). This process becomes increasingly critical under sea level rise scenarios. As sea level rises, increased water depth allows waves with larger periods and greater amplitudes to reach the shore, resulting in higher run-up values (Brocchini and Baldock, 2008). Research indicates that sea level driven changes in wave characteristics increase the resulting design heights by an average of 48–56%, relative to changes caused by sea level rise alone (Arns et al., 2017). This suggests that future storm events similar to the 2013/2014 winter storms could have substantially greater impacts on Irish coast, as rising seas allow larger waves to reach the shore.

Taken together, these observations highlight the urgent need for comprehensive, location specific wave studies and their impacts on the coast. Such studies are vital for improving coastal resilience, guiding sustainable marine spatial planning, and informing the development of offshore infrastructure.

As the climate changes, shifts are expected in the ocean wave characteristics such as wave height, direction and frequency due to changing climate factors like shifting wind patterns, rising sea level and sea ice concentration (Gaffet et al., 2025; Maia et al., 2022; Lobeto et al., 2021). Understanding these shifts is not only crucial for managing coastal risks in Ireland, but also supports sectors such as offshore renewable energy (Gallagher et al., 2016c), which are highly sensitive to sea state conditions. To prepare for these

impacts, we need sophisticated wave prediction systems that can capture both present conditions and project future scenarios.

This thesis explores how remotely generated swells influence Irish waters, how future wave conditions may evolve under rising seas and shifting winds, and how these changes could affect our coasts. From large-scale swell tracking across the NA to fine-scale wave run-up at the shoreline, each chapter builds a clearer picture of Ireland's wave climate and its impacts on the coast.

1.2 Bridging Gaps from Atlantic Swells to Nearshore Wave Run-up

To simulate waves near Ireland, it is essential to account for waves generated by distant storms across the NA (Calvino et al., 2022; Brown et al., 2010; Pilar et al., 2008). Inadequate representation of remotely generated swells can lead to significant underestimation of wave energy near the coast (Gaffet et al., 2025). Understanding which regions contribute to swells reaching Irish waters and how this influence varies seasonally and interannually is the first step taken in the thesis for long-term wave climate study in Ireland. Most previous studies focus on wind-wave correlations or examine general wave patterns (detailed in section 3.1 of Chapter 3, without tracing origin and influence of swells from distant sources to the Irish coast. This represents a key research gap that this thesis aims to address through detailed swell analysis.

Building on this, robust wave modelling tools are used for this research to capture both local and remotely generated waves. Spectral wave models like WAM (WAve Model; Wamdi Group, 1988; Guenther et al., 1992), WW3 (WaveWatchIII; Tolman, 1989), and SWAN (Simulating Waves Nearshore; Booij et al., 1999) are widely used to simulate waves at global, regional and local scales. These models are driven mainly by wind data as it is the major force that generates waves (NOAA Ocean Service, 2024; Holthuijsen, 2007). The primary source of wind for climate applications is climate models. Though their outputs extend into the future, climate model data often lack the spatial and temporal resolution required for accurate wave simulations (Islek et al., 2022). On the other hand, reanalysis datasets are high in resolution but are limited to historical periods and do not provide future projections (ECMWF, 2016). This mismatch between resolution and projection capability presents a major challenge in climate-scale wave modelling. To address this, regional weather models are commonly used to dynamically downscale climate model wind fields (Markina et al., 2018; Bento et al., 2018; Tiron et al.,

2015). However, this approach is computationally expensive and time-consuming. Recently, large data-driven techniques and expert guided machine learning have also been explored. While promising, these methods often require extensive training datasets, tuning, and may lack physical consistency (Benton et al., 2024; Annau et al., 2023). Consequently, there is an increasing need for alternative methods that are both computationally efficient and physically consistent to enable high-resolution wave modelling over climatological time scale (Camps-Valls et al., 2025; Trindade et al., 2019).

In this context, the surrogate data generated from reanalysis datasets by the analogue method is an efficient alternative for creating high-resolution wind fields for both present and future conditions. These surrogate datasets statistically reflect the large-scale characteristics of climate model projections, while retaining the spatio-temporal detail of reanalysis products. This makes them well suited for long-term wave modelling studies. In this study, surrogate wind data are used along with climate-driven sea level and sea ice to simulate wave conditions under present and future scenarios. While this approach offers valuable insights into offshore and regional wave patterns, understanding how these changing wave climates impact the shoreline requires closer examination of nearshore processes.

When waves travel from deep to shallow water, they undergo complex transformations (Dodet et al., 2019) such as shoaling, breaking, and run-up which are further influenced by rising sea levels (Melet et al., 2018; Atkinson et al., 2013) and coastal topography (Webb, 2021). Melet et al. (2018) showed that as the sea levels rise, the interaction between waves and coastline is expected to intensify, altering wave transformation processes near the shore and amplifying the risk of coastal flooding and erosion. While spectral models are effective in simulating offshore and nearshore wave conditions, they do not resolve the non-linear processes that occur close to shore (such as shoaling, breaking and run-up; Thomas and Dwarakish, 2015). To capture these complex coastal dynamics, researchers often solve the non-linear shallow water equations (SFINCS, XBeach; van Ormondt et al., 2025; Smit et al., 2010), Boussinesq equations (MIKE21, FUNWAVE; Warren and Bach, 1992; Kirby et al., 1998) or Navier-Stokes equations (IH-3VOF; Lara et al., 2010). These models are widely used to study wave transformations in the surf zone, wave-structure and coastal interactions under varying beach slopes and sea level conditions. Continuous developments in numerical techniques aim to reduce the computational cost of such models while maintaining physical accuracy (Lara et al., 2010). Motivated by this need for efficiency, the present study develops a one-dimensional model that enables the translation of offshore wave information to coastal conditions. The

model can be used to simulate wave run-up and assess how future changes in offshore waves and sea level may affect the coast.

1.3 Objectives of the Study

The main objectives of this study are to :

- Investigate how swells from different regions of the NA influence Irish waters and assess how this influence varies across seasons.
- Develop a nested modelling framework that uses surrogate winds and other climate drivers such as sea ice and sea level for long-term wave simulations.
- Simulate waves under present and future conditions to assess projected changes in wave height characteristics.
- Develop a computationally efficient one-dimensional wave run up model to understand localised impacts on the coast.
- Understand how offshore wave conditions impact the coast through wave run-up processes and assess the effects of future sea level rise on run-up values.

Thus the thesis aims to understand and project wave conditions and their impacts along the Irish coast on climatological timescale using nested modelling framework that extends from NA deep water to the Irish coast. The study begins with a swell analysis to understand the influence of swells from different regions of the NA on Ireland. The results then guide the selection of an appropriate model domain for capturing swell effects. The modelling approach then combines WAM and SWAN spectral wave models, driven by climate drivers to project waves from present day to future conditions. A key contribution from this part is the development of high-resolution surrogate wind data that combines the large-scale features of climate model winds with the spatial and temporal detail of reanalysis data. This enables efficient long-term simulations without using computationally expensive dynamical models for downscaling of winds.
Finally, to assess how offshore wave conditions affect the coastline, it needs to be modelled outside the SWAN. So, a one dimensional wave run up model, SWARM-1D (Shallow WAter WAve Run-up Model in 1 Dimension) is developed to investigate wave run-up at a selected location at entrance of Galway bay (the west coast of Ireland). The model

developed is highly computationally efficient, takes boundary conditions from SWAN, and includes future sea level rise scenario to evaluate the combined effects of changing wave conditions and elevated water levels on coastal run-up.

1.4 Research questions

Understanding how waves change in the future is of great importance for coastal planning, infrastructure design and better adaptation strategies, especially for Ireland, which is directly exposed to the energetic Atlantic swells. However, long-term simulation of waves is challenging due to the limitations of adequate wind forcing, computational cost, and uncertainties in climate projections. This study addresses these challenges by driving nested WAM-SWAN wave models with high-resolution surrogate winds, also incorporating other climate-driven factors such as sea ice and sea level rise, to simulate the present and future wave conditions with a focus on the distributional changes of wave heights.

Additionally, understanding how these changes manifest in the nearshore zone is essential for assessing potential coastal impacts. By integrating SWARM-1D model into the workflow, this research links large-scale wave climate projections to local-scale coastal responses.

Accordingly, this thesis is guided by the following three main research questions:

1. Which are the dominant North Atlantic swell source regions influencing the west of Ireland, and how does their influence vary with season?

2. Is it possible to predict wave climate around Ireland using WAM–SWAN modelling system driven by statistically generated surrogate wind data over multi-year periods representative of climatological timescales? What are the projected changes in wave heights under a future high-emission climate scenario (SSP5-8.5)?

3. How do waves transform near the shore under future conditions, and what are the implications for coastal impacts such as run-up?

1.5 Outline of the thesis

Chapter 2 presents a review of existing literature on global and regional wave climate to provide the scientific background for the thesis. It introduces fundamental concepts of ocean waves, the distinction between wind-sea and swell, and the importance of studying

wave climate. The chapter then discusses changing climate conditions and their influence on wave projections. This is followed by an overview of NA wave characteristics and key atmospheric drivers. It also outlines major wave modelling approaches and examines wave transformation and sea level rise effects, and the vulnerability of the Irish coast to the climate-driven wave impacts. The chapter further presents the rationale underpinning the key methodological choices made in this study, including the selection of models and forcing datasets, the adoption of the SSP5-8.5 high-emission scenario, and the climate drivers incorporated such as wind, sea ice and sea level. The associated uncertainties inherent in climate-scale wave projections are also identifiedTogether, these sections establish the foundation for the thesis, while studies directly supporting each research chapter are discussed within the respective introductions.

Chapter 3 investigates the influence of swells from the NA on the west coast of Ireland through statistical methods. The chapter begins by defining the regional domains chosen as swell sources and outlines the key hypotheses and assumptions which guided the analysis. The datasets and methods are then described, including the application of swell period from ERA5 to estimate swell travel time and identify the dominant source regions. The chapter then presents the results from the climatology of swell propagation, followed by case studies illustrating seasonal and interannual variability in swell travel times. The discussion interprets the physical drivers behind the observed patterns, evaluates the methodological strengths and limitations and highlights broader implications for understanding Ireland's wave climate and future research direction. The understanding of the NA swell influence on the west coast of Ireland from this chapter form the foundation for Chapter 4.

Chapter 4 investigates wave climate simulations from the NA to Irish waters under changing climate conditions. It begins by reviewing previous studies on wave projections and regional downscaling approaches, highlighting common practices used to translate coarse-resolution climate model outputs into regional wave information. The chapter then provides an overview of the study area and the model domains used for wave simulations, along with the datasets used for model forcing and validation. A key component of this chapter is the generation of high-resolution surrogate wind using analogue-based approach. The methodology and results of present and future wave simulations are described in detail. The results presented in this chapter emphasise on analysing changes in the full distribution of wave heights, rather than just mean or extreme values, and how these changes vary seasonally and spatially along the NEA region around Ireland. The chapter concludes with a discussion of key findings, methodological considerations, and

study-specific limitations, providing the basis for the coastal impact analysis presented in the following chapter.

Chapter 5 introduces a one-dimensional non-linear shallow water wave run-up model (SWARM-1D). The model is designed to simulate wave run-up on the Irish coast, thereby translating the offshore waves into coastal impacts. It begins by defining the run-up formulation adopted in this study and reviewing previous research on wave run-up in Ireland, noting the absence of studies that quantify run-up values. The chapter then describes the development of the one-dimensional SWARM model, outlining the governing equations, numerical scheme, and boundary conditions. Model performance is compared with empirical formulations, followed by an application to Fanore Beach in Galway Bay to evaluate run-up behaviour under varying wave and sea level conditions. The discussion highlights the role of sea level rise in modifying waves near the coast, methodological limitations, and the broader applicability of the model for future coastal hazard assessments.

Chapter 6 brings together the main findings of the thesis and reflects on how they address the research questions outlined in Section 1.4. It summarises the key scientific and methodological contributions, highlighting how the work advances understanding of wave dynamics and coastal processes around Ireland. The chapter also outlines the broader relevance of the findings, identifying who can benefit from this research, including coastal communities, policymakers, and the renewable energy sector. Finally, it discusses potential paths for future research and model development to further enhance projections of coastal wave impacts under changing climate conditions.

CHAPTER 2

Literature Review

In this chapter, I review existing knowledge on wave climate, with emphasis on global mechanisms, the NA wave dynamics, and the broader context of Irish conditions. It also presents the development of wave modelling framework, climate change projections and associated coastal impacts. Together these sections establish the background for the thesis, while studies directly supporting the aims and methods of each chapter are cited and discussed within the introduction of each respective chapters.

2.1 Introduction to ocean waves

Ocean surface waves are generated through the complex interaction between wind and the ocean surface, a process first described in the pioneering theoretical work of Phillips (1957) and Miles (1957). Phillips (1957) described the initial generation of waves through pressure fluctuations associated with turbulent wind flow. Miles (1957) developed a theory for wave growth due to wind-induced pressure variations and waves orbital motion. A complete understanding of wave evolution was later provided by Hasselmann et al. (1973), who demonstrated that energy transfer from the atmosphere to the ocean surface involves a series of mechanisms, including pressure fluctuations, viscous stresses and wave-turbulence interactions.

Modern understanding of wave generation is encapsulated in the spectral energy balance approach, where the evolution of wave energy is described by action balance equation (Wamdi Group, 1988). This approach recognizes that sea state can be represented by a two-dimensional wave spectrum that describes the distribution of wave energy as a

function of frequency and direction (Hasselmann et al., 1973).

The process of wave generation begins with the formation of small ripples on the water surface due to wind stress, creating surface roughness that enhances further energy transfer from the wind to the waves (Phillips, 1957). As these waves grow, they become more efficient at extracting energy from the wind through a feedback mechanism in which longer waves travel faster and can more effectively capture wind energy.

Beyond initial generation, the evolution of a wave field is governed by three principal source term categories in the spectral energy balance equation. The first is atmospheric input (S_{in}), representing the transfer of energy from wind to waves. The second is nonlinear wave-wave interactions (S_{nl}), which redistribute energy across the spectrum through resonant quadruplet interactions among four wave components (Komen et al., 1994; Hasselmann et al., 1973). These interactions are responsible for the downshift of spectral peak frequency as waves grow, and their accurate representation distinguishes third-generation wave models from earlier approaches. The third category is dissipation (S_{ds}), which encompasses several mechanisms: whitecapping, the dominant dissipation process in deep water caused by wave steepening and breaking at the sea surface; depth-induced wave breaking, which occurs as waves enter shallow water and the ratio of wave height to water depth becomes critical; and bottom friction, which attenuates wave energy as waves propagate over a shallow seabed (Komen et al., 1994; Hasselmann et al., 1973). Together these processes determine the growth, propagation, and decay of ocean waves across all scales.

The goals of wind-wave research are well defined: to predict the wind-wave field and its effects on the environment (Young, 1999b). The environment may be natural such as beaches and the atmosphere or shaped by human activity such as ports, harbours, and coastal settlements. While the goals are similar, the specific requirements vary across disciplines. For example, coastal engineering applications may only require the integral wave parameters (such as wave height and peak period), whereas studies of air-sea interaction generally need a detailed description of the full wave spectrum (Young, 1999b; Janssen, 1991; Miles, 1957).

2.1.1 Distinction between wind-sea and swell

The wave condition at a given location is influenced by the recent history of wind over the generation area (fetch), resulting either locally generated wind-seas or swells that originate from distant storms (Méndez and Rueda, 2020). This distinction between wind-sea and swell represents the fundamental concept in wave climatology that was first clearly

articulated by Sverdrup and Munk (1947).

Wind-sea refers to waves that are actively generated by local wind forcing, while swell consists of waves that have propagated away from their generation area (Hasselmann et al., 1973; Pierson Jr, 1955). The physical characteristics of these two wave types differ significantly. Wind-sea exhibits shorter periods and greater directional spread (Hasselmann et al., 1973). The frequency spectrum of wind-sea often displays a peak at higher frequencies with a relatively broad spectral shape (Pierson Jr and Moskowitz, 1964). In contrast, swells are characterised by longer periods and narrow directional spread (Barber and Ursell, 1948).

This distinction has important implications for wave modelling. Studies show that regional wave climate simulations often neglect remotely generated swell (Mora-Escalante et al., 2025), which requires special attention in swell dominated regions.

In spectral wave models, wind-sea and swell are separated using a method called spectral partitioning. The simplest and most widely used approach compares the speed of each wave component to the local wind speed. If a wave is travelling faster than the wind, it is no longer being pushed by the wind and is therefore classified as swell; if it is still being driven by the wind, it is classified as wind-sea (Komen et al., 1994). More advanced methods scan the full two-dimensional wave spectrum and identify separate peaks. This allows the model to detect and track multiple swell systems and wind-sea systems that may be present at the same time (Portilla-Yandún, 2018). The choice of method matters because, in many real-ocean situations, swell and wind-sea overlap across similar wave frequencies, making a clean separation difficult regardless of the technique used.

Different spectral wave models implement these partitioning approaches differently, with some applying only the wave-age criterion and others offering more advanced watershed-based separation (Portilla-Yandún, 2018). WAM uses the wave-age criterion as its default separation method (Wamdi Group, 1988). SWAN also applies a wave-age threshold but gives the user more flexibility to adjust this threshold (SWAN Team, 2023). WaveWatchIII (WW3) goes further and includes a built-in spectral partitioning routine based on the watershed approach, making it better suited to studies that specifically analyse swell sources and propagation paths (Brus et al., 2021). The ERA5 wave output from the ECMWF model uses a combination of both; the wave-age criterion at the model level and post-processed spectral partitioning for derived swell products (Janssen and Bidlot, 2003). The specific models used in this thesis for swell analysis and their respective separation approaches are described in Section 3.4.1.

2.1.2 Basic wave parameters

Ocean waves are characterised by several key parameters that describe their physical behaviour (Figure 2.1). The definitions of the basic parameters explained in this section are adapted from Massel (2017); Young (1999b).

Wave height (H) represents the vertical distance between a wave crest and the preceding trough, while amplitude ($a = \frac{H}{2}$) describes half of this vertical distance. The wavelength (λ) is the horizontal distance between two successive crests or troughs and the wave period (T) is the time interval between successive crests or troughs passing a fixed point.

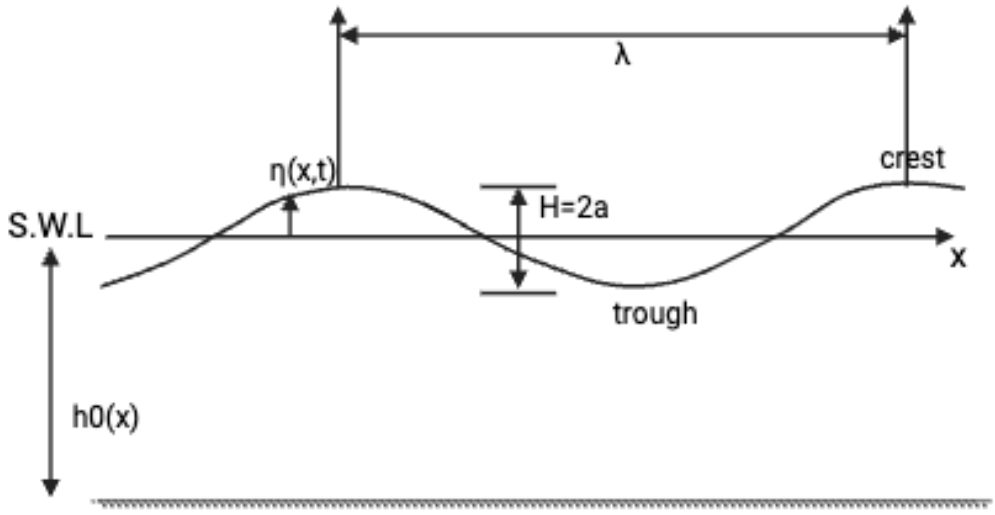

Figure 2.1: Definition of fundamental wave parameters: wave height (H), wavelength (λ) and wave amplitude (a) for an idealized sinusoidal wave.

These individual wave parameters are important for understanding wave mechanics, but are insufficient for describing the complex, irregular nature of real ocean waves. This ocean surface complexity, characterised by continuous spectra of wave components with varying heights, periods and directions (Longuet-Higgins, 1953), led to the development of statistical parameters of waves such as significant wave height (H_s) and peak period (T_p).

Significant wave height is defined as the average height of the highest one-third of waves in a given time series and peak period is defined as period at which the maximum spectral energy density occurs (Holthuijsen, 2007). The analysis presented in this thesis utilises

these two fundamental statistical wave parameters of wind-generated waves (hereafter referred to simply as *waves*).

2.1.3 Importance of studying wave climate

Studies of global and regional wave climates are important from both scientific and societal perspectives. Wave climate is the long-term statistical description of ocean waves, usually expressed using parameters such as significant wave height, period and direction (Méndez and Rueda, 2020).

Wind-generated surface waves are a significant renewable energy source (Farrok et al., 2024), and are important for many coastal processes, including erosion (Palermo et al., 2024; Scott et al., 2019) and the modulation of local trends of sea level (Dodet et al., 2019; Melet et al., 2018; Vousdoukas et al., 2017). This interaction between the wind and ocean surface waves is a fundamental component of the Earth system, with significant implications for climate modelling, coastal processes, and marine operations. These waves are not just surface phenomena but also critical components of complex Earth system interactions, influencing processes ranging from marine ecosystems to global climate patterns (Cavaleri et al., 2012).

It is important to recognise that coastlines are not only shaped by extreme storm events but also by the steady, everyday action of ordinary waves over long periods of time. These regular waves move sediment, wear away cliff faces, and maintain the shape of beaches across seasons and decades (Leach et al., 2021). Along the west coast of Ireland, where energetic Atlantic swell arrives persistently throughout the year, this background wave forcing acts continuously on an already storm-exposed coastline, increasing the cumulative impact on coastal morphology (Guisado-Pintado and Jackson, 2019).

Waves play a central role in Earth system dynamics through air-sea interactions, influencing energy exchange across the ocean-atmosphere boundary and shaping the structure of the atmospheric boundary layer (Casas-Prat et al., 2024; Jenkins et al., 2012). They also act as primary drivers of coastal morphodynamics by determining how beaches evolve, how sediments are transported and how ecosystems respond to changing wave conditions (Leach et al., 2021).

From a societal perspective, wave climate directly affects coastal communities, infrastructure, and marine operations. Even small shifts in dominant wave direction can alter sediment transport patterns, reshaping coastlines and influencing erosion and accretion processes (Bramante, 2017). These effects can be further exacerbated during extreme wave events, generating threats to the coast. Knowledge of wave climate is also crucial

for the design and operation of coastal facilities and offshore industries (Ambarita et al., 2023; O'Connell et al., 2020). The long-term wave climate studies are particularly important as offshore wind and wave energy projects expand near coasts (Bento. et al., 2011). Therefore, detailed information on waves is needed for designing reliable and efficient systems (Ribal et al., 2020).

In the context of a changing climate, shifts in global wind patterns are expected to alter ocean wave regimes worldwide (Gaffet et al., 2025; Maia et al., 2022; Lobeto et al., 2021). This has far-reaching implications not only for regional coastal hazards but also for ecosystems, infrastructure resilience, and adaptation planning. As a result, wave climate studies are increasingly recognised as fundamental for linking atmospheric variability to oceanic response and for supporting sustainable coastal management under future climate scenarios (Morim et al., 2019).

2.2 Changing climate and wave projections

Wave climate is influenced by multiple interconnected climate drivers including atmospheric circulation patterns, ocean temperatures, sea level rise, ice coverage, and ocean currents (Lobeto et al., 2021; Fox-Kemper, 2021; Hemer et al., 2013). Changes in wind patterns and storm activity affect the amount of energy transferred to the ocean surface (Lobeto et al., 2021; Reguero et al., 2019). Ocean temperatures modulate atmospheric stability and storm intensity thereby influencing wave generation (Chen, 2024). In addition, atmospheric climate change drives shifts in large-scale ocean circulation, including changes in thermohaline circulation and the position of boundary currents, which can modify wave propagation conditions through wave-current interactions, even in regions where local wind changes are modest (Casas-Prat et al., 2024). While sea level rise does not directly affect wave generation in deep water, it alters how waves interact with coastal environments by raising the baseline water level (Melet et al., 2018). Reductions in sea ice cover increase available fetch for wave growth (Chen et al., 2021), and ocean currents modify wave heights through wave-current interactions during propagation (Kumar and Hayatdavoodi, 2023).

Additionally, the global wave climate responds to large-scale atmospheric oscillations such as the North Atlantic Oscillation (NAO) and the El Niño-Southern Oscillation (ENSO), which drive interannual variability and long-term trends in wave climate (Reguero et al., 2019). Thus, both gradual climate change and natural modes of variability shape the future wave climate.

2.2.1 Approach to wave projections

To understand how waves might change in the future, scientists use General Circulation Models (GCMs). GCMs are the primary tool to investigate the response of the climate system to different forcings (Fox-Kemper, 2021; Loarca et al., 2021). These models simulate how the atmosphere, ocean, ice and land surface respond to changing climate conditions. However, GCMs do not simulate surface waves as part of their ocean components (Lobeto et al., 2021). Therefore, wave climate projections must be generated from GCM outputs such as sea level pressure, surface winds, and sea ice coverage (Kumar et al., 2025; Lobeto et al., 2021). Two main approaches are used: dynamical downscaling, where spectral wave models (explained in section 2.5) are forced with the climate model winds and statistical downscaling which develops an empirical relationship between atmospheric variables and wave parameters.

2.2.2 Observations, Variability and Uncertainties

Studies show that wave climate changes will vary significantly between different ocean regions by the end of the 21^{st} century. Recent studies by Casas-Prat et al. (2024) indicate that mean wave height is projected to rise by 5-10% in the Southern Ocean and eastern tropical South Pacific, and by more than 100% in the Arctic Ocean as sea ice retreats, while reductions of up to 10% are expected in the North Atlantic and North Pacific under the RCP8.5 scenario (relative to 1979–2004). In the NA specifically, wave heights have been observed to increase over the last 70 years, with typical winter trends showing increases of up to 20 cm per decade, alongside a northward displacement of storm tracks (Noone et al., 2024). This observed increase contrasts with future projections of decreasing mean wave heights in the basin under high-emission scenarios, reflecting the effects changes in atmospheric circulation patterns.

These changes also vary by season. Patra et al. (2021) showed increases in seasonal extreme waves under the high-emission SSP5-8.5 scenario, with changes of up to 15% (approximately 1 m, relative to the 1986–2005 period), particularly in the Southern Hemisphere high latitudes. More recently, Meucci et al. (2024), introduced an eight-model global wind-wave climate ensemble under CMIP6 scenarios SSP1-2.6 and SSP5-8.5, showing broad consistency in projected wave height increases in high latitudes but considerable variability in tropical and mid-latitude regions, including the North Atlantic.

However these projections should be interpreted with caution due to several methodolog-

ical limitations. As shown by Morim et al. (2019), wave climates are not adequately represented when wave models are forced with coarse-resolution wind fields. High-resolution forcing is required to properly resolve wave transformations into shallow water and to capture extreme events, which are critical for coastal impact assessments (Bricheno and Wolf, 2018). In addition, recent assessments by Lobeto et al. (2023) show that wave model choice is the dominant source of uncertainty across much of the global ocean, with projected changes differing by more than 75% of the ensemble mean in several regions. Uncertainties related to different wave model physics can often exceed those associated with the choice of climate model, underscoring the need for multi-model wave ensembles in future projection studies (Lobeto et al., 2023).

Further uncertainties arise from differences in climate model projections and emission scenarios, as well as from natural climate variability (Snyder et al., 2024), particularly in regions such as the North Atlantic where modes such as the NAO strongly influence wave conditions. In addition, the representation of swell and boundary conditions remains a challenge in regional studies, as many models do not fully capture the influence of remotely generated waves (Siegelman et al., 2025). These combined uncertainties highlight the importance of using appropriate modelling frameworks and long-term simulations to better represent wave climate variability and its potential changes, particularly for coastal impact assessments.

2.3 North Atlantic wave climate characteristics

The NA experiences one of the most energetic wave climates in the world (Martínez-Asensio et al., 2016). Waves in this basin show pronounced seasonal variability, with the highest values observed during winter when storm activity peaks (Prestes et al., 2025; Dobrynin et al., 2019). The northeastern Atlantic and adjacent shelf seas show high interannual variability with monthly mean H_s varying from year to year (Morim et al., 2021, 2019; Aarnes et al., 2017; Woolf et al., 2002). This variability reflects the NA basin's sensitivity to large-scale atmospheric patterns, particularly the NAO (explained in detail in Section **??**), which has been identified as the dominant driver of wave height predictability in the Atlantic.

Dobrynin et al. (2019) demonstrated that winds from the climate model MPI-ESM, can skilfully reproduce this NAO-wave height relationship in the North Atlantic when used to force the WAM spectral wave model, providing confidence in using the MPI-ESM as a climate driver for North Atlantic wave simulations. Li et al. (2022b) used WAM forced

by winds from a regional climate model downscaled from MPI-ESM for wave climate projections under the RCP2.6 and RCP8.5 scenarios, with ERA5-forced simulations run in parallel as the present-day validation baseline. More recently, MPI-ESM has been included as one of eight CMIP6 models used to force wave climate projections in global ensemble studies (Meucci et al., 2024), further establishing its suitability for wave climate research in this basin.

Multiple studies have consistently projected reductions in mean H_s across NA by the end of the 21^{st} century (Casas-Prat et al., 2024; Morim et al., 2019; Aarnes et al., 2017; Dobrynin et al., 2015). These projected decreases are most pronounced under high-emission scenarios such as RCP8.5, affecting both seasonal and annual averages (Bernardino et al., 2021; Lemos et al., 2020, 2019; Morim et al., 2019; Gallagher et al., 2016a; Hemer et al., 2013; Semedo et al., 2012).

2.4 Atmospheric drivers of the North Atlantic wave variability

Large-scale atmospheric circulation patterns exhibit distinct modes of variability that influence regional and remote areas through teleconnections – statistically defined relationships between climate anomalies in widely separated regions (Wallace and Gutzler, 1981). Four primary atmospheric modes dominate the NA and European variability: the North Atlantic Oscillation (NAO), the East Atlantic (EA) pattern, the Scandinavian (SCAND) pattern, and the East Atlantic-Western Russian (EA/WR) pattern (Morales-Márquez et al., 2020). These circulation modes operate across multiple spatial and temporal scales, generating complex wave climate responses.

The NAO represents the primary atmospheric mode controlling wave climate across the NA basin (Dobrynin et al., 2019; Martínez-Asensio et al., 2016). It is defined by the pressure difference between the Icelandic and the Azores systems (Hurrell, 2001). It controls westerly wind strength and storm track locations across the NA (Marshall et al., 2001). Woolf et al. (2002) identified strong connections between the NAO and interannual NA wave climate variability. Dodet et al. (2010) demonstrated significant winter NAO contributions to interannual variability of H_s, mean wave direction, and mean wave period over the NEA using five decades of hindcast data. Bertin et al. (2013) established NAO relationships with NA annual mean H_s throughout the 20^{th} century. Martínez-Asensio et al. (2016) quantified NAO impacts, showing H_s increases up to 1.0 m per NAO unit in the northwest of Britain during positive phases and 0.6 m increases

near the Azores during negative phases. Furthermore, Bernardino and Guedes Soares (2016) found that negative NAO winters produce longer storms with higher maximum wave heights.Dobrynin et al. (2019) demonstrated, using a 30-member MPI-ESM ensemble to force the WAM wave model over 1982–2017, that the correlation between the winter NAO index and seasonal mean H_s reaches 0.92 in the region 50°N–68°N, directly encompassing the waters west and northwest of Ireland. Scott et al. (2021) further confirmed the dominant role of atmospheric circulation indices, particularly the NAO, in controlling inshore wave direction and height variability specifically along the UK and Irish coasts, reinforcing the importance of capturing the NAO variability when simulating the wave climate of the study region.

The NAO operates on interannual-to-decadal timescales, with prolonged phases of positive or negative index that can persist for several years before reversing (Hurrell, 2001). As a consequence, wave climate statistics derived from short observational or simulation periods risk being biased towards the particular NAO phase that prevailed during that period, rather than representing the full climatological range of conditions. Long-term studies spanning multiple NAO cycles are therefore essential to obtain robust estimates of mean wave conditions, extreme wave statistics, and directional variability in the NEA (Viñes et al., 2026).

The EA pattern consists of north-south pressure dipoles with multidecadal variability and represents the second major mode affecting the NA wave climate (Morales-Márquez et al., 2020). Woolf et al. (2002) noted EA influences on NA waves, though these were weaker than the NAO effects. Charles et al. (2012) demonstrated the EA relationship with significant wave height, mean wave direction and mean wave period variability in the NA. Martínez-Asensio et al. (2016) showed that EA positive phases generate waves that increase up to 0.86 m between Britain and Iberia, primarily through swell modifications. Furthermore, Izaguirre Lasa et al. (2010) detected EA connections to the extreme wave climate in the NEA.

The other two atmospheric modes exert weaker yet meaningful influences on the NA conditions relative to the dominant NAO (Santo et al., 2016). Izaguirre et al. (2011) demonstrated connections between extreme wave events and the EA/WR and the SCAND circulation indices during 1992–2010. They found that both patterns modulate the frequency and intensity of extreme wave events in the northeastern Atlantic. These secondary modes exhibit more spatially confined influences compared to the NAO and EA effects (Martínez-Asensio et al., 2016). Analysis by Shimura et al. (2013), during the period 1960–1990, revealed that atmospheric teleconnections affect the eastern

NA more strongly than the western regions, highlighting the importance of geographic considerations in wave-atmosphere studies.

2.4.1 Regional focus to the Northeast Atlantic

The NEA lies directly in the path of major NA storm tracks (Feser et al., 2015), which amplifies its response to large-scale atmospheric patterns. It is also a transition zone where locally generated wind-sea meets the long-travelled Atlantic swells, creating a complex and highly variable wave climate (Morim et al., 2019; Aarnes et al., 2017; Charles et al., 2012; Dodet et al., 2010).

The wave climate of this region is energetic and strongly seasonal (Dabrowski et al., 2023), with winter dominated by large, long-period waves from the southwest to the northwest and summer by smaller, shorter waves from the north (Dodet et al., 2010). Strong interannual variability is observed, with positive correlations between winter H_S and the NAO index at northern latitudes and negative correlations at southern latitudes (Dodet et al., 2010). Multi-model projection studies further indicate robust decreases in mean H_s across the NEA by the end of the 21^{st} century (Aarnes et al., 2017).

Understanding wave climate variability is particularly important in dynamic regions like the NEA, where the wave climate is significantly influenced by atmospheric patterns (Morales-Márquez et al., 2020), climate change and seasonal patterns (Bitner-Gregersen et al., 2022; Morales-Márquez et al., 2020; Markina et al., 2019).

The NEA region around Ireland is the main focus of the thesis because of its sensitivity to atmospheric forcing and its complex geomorphology (detailed in Section 4.2). Although the current study does not directly analyse the influence of atmospheric teleconnections, the extensive literature on these processes provide important guidance for setting simulation periods and model domains. Previous studies on the variability of wave climate and sensitivity to atmospheric patterns highlight the need for a longer study period to capture wide range of conditions. It is therefore essential to capture representative wave conditions for model boundaries that should include the main physical drivers influencing the region.

2.5 Wave modelling approaches

Ocean wave characteristics can be determined through various methods including field measurements, physical models, analytical solutions, and numerical simulations (Thomas and Dwarakish, 2015). Among these, numerical models have emerged as powerful tools

for studying surface waves, with their performance depending on how accurately the physical phenomena are represented in the numerical scheme (Janssen, 2008). In addition, these models should be capable of representing complex conditions including locally generated wind-sea, remotely generated swells, spatially and temporally varying winds, and irregular bathymetry and coastlines (Komen et al., 1994).

2.5.1 Types of Wave models

Wave models are fundamentally divided into two categories based on their approach to representing waves: phase-averaging models and phase-resolving models (Komen et al., 1994).

Phase-averaging models predict statistical properties of the wave field such as significant wave height, mean period and directional spectra (Komen et al., 1994). They do not treat waves individually instead, they use the wave spectrum and because of this they are sometimes called *spectral models* (Rogers, 2020). These models are computationally efficient, making them suitable for long-term simulations and large domains, such as the open ocean or regional basins (Thomas and Dwarakish, 2015). Importantly, phase-averaging models such as WAM are capable of simulating shoaling and refraction due to depth and currents, though they are less suited to resolving the fine-scale processes of the immediate nearshore zone, including wave reflection, diffraction, infragravity wave generation, swash zone dynamics, and the turbulent structure of individual breaking waves (Booij et al., 1999; Wamdi Group, 1988)

Phase-resolving models predict the water surface and phase of individual waves in time and space (e.g., Boussinesq equations, non-linear shallow water equations (non-hyrdrostatic), mild slope equations; Lowe et al., 2019; Van Der Meer et al., 2016; Nwogu and Demirbilek, 2001; Komen et al., 1994). By simulating individual waves, phase-resolving models capture short-scale processes such as wave reflection, diffraction, shoaling or wave steepening that cannot be represented by phase-averaged models (Nwogu and Demirbilek, 2001). However, this detail comes with a high computational cost as resolving individual waves over large domains would require enormous computer memory and processing time (Battjes and Beji, 1992). As a result, phase-resolving models are typically applied in small, high-resolution domains (e.g., nearshore zones, harbours, or in run-up studies).

2.5.2 Evolution of Spectral wave models

The first attempt to numerically predict ocean waves emerged in the 1950s and 1960s (Cardone and Greenwood, 1986). The basis of spectral models is the spectral energy balance equation, which in deep water and in the absence of currents is given by,

$$\frac{\partial F}{\partial t} + \vec{V_g} \cdot \nabla F = S = S_{in} + S_{nl} + S_{ds} \tag{2.1}$$

where, F is the two-dimensional wave spectrum that depends on space, time (t), frequency, and propagation direction, V_g is the group velocity and source function S is expressed as the sum of S_{in} (input energy from the atmosphere), S_{nl} (non-linear energy transfer by wave-wave interaction) and S_{ds} (energy losses to dissipative forces).

These models are generally classified as first, second, and third generation models. The first-generation models were based on simple wind fields and linear wave growth and neglected the other two source terms (Komen et al., 1994). As a result, they could not realistically reproduce the full spectrum of ocean waves.

To overcome this, second-generation models were developed during the 1970s and early 1980s. These models incorporated varying wind fields and included simplified treatments of non-linear interactions and dissipation (Komen et al., 1994). However, Forristall and Reece (1985) systematically tested second-generation models using idealised cases and found that the parameterisations used to represent non-linear transfers could not adequately describe the evolution of the wave spectrum.

In response to these shortcomings, efforts intensified in the mid 1980s to develop models that did not rely on pre-specified spectral shapes. This resulted in the development of the third-generation wave models, which explicitly solve the full spectral action balance equation without assuming a predefined spectral form. The most significant outcome of this was WAM (Wamdi Group, 1988). WAM could simulate the growth, propagation, and decay of wind waves and swell in deep water more realistically than earlier generations. Building on WAM, other third-generation models were developed, including WW3 (Tolman, 1989), widely used for global and regional scales, and SWAN (Booij et al., 1999), which was designed specifically for shallow-water and nearshore applications.

2.5.3 Why do we need more than one model?

No single wave model can efficiently represent processes from the open ocean to the nearshore (Guisado-Pintado, 2020). Therefore, different models are typically combined

depending on scale and purpose. For example, WAM is widely applied at the oceanic scale to represent wave growth and propagation in deep and intermediate waters (Wittmann and Farrar, 1997; Swain et al., 2019). Although, modern versions of WAM have been extended to include depth refraction and depth-induced wave breaking, the model uses explicit spatial schemes that require very small grid sizes in shallow water, making it computationally impractical for direct coastal applications (Bingölbali et al., 2019). In contrast, SWAN is commonly used in nearshore areas where higher resolution and shallow water processes must be represented (Booij et al., 1999; Neill, 2024; Zed et al., 2022; Anton and Nash, 2020; Guisado-Pintado, 2020; Reduan Atan and Goggins, 2017; Atan et al., 2016; Bento et al., 2016; Bento. et al., 2011). Applying models like WAM directly in nearshore regions would be computationally expensive due to the need for very fine spatial and directional resolution, as well as stability constraints that require very small time steps (Luo and Flather, 1997; Yuan et al., 2024).

To address this, a nested approach is often adopted. In nesting, a coarser large-domain model is used as boundary conditions for a finer local domain model (Luo and Flather, 1997). This downscaling can be applied in multiple stages, for example from global to regional and finally to coastal domains, ensuring that offshore wave information is consistently transferred into nearshore simulations (Reduan Atan and Goggins, 2017). Nesting is a widely used approach in wave models and is particularly important in the NEA and Ireland, where long-travelled swells interact with locally generated seas over complex bathymetry (Calvino et al., 2022; Anton and Nash, 2020; Reduan Atan and Goggins, 2017; Atan et al., 2016; Bento et al., 2016).

2.6 Waves at the coast and their impacts

2.6.1 Wave transformation in shallow water

In the open ocean, waves transfer energy without moving water mass significantly, but this changes dramatically when waves enter shallow waters (Deacon, 1946; Hughes, 2016). As waves approach the shore, the circular orbital motion extends to roughly half the wave length below the surface. Thus waves start interacting with the sea bed. The friction with the sea bed slows the lower part while the upper part continues forward, and causes the wave to steepen and grow taller until it becomes unstable and breaks.

The transformation from deep to shallow water involves competing processes. Wave steepness increases due to non-linear effects while the wave shortness changes due to frequency dispersion (Stelling and Zijlema, 2009). These effects normally balance each

other in deep water. However, when the sea bed rises towards the coast, this balance breaks leading to instability and finally the breaking of waves. After breaking, turbulence dominates the flow and prevents further steepening, allowing broken waves to move shoreward as bores that gradually flatten and extend before running up the beach (Stelling and Zijlema, 2009).

The region from where waves break to the shoreline is the surf zone and from the shoreline to where they reach their maximum inland extent is the swash zone. The two zones are characterised by highly complex wave and current patterns. Here, wave setup (the elevation of mean water level), wave run-up (the maximum vertical extent of wave uprush), and nearshore currents control how sediment moves and how pollutants disperse (Tao, 2020). These processes become particularly important during coastal flooding, when the total water level results from the combined effect of mean sea level, tides, and storm-driven surge with wave effects (Wolf, 2009).

2.6.2 Sea level rise effects on wave-coast interactions

The natural wave transformation processes are fundamentally altered when sea level changes the baseline conditions. That is, sea level rise alters how waves interact with the coast by shifting the point at which waves begin to shoal and break further landward (Arns et al., 2017). Therefore, waves that previously dissipated much of their energy in deep water will increasingly reach the shore, producing higher run-up heights (Chini et al., 2010).

While sea level rise has minimal influence on offshore wave climate, its effects become pronounced at the shore (Chini et al., 2010). The elevated water level allows longer period and higher amplitude waves to propagate closer to the shoreline before losing energy (Arns et al., 2017). This amplification of wave impacts represents a critical but underestimated component of future coastal flooding risk.

2.6.3 Is Ireland vulnerable to sea level rise?

Relative sea level (RSL), the sea level relative to the land at a given location, is determined not only by changes in ocean water volume but also by vertical land motion including land uplift and coastal subsidence (Fox-Kemper, 2021). Global mean sea level rise is primarily caused by the thermal expansion of seawater and the melting of glaciers and ice sheets (Fox-Kemper, 2021). These processes, combined with regional land movements, determine the actual sea level changes experienced along the Irish coast. Glacial Isostatic Adjustment (GIA), the ongoing response of the Earth's surface to the retreat

of ice sheets since the Last Glacial Maximum (Whitehouse, 2018), drives vertical land motion across Ireland. This results in spatially variable land movement, with uplift in some regions and subsidence in others. In the north and northeast of Ireland, post-glacial rebound leads to slow land uplift, partially offsetting ocean-driven sea level rise and resulting in lower rates of relative sea level increase (Bradley et al., 2023). In contrast, much of southern and western Ireland experiences land subsidence. This is driven by two main mechanisms: forebulge collapse associated with GIA, and localised subsidence due to compaction of soft estuarine and coastal sediments (Bradley et al., 2023). Areas such as Cork, Tarbert, and Galway are particularly affected, where subsidence adds to ocean-driven sea level rise and increases local coastal exposure beyond what global mean projections alone would suggest (Bradley et al., 2023). These regional land motion effects are critical when interpreting tide gauge records and projecting future sea levels, as neglecting them can lead to misinterpretation of long-term trends (Bradley et al., 2023).
Tide gauge data show rising sea levels at rates consistent with global trends, but with local variations. Dublin has accelerated from about 7 mm/year in the mid 20^{th} century to over 3 mm/year since the 1990s (Shoari Nejad et al., 2022), while Cork has experienced rates of around 2.2 mm/year in recent decades (Pugh et al., 2021). Projections suggest global sea level could rise by 0.3-0.6 m by 2100 under moderate emission scenarios and up to 1 m or more under high emissions (Slangen et al., 2014).
Even modest increases in sea level could transform coastal flooding risk in Ireland. An additional 0.5 m of sea level rise could permanently inundate around 200 km^2 of land, particularly in Wexford, Kerry, and Cork, while combined events of sea level rise and storm surge could flood around 600 km^2 (Noone et al., 2024). Ireland's exposure to energetic Atlantic swells further amplifies this risk (Gallagher et al., 2016b), as elevated water levels allow larger waves to reach further inland and enhance wave run-up during storms (Melet et al., 2018; Arns et al., 2017).
Storm surges and extreme waves pose an increasing threat to Ireland as sea level continues to rise (Noone et al., 2024; McGrath et al., 2008). This is a major threat to coastal cities such as Cork, Dublin, Galway, and Limerick and can cause damage to infrastructure including ports and energy facilities. Ireland's soft sediment shorelines are particularly at risk due to their vulnerability to erosion and inundation under rising seas (Noone et al., 2024).
The evidence reviewed above, from energetic Atlantic swell exposure, to rising relative sea levels driven by both ocean warming and land subsidence, collectively establishes that Ireland represents a particularly vulnerable and scientifically compelling case study.

Addressing these risks, however, requires a modelling framework capable of connecting large-scale atmospheric forcing to local-scale coastal response. The following section outlines the rationale for the design choices made in this thesis to achieve this aim.

2.7 Rationale for the study design

Despite this extensive body of work, several gaps remain. Swell contributions are still under represented in regional projections (detailed in Section 3.1 of Chapter 3). Downscaling of climate model winds requires computationally demanding regional weather models or simplified statistical approaches. Most critically, no existing study has explicitly integrated large-scale wave climate, nearshore transformation, and coastal run-up under rising sea levels for Ireland.

This thesis addresses these gaps by applying surrogate wind driven nested WAM-SWAN framework tailored to the NEA and the Irish shelf to capture both offshore swell and locally generated seas that shape Irish wave climate. In addition, a one-dimensional non-linear shallow water model is developed to study wave run-up under varying sea level conditions. Together, these modelling components establish a direct link between large-scale atmospheric forcing and local coastal impacts, providing a framework to assess present and future wave climate and its implications for Ireland's coasts.

The modelling framework employed in this thesis involves a series of choices regarding observational data, climate model forcing, climate drivers, emission scenarios, simulation length, and ensemble strategy. These choices are grounded in the existing literature and in the specific requirements of studying the wave climate of the NEA and the Irish coast. This section reviews the evidence supporting each choices.

2.7.1 ERA5 wave data for swell propagation analysis

ERA5 wave parameters are produced by the ECMWF WAM wave model, which is fully coupled to the atmospheric model within the ERA5 system and benefits from the assimilation of satellite altimeter significant wave height observations (Soci et al., 2024; Hersbach et al., 2020). This makes ERA5 wave output more physically consistent than wave parameters derived from uncoupled reanalysis-forced wave models, because the sea surface roughness fed back from the wave model influences the atmospheric boundary layer, improving the representation of both wind and wave fields simultaneously. The ERA5 wave dataset has been widely used for swell climatology and source region studies in the North Atlantic (Semedo et al., 2011; Gulev and Grigorieva, 2006) and its swell pe-

riod parameters have been shown to capture the propagation characteristics of Atlantic swell with sufficient fidelity for cross-correlation based travel time analysis (Ardhuin et al., 2009).

Swell period was chosen as the cross-correlation variable in preference to swell height because it is less affected by dissipation and wind-sea contamination along the propagation path, providing a more reliable tracer of swell origin (Ardhuin et al., 2009; Barber and Ursell, 1948). The results of the swell propagation analysis directly inform the choice of the North Atlantic as the outer wave model domain in Chapter 4.

2.7.2 ERA5 Reanalysis as reference for MPI-ESM

The ERA5 global atmospheric reanalysis (Hersbach et al., 2020), produced by the European Centre for Medium-Range Weather Forecasts (ECMWF) at approximately 31 km horizontal resolution, was used as the reference for surrogates for MPI-ESM climate model winds. ERA5 was selected because it has been extensively evaluated for surface wind fields over the North Atlantic and the NEA. It demonstrated substantially improved performance relative to its predecessor ERA-Interim, particularly in capturing mid-latitude storm track winds that are the principal generators of Atlantic swell reaching Ireland (Bricheno et al., 2023; Hersbach et al., 2020). Studies evaluating ERA5 against Irish Marine Institute buoy observations have confirmed good agreement for both mean and extreme significant wave height in the NEA (Nic Guidhir et al., 2022; Gallagher et al., 2014). ERA5-forced wave model hindcasts have also been shown to perform more consistently than other reanalysis products for North Atlantic wave height trends, particularly in the extratropical storm track region (Sharmar et al., 2021; Markina et al., 2018). ERA5 wind fields serve as the reference dataset for generating high-resolution surrogate wind fields for both the present-day and future climate simulations.

2.7.3 MPI-ESM as the climate model driver

The MPI-ESM was selected as the source of climate model wind fields for driving the future wave climate simulations. MPI-ESM is a comprehensive coupled Earth System Model contributing to CMIP6 (Mauritsen et al., 2019). The choice was motivated by its reliable performance in simulating North Atlantic atmospheric circulation including the NAO variability and storm tracks (Olonscheck et al., 2023), its ability to capture the NAO-driven wave variability when used to force WAM (Dobrynin et al., 2019), and the fact that its projected changes in the North Atlantic circulation under RCP8.5 are broadly consistent with the CMIP6 ensemble mean (Casas-Prat et al., 2024). MPI-ESM

has also been included as one of eight CMIP6 models in the global wave climate ensemble of (Meucci et al., 2024), confirming its suitability for wave climate projection studies.

2.7.4 Selection of climate drivers

The wave climate simulations in this thesis are driven by three climate variables: surface wind fields, sea ice concentration, and sea level. This selection reflects both the physical processes governing wave generation and propagation in the North Atlantic and the practical constraints of the modelling framework. The decision to include these three drivers and exclude others, specifically ocean currents, sea surface temperature (SST), and ocean salinity, is justified below.

Wind fields are the primary driver of wave generation in the open ocean. As established in Section 2.1, the transfer of energy from wind to waves through the atmospheric input source term (Sin) is the fundamental mechanism controlling significant wave height, peak period, and directional distribution across the North Atlantic. Changes in wind speed, direction, and storm track position under future climate scenarios therefore constitute the most direct pathway through which climate change affects the wave climate around Ireland **??**. Wind forcing is accordingly the most important climate variable for wave projections..

Sea ice concentration is included because changes in Arctic and sub-Arctic sea ice extent directly affect the fetch available for wave growth in the northern North Atlantic and the wave boundary conditions entering the model domain from the north (Christakos et al., 2024). As sea ice retreats under climate change, the open water area available for wave generation expands, leading to increases in swell energy propagating southward into the North Atlantic basin (Chen et al., 2021). For a study covering the full North Atlantic domain, neglecting sea ice changes would result in an underestimate of future swell energy at the northern boundary and an incomplete representation of how the wave climate of the NEA is affected by Arctic changes. Sea ice concentration from MPI-ESM is therefore included as a boundary condition in the North Atlantic domain.

Sea level is included specifically for the coastal wave run-up simulations in Chapter 5, where projected sea level rise under RCP8.5 is applied as an elevated baseline water level in the SWARM-1D model. As discussed in Section **??**, sea level rise shifts the point of depth-induced wave breaking landward, allowing larger waves to reach the shoreline and increasing wave run-up heights. Without incorporating sea level change, the coastal impact assessment would be limited to changes in offshore wave conditions alone and would miss the amplification of run-up caused by the changing baseline water depth.

This is one of the most significant but often underestimated components of future coastal flooding risk in Ireland (Melet et al., 2018; Aarnes et al., 2017).
Ocean currents, SST, and salinity were not included as explicit climate drivers in the wave modelling framework. Ocean currents influence wave heights through wave-current interactions (Kumar and Hayatdavoodi, 2023), but Calvino et al. (2022) demonstrated specifically for Irish waters that including currents improves overall significant wave height accuracy by only 1%. They also identified that current effects become significant at spatial scales below 50 km and dominate wave energy variability only at scales below 50 m. Since the region surrounding Ireland features weaker currents compared to regions such as the Gulf Stream or the Agulhas Current (Calvino et al., 2022), the exclusion of current fields is justified.

2.7.5 Choice of Emission Scenario: RCP8.5 / SSP5-8.5

RCP8.5 was selected because the projected changes in wave heights around Ireland are substantially larger under RCP8.5 than under lower emission scenarios, making the climate change signal more clearly detectable above natural variability . Gallagher et al. (2016a) directly compared RCP4.5 and RCP8.5 for Irish waters using the EC-Earth climate model and WAVEWATCH III. Their study projected decreases in annual mean significant wave height of up to 3.5% under RCP8.5 compared to only 2% under RCP4.5, with no statistically significant decrease found for RCP4.5 off the west coast of Ireland in spring and autumn. Similarly, Lemos et al. (2021) compared projected changes in North Atlantic wave heights under RCP4.5 and RCP8.5 using ten different climate models. They found that under RCP8.5, the projected decreases in wave height are larger and more consistent across models, while under RCP4.5 the changes are smaller and harder to distinguish from the natural year-to-year variability of the climate system. This is particularly important for the present study, which uses only a single climate model member over a 20-year period. Under these conditions, using a weaker scenario such as RCP4.5 would risk producing projected changes too small to be confidently attributed to climate change rather than natural variability. RCP8.5 therefore provides a clearer and more detectable climate change signal given the constraints of the study design. In addition, RCP8.5 produces the largest projected sea level rise by 2100, which is directly relevant to the wave run-up simulations in Chapter 5.1, where sea level rise is the primary factor amplifying coastal flooding risk (Allan et al., 2023; Fox-Kemper, 2021).

2.7.6 Choice of simulation length and period

The 20-year duration was selected for both present and future simulations, to ensure wave climate statistics represent the climatological regime rather than being dominated by individual anomalous years. The primary driver of interannual wave climate variability in the NEA is the NAO, which operates on timescales of years to decades with clustering of positive and negative phases that can persist for several years (Dobrynin et al., 2019). A period of fewer than 15–20 years risks producing wave statistics biased by a single NAO phase. A 20-year window is sufficient to sample multiple NAO phase transitions (Viñes et al., 2026) and is the standard in comparable NEA wave climate studies (Gallagher et al., 2016a; Aarnes et al., 2017). The 20-year window also partially captures variability associated with the East Atlantic pattern, which modulates NEA wave heights on decadal timescales (Morales-Márquez et al., 2020). From a computational perspective, 20 years represents the longest practically feasible period given the demands of the nested WAM-SWAN system with surrogate wind generation.

The present-day simulation (2004–2023) aligns with the expansion of the Irish Marine Institute buoy network, providing the best available observational record for validation (Marine Institute, 2022). The future period (2081–2100) follows the standard CMIP6 convention for end-of-century projections, maximising the detectable climate change signal under RCP8.5 (Morim et al., 2019). Both windows span 20 years, which is sufficient to sample multiple NAO phase transitions and avoid statistics biased by a single NAO phase – the primary mode of interannual wave climate variability in the NEA, with correlations between the NAO and seasonal H_s reaching 0.92 in the region west of Ireland (Dobrynin et al., 2019). This 20-year standard is consistent with comparable NEA wave climate studies (Lemos et al., 2020, 2019; Gallagher et al., 2016a), and represents the longest computationally feasible period given the nested WAM-SWAN system with surrogate wind generation.

2.7.7 Model Uncertainty in Wave Climate Projections

Wave climate projections are subject to multiple sources of uncertainty that must be considered when interpreting future changes. The primary sources include: (1) climate model uncertainty, arising from differences in the physical parameterisations and numerical schemes used by different models (Morim et al., 2019); (2) internal climate variability, which represents the natural random fluctuations in the climate system that cannot be predicted beyond seasonal timescales (Hemer et al., 2013); (3) emissions scenario uncer-

tainty, reflecting the range of possible future greenhouse gas concentrations depending on societal choices (Meucci et al., 2024); and (4) wave model uncertainty, introduced by differences in model physics, spatial resolution and spectral discretisation (Alonso and Solari, 2021).

Climate model uncertainty arises from differences in the physical parameterisations, numerical schemes and spatial resolutions used by different global climate models. Different models can produce different atmospheric circulation patterns and wind fields under the same emission scenario, leading to different projected wave climates (Morim et al., 2019; Hemer et al., 2013).

Emissions scenario uncertainty reflects the range of possible future greenhouse gas concentrations depending on societal and political choices (Patra et al., 2024). Studies have shown that under lower emission scenarios such as RCP4.5 or SSP2-4.5, signals of wave climate change are unlikely to exceed the magnitude of natural climate variability, whereas under high emissions scenarios such as RCP8.5 or SSP5-8.5, robust changes in wave height, period and direction are projected across large parts of the global ocean (Patra et al., 2024; Meucci et al., 2020; Morim et al., 2019). The choice of emissions scenario therefore significantly influences the magnitude and spatial extent of projected wave climate changes, and projections based on a single scenario should be interpreted accordingly.

Wave model uncertainty is introduced by differences in the numerical wave models used for downscaling, including their physical parameterisations of wave generation, dissipation and nonlinear interactions, as well as their spectral and spatial resolutions. Alonso and Solari (2021) found that methodology-related uncertainty, including the choice of wave model and downscaling approach, dominates other sources of uncertainty in current global wave climate projections. The use of different wave models, such as WAM, WWW3 or SWAN, can produce different results even when forced with the same climate model output, highlighting the importance of carefully evaluating wave model performance through validation studies.

Internal climate variability represents the natural random fluctuations in the climate system, such as those associated with the NAO and ENSO, that are not driven by external forcing. A single ensemble member cannot capture this full range of natural variability, and projections from different ensemble members of the same model can differ substantially over regional scales (Morim et al., 2019).

2.8 Summary

This chapter reviewed the fundamental processes of wind-wave generation, the distinction between wind-sea and swell, and the statistical parameters used to describe sea states. These concepts form the foundation of wave climate studies and underpin the numerical modelling approaches applied in this thesis. The review also highlights that modern wave modelling relies on spectral representations to capture wave energy across frequencies and directions. This framework enables third-generation models such as WAM and SWAN to simulate the growth, propagation, and transformation of waves. WAM is well suited for large-scale ocean simulations, while SWAN is designed for coastal areas, and nesting the two allows offshore wave conditions to be transferred to nearshore regions.

The literature also shows that the NA, especially the NEA has one of the most energetic wave climates in the world. This region experiences strong seasonal and interannual variability linked to large-scale atmospheric patterns. Future projections indicate decreases in mean wave height in this region, but with considerable uncertainty about extreme waves.

The chapter further reviewed on how waves transform as they approach the coast, and how rising sea levels can amplify coastal impacts. For Ireland, where sea level is rising, even a small increase poses high risk of flooding and erosion, especially when combined with storm surges and powerful Atlantic swells.

Together, the literature reviewed in this chapter establishes that understanding the wave climate of the NEA and its coastal impacts requires a multi-scale approach - one that connects large-scale atmospheric forcing to regional wave conditions and ultimately to local coastal responses. The gaps identified in this review, particularly the underrepresentation of swell in regional projections, the absence of an integrated wave-to-runup framework for Ireland, and the limited treatment of sea level rise in wave impact studies, motivate the modelling framework developed in this thesis. The choices reviewed in Section 2.7, including the use of ERA5, MPI-ESM, the climate variables for modelling and ahigh emissions scenario are each grounded in the evidence presented above and are designed to address these gaps within the practical constraints of the study.

CHAPTER 3

Swell Propagation Analysis in the North Atlantic

This chapter investigates the influence of remotely generated swells on the NEA region around Ireland from different regions of the NA. Using 20 years of swell period data, the analysis identifies key regions that consistently influence Irish waters and estimates the typical time lags associated with swell arrival. Statistical methods, including normalised cross-correlation and bootstrapping, are employed to ensure the robustness of the observed patterns. The results highlight the dominant role of certain regions while also revealing the variability linked to large-scale atmospheric conditions such as the NAO. By combining spatial and temporal insights, this chapter provides a clearer understanding of the remote swell influence on the west of Ireland. These findings lay the groundwork for the following chapter, which uses this information to inform the spatial domain selection for the wave model configuration.

3.1 Introduction

Ocean surface waves are the surface signature of atmospheric forcing over the ocean. Among these waves, swells are long-period waves that are generated by distant storms (Markina et al., 2018; Semedo et al., 2015; B. Kinsman, 1965). Once formed, they propagate thousands of kilometres with little loss of energy and travel across the entire ocean

basin (Wu et al., 2024b; Alves, 2006; Snodgrass et al., 1966). Unlike wind-sea, which is generated by local winds, swells shaped by remote wind systems reflect large-scale atmospheric activity (Gulev and Grigorieva, 2006). Swell generation begins when wind waves reach a stage where the phase speed of the peak wave exceeds local wind speed, allowing the waves to radiate outward from the storm centre as swell (Holthuijsen, 2007). Consequently, swell fields are less correlated with local winds, in contrast to wind-seas which show strong wind-wave dependence (Collard et al., 2009; Pierson and Moskowitz, 1964). Because of their ability to travel from their origin, swells are particularly important for understanding how ocean wave climate responds to regional and global changes in wind patterns.

Continental landmasses significantly influence global swell propagation (Li, 2016; Alves, 2006; Ardhuin et al., 2002). Swells generated in the Southern Oceans can spread energy across the entire global ocean, affecting wave climate in both hemispheres (Li, 2016; Young, 1999a). Even in the presence of vast land barriers blocking the path, swells from the Northern Hemisphere still reach remote locations (Alves, 2006). This shows how effectively these swell waves travel across ocean basins. The dominance of swell over wind-sea has been observed globally, with swell comprising more than 80% of wave energy in most oceanic regions (Zhang et al., 2023; Semedo et al., 2011; Chen et al., 2002). The NA exhibits significant long-term changes in wave climate with seasonally pronounced swell dominance. For example, a 45-year (1958–2002) wind-wave climatology analysis by Gulev and Grigorieva (2006) revealed the varying trends for wind-sea and swells in the NA during winter. Their study found that the over all increase in significant wave height in the central subpolar NA is primarily driven by the growing swell rather than the wind-sea. Supporting this, Gentil et al. (2012) analysed both satellite observations and wave model outputs from 2002 to 2008 and found that swell energy overwhelmingly dominated the wave regimes across mid-latitudes and the tropical NA. Additionally, Markina et al. (2018) used WW3 model outputs to examine the spatial distribution of wind-sea and swell influence in the NA. Their study showed that the 99^{th} percentile swell height reached up to 5.3 m, particularly in the central mid-latitudes and the North Sea, regions which are strongly affected by remotely generated long-period swell waves. Further supporting the importance of this region, a study by Amores and Marcos (2020) using WW3 modelling revealed that the Southern Ocean is the dominant global swell source. Their study also identified the NA as a direct and significant source of swell events affecting Ireland, with this region historically producing up to 28 major swell events per year. Although swells from the South Atlantic can reach the NA, their

influence near Ireland is relatively minor and short-lived, typically limited to less than 30 days annually (Alves, 2006). Therefore, the NA is the most relevant domain for investigating swell propagation and variability affecting wind-waves in the west of Ireland, and is the focus of this study.

Off the west coast of Ireland, these swells arrive after travelling thousands of kilometres, largely uninhibited due to long fetch and lack of land barriers (Shanahan and Fitzgerald, 2025; Nic Guidhir et al., 2022; Gaughan and Fitzgerald, 2020; Gallagher et al., 2014). This region experiences long-period waves (~8-8.5 seconds) confirming the presence of distant swells, in contrast to the Irish sea where wave periods are shorter (~4 seconds; Horrillo-Caraballo et al., 2021; Scott et al., 2021). Observational studies reveal a strong wind-wave correlation on the east coast (> 0.7), but much weaker correlations in the northwest and southwest, where Atlantic swells dominate (Gaughan and Fitzgerald, 2020; Fusco et al., 2010).

Although these studies clearly establish the presence and importance of swells around Ireland, especially on the Atlantic-facing coast, there is limited knowledge about specific propagation paths, travel durations and how these vary seasonally or interannually. Most previous research focuses on wind-wave correlations or examines general wave patterns, without explicitly tracing swell waves from distant regions to the Irish coast. This lack of targeted analysis represents a key research gap. To address this, the current chapter investigates how long it takes swells from different regions of the NA to reach the west of Ireland. The current study uses a cross-correlation approach similar to that used by Zheng et al. (2022, 2018) to study the influence of swell source regions on target areas in the Indian and Pacific Oceans. A 20-year time series of swell period data from various source regions is analysed, and the time lag that gives the highest correlation with swell data off the Irish west coast is identified. The same method is also applied on a seasonal basis to examine whether the influence of different swell source regions changes throughout the year. This analysis offers new insights into the spatio-temporal variability of swell propagation towards Ireland and improves our understanding of the dynamic nature of its wave climate.

3.2 Regional Definition

To explore the influence of swell from different parts of the NA, on waves off the west coast of Ireland, the NA domain was divided into multiple rectangular source regions (named A, B, C, D, E, F, and G) and a single target region, T. This division was

based on the work of Alves (2006), who identified regions of the global ocean with high storm activity or strong potential for swell generation. For the current study, five source regions were selected within the extratropical North Atlantic (ETNA), along with two additional regions located in the tropical North Atlantic (TNA). The spatial extents of each box are detailed in Table 3.1.

Box name	**Region**	**Latitude**		**Longitude**	
		North (°)	**South(°)**	**East(°)**	**West(°)**
A	ETNA	50	35	-70	-50
B	ETNA	50	35	-50	-30
C	ETNA	49	35	-25	-10
D	ETNA	65	55	-63	-50
E	ETNA	68	58	-40	-23
F	TNA	25	10	-80	-60
G	TNA	30	10	-40	-18

Table 3.1: Coordinates of Source boxes in ETNA and TNA regions

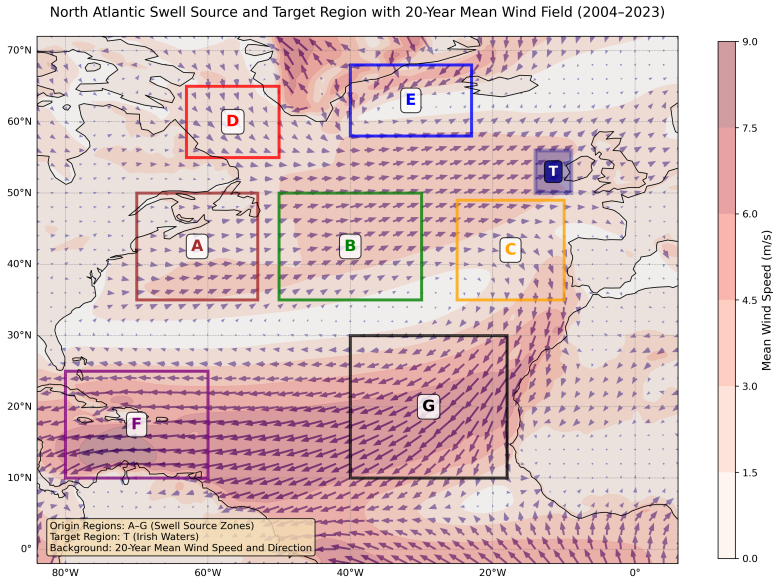

Figure 3.1: Source (A–G) and target (T) regions used in the swell analysis over the North Atlantic. The outlined boxes represent the source regions, while the filled blue box indicates the target region off the west coast of Ireland. The background shading shows the 20-year (2004 to 2023) mean wind speed, and arrows indicate the corresponding mean wind direction, based on ERA5 wind data

3.3 Hypothesis and Assumptions

The following section presents the main hypothesis of this study and the key assumptions underlying the use of lagged correlation to track swell propagation across the NA basin.
Hypothesis: If swell generated at point A travels to point T, then wave properties at A and T will be highly correlated, but with a time lag equal to the travel time.
Assumptions:

1. Swell generation zones are geographically consistent over time (Alves, 2006).
2. Swell can propagate over long distances with minimal energy loss (Ardhuin et al., 2009; Alves, 2006).
3. Time lag at which maximum correlation occurs between source and target regions reflects the swell travel time (Zheng et al., 2018, 2022).

3.4 Data and Methods

3.4.1 ERA5 Dataset

The mean period of total swell (mpts) was used in this analysis in preference to swell wave height, due to its more stable behaviour over long distance propagation (Ardhuin et al., 2009; Donn, 1949). The mpts values were extracted from the ERA5 wave reanalysis dataset, which is generated using four-dimensional variational data assimilation (4D-Var) within the ECMWF Integrated Forecasting System (IFS), Cycle 41r2 (Hersbach et al., 2020). The wave model (WAM) employed in ERA5 operates at a horizontal resolution of approximately 0.36°, while the reanalysis dataset provides forecast output at hourly intervals interpolated into a spatial resolution of 0.5°(Bruno et al., 2020). WAM computes 2D wave spectrum, F(f,θ) as a function of frequency f and propagation direction θ, at each grid point. Then the wave components in the spectrum are differentiated as wind-sea and swell. WAM considers wave components which are subjected to wind forcing as wind-sea while the remaining part of the spectrum is considered as swell (Janssen and Bidlot, 2003). For the current study, 3-hourly data spanning a 20-year period (2004–2023) were analysed over the NA region, bounded by 72°N to 2°S latitude and 84°W to 6°E longitude.
A 3-hour lag step was chosen based on the group velocity of typical Atlantic swell. For swell periods of 12-15 s, deep-water group velocity theory gives approximately 9-12 m/s (Holthuijsen, 2007), meaning swell travels roughly 100–130 km in 3 hours. Since each

source region spans several hundred kilometres, a 3-hour step provides multiple detection windows as the swell crosses any region. This ensures that the peak lag-time signal is not missed. Additionally, 3-hourly sampling reduces the dataset to one-third the size of hourly data, making the cross-correlation computationally practical.

3.4.2 Methodology

This section outlines the methodology used to investigate the influence of remotely generated NA swell on wave climate along the Irish coast. For this study, I am using normalised cross-correlation (NCC) as the primary analysis method to identify the timing and spatial patterns of swell propagation. A similar study to estimate the swell travel time in the Indian and Pacific ocean was done by Zheng et al. (2022, 2018). A comparable method is adopted here with two key distinctions: instead of swell wave height, the analysis is based on swell period, which is more stable over long distances and thus a reliable indicator of swell propagation, and NCC is used instead of ordinary cross correlation to eliminate the biases due to differences in magnitude across regions. To quantify uncertainties in the correlation estimates, bootstrapped samples were generated. Cross-correlation is computed for each resampled pair to obtain a distribution of correlation values for non-parametric error estimation.

A combination of lagged NCC and non-parametric block bootstrapping is used in this chapter. The NCC approach estimates the time delay (lag) and strength of similarity between source and target swell signals. The bootstrapping estimates the uncertainty range that is used to evaluate the statistical significance of observed correlations. Thus the method adopted helps to determine whether swell signals originating from different regions of the NA exhibit lagged correlation with swells observed near the Irish coast and to assess the statistical significance of the identified lag-times.

3.4.2.1 Lagged Normalised Cross Correlation

NCC is a statistical measure of similarity that quantifies the temporal correspondence between two signals while eliminating dependency on signal amplitude (Lewis, 2001), computed using Eq 3.1.

$$\mathrm{Corr}(k) = \frac{1}{N} \sum_{t=1}^{N-k} \frac{(x(t) - \mu_x)\,(z(t+k) - \mu_y)}{\sigma_x \sigma_y} \tag{3.1}$$

where $x(t)$ and $z(t)$ are the two time series, μ and σ represent their means and standard deviations, respectively, and N is the number of overlapping data points at lag k.

NCC ensures that correlation strength reflects actual temporal relationships rather than differences in absolute period values between locations. As done in time lagged cross correlations (Wu et al., 2024a), lagged NCC involves computing the correlation between normalised time series, then progressively shifting one series by a fixed time step and recalculating the correlation. This process continues up to a defined maximum lag of 8 days. The time lag that produces the highest correlation is the estimated delay between variations in the two time series.

Spatial averaging of ERA5 swell period data over each predefined region was performed prior to the cross-correlation analysis. This approach reduces the influence of local sub-regional variability and noise, yielding a single representative time series per region. A similar spatial averaging strategy was used by Zheng et al. (2022, 2018). Following spatial averaging, regional time series were normalised by subtracting the regional mean and dividing by the regional standard deviation (z-score normalisation) using Eq 3.1. This removes differences in absolute swell period magnitude across regions and ensures that the NCC reflects temporal variability rather than amplitude differences. Normalised values may occasionally be negative (as in Figure 3.2), which simply indicates swell periods below the regional mean. Negative normalised values do not imply physically negative wave periods.

The process is illustrated in Figure 3.2, which shows an example application of NCC using time series of normalised swell period. In Figure 3.2(a), the original normalised time series (January 2023) from a source region (Region E) and a target location (T) are shown. At zero lag, the signals appear unaligned, with a negative correlation of 0.55. In Figure 3.2(b), the source signal shifted by a lag of 132 hours ($\sim$ 5.5 days) resulted in good alignment with the target signal with a correlation value of 0.92. This is further shown with lagged cross correlation curves in Figure 3.2(c), where the red dotted line represents the lag at which maximum correlation was obtained. This lag is interpreted as the estimated swell travel time from Region E to T.

This example demonstrates the fundamental approach used in this study, which is applied to 20-years of swell period data. The technique is repeated for multiple predefined source regions and one target region, with the goal of estimating swell travel times and understanding seasonal variability in swell propagation.

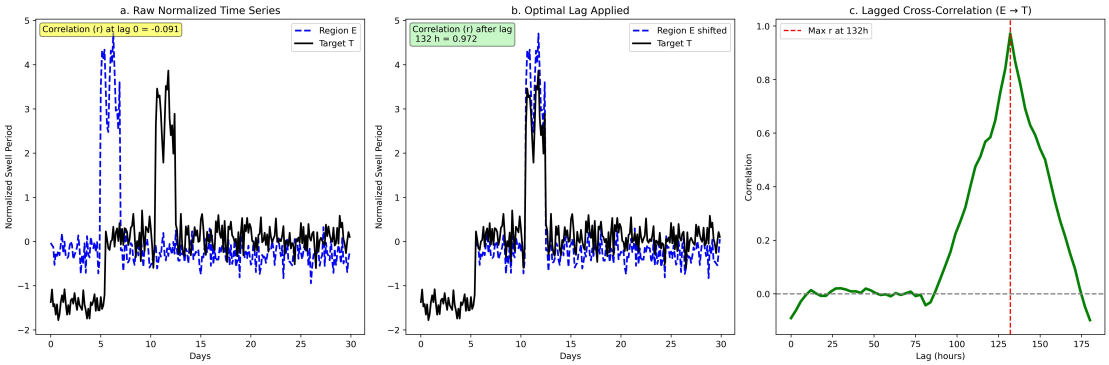

Figure 3.2: Illustration of NCC applied to detect swell propagation lag. a. Normalised original swell period time series at zero lag; b. alignment after applying optimal lag of 132 hours; c. Lagged corss-correlation curve (green) with the red dotted line representing the lag at which maximum correlation occurs.

3.4.2.2 Block bootstrapping

The block bootstrap (Hall et al., 1995; Künsch, 1989) method is used to assess the uncertainty in the correlation strength at the lag derived from NCC. Bootstrapping is a statistical resampling technique used to estimate the variability or distribution of a given statistic such as mean, correlation, or standard deviation (Efron, 1992). Rather than resampling individual data, block bootstrapping involves resampling blocks of consecutive data, making it well suited for autocorrelated time series, like swell period.

Swells exhibit strong temporal coherence over distances up to 10,000 km and durations approaching 10 days (Delpey et al., 2010). This persistence is also evident in the autocorrelation structure of the data. For each region, an e-folding decorrelation time was computed. This was done by computing the autocorrelation function of the time series and identifying the first time lag at which the autocorrelation dropped below 1/e ($\sim$0.37; Bellomo et al., 2014). This threshold is commonly used in oceanographic and climate studies as a measure of the dominant timescale over which the signal retains memory before losing coherence (Piles et al., 2021; Eastman et al., 2016; Bellomo et al., 2014; Ruiz-Barradas et al., 2013; Ardhuin et al., 2009; Gerber et al., 2008). Across all source and target regions, the estimated e-folding timescale ranged between 2.4 and 40.8 days with a median value of around 15 days.

To balance the statistical robustness and the physical relevance, a 10 day block length was chosen for bootstrap resampling. This choice remains within the observed range and is supported by studies indicating swell coherence over similar timescales.

3.4.2.3 Correlation Analysis and Significance Evaluation

The methods outlined above were applied in three stages to investigate seasonal and interannual patterns of remotely generated swells reaching the Irish coast. First, a 20-year seasonal climatology was established by computing lagged NCC between swell period time series from different source regions (A-G) across the NA and the fixed target region, T, near Ireland. These time series were derived by spatially averaging the swell data over each predefined region. The lag corresponding to the highest correlation was estimated as the swell travel time from each source. Heat maps were created to visualise the evolution of correlation values over different lags for each source-target pair.

To quantify the uncertainty range around observed correlations, a non-parametric block bootstrap approach was used, to generate a distribution of correlation coefficients. At every lag, 5000 unique bootstrap pairs of source and target time series were created by randomly resampling 10-day block with replacement. This approach helps to capture a wide range of possible variations and provides more reliable uncertainty estimates.

For each bootstrap pair, the correlation was computed at the specific lag, yielding 5000 correlation values per lag. This process generates a distribution of correlation coefficients for each lag, representing the natural variability of correlation estimates due to sampling uncertainty. From each lag's bootstrap distribution, the 2.5^{th} and 97.5^{th} percentiles were extracted to establish a 95% uncertainty range around the observed correlation at that lag.

A lag was considered statistically significant if zero fell outside the 95% bootstrap uncertainty range of the correlation at that lag. This determines whether the estimated swell travel time represents a meaningful propagation delay rather than random temporal alignment.

In the second analysis, NCC and bootstrapping approach were repeated on individual years to examine the interannual and seasonal variability in swell propagation. Lag maps were generated for selected years, to determine which regions dominated and how long swells took to reach the target. Finally, two contrasting years (2008 and 20203) were selected to highlight the seasonal shifts (during winter and summer). This multistep approach provides a robust and physically meaningful assessment of the influence of different NA swell source regions on Irish wave climate.

3.5 Swell Event Climatology at the Irish Coast

Understanding the swell climate at the Irish coast is an important step before investigating where these swells come from. This section provides a basic description of how often significant swell events arrive at the west coast of Ireland, and the wave periods associated with these events. This provides context for the detailed cross-correlation analysis presented in the sections that follow.

3.5.1 Frequency and magnitude of swell events off the west coast of Ireland

Significant swell events at T were identified by scanning the full 20-year swell period time series and selecting all periods during which the swell period rose above the 75th percentile threshold of approximately 13 seconds. Each continuous exceedance lasting at least 24 hours was counted as one event. A total of 738 significant swell events were identified at T over the 20-year record, corresponding to a mean of approximately 33.5 events per year. Figure 3.3 presents the seasonal distribution of these events. Winter (DJF) is by far the most active season, accounting for 268 events over the 20-year period. Autumn (SON) is the second most active season with 236 events, followed by spring (MAM) with 204 events. Summer (JJA) is markedly inactive, contributing only 30 events over the full 20-year record. This pronounced seasonal asymmetry is consistent with the dominant influence of the North Atlantic storm track, which is most active during the cold season and largely absent in summer, resulting in far fewer opportunities for long-period swell generation and propagation towards Ireland.

Figure 3.4 presents the distribution of peak swell period for events in each season. Winter events exhibit the greatest magnitude and variability, with a median peak period of approximately 13 seconds and individual events reaching 17 to 18 seconds. These exceptionally long periods correspond to swells generated by particularly intense and distant North Atlantic storms, and represent the conditions of greatest relevance for coastal engineering design and hazard assessment along the Irish coast. Autumn events show a similarly broad distribution, though with slightly lower median values, while spring events are more tightly clustered around the median. Summer events are characterised by the shortest and most uniform peak swell periods, with a median of approximately 12 seconds and limited variability, consistent with the weak and infrequent storm activity during this season. This finding motivates the detailed seasonal analysis presented in Case Study I (Section 3.6.2.1), which examines how swell source patterns vary across all

seasons within a single year, and the interannual comparison in Case Study II (Section 3.6.2.2), which focuses specifically on winter, the season of greatest swell activity, and summer, least active season, to investigate how atmospheric conditions between 2008 and 2023 alter the regional swell influence on Ireland.

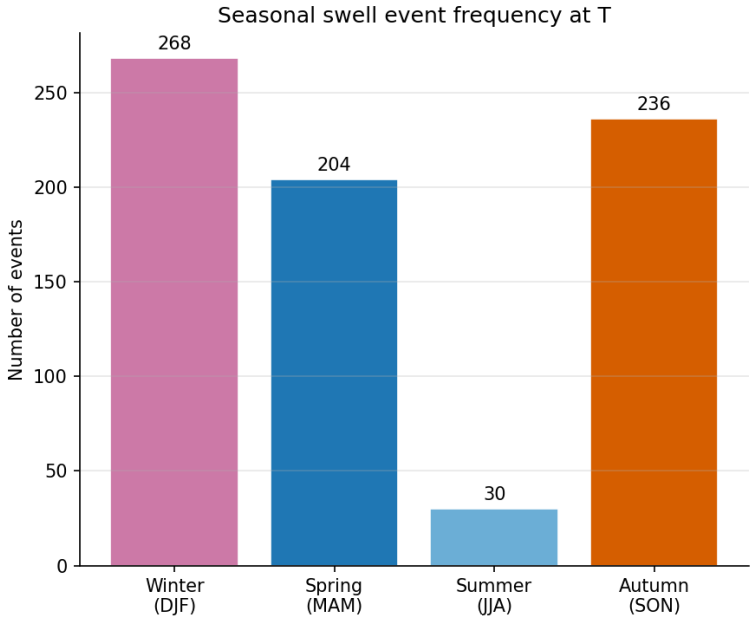

Figure 3.3: Seasonal distribution of significant swell events at the target region T, off the west coast of Ireland, identified from the ERA5 swell period record over the 20-year period 2004–2023.

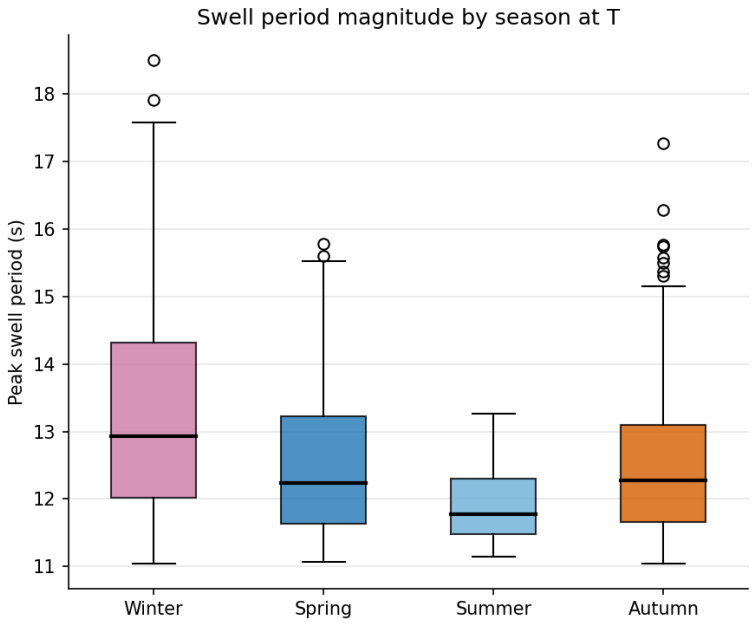

Figure 3.4: Seasonal distribution of swell periods at the target region T, off the west coast of Ireland, identified from the ERA5 swell period record over the 20-year period 2004–2023.

However, these figures alone do not reveal where these swells are coming from, how strongly each part of the North Atlantic influences conditions at Ireland, or how long it takes swell from different regions to arrive. Understanding these aspects, the source regions, the strength of their influence, the typical travel times, and how all of these vary seasonally and across years, is essential for correctly configuring a wave model that can capture the full swell forcing experienced at the Irish coast. This is the motivation for the normalised cross-correlation analysis presented in Section 4.7, which systematically examines the relationship between swell conditions across the North Atlantic and at T, and statistically estimates the typical propagation delay from each source region to the Irish coast.

3.6 Results

This section presents the outcome of the lagged correlation analysis between source and target regions. The goal is to identify the regions influencing the swell climate near Ireland and how this varies seasonally and interannually.

The results are organised to first establish a long-term seasonal climatology of swell

propagation patterns, followed by selected year specific visualisation to highlight inter-annual variability. Finally, two contrasting years (2008 and 2023) are examined in detail to illustrate shifts in swell influence during winter and summer in those years.

3.6.1 Seasonal Swell Climatology

To understand the seasonal patterns of swell influence on the target region, the results are presented using heat maps of lagged correlation and plots of maximum correlation with 95% uncertainty range. These visualisations capture dominant swell propagation pathways across different seasons over the period.

3.6.1.1 Trends from Heat map

Lagged correlation heat maps for each season over a 20-year period are shown in Figure 3.5. They capture the correlation strength across different lags between swell period from each source to target region. In the heat maps, the y axis represents the time lags (in hours), while the x axis indicates the source region compared with T for finding lagged NCC. Red shades indicate positive correlations and blue shades represent negative correlations. For each region and season, a black box highlights the time lag at which the maximum correlation occurred and a '$\star$' beside the correlation value indicates significance.

From Figure 3.5, it is evident that most source regions show positive lagged correlation with T across all seasons, indicating swell propagation towards the Irish coast. However, in winter, Regions A and D exhibit weak or negative correlation, suggesting limited influence from these regions. Notably, Region C shows strong correlation ($\sim$ 0.7 to 0.8) across all seasons, particularly at short time lags (0-12 h). This likely reflects C's close proximity to T, resulting in faster and more direct swell transmission, while E shows moderate correlation around 0.5 in all seasons, with peak often occurring at 0 lag. B also shows similar behaviour except in winter.

A peak correlation at zero lag suggests that the swell signals in those regions and the target occur at the same time. However, a zero lag-time requires careful interpretation and may reflect one of several mechanisms: (i) simultaneous swell generation in both regions due to the same large weather system; (ii) geographic proximity enabling faster-than-detectable propagation given the 3-hour temporal resolution; (iii) a statistical artefact of the NCC maximisation algorithm, in which the algorithm assigns zero lag as the maximum because it cannot resolve the true short delay; or (iv) a consequence

of interannual variability in true propagation delays. Accordingly, zero lag-times should not be taken uncritically as evidence of simultaneous generation.

For Region B, which shares broadly similar mean wind climatology with T (Figure 3.1), the zero lag most likely reflects mechanism (ii). B is relatively close to T and the true propagation delay may simply be shorter than the 3-hour temporal resolution can resolve. However, mean wind similarity alone is not sufficient to explain simultaneous swell generation, as swell is driven by instantaneous storm dynamics rather than mean atmospheric conditions.

The mean wind map reveals that E experiences strong winds, consistent with its location within the subpolar low-pressure zone which intensifies during positive NAO phases (Hurrell, 2001; Huang et al., 2006; Walker, 1924). These conditions are favourable for generating long-period swells that influence T (Semedo, 2005). However, E is located more than 2000 km from T, meaning proximity cannot explain the zero lag. The zero lag here is most likely mechanism (iii) — a statistical artefact of the long-term NCC averaging. When NCC is computed over the full 20-year record, year-to-year variability in the actual swell lag means no single non-zero lag consistently dominates, causing the algorithm to converge on zero as the best aggregate fit. This is supported by the individual year results, which frequently show non-zero lag-times for these regions and are therefore considered a more physically meaningful estimate of true propagation delay; accordingly, they are given greater emphasis in Section 3.6.2.

While the strongest signals are observed from C, E, and B in the heat map, it is important to note that G in the far southern NA shows a correlation of 0.33 at a lag of 48 hours during spring and autumn. This suggests that swells from the subtropical NA region may occasionally influence T.

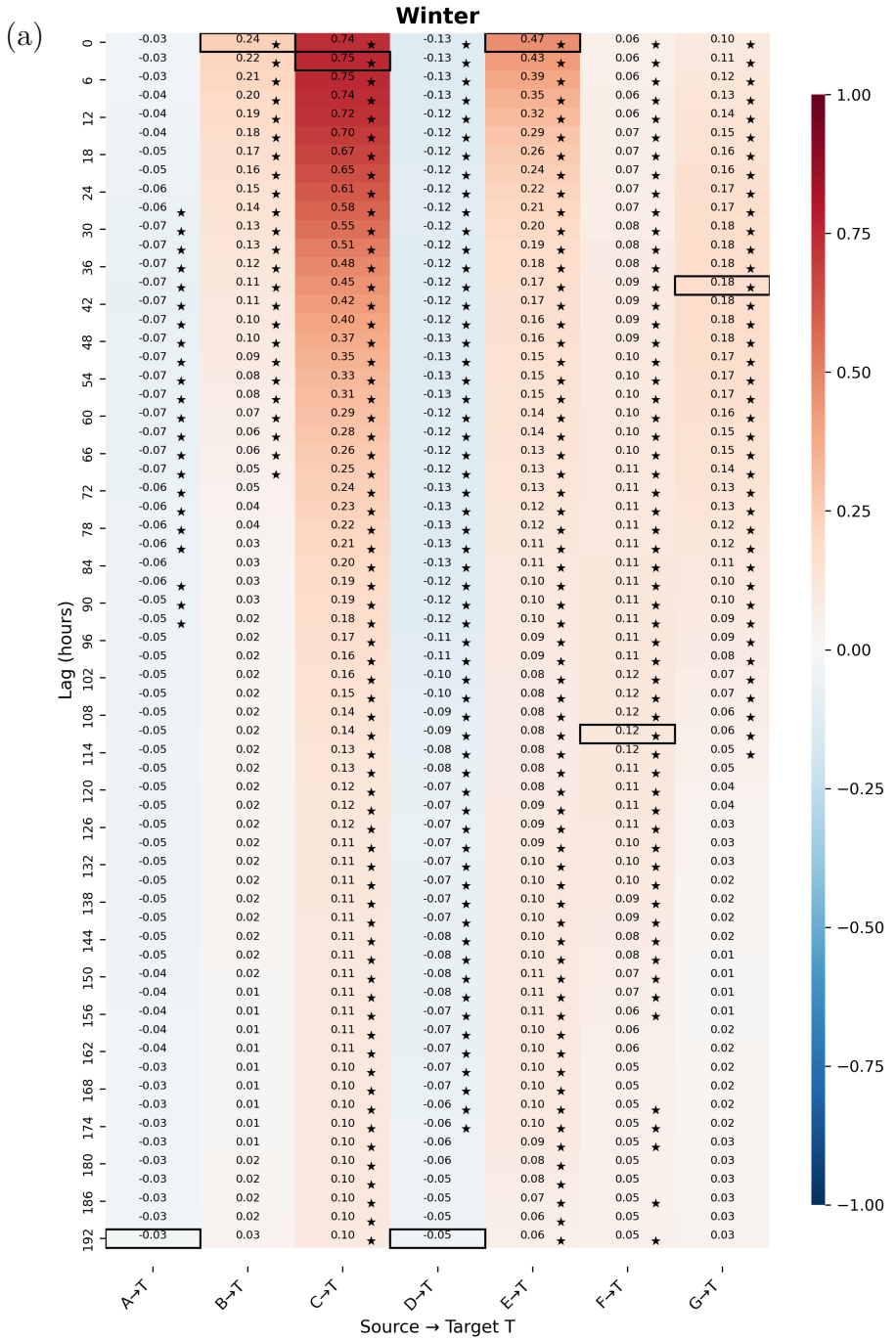

Figure 3.5: Lagged cross-correlation heat maps between swell periods in source regions (A–G) and the target region (T), based on 20-years of data. Panels show (a) winter, (b) spring, (c) summer, and (d) autumn on separate pages. The x-axis represents each source-to-target pair, and the y-axis indicates time lag. Red shading denotes positive correlation and blue shading denotes negative correlation. The black box marks the lag at which the maximum correlation occurs and '⋆' indicates the significance of lag because uncertainty range excluded zero.

(b)

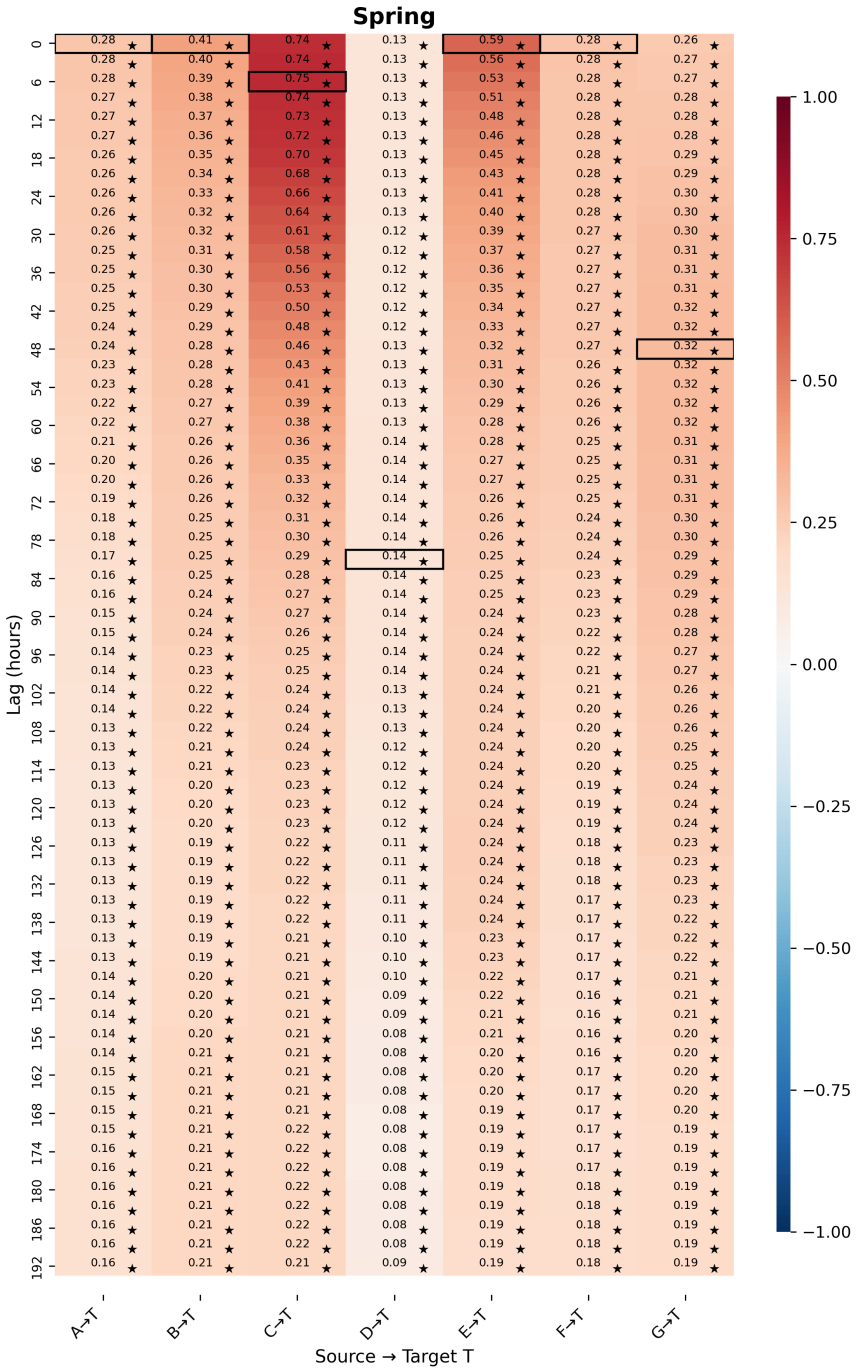
Spring
Lag (hours)
Source → Target T
A→T
B→T
C→T
D→T
E→T
F→T
G→T
1.00
0.75
0.50
0.25
0.00
−0.25
−0.50
−0.75
−1.00

(c)

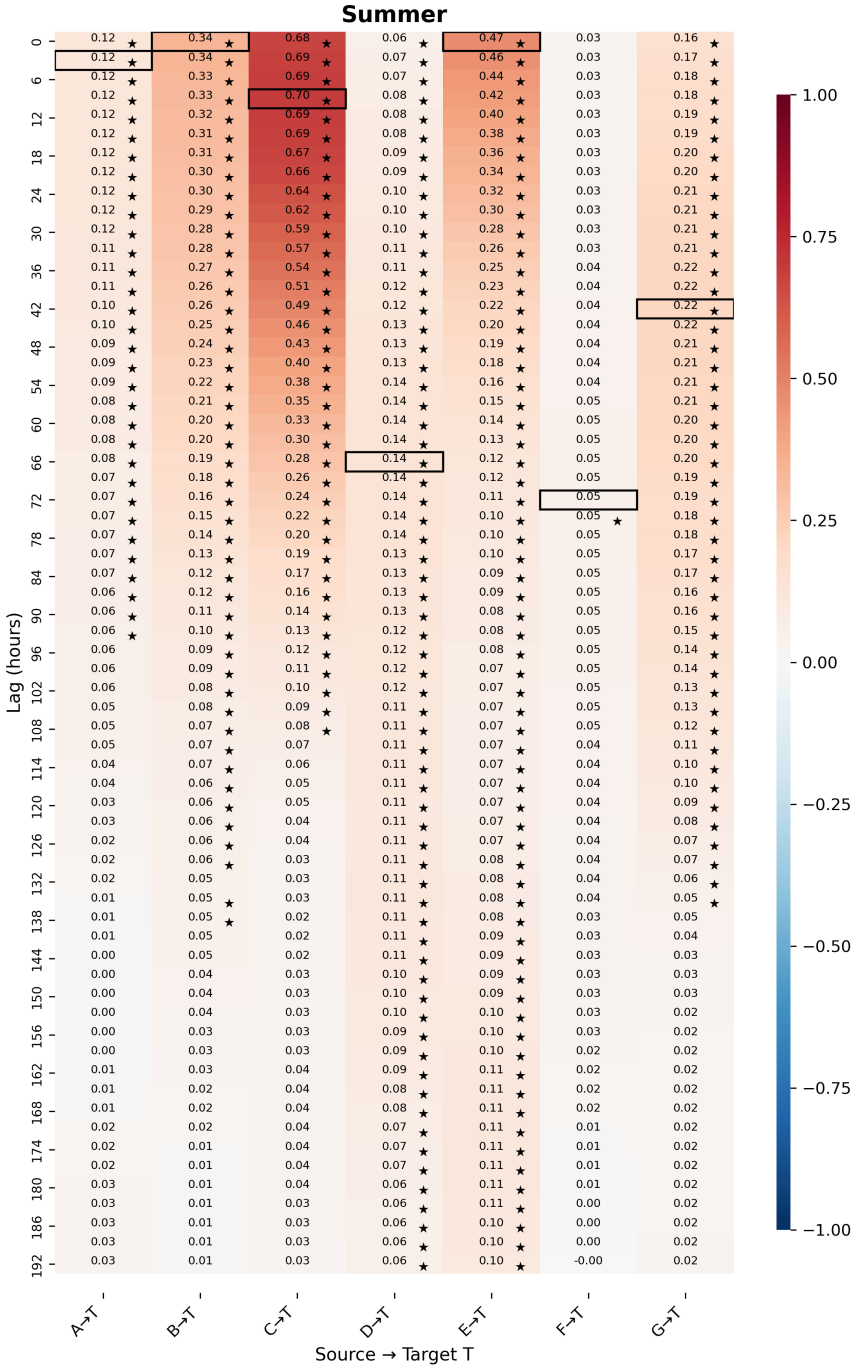
Summer
Lag (hours)
Source → Target T
A→T
B→T
C→T
D→T
E→T
F→T
G→T
1.00
0.75
0.50
0.25
0.00
−0.25
−0.50
−0.75
−1.00

(d)

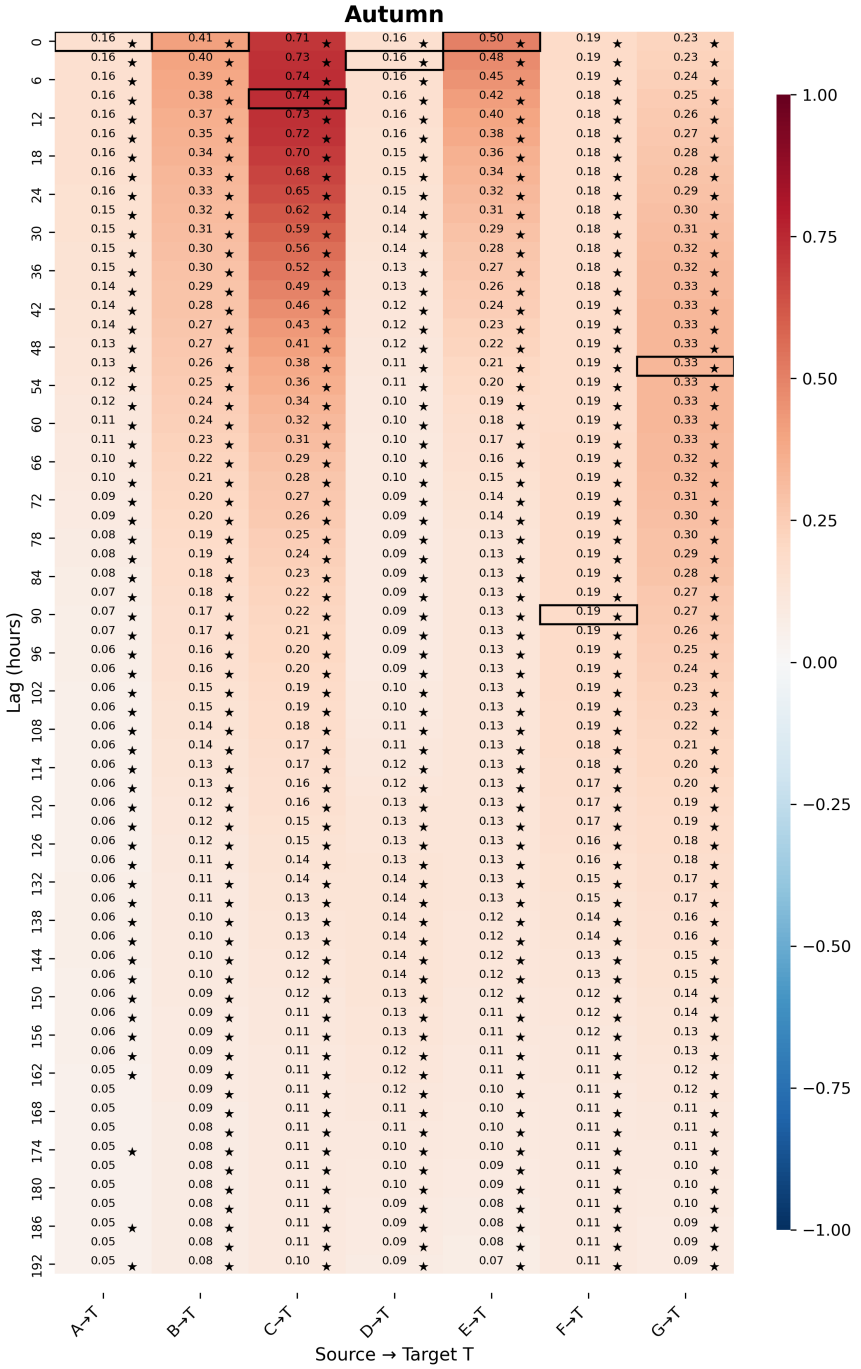
Autumn
Lag (hours)
Source → Target T
A→T
B→T
C→T
D→T
E→T
F→T
G→T
1.00
0.75
0.50
0.25
0.00
−0.25
−0.50
−0.75
−1.00

3.6.1.2 Statistical Significance from Bootstrap sampling distribution

To determine whether the estimated swell travel time (identified as the lag producing maximum correlation) is statistically reliable, the maximum correlation values were plotted with their bootstrap derived uncertainty range, as shown in Figure 3.6. The dots in each case in Figure 3.6, represent the maximum correlation at the identified lag, and the vertical bars show the range (95%) of correlation value derived from sampling. The grey line (provides the mean correlation across all seasons at each region) in the error bar plot provide a clear overview of which regions consistently influence the target.
It can be clearly seen that C, B, and E have strong influence on T. Region C, in particular, display consistently high average correlation around 0.75, reinforcing its role as a dominant and persistent swell source across seasons. This pattern is further supported statistically by the 95% sampling distribution which does not include zero. This suggest that the lags at which observed correlations occurred for these regions are unlikely to be the result of random variation, providing robust evidence of physical swell propagation. In contrast, A and D in winter and F in summer exhibit uncertainty ranges that include 0, indicating that these are not statistically significant based on the hypothesis testing framework: whereby a lag is considered statistically insignificant if the 95% uncertainty range includes zero. However, from a physical perspective, the behaviour of A and D can be attributed to their strong dependence on the NAO. These regions lie in areas highly affected by theNAO phase changes. This behaviour is discussed further in Section 3.7.2

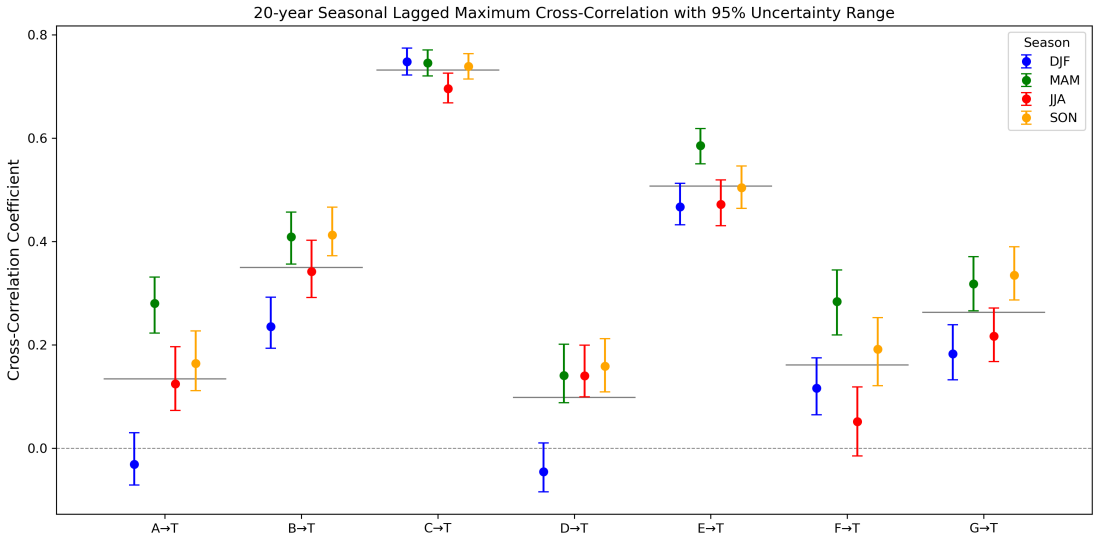

Figure 3.6: Maximum cross-correlation coefficients for seasonal swell propagation from North Atlantic source regions (A-G) to Irish target region (T) over 20-year climatology (2004–2023).Grey horizontal lines indicate average correlation values. Error bars represent 95% bootstrap uncertainty range (5^{th} - 95^{th} percentile) based on 5000 bootstrapped samples. Seasons: blue - DJF (winter), green - MAM (spring), red - JJA (summer), yellow -SON (autumn). The x-axis represents each source-to-target pair, and the y-axis indicates maximum correlations.

3.6.2 Case studies: Seasonal and Interannual Variability in Swell travel time

To explore the variability in swell propagation towards Irish waters, two illustrative case studies are presented. The first one examines seasonal patterns within a single year (2023), while the second one compares selected seasons in two years (2008 and 2023) to highlight interannual differences. A different visualisation approach is adopted here. While the previous section analysed long-term swell propagation patterns using 20-year seasonal lagged correlation heat maps, in this section I am presenting seasonal spatial map of a single year that summarises swell arrival times to T from source regions.
The map in Figure 3.8 (b) displays labelled boxes over the predefined source and target regions, with the values indicating time lag at which maximum correlation with T was observed (in days: d or hours: hr) which is assumed as the statistical swell arrival time from the source to T. The values are extracted from the heat map of seasonal lagged correlation with significance (Figure 3.8 a) for Winter 2023. This figure is presented as a demonstration of how lag information is spatially summarised.

For example, in Figure 3.8 (b), Region E (blue box), labelled as EH, exhibited high correlation at a lag of 15 hours, and the '⋆' after the travel time indicate that the estimated travel time is statistically significant. If '⋆' is missing then the travel time is not significant. Labels in other boxes include tags like VL: very low, L: low, H: High and X: negative values indicating the strength of observed correlations.
The background shading shows the frequency of wind speed exceeding 10 m/s. This wind metric helps to assess whether regions A-G are in active wind zones and tend to act as effective swell sources. Together, the seasonal maps generated provide a clear seasonal picture of swell transmission across the NA and highlight both temporal and spatial influence on Irish waters.

(a)

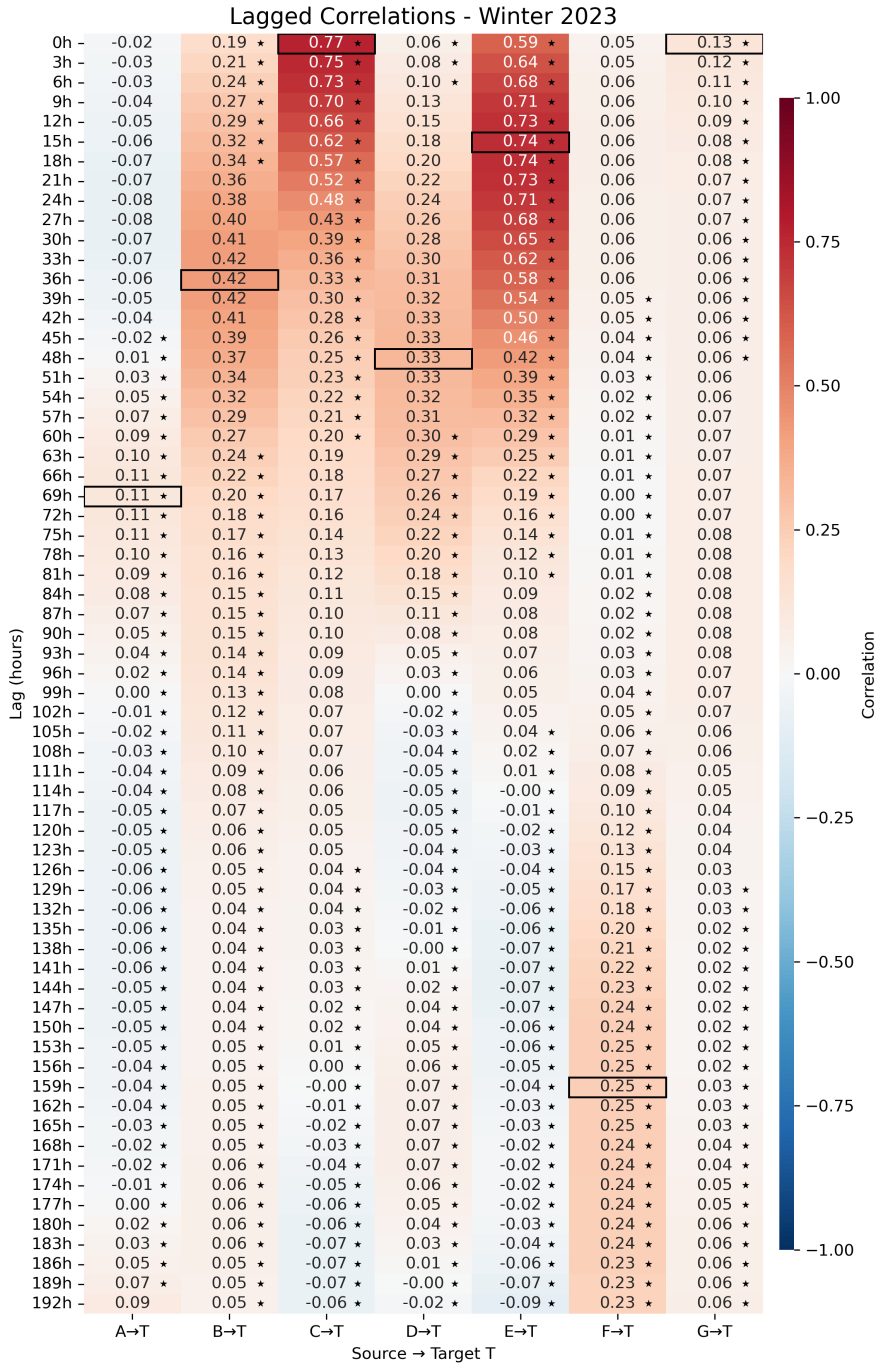
Lagged Correlations - Winter 2023
Lag (hours)
Source → Target T
A→T
B→T
C→T
D→T
E→T
F→T
G→T
Correlation
1.00
0.75
0.50
0.25
0.00
−0.25
−0.50
−0.75
−1.00

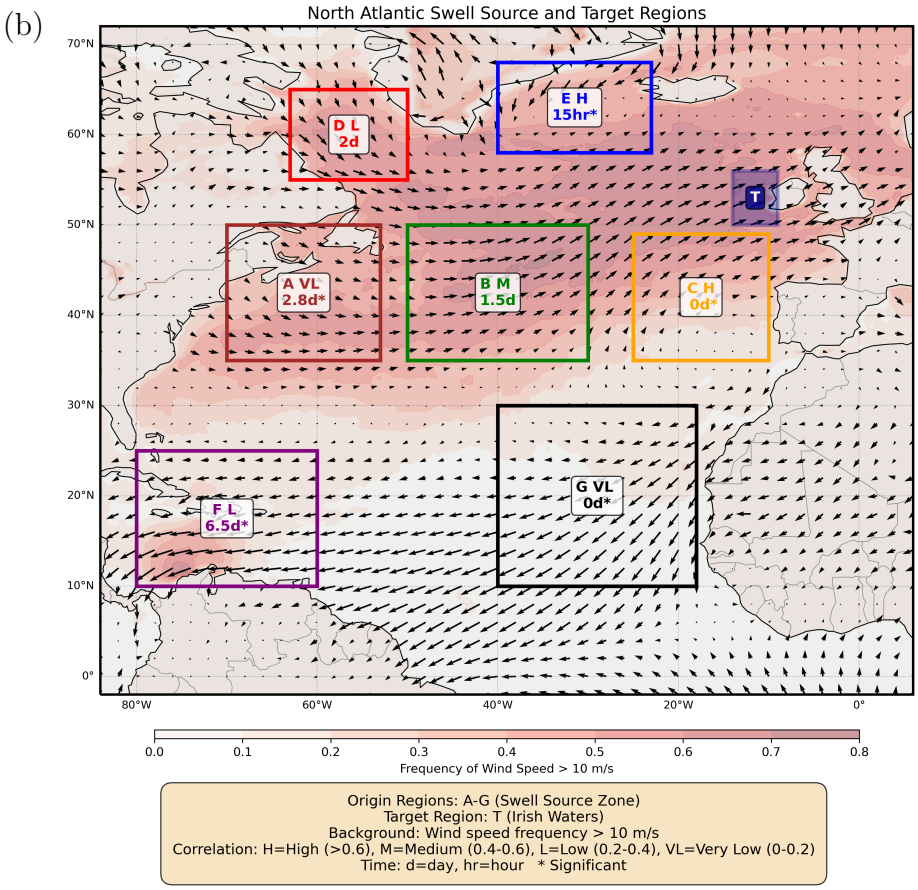

Figure 3.8: Demonstration of seasonal swell influence interpretation using lagged correlation and spatial mapping (Winter 2023 example). a. Heat map showing lagged correlation between A-G and T for Winter 2023. The x-axis represents each source-to-target pair, and the y-axis indicates time lag (in hours). Color intensity indicates the correlation strength. The black box marks the lag at which the maximum correlation occurs, indicating the swell travel time from source to target. The '$\star$' indicates the significance of lag because uncertainty range excluded zero ie unlikely to arise from random fluctuations. b. Corresponding spatial map summarising swell travel from each source region. Numbers within the boxes indicate the time lags (converted to days or hours) at which maximum correlation with T occurred, along with the labels for correlation strength. The background shading represents the frequency of mean speeds exceeding 10m/s, included to interpret the potential of different source region to generate swells.

3.6.2.1 Case Study I: Seasonal Swell Propagation in 2023

This section presents the spatial maps from a case study conducted for 2023 to understand the seasonal variability in the influence of swells from different NA sources on T. The lag represents the average delay in the propagation of the swell period signal from each source region to T, estimated statistically across all events within that season. It should not be interpreted as the physical travel time of any individual swell event.
In Figure 3.9 (a,b,c,d), C, E, and B consistently influence target T across all seasons. Region C shows high correlation (~ 0.7), indicating immediate swell arrival or the same weather system in both regions due to close proximity. B exhibits low to moderate correlations with swell reaching T within 1 to 1.5 days. Region E shows high correlations (0.6-0.7) in all seasons except summer and swell from this region arrives at T within less than a day.
A exhibits almost no correlation in all seasons except for spring, where it shows low correlation with an estimated swell travel time of 7 days. D generally lacks significant correlation, though a moderate signal is observed in spring. The correlation from F to T is low in winter, spring and in summer. Swell propagating from F reaches T during the correlated seasons after 2 to 6 days with no influence in autumn. It is noted that some of these lag-times, particularly from Region F, appear shorter than physically expected given the large separation from the Irish coast. This suggests they may reflect the statistical propagation of the swell period signal averaged across all events within the season, rather than the true travel time of any individual swell event. In contrast, G exhibits low but detectable correlations, with swells reaching the Irish coast in approximately 4 days during autumn. During spring and summer, the travel times are around 6 days and 2 days, respectively. However, correlations in winter are very weak, indicating minimal influence from G during that season.
Statistical significance assessment revealed that swell travel times from most regions were statistically reliable across all seasons. However, exceptions included Regions B and D, which lacked significance in winter and G, which showed no significance in summer. This indicates that swell propagation from these sources during these specific seasons cannot be reliably distinguished from random variability. It should be noted that the significance of regions showing negative correlations are not discussed further, as they do not represent meaningful swell propagation to T.

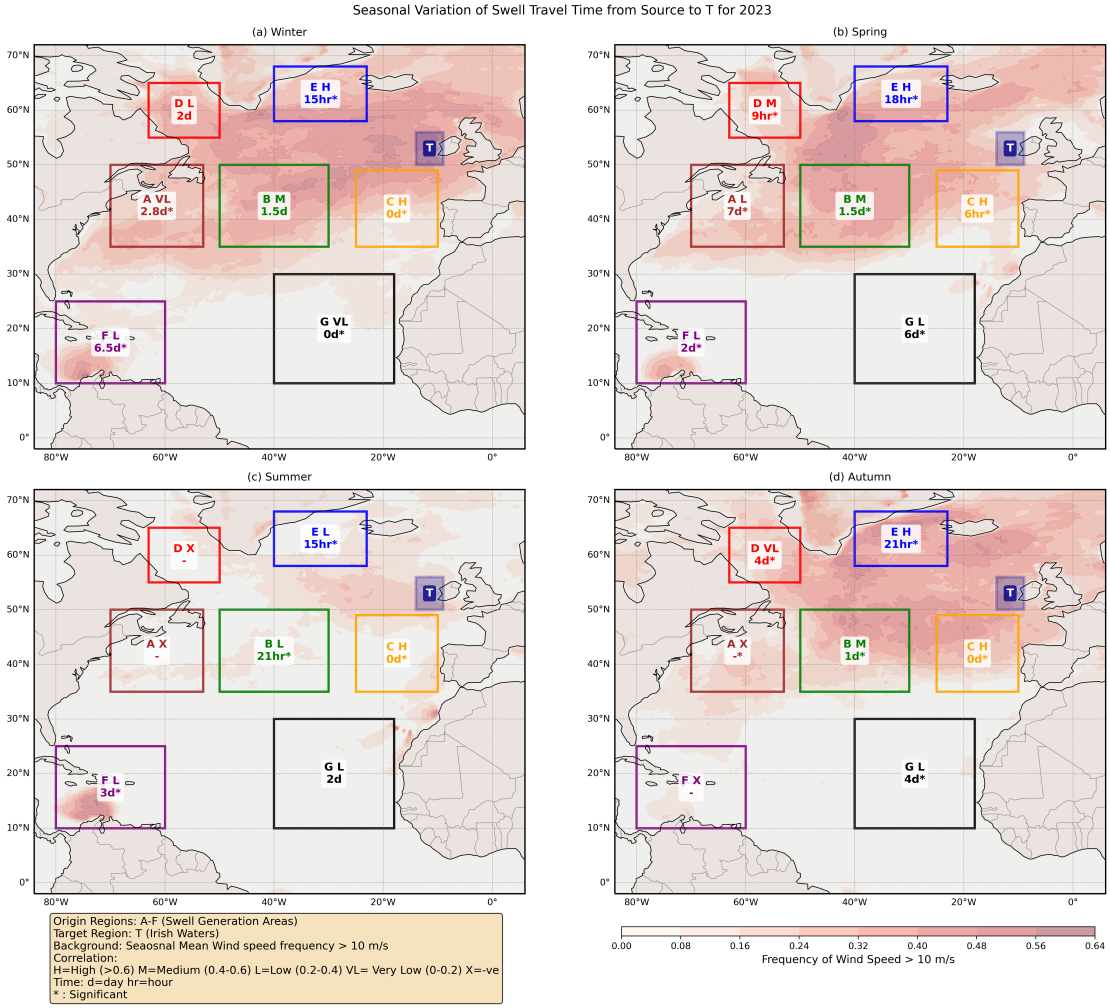

Figure 3.9: Seasonal spatial maps of swell travel times to target T from NA source regions (A-G) for 2023. Colored boxes show regional swell travel time (in days (d) or in hours (hr)) at maximum lagged correlation. The correlation strength is indicates as H (High), M (Moderate), L (Low) or VL (very Low). Background shading represents frequency of wind speed exceeding 10 m/s. Panels show (a) winter, (b) spring, (c) summer and (d) autumn. B,C, and E demonstrate consistent seasonal influence with short travel times, while remote regions show variable seasonal activity.

3.6.2.2 Case Study II: Interannual comparison between 2008 and 2023

This section presents spatial maps comparing winter and summer seasons of 2008 and 2023 to examine interannual variability in swell propagation from different North Atlantic source regions to T.
The two years were deliberately selected to represent contrasting large-scale atmospheric states. The year 2008 was characterised by a predominantly positive NAO phase, associated with a strengthened Azores High and deepened Icelandic Low, which drives an intensified and zonal jet stream tracking northeastward across the central North Atlantic. In contrast, 2023 was a highly negative NAO year, associated with a weaker pressure gradient that allows the jet stream to adopt a more meridional, southward-displaced path, reducing sustained storm activity across the central North Atlantic.

From the spatial plots in Figure 3.10, Regions C, E, and B emerge as consistent contributors across both years and seasons, reaffirming their importance in influencing the Irish coast. However, notable differences exist between the two years in the behaviour of individual regions. During Winter 2008, Region E shows high correlation with a lag-time of 18 hours, while Region B shows low correlation with a lag-time of 1 day. Regions A, D, F, and G all show negative correlations, indicating no meaningful swell propagation toward T during this season. Region C shows high correlation at zero lag, consistent with its behaviour across all analyses.
During Winter 2023, the pattern shifts considerably. Region D shows a low but statistically significant lag-time of 2 days, a signal entirely absent in Winter 2008. Region A shows a very low but detectable correlation with a lag-time of 2.8 days. Region F shows a low correlation with a lag-time of 6.5 days. Region B exhibits a medium correlation with a lag-time of 1.5 days, though this is not statistically significant. Region E maintains high and statistically significant lag-time of 15 hours. These contrasting patterns between the two winters suggest that the NAO phase plays an important role in determining which source regions actively contribute to swell at T, a point explored further in the Section 3.7.2.
During Summer 2008, Region E shows a moderate and a lag-time of 3 hours. Region B shows a very low correlation with a lag-time of 1.3 days. Region A shows a very low correlation with a lag-time of 3 days though this is not statistically significant. Region F shows a very low detectable correlation with a lag-time of 3 days. Regions D and G show negative correlations.

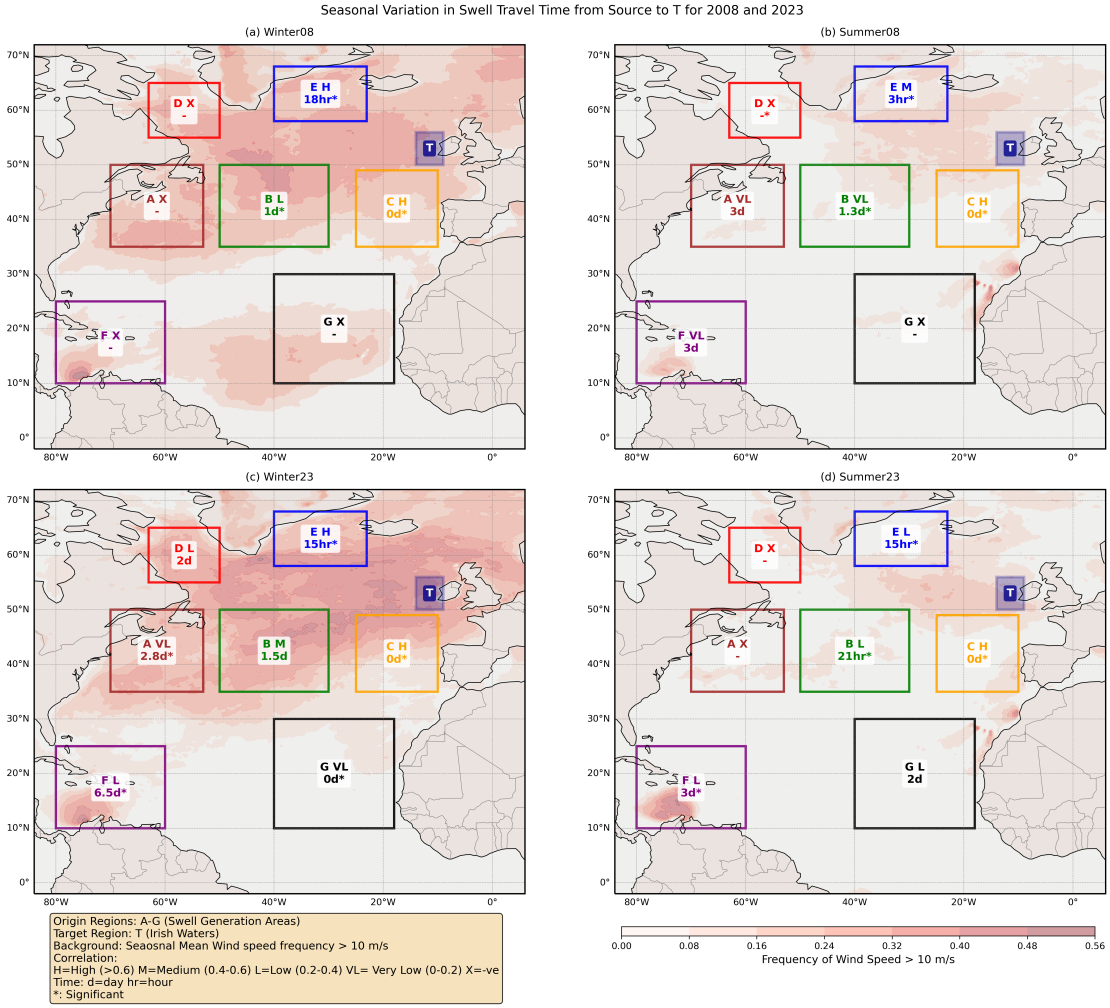

Figure 3.10: Winter and Summer spatial maps of swell travel times to target T from NA source regions (A-G) for 2008 and 2023. Colored boxes show regional swell travel time (in days: d or in hours: hr) at maximum lagged correlation. The correlation strength is indicates as H (High), M (Moderate), L (Low) or VL (very Low). Background shading represents frequency of wind speed exceeding 10 m/s. Panels show (a) Winter 2008, (b) Summer 2008, (c) Winter 2023 and (d) Summer 2023. B, C, and E demonstrate consistent seasonal influence with short travel times

During Summer 2023, Region C maintains high correlation at zero lag. Region B shows a low correlation with a lag-time of 21 hours. Region E shows a low correlation with a lag-time of 15 hours, a decrease in correlation strength compared to Summer 2008. Region F shows a low correlation with a lag-time of 3 days, consistent with Summer 2008. Region G shows a low correlation with a lag-time of 2 days though this is not statistically significant. Region D shows negative correlation.
Regarding statistical significance across the interannual comparison, travel times from C and E are statistically significant across both seasons examined and in both years. Region B showed statistically significant travel time during summer for both years but lacked significance in Winter 2023 under negative NAO conditions. Travel times from F became statistically significant in both seasons in 2023 after being insignificant in Winter 2008. Regions A and D showed statistically significant travel times only in Winter 2023, while D showed no significant travel times in any other analysis.

3.7 Discussion

The results presented in this chapter highlight the spatial and temporal variability in swell propagation from the NA source region to Irish waters (T). This section discusses the dominant patterns identified in the lagged correlation analysis and explores possible atmospheric drivers, such as wind intensity and large-scale circulation patterns (e.g., the NAO). While certain sources exhibit a relationship that align with meteorological conditions, other regions show high variability that may not be attributed to seasonal wind activity alone. The discussion also reflects the limitations of the current methodological approach in calculating precise swell travel times or detailed wave transformation processes. Nevertheless, it is well suited for the present study aiming to identify dominant swell region and assessing their influence on Irish waters.

3.7.1 Summary of key findings

The analyses presented in this chapter, the 20-year seasonal climatology, the 2023 seasonal case study, and the 2008 vs 2023 interannual comparison, collectively reveal a consistent picture of swell propagation from North Atlantic source regions to Irish waters.
Across all three analyses, Regions C, B, and E emerge as the dominant and most consistent swell sources for T. Region C shows the highest and most reliable correlation in all seasons and both years, owing to its close proximity to T. Region E shows consistently

high correlation during winter across all analyses, maintaining its influence regardless of year or NAO phase. Region B shows consistent contributions during winter and summer in the long-term climatology and in 2023, though its influence is more sensitive to interannual atmospheric variability.

Regions A, D, F, and G show weak and variable correlations in the long-term climatology, with limited statistical significance. However, the interannual comparison reveals that these regions are not entirely negligible. In Winter 2023, under highly negative NAO conditions, Regions A, D, and F all show statistically significant correlations with T, demonstrating that their influence is conditional on the prevailing atmospheric state rather than absent altogether.

The contrast between 2008 and 2023 is consistent with their differing NAO states. The positive NAO year (2008) was associated with concentrated swell activity from mid-latitude regions B and E, while the negative NAO year (2023) activated lower-latitude and western boundary regions such as D, A, and F through the southward displacement of the storm track. The 20-year mixed NAO record captures the aggregate of both regimes, explaining why the long-term climatology shows dominant contributions from C, B, and E while peripheral regions appear weak or insignificant on average.

3.7.2 Physical Drivers Behind Observed Patterns

The observed patterns of lagged correlation and swell travel time can be understood in terms of the underlying physical processes governing swell generation and propagation across the North Atlantic.

Region C's consistently high correlation with T at zero lag can be attributed to its close geographic proximity to T, which enables near-immediate swell propagation with travel times shorter than the 3-hour temporal resolution of the dataset. Despite this proximity, both regions experience different local wind patterns, making simultaneous independent generation unlikely. The zero lag therefore reflects fast propagation rather than simultaneous generation, and this interpretation is consistent across all seasons and both years examined.

Region E shows reliable and NAO-independent swell contributions during winter. This is consistent with its location within the subpolar low-pressure zone, which is dominated by the Icelandic Low, a persistent feature of the North Atlantic atmospheric circulation that remains active regardless of NAO phase. Whether the jet stream is zonal or meridional, Region E remains under the influence of this storm-generating zone and continues to generate swell toward T. Supporting this interpretation, Semedo (2005) showed that

the pressure gradient associated with the Icelandic Low is particularly favourable for generating long-period swells. During summer, E's correlation weakens considerably, reflecting the seasonal reduction in storm activity across all mid-latitude regions rather than any NAO-related change.

Region B shows a more NAO-sensitive response. During positive NAO conditions (Winter 2008), the intensified westerly storm track passes directly over Region B, generating significant swell that propagates toward T with a statistically significant lag-time of 1 day. During negative NAO conditions (Winter 2023), the southward displacement of the jet stream reduces sustained storm activity over Region B, resulting in a medium but statistically insignificant correlation. This NAO sensitivity is consistent with studies showing a strong positive relationship between NAO phase and wind speed and storm frequency over the central North Atlantic (Iversen and Burningham, 2015; Phillips et al., 2013).

The contrasting behaviour of Regions A and D between the two years reflects NAO-driven shifts in jet stream position. During positive NAO conditions (Winter 2008), the strong zonal jet stream tracks northeastward at high latitudes, directing storm activity away from the latitudes occupied by Regions A and D. As a result, both regions show negative correlations with T in Winter 2008. During negative NAO conditions (Winter 2023), the weakened and more meridional jet stream shifts southward, bringing the storm track closer to the latitude of Region D. This directly activates Region D as a swell source, which shows a low but statistically significant correlation with a lag-time of 2 days in Winter 2023, a signal entirely absent in Winter 2008. This demonstrates that NAO-driven shifts in jet stream position can activate or suppress individual source regions as swell contributors to Irish waters.

Region D's low correlation in winter can also be partly attributed to persistent sea ice cover during the period (Rasmussen et al., 2016), which can significantly inhibit swell generation (Han and Li, 2018). The results from seasonal analysis further supports this interpretation, with the region consistently showing minimal or no swell influence on the target.

The seasonal weakening of B and E during summer reflects the annual cycle of North Atlantic storm activity rather than NAO variability. Both regions lie within the mid-to-high latitude zone of cyclogenesis, which is highly active during winter but experiences substantially reduced storm frequency and intensity during summer. This seasonal control dominates over NAO variability and explains why B and E show consistently weak correlations during summer across all years in the record. Regions F and G show weak

and variable correlations throughout the analyses. Their limited influence can be attributed to two factors: first, their large distance from T means that swell undergoes significant dissipation during propagation, reducing the detectable signal at the target; second, swell generation in the tropical North Atlantic is tied to hurricane and tropical storm activity, which is highly variable interannually and concentrated in the summer and autumn months (Klotzbach, 2011). The occasional statistically significant signal from F, particularly in Winter 2023, suggests that under specific atmospheric conditions the tropical North Atlantic can make a marginal but detectable contribution to Irish swell conditions.

3.7.3 Methodological Strengths and Limitations

The study introduces a statistically robust approach for identifying and characterising the influence of remote swell sources on Irish waters. The application of NCC enables consistent detection of temporal relationships between source and target regions, independent of amplitude differences. By applying this method to long-term (20-year) data and integrating block bootstrap method for uncertainty quantification, the analysis offers a robust framework for detecting swell propagation patterns on climatological scale. Another key strength lies in the choice of swell period as the primary variable. While many previous studies relied on significant wave height (H_s) or swell height to study swell propagation (Sabique et al., 2012; Bhowmick et al., 2011; Semedo et al., 2011; Alves, 2006), others have used swell power and energy flux to characterise the global swell distribution (Sreelakshmi and Bhaskaran, 2022; Arinaga and Cheung, 2012). Significant wave height inherently includes contributions from both local wind-sea and remotely generated swell (Colosi et al., 2021) and can be misleading, swell period is more stable during long distance propagation (Donn, 1949) than swell wave height. Thus, swell period, less susceptible to local wind-sea interference and more stable, makes it better suited for tracking swell origin and arrival times over basin scales.

Although the approach has several strengths, it also carries limitations. While swell period is fundamentally related to wave energy transport (Ponce de León et al., 2023), using period alone as a variable does not capture complete wave energy information. This means it cannot be directly applied to energy or hazard assessments. The lag times derived from correlation peaks should not be interpreted as exact physical travel times, instead they are a statistical estimation of the delay in the propagation of swell signals. The analysis does not consider wave spectra, which could refine the identification of source contribution in more complex sea states (Portilla et al., 2009).

The lag-times derived from the NCC analysis are statistical estimates of the delay in the propagation of swell signals rather than the physical travel time of individual swell events. Since the NCC is computed over the full time series, some lag-times, particularly from distant regions such as F, may appear shorter than physically expected. The method also cannot distinguish between regions where swell is generated and regions that swell simply passes through on its way to T, and for this reason the results are described as identifying regions of significant swell influence rather than definitive swell origin regions. Additionally, crossing swell conditions, where ERA5 switches between competing swell partitions, can temporarily misalign the two time series and reduce the cross-correlation coefficient, while swell dissipation over long propagation distances limits the detectability of signals from the most remote regions, meaning the influence of regions F and G may be underrepresented in the results.

Swell generation areas can shift over time due to changes in climate or storm activity (Fan et al., 2014). The fixed source regions in this study favour a consistent analysis, but may not capture all changes. Also, averaging data across each region to create a single time series may miss swell events occurring near the boundaries of each region. This may not capture smaller or short lived swell signals, but works well for understanding general patterns as shown by Zheng et al. (2018).

However, these limitations do not undermine the primary objective of the study. The goal is not to resolve precise travel times or quantify energy flux, but to identify which source regions consistently influence Irish swell conditions over seasonal and interannual timescales. In this context the use of total swell period, fixed regional boxes and statistical lags are appropriate and effective. The method provides an estimate of influence based on signal similarity, which is sufficient to determine dominant and persistent swell contributors.

3.7.4 Implications and Future Directions

The findings from this chapter directly informed the design of the wave model configuration developed in Chapter 4. The identification of Regions B, C, and E as the most consistent and dominant swell sources established that the outer model domain must extend sufficiently far into the west and northwest North Atlantic to capture the full propagation pathway of swell from these regions before it enters the regional model boundary. The lag-time results, showing that swells from these regions arrive at Irish waters within hours to approximately 1.5 days, confirm that even relatively short simulation periods must account for remotely generated swell already present within the

domain at the start of the simulation, highlighting the importance of an adequate model spin-up period. The strong seasonal variability identified in this chapter, with winter emerging as the period of peak swell activity, highlighted the importance of running a sufficiently long simulation to capture the full range of seasonal and interannual variability in swell conditions. This seasonal dependence was also considered during the generation of surrogate wind forcing data, where preserving the seasonal structure of the wind fields was identified as essential to ensure that the modelled swell climate reflects the observed seasonal swell propagation patterns. The NAO-driven interannual variability further revealed that under negative NAO conditions Region D became an active swell source, indicating that the model domain must be broad enough to represent swell contributions from higher latitude western North Atlantic regions that are only occasionally active. Finally, the statistically significant seasonal contributions from Regions F and G demonstrate that swell generated in the tropical North Atlantic can reach Irish waters under certain atmospheric conditions, suggesting that the southern boundary of the model domain should extend far enough into the tropical Atlantic to capture these occasional but physically meaningful swell pathways. Collectively, these lessons shaped both the spatial extent of the model domain and the choice of simulation periods adopted in Chapter 4.

The study and findings have several practical implications. The approach is particularly well suited for tracking swell systems across ocean basins and informing early warning frameworks that can predict the timing of swell arrivals along the coastline. It also holds potential value for coastal engineering design and wave energy site planning (Babanin and Jiang, 2017), and long-term assessments of climate impacts on ocean wave conditions (Cavaleri et al., 2012; Semedo et al., 2011; Ardhuin et al., 2009). Stakeholders involved in infrastructure development or coastal adaptation strategies can benefit from identifying remote regions that consistently influence wave conditions along the Irish coast, especially under changing climate conditions. Furthermore, identifying remote regions that consistently generate swells reaching Ireland can support more accurate wave forecasting. By monitoring these key swell source areas, early warnings and operational forecasts for the Irish coast can be improved. This becomes particularly important for predicting swell-induced hazards-such as wave run up, coastal flooding, and erosion (Palmer et al., 2014; Lefèvre, 2009). These hazards may pose significant threats to densely populated coastal zones, especially under rising sea levels (Harley et al., 2017; Wang et al., 2016). Inaccurate swell predictions can also impact offshore activities, including port operations and the functioning of marine energy infrastructure (Babanin and Jiang, 2017).

Therefore, understanding swell propagation patterns are essential not only for improving forecast reliability but also for guiding coastal planning and strengthening resilience to climate-related risks.
However, further development is needed before this method can be fully applied in these operational and planning contexts. Future work could improve the current framework by incorporating directional swell spectra, energy based wave parameters, and incorporating numerical wave models to validate the estimated travel times. Expanding the analysis to multiple coastal sites and testing its robustness under different climate scenarios would help to generalise the findings and strengthen their relevance for regional wave climate projections and adaptation planning.

3.8 Conclusion

In conclusion, this study provides a comprehensive and statistically grounded understanding of swell propagation patterns to the Irish coast. The analysis offers valuable insights into spatial patterns, long-term consistency, and the role of large-scale atmospheric variability in shaping swell behavior. The findings identify key source regions and demonstrate notable seasonal and interannual variability in how distant NA areas influence wave conditions in Irish waters. Overall, the study provides a meaningful advancement in our understanding of remote swell contributions to the Irish coastal wave climate.

CHAPTER 4

Wave simulations from North Atlantic to Irish Waters under Changing Climate Conditions

The previous chapter examined swell propagation in the NA and identified the swells from the NA region influence the Irish wave climate. This chapter focuses on simulating present and future wave conditions in the NEA using a nested WAM-SWAN modelling framework. The simulations are driven by climate drivers such wind, sea ice and sea level. A key contribution of this chapter is the development of an innovative analogue-based approach for generating high-resolution surrogates for the MPI-ESM climate model winds and its application to wave modelling. The model results are then analysed to understand the seasonal variations across the NEA and location-specific assessments along the west of Ireland. Unlike previous studies that focus primarily on time series or extreme events, the results presented here examine the full distribution of wave heights, providing a more comprehensive view of the projected wave changes. The simulated wave data produced in this chapter also serve as input for the run-up analysis presented in the following chapter.

4.1 Introduction

The general concept of wave generation, propagation, and the transition from the deep ocean to the coastal environment involves downscaling the wave processes from the oceanic scale to the regional and coastal scales. The state-of-the-art wave models such as WAM, WW3, and SWAN are implemented on nested grids to achieve fine-resolution wave simulations. For instance, Brown et al. (2010) and Pilar et al. (2008) effectively demonstrated that the NA domain, when used with a nested WAM model, is sufficient to capture swells influencing wave conditions in the NEA. In contrast, Calvino et al. (2022) employed a nested WW3 model with a larger outer domain covering the entire Atlantic to investigate the large-scale processes, such as the NA current, on wave propagation.

Nesting SWAN within large-scale models such as WAM and WW3 is a common practice. Swain et al. (2019) demonstrated that SWAN hindcasts using WAM boundary conditions showed a 5–15% error in significant wave height (H_s) compared to deep-water models, yet achieved lower RMSE and higher correlation in nearshore wave predictions at buoy locations in the North Indian Ocean, compared to SWAN hindcasts using WW3 boundary conditions. Additionally, the nested WAM-SWAN approach by Lalbeharry and Ritchie (2009) demonstrated that coarse-grid (0.5°) WAM outputs can provide effective boundary conditions for SWAN, enabling accurate simulation of wave transformation from deep to shallow waters. These studies collectively support the nesting approach employed in the present study, which uses WAM and SWAN to capture the full wave spectrum, from the swell generation in the open ocean to the wave transformation in shallow coastal waters.

Accurate wave predictions rely heavily on high-resolution wind forcing, as wind serves as the primary mechanism for wave generation (Barbariol et al., 2022; Baordo et al., 2020). The generation of such high-resolution wind data at regional scales typically involves downscaling techniques. Dynamical downscaling employs atmospheric models to enhance the spatial and temporal resolution of wind fields, providing more robust solutions for wave modelling. For instance, Markina et al. (2018), utilised the WRF model to downscale wind fields in the NA, achieving a 14 km resolution to improve wave prediction accuracy in this region. Similarly, HARMONIE mesoscale model was used to dynamically downscale ERA-Interim reanalysis data to 2.5 km resolution for wave hindcasts in Ireland (Gallagher et al., 2016c). In Galway Bay (west coast of Ireland), regional weather model, WRF, provided atmospheric forcing for SWAN, further demonstrating the effectiveness of localised wind inputs for wave simulations (Ana Rute Bento and Soares, 2018). While these dynamical approaches significantly enhance the accu-

racy of wave predictions, their computational demands and resource intensity are still a challenge. On the other hand, statistical downscaling methods have been widely utilised to refine coarse global climate model (GCM) outputs for wave studies. For instance, Weibull-based downscaling techniques (Alizadeh et al., 2020) and multi step statistical algorithms (Towe et al., 2017) have been applied to improve wind fields for wave climate analysis in the Persian Gulf and the North Sea. However, statistical downscaling often assumes stationary relationships between large-scale predictors and local-scale predictands, which may limit its applicability under changing climate conditions (Alizadeh et al., 2020).

This chapter aims to overcome the limitations associated with low-resolution climate model data and the challenges in downscaling wind data for wave modelling. For this I am implementing an analogue approach to generate surrogate wind data for the MPI-ESM climate model, utilising high-resolution ERA5 reanalysis data. The surrogate wind data is used to drive WAM and SWAN wave models in the NEA, with a particular emphasis on Ireland, to explore the wave dynamics for present day and future climate. This approach aims to provide a computationally efficient and accurate framework for studying wave climate variability in dynamic and high-energy coastal regions.

4.2 Study region

The wind-wave dynamics of the NEA are driven predominantly by westerly and south-westerly winds blowing over the NA ocean (Gleeson et al., 2019; Gallagher et al., 2014; Bertin et al., 2013). Figure 4.1(a) illustrates the mean ERA5 wind speed and direction for 2018 for the NA domain, highlighting that most of the wind in the NEA (shown in the red box), particularly around Ireland, is predominantly westerlies. The NA swells, influenced by wind patterns and mid-latitude cyclones, significantly affect the wave climate around Ireland (Loureiro and Cooper, 2019; Gallagher et al., 2016a). These swells propagate eastward and play a critical role in shaping nearshore wave characteristics of Ireland, including significant wave heights and the occurrence of extreme wave events (Gallagher et al., 2016b). Analysis of nearshore waves during major storm events in 2015–2017 highlights how these swells contribute to high-energy waves in the NEA, particularly along Ireland's Atlantic coast (Fedele et al., 2019). These waves are further influenced by the complex geomorphology of the Irish coast (O'Brien et al., 2013) and climate phenomena such as the NAO. During the positive NAO phase, stronger westerly winds intensify wave heights and increase the frequency of storm events making the re-

gion highly energetic and dynamic (Gleeson et al., 2019; Dodet et al., 2010).
Projections using global climate models such as EC-Earth, indicate a potential decrease in wind speeds over the NA by up to 3.5% by the end of the century, which may reduce swell generation and significant wave heights near Ireland (up to 15% in some seasons; Gallagher et al., 2016a). Similarly, WW3 model predicts a decline in both mean and extreme wave heights, with the most pronounced reductions occurring in winter and summer around Ireland (Gallagher et al., 2016b). Other regionally downscaled wave climate studies by Lemos et al. (2021); Wolf et al. (2020); Aarnes et al. (2017), confirmed a trend towards decreasing seasonal averages of H_s around Ireland. The magnitude of change depends on the emissions scenario with the strongest occurring under RCP8.5. Gallagher et al. (2016a) study revealed largest reductions in H_s are projected in winter and summer.
Most studies project decreases in mean H_s around Ireland, while future changes in extreme waves are less certain. Some projections suggest increases in extreme wave heights (Bernardino et al., 2021; Lobeto et al., 2021; Wolf et al., 2020; Bricheno and Wolf, 2018), while others indicate little change or even decreases (Aarnes et al., 2017; Gallagher et al., 2016a,b).
The western Irish coast, directly exposed to NA weather systems, experiences a wave climate dominated by long-period swells superimposed with locally generated wind waves (Gaughan and Fitzgerald, 2020). This combination, along with the influence of climate drivers and the extensive fetch of the Atlantic, underscores the importance of understanding wave dynamics in the region and its implications for natural and socio-economic systems, particularly in the context of future climate change.

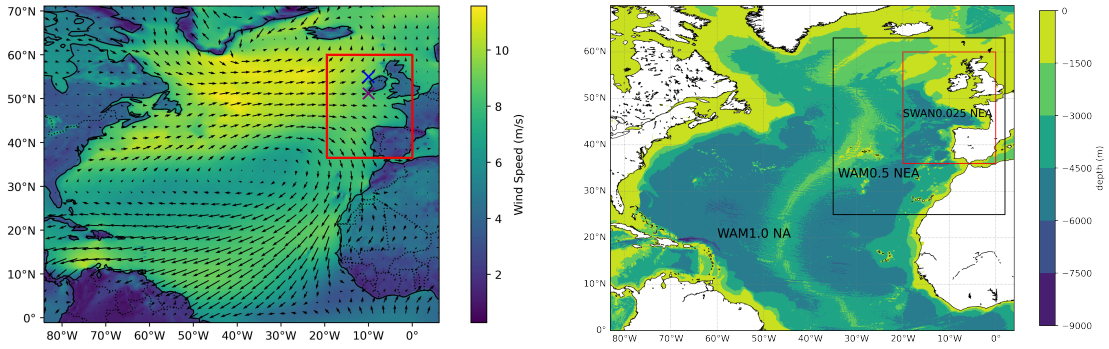

(a) (b)

Figure 4.1: a. Study region in the North Atlantic, illustrating the mean wind speed (color shading) and direction (black arrows) for 2018 based on ERA5 data. The red box highlights the main area of interest of this study. The blue cross denotes the location of the M4 buoy, while the purple cross represents the M3 buoy. b. Spatial map of the model domains used in the study. The entire domain represents the WAM1.0NA (North Atlantic) domain, with the black box representing WAM0.5NEA (Northeast Atlantic) domain and the red box representing SWAN0.025 domain. The color shading shows GEBCO bathymetry for the entire region, highlighting variations in seafloor depth.

4.3 Wave Model and Data

4.3.1 WAM Model

WAM (Günther et al., 1992) is a third generation model that describes the evolution of the wave spectrum by solving the wave energy equation. WAM, which is used here with its latest version Cycle 6, is an open-source code developed by the WAMD Group and maintained by the German Institute HZG (Helmholtz-Zentrum Geesthacht; Baordo et al., 2020).

A domain covering the entire NA was chosen to capture the swell waves generated in mid-latitudes. The WAM model, with a spatial resolution of 1.0°× 1.0° (WAM1.0NA) on a regular latitude-longitude grid, simulates large-scale wave generation and propagation across the Atlantic basin (refer Figure 4.1.b). This model serves as the outer boundary for subsequent nested models, enabling the transition of oceanic waves into more detailed regional and coastal simulations. Daily sea ice concentration was incorporated into WAM1.0NA simulations. As highlighted by Tuomi et al. (2019), the choice of sea ice data source significantly influences the results, irrespective of the method employed. For the current model setup, grid points with an ice concentration exceeding 30% were excluded from model computations. To provide higher resolution boundary conditions

for coastal modelling, one way nesting technique is applied in the WAM model. A finer resolution WAM model with a spatial resolution of 0.5° (WAM0.5NEA) was set up for the NEA, refining the wave field for regional analysis (black box in Figure 4.1(b) represents the WAM0.5NEA domain). This domain covers the waters surrounding Ireland and accounts for the wave transformations that occur as waves propagate from the deeper NA towards the continental shelf. Wave boundary conditions for this domain are supplied by the coarser WAM1.0NA model. However, sea ice was excluded from the WAM0.5NEA simulations, as it was observed only in the Northwest Atlantic, outside the primary domain of interest.

Both WAM models were implemented with 12 directional bins and 25 frequency bands, with the energy balance equation integrated using a propagation time step of 10 minutes. The lowest frequency resolved is 0.0418 Hz and all other settings were kept to default values. The WAM model simulations were conducted using default ECMWF Cycle 45R1 physics for input and open ocean dissipation (IPHYS set to 0). Wave breaking (BREAK) and the Phillips source function (PHILL) were both set to 0 as the focus was on large-scale wave simulations where these processes are less critical. Depth scaling of the source function (ISNL) was set to 0 making it suitable for deep water conditions (Janssen and Bidlot, 2003).

4.3.2 SWAN Model

Another third-generation spectral wave model SWAN is used to simulate wave climate around Ireland. Although WAM and SWAN have the same scientific principle, SWAN has some additional formulations for shallow water simulations (Lemos et al., 2023; Rusu et al., 2008). SWAN Cycle III 41.45 version is used to set up the regional model for NEA. The current method uses one-way nesting, where WAM0.5NEA provides wave boundary conditions to the finer SWAN model. This ensures that large-scale wave processes are accurately represented while allowing the high-resolution SWAN model to simulate local wave conditions at reduced computational cost. The nesting approach dynamically downscales the wave field, ensuring that swells generated in the open ocean are transferred effectively to the regional and coastal models. The SWAN model, with a spatial resolution of 0.025°× 0.025° (SWAN0.025), provides detailed simulations of the wave climate around the Irish coast (red box in Figure 4.1(b) represents the SWAN domain). The geographical extent of WAM and SWAN domains along with grid information and inputs used are provided in Table 4.1. The model captures the wave transformation processes as waves move into shallow coastal waters, influenced by local bathymetry and

coastline features.

SWAN was configured with the same directional discretisation as WAM (12 bins), and sensitivity tests showed only minor differences when using higher spectral resolution (refer Figure A.5). The current SWAN set up consists of of 12 uniformly distributed directions and 25 frequencies, which are logarithmically spaced from 0.046 Hz to 1.0 Hz. The SWAN model simulations are run in a non-stationary mode with a 30 minute time step. SWAN is run in third-generation mode, incorporating the WESTH (non-linear saturation-based white capping combined with wind input; SWAN Team, 2023) formulation for wind-driven wave growth, the BSBT (Backward Space Backward Time) scheme for wave propagation, and both triad and quadruplet wave-wave interactions. The model incorporated white-capping as the primary open ocean wave energy dissipation mechanism, along with bottom friction in transitional waters. Depth-induced wave breaking is additionally activated to capture wave transformation processes in shallow coastal waters near the Irish coast. SWAN default formulations and coefficients are used for all other physical processes.

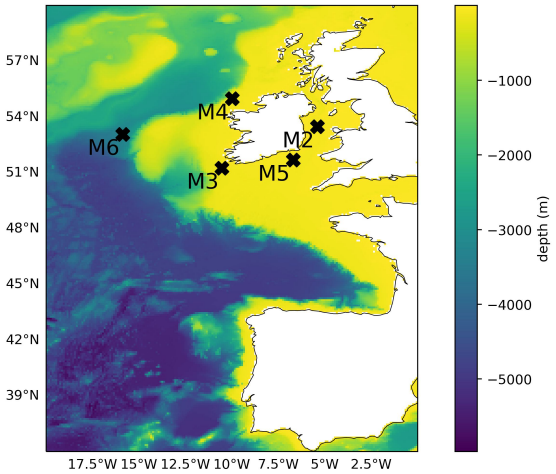

Figure 4.2: Domain covering SWAN0.025 grid, showing high-resolution bathymetry used for SWAN model set up. The bathymetry is derived from combination of INFOMAR and GEBCO datasets. The locations of Irish observational buoys used for validation are marked (cross) within the domain.

Table 4.1: Computational Grids, Spectral Configuration, Time Steps and Inputs used for Model Simulations

Grid	**Geographical Extent**				**Spatial Resolution**		**Spectral Resolution**	**Time Step**		**Inputs**			
	N	S	W	E	$\Delta x \times \Delta y$	$nx \times ny$	$\Delta\theta \times \Delta f$	Prop. (min)	Source (min)	Wave	Wind	Sea ice	Sea level
WAM1.0NA	69°	0°	-82°	4°	$1° \times 1°$	70×87	$30° \times 25$	10	10	–	×	×	–
WAM0.5NEA	63°	25°	-35°	2°	$0.5° \times 0.5°$	77×75	$30° \times 25$	10	10	×	×	–	–
SWAN0.025	60°	36.5°	-19.5°	0°	$0.025° \times 0.025°$	780×940	$30° \times 25$	30	30	×	×	–	×

Δx: spatial resolution in x direction; Δy: spatial resolution in y direction; nx: number of grid points in x direction; ny: number of grid points in y direction.
$\Delta\theta$: directional resolution (degrees); Δf: number of frequency bins; Prop.: wave propagation time step; Source: source term integration time step.
×: input applied; –: not applied.

4.3.3 Data

4.3.3.1 Bathymetry

Two datasets were used for model bathymetry development. GEBCO_2023 (General Bathymetric Chart of the Oceans_2023) grid is a global model of ocean and land that provides elevation data which is available on 15 arc-second interval grid (GEBCO Bathymetric Compilation Group, 2023). Both WAM models use GEBCO bathymetry interpolated to a 0.5° grid. INFOMAR (Integrated Mapping for the Sustainable Development of Ireland's Marine Resources) maps Irish coastal and offshore waters at resolutions ranging from 500 m to 2 m and is managed by the Geological Survey of Ireland (GSI) and the Marine Institute (Sheehan, Kevin and INFOMAR Survey Team, 2021). To obtain high-resolution bathymetry near the shore, SWAN uses INFOMAR and GEBCO bathymetry interpolated to a grid of 0.025° resolution.

4.3.3.2 Wind

The study utilises two distinct wind datasets: the low-resolution MPI-ESM wind data from the CMIP6 ensemble and the high-resolution ERA5 reanalysis data. To mitigate the limitations associated with the coarse resolution wind data for wave modelling, I employed ERA5 data as a high-resolution reference for generating surrogates for the MPI-ESM winds. This is explained in detail in Section 4.4.

ERA5 is the fifth generation of ECMWF atmospheric reanalysis of the global climate (ECMWF, 2019) which delivers atmospheric, land surface, and ocean wind wave data. Wind components are available at 0.25° (31km) grid spacing and at an hourly frequency (Hersbach et al., 2023; ECMWF, 2016). This work utilises 10 m u (u10) and v (v10) components of wind spanning from period 2004–2023.

MPI-ESM (Max-Planck Institute of Earth System Model) is a comprehensive climate model used for simulating Earth's climate system and developed by Max-Plank Institute of Meteorology, Hamburg, Germany (Garcia-Pereira et al., 2023). It couples different components of the Earth system including the atmosphere - ECHAM6 (Stevens et al., 2013), ocean dynamics and sea ice - MPIOM (Jungclaus et al., 2013), land surface processes - JSBACH (Reick et al., 2013) and marine biogeochemistry - HAMOCC (Ilyina et al., 2013).

The 10m u (uas) and v (vas) components of wind used in this study is obtained from the first realisation (r1i1p1f1) model simulation of the CMIP6 version of the Max Planck Institute Grand Ensemble (MPI-GE CMIP6) which is based on the MPI-ESM version

1.201p7 (Olonscheck et al., 2023). The model includes simulations under five emissions scenarios and the data used in the current study corresponds to SSP5-8.5. The low-resolution (LR) configuration, MPI–ESM LR, has a horizontal atmospheric resolution of 1.875° (200 km) and includes 47 vertical layers (Düsterhus and Brune, 2024).
For the present study, MPI-ESM LR wind from 2004 to 2023 (representing the present climate) and 2081 to 2100 (representing future climate projections) were used.

4.3.3.3 Sea ice

The sea ice model is integrated within the ocean general circulation model MPIOM. It provides daily sea ice concentration on a bipolar grid with a nominal resolution of 1.5° (Jungclaus et al., 2013). To make the sea ice data compatible with the wave models, the data were interpolated to a regular grid of resolution 0.5°. According to recent studies, Arctic sea ice is projected to experience a significant decline by 2100 (Ivanov and Repina, 2018), with the oldest ice potentially disappearing around mid-century (Chen et al., 2021). Chen et al. (2021), further indicates that sea ice thickness is anticipated to decrease at an average rate of 0.22 m per decade after September 2060, accompanied by a comprehensive decline in sea ice concentration and volume. Similarly, Dauner et al. (2024), highlights a long-term decline in sea ice extent in the Greenland and the NA sector based on historical data, model simulations, and proxy-based reconstructions, which consistently predict significant reductions in sea ice. Considering these projections, the presence of sea ice in the study region was neglected for the future simulations.

4.3.3.4 Sea level

Regional sea level data from the IPCC 6^{th} Assessment Report (AR6; Fox-Kemper, 2021)under SSP5-8.5 are used for the present study. Data are available from 2020 to 2150 along with how these projections differ depending on future scenarios (Kopp et al., 2023). To account for the effects of storm surges on sea level, the storm surge anomaly (tideSurgeAnom) from the UK Climate Projections 2018 (UKCP18), based on RCP8.5, was added to the regional sea level projection, creating a combined sea level dataset used as input to the SWAN wave model. UKCP18 offers updated observations and climate change projections extending to 2100 for the UK and globally (Lowe et al., 2018). Since the UKCP18 data is available on an irregular grid, they were interpolated to a 0.5° regular grid before being integrated with the sea level projections.

4.3.3.5 Wave buoy data

Wave height data from observational buoys (M2-M6) are used to validate the models. These buoys form part of the Irish Marine Data Buoy Observation Network (IMDBON), which is managed by the Marine Institute and Met Éireann, and funded by the Department of Agriculture, Food and the Marine (Marine Institute, 2022). IMDBON provides hourly weather measurements as well as wave height and wave period since 2001.
The locations of the wave buoys are shown in Figure 4.2 and the distance from shore along with latitude and longitude values are provided in Table 4.2. Buoy M6, situated off the west coast of Ireland in deep water, was used to validate significant wave height (H_s) outputs from the WAM0.5NEA model. The other buoys, M2 to M5, are located closer to the shore and were employed for validating the SWAN model. Among these, buoys M3 and M4, positioned along the west coast of Ireland, were of particular interest as this region is directly influenced by NA swells. For further details on the validation process, refer to Section 4.5.

4.4 Downscaling wind via surrogate data generation

Dynamical downscaling of winds, which uses regional weather models to drive wave simulations (Markina et al., 2018) or coupling them with wave models (Bento et al., 2016) is a common approach in wave modelling. Instead I am using an analogue method to downscale the climate model output. High-resolution ERA5 reanalysis data are used to generate surrogate winds for the low-resolution MPI-ESM winds. The surrogate winds follow daily evolution of MPI-ESM and preserve its large-scale spatio-temporal characteristics, while providing realistic high-resolution representation through selected ERA fields. This ensures temporal and spatial consistency between the coarse-resolution driving model and the high-resolution surrogate data.

4.4.1 Analogue method for surrogate data generation

The analogue approach used here involves finding analogues or similar instances in a reference dataset that match certain characteristics of the target dataset. This method relies on identifying the instances from the reference dataset that closely resemble the conditions observed in the target dataset. The corresponding values from the reference dataset are then used as surrogates for the target dataset.

In this study, the analogue approach is applied to generate surrogate wind data for both present and future MPI-ESM simulations using ERA5 as the reference. The goal is to construct surrogates that retain the large-scale structure and long-term trends of MPI-ESM wind while preserving the resolution (both in time and space) of ERA5.

To ensure a consistent comparison during analogue selection, it is necessary to bring both datasets to the same spatial and temporal resolution. Accordingly, the ERA5 data, available at 0.25° are first spatially regridded to match the coarser MPI-ESM grid (1.8°). Then, daily averages of the u10 and v10 wind components are computed from ERA5. This preprocessing ensures that both datasets are aligned in space and time, enabling a direct comparison of wind conditions over a defined spatial domain.

The choice of this spatial domain is a key aspect of the surrogate generation process, as it strongly influences the ability of the selected analogues to reproduce relevant physical conditions. In particular, the spatial domain determines which atmospheric features are prioritised when computing similarity between the target and candidate wind fields. A larger domain may emphasise large-scale wind patterns, while a smaller, regional domain focuses the comparison on localised wind conditions. A detailed discussion on the sensitivity to domain size is provided in the Section 4.5.3.

To identify analogues, the daily wind fields from MPI-ESM are compared with daily averaged wind fields from ERA5. For each target day in MPI-ESM (M_{ref}), a search window of ±14 days around the same calendar day is applied to each year in the ERA5 dataset spanning from 2004 to 2023. This rolling 29-day window across 20 years resulted in a candidate pool of 580 ERA5 days (E_n, n = 1, 2, ..., N; N is the total number of candidates) for each M_{ref}. The ±14-day window was chosen to preserve seasonal consistency, as wave climate along the Irish coast is strongly seasonal. Thus it is important that the analogues must reflect the atmospheric conditions relevant to the target season, including transitional days between seasons where wind patterns shift gradually. Extending the window beyond ±14 days would risk combining days from climatologically distinct seasons, introducing spurious variability into the surrogate time series.

The similarity between M_{ref} and E_n was quantified using the vector difference (VD) in wind components. Specifically, the Euclidean distance (Senter and Lupo, 2024) between the wind vectors was computed at each grid point using the formula:

$$VD_n = \sqrt{(M_{ref_u} - E_{n_u})^2 + (M_{ref_v} - E_{n_v})^2}, \quad n = 1, 2, \ldots, N \tag{4.1}$$

where N=580, depending on data availability (eg: leap year).

The VD field then quantifies the difference between MPI-ESM and ERA5 wind vectors

at each grid point. The VD field is then spatially averaged over the domain to obtain a single similarity score for each candidate day. The ERA5 day with the minimum spatially averaged VD is selected as the best analogue for the corresponding M_{ref}. The schematic diagram Figure 4.3 illustrates the process of analogue selection for MPI-ESM surrogate generation. An advantage of using the vector difference as the similarity metric is that it inherently captures both wind speed and wind direction differences, thereby simplifying the similarity assessment while still retaining the full vector characteristics of the wind field.

Once the best analogue day is identified for each MPI-ESM day, the corresponding high-resolution wind fields from ERA5 (u10 and v10) are extracted. These extracted wind fields are then connected in temporal order to construct a continuous high-resolution surrogate wind time series. As the analogue days are selected based on daily similarity to MPI-ESM wind fields, the resulting sequence of surrogate days reflects the trends and variability embedded in the original MPI-ESM simulations, while attaining the spatial and temporal resolution of ERA5.

As an example, consider January 18, 2080, from the MPI-ESM simulation. A ± 14 day search window is applied around this date, spanning from January 4 to February 1. All dates within this window are extracted from each of the 20 years in the regridded ERA5 record (2004 to 2023), resulting in a total of 580 candidate days. For each candidate day, the spatially distributed vector difference between the MPI-ESM and ERA5 wind components is computed, and the mean VD over the domain is calculated. Suppose January 22, 2007, is identified as the day with the minimum spatially averaged VD, this day is then selected as the best analogue for January 18, 2080.

If 3-hourly ERA5 wind data are used as the high-resolution reference, then the full 3-hourly wind fields from the selected analogue day (in this case, January 22, 2007) are used as the surrogate wind input for the MPI-ESM target day. This process is repeated for each day in the MPI-ESM time series, resulting in a surrogate dataset with the resolution of ERA5 and the large-scale variability of the MPI-ESM simulation.

Using the same ERA5 dataset for both present and future scenarios offers a consistent baseline, reducing the risk of introducing biases that could arise from using different datasets. While this method assumes that present day ERA5 variability is a reasonable proxy for the structure of future variability, it is a standard and robust approach in climate modelling, especially when high-resolution observational datasets for the future are unavailable. A similar approach was employed by Noël et al. (2021), who performed statistical downscaling of CMIP5 projections using ERA5 as a reference dataset. In their

study, they statistically downscaled historical data, validated it against ERA5, and used the identified biases to correct the projected downscaled data. This demonstrates the viability of using ERA5 as a reliable baseline for generating high-resolution data and correcting model biases, further supporting the assumption that present day ERA5 variability can serve as a reasonable proxy for future scenarios in surrogate data generation.

4.4.2 Surrogate wind quality assessment

To assess the quality of the surrogate wind fields generated through the analogue method, two complementary analyses were conducted. First, the distribution of minimum VD scores across all analogue selections was examined to quantify the overall match quality. Second, the surrogate wind fields were compared visually against the corresponding MPI-ESM and ERA5 wind fields for days representing different VD score ranges, to confirm that the large-scale atmospheric patterns relevant for wave generation are well reproduced.

The distribution of minimum VD scores across all analogue selections is shown in Appendix A.6. For the present period (2004–2023), the minimum VD scores range from approximately 2 m/s to 8 m/s, with a median of 3.54 m/s, indicating that the ERA5 archive consistently provides good analogues for MPI-ESM wind patterns. For the future period (2081–2100), the distribution is similar, with a slightly lower median of 3.44 m/s, suggesting comparable analogue quality. Only 10% of days in both periods yield VD scores above approximately 5 m/s, representing cases where the MPI-ESM circulation pattern is less well represented in the ERA5 candidate pool (an inherent limitation of any analogue-based downscaling approach).

To further assess the quality of the analogue selection across different VD score ranges, the MPI-ESM, ERA5 and surrogate wind fields were compared for three example days representing low, medium and high VD scores (Appendix A.7). Across all three cases, the surrogate wind fields successfully reproduce the dominant large-scale circulation patterns of MPI-ESM over the full NA domain, confirming that the analogue selection captures synoptically relevant conditions for both local wind-sea and remotely generated swell reaching the Irish coast, even for days with relatively high VD scores.

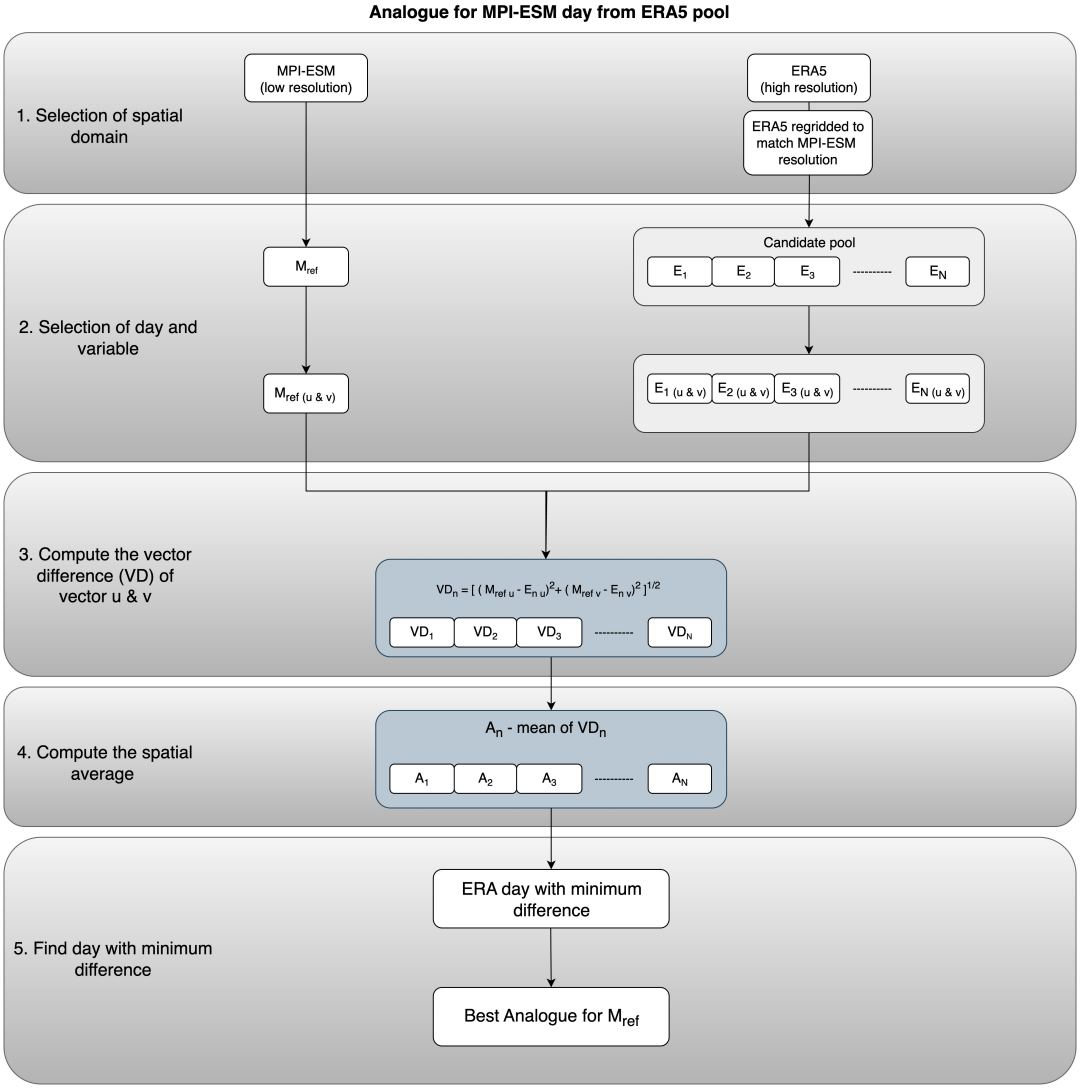

Figure 4.3: Schematic representation of analogue finding for the surrogate wind data generation. The method integrates coarser MPI-ESM and fine ERA5 data. The process begins with selecting the spatial domain, after which datasets are regridded and resampled to ensure consistent spatial and temporal resolution. For selected day in MPI-ESM (M_{ref}), the vector difference (VD_n) between ERA5 ($E_{n(u\&v)}$) and MPI-ESM ($M_{ref(u\&v)}$) wind components is computed over the selected domain. The spatially averaged vector difference (A_n) is then used to identify the ERA day with minimum difference, which is selected as the best analogue.

4.5 Model Validation and Sensitivity Analysis

In this section, the two experiments, validation and the temporal sensitivity analysis, are conducted using real wind data from ERA5 to assess the model's ability to represent current conditions. The validation involves computing the statistical metrics of model outputs driven by high-resolution ERA5 winds against observed data. Following this, a sensitivity analysis examines the impact of wind data resolution by comparing model performance using high to low-resolution wind inputs. Based on the conclusions drawn from this analysis, a second sensitivity experiment is carried out using surrogate winds generated by selecting a different domain for computing the VD between the climate model and reanalysis data.

4.5.1 Model Validation against Observational buoys

The study area chosen benefits from a dense network of in-situ buoy observations (refer Figure 4.2 for locations). The validation period from 21 September 2023 to 10 October 2023 was carefully chosen, to ensure the availability of continuous, error-free observational data, thereby eliminating potential uncertainties associated with data gaps or inaccuracies. For this simulation period, model outputs were saved at hourly intervals to allow for detailed temporal comparison with observations.

Statistical validation of modelled H_s against buoy observation was undertaken to understand the skill of the models WAM0.5NEA and SWAN0.025. The computed statistics of H_s (refer Table 4.2) are the mean of measurements (Bm) and model simulations (Sm), the bias, root mean square error (RMSE), scatter index (SI) and the Pearson Correlation Coefficient (r).

The locations on the west coast of Ireland (M6, M4 and M3), directly influenced by the NA swells, exhibit higher mean H_s than the locations on the east coast of Ireland (M2 and M5) during the validation period. In contrast, M2 and M5, which are sheltered from the direct influence of swells and dominated by wind-sea conditions, have different statistical characteristics than M6, M4, and M3. Negative bias across all locations suggests that the model tends to underpredict H_s relative to the observations, with higher bias in the west coast locations where the influence of swell is stronger. RMSE follows a similar pattern with higher values in the west coast. The lower bias and RMSE in the east coast reflects the dominance of local wind-driven waves. Conversely, the lower scatter index (SI) in the west coast indicates that the model predictions are more consistent for swell-dominated locations but show greater variability (high SI on the east coast) in

regions where wind-driven waves dominate.

Correlation coefficients (r) further support these findings, with the highest correlations observed on the east coast (M5: 0.922, M2: 0.899) and slightly lower values in the west (M3: 0.871, M4: 0.867, M6: 0.766). The strong correlation across all locations suggests that the model successfully captures temporal variations in wave height.

4.5.2 Sensitivity to temporal resolution of ERA5 wind forcing

Simulations, similar to the validation period, were conducted by driving WAM-SWAN setup using ERA5 wind data at different temporal resolutions – 1 hour, 3 hours, 6 hours, and 24 hours – to assess the influence of wind forcing on wave model performance. Most of the studies focus on the direct matching of wave time series or extreme events. The focus of the present study is on the full distribution of wave heights along the Irish coast, as it provides valuable insights for adaptation strategies.

The H_s distribution from SWAN0.025 simulations, driven by ERA5 winds, was compared to observations from the M4 buoy. The temporal sensitivity analysis was conducted at M4 as a representative western station, as the west coast of Ireland is the primary focus of this study due to its direct exposure to the NA swell. As shown in Table 4.2, M3 and M4 exhibit very similar statistical performance (bias: -0.229 and -0.223; RMSE: 0.627 and 0.528; r: 0.871 and 0.867 respectively), and M4 was therefore selected as representative of the west coast with results considered applicable to M3.

The results, as illustrated in Figure 4.4, indicated good alignment of the distribution curve of H_s from the model (blue lines) with observations (orange lines) for 1-hourly and 3-hourly wind data, while significant deviations were noted with 6-hourly and daily forcings. In addition, the models successfully reproduced the frequent waves with heights ranging between 2.5 and 4 m when driven by hourly and three-hourly wind forcing. However, this was not achieved with six-hourly and daily wind forcing.

To quantitatively assess the similarity between modelled and observed wave height distributions, the Earth Mover's Distance (EMD) was computed for model H_s from each wind forcing case with the buoy H_s. EMD is a metric used to compare two distributions (Luzia et al., 2022; Düsterhus and Hense, 2012). It measures the effort required to transform one distribution into another by considering the amount and distance of "mass" that must be shifted (Luzia et al., 2022). The results provided in Phase I of Table 4.3 revealed that 3-hourly forcing produced a lower EMD value (0.38), indicating the closest

Table 4.2: Statistical results of H_s at each locations

	Lat	Lon	Distance from Irish shore	Bm	H_s **from WAM0.5NEA**				
	(°)	(°)	(km)		Sm	Bias	RMSE	SI	r
M6	52.986	-15.866	389	3.912	3.514	-0.397	0.768	0.196	0.766
	Lat	Lon	Distance from shore	Bm	H_s **from SWAN0.025**				
	(°)	(°)	(km)		Sm	Bias	RMSE	SI	r
M3	51.217	-10.550	56	3.656	3.427	-0.229	0.627	0.171	0.871
M4	55.000	-10.000	83	3.742	3.519	-0.223	0.528	0.146	0.867
M2	53.480	-5.425	37	1.671	1.527	-0.143	0.419	0.250	0.899
M5	51.690	-6.704	56	2.717	2.552	-0.165	0.570	0.209	0.922

Bm: mean H_s from buoy, Sm: mean H_s from model simulations
RMSE: root mean square error, SI: scatter index
r: Pearson's Correlation Coefficient.

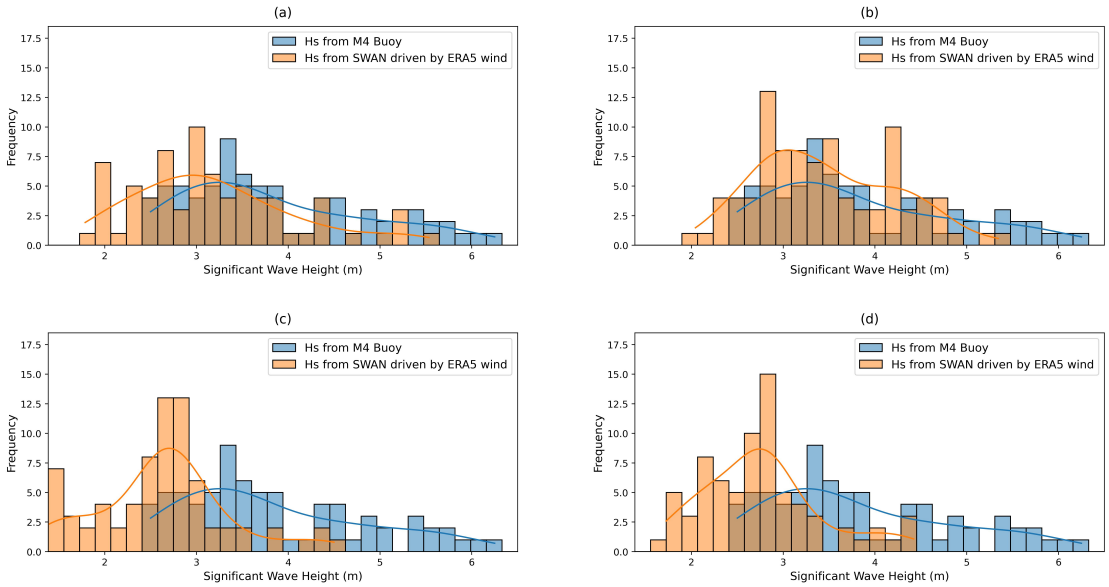

Figure 4.4: Comparison of H_s distribution from SWAN driven by ERA5 winds having temporal resolution of 1 hour (a), 3 hours (b), 6 hours (c) and 24 hours (d) with significant wave height from M4 buoy. The blue line represents the distribution curve of H_s from M4 buoy, while the orange line represent the distribution curve of H_s from SWAN0.025 model. The blue bars indicate the wave height distribution derived from M4 buoy while the orange bars indicate the wave height distribution derived from the model simulations.

match to the observed distribution. Although model results from the 1-hour wind forcing appeared visually similar to the observations, they have a higher EMD than 3-hourly wind forcing because the metric captures even small shifts across the full distribution. The 6-hourly and 24-hourly wind forcing produced higher EMD values (1.44 and 1.08), reflecting their inability to reproduce the observed H_s distribution accurately. Considering these findings, along with computational and storage requirements, 3-hourly ERA5 data were selected for generating surrogate winds for MPI–ESM simulations.

4.5.3 Sensitivity to spatial domain selection for surrogate winds

To investigate the influence of spatial domain selection (represented as the first step in the schematic diagram Figure 4.3) on surrogate wind quality and wave model performance, surrogate datasets were generated using three different domains: the full NA, the NEA region consistent with the WAM0.5NEA domain and the region around Ireland

matching the SWAN0.025 model. In all cases, high-resolution surrogate wind fields were generated by rearranging 3-hourly ERA5 wind data from the entire NA, based on time indices identified through analogue matching. The resulting surrogate wind forcing was then used to drive the nested model system to simulate wave conditions for the year 2023. The modelled daily H_s from each experiment was compared against observations from the M3 and M4 buoys. Model performance was also evaluated by calculating the EMD between the modelled and observed H_s distribution at both locations.

The wave height distribution curves shown in Figure 4.5 from the three surrogate wind experiments show good overall agreement with observations at both M3 and M4 over the one-year simulation period (2023). Examining the peak of the distribution, which represents the most common wave states, all three surrogate configurations reproduce the most frequently occurring wave heights reasonably well. However, differences emerge in the high wave height tail of the distribution, representing extreme wave conditions, where the choice of surrogate domain has a more pronounced effect.

The surrogate winds generated using the VD-Ireland domain produced the closest overall match to observations, supported by the lowest EMD values at both buoy locations (0.09 at M3 and 0.10 at M4). However, it is noted that the use of the VD-Ireland domain for analogue selection leads to a slight overprediction of wave heights at M3, particularly in the high wave height tail of the distribution. This is attributed to the optimisation of analogue selection over the smaller coastal domain, which may amplify local wind conditions at this exposed western station. Despite this, the overall performance of the VD-Ireland surrogate forcing remains superior to the NA and the NEA domain configurations, highlighting that selecting analogues based on local wind conditions significantly improves model performance in the nearshore region around Ireland.

The experiments described above determine the final model set up in this study. Using ERA5 winds, the validation against buoy observations demonstrates that the nested WAM-SWAN framework can reproduce observed wave conditions in Irish waters with reasonable accuracy. The sensitivity analyses further indicate that 3-hourly wind forcing provides the best representation of the full distribution of significant wave heights, and that selecting analogues based on the Ireland domain produces surrogate wind fields that generate realistic wave conditions. Based on these findings, 3-hourly wind data and the Ireland domain were selected for generating surrogate winds. These surrogate winds, derived from climate model data, are used to simulate wave conditions to examine the present and future wave climate around Ireland. While biases exist in climate model

Table 4.3: Summary of data inputs for wave simulations, resolution of input data, and agreement of model H_s with observations

	Input data	Temporal resolution (hr)	Spatial resolution (°)	Buoy used for comparison	EMD (buoy vs model H_s)
Phase I	ERA5	1	0.25	M4	0.656
	ERA5	3	0.25	M4	0.386
	ERA5	6	0.25	M4	1.449
	ERA5	24	0.25	M4	1.083
Phase II	VD-NA	3	0.25	M3	0.156
	VD-NEA	3	0.25	M3	0.146
	VD-Ireland	3	0.25	M3	0.091
	VD-NA	3	0.25	M4	0.173
	VD-NEA	3	0.25	M4	0.129
	VD-Ireland	3	0.25	M4	0.103

Notes: In Phase I, 3-hourly ERA5 (highlighted in grey) wind was chosen for surrogate wind data generation in Phase II.
In Phase II, the model was driven using surrogate winds generated using different domains selected for computing vector difference, and model performance was compared. VD-Ireland (grey rows) was selected for our study.
VD-NA: Surrogate data generated by computing vector difference between MPI-ESM and ERA5 winds over the North Atlantic.
VD-NEA: Surrogate data generated by computing vector difference over the Northeast Atlantic.
VD-Ireland: Surrogate data generated by computing vector difference over a domain around Ireland.

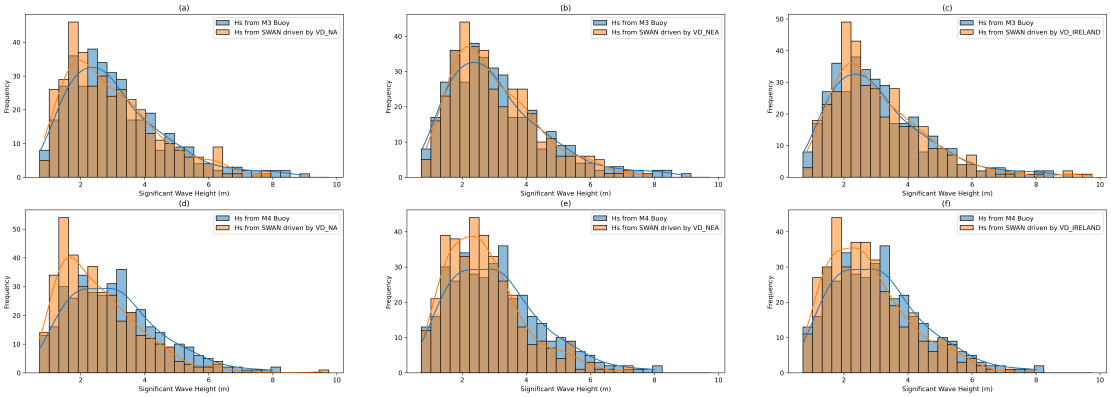

Figure 4.5: Comparison of significant wave height distribution from SWAN driven by surrogate winds generated through selecting different domain with significant wave height from M4 and M4 buoy. The blue line represents the distribution curve of H_s from buoy and the orange line represent the distribution curve of H_s from SWAN0.025 model driven by VD-NA winds (a and d), VD-NEA winds (b and e), and VD-Ireland winds (c and f). The top three plots represent comparison of model H_s with M3 buoy and bottom three for that with M4 buoy. The bars indicate the histogram of wave heights from buoy (blue) and model (orange).

winds, the focus of this study is the relative differences between present and future simulations, rather than the absolute magnitude of wave heights.

4.6 Model Simulations and Computational Resources

All wave model simulations were carried out on the Levante high-performance computing system at the German Climate Computing Centre (DKRZ) under project ID uo1075. The WAM simulations were executed in parallel using MPI across 5 nodes with 3 tasks per node. For a 2-year simulation, WAM1.0NA required approximately 23 minutes and WAM0.5NEA approximately 24 minutes of wall-clock time, corresponding to roughly 42–44 seconds of compute time per simulated day. The SWAN model was run in parallel using OpenMP on a single shared node with 20 CPUs, requiring approximately 4.9 minutes of compute time per simulated day, with a peak memory usage of approximately 2.1 GB. Each 20-year SWAN simulation required approximately 25 days of wall-clock time.

Two sets of 20-year simulations were conducted using the nested WAM-SWAN framework, as summarised in Table 4.4:

1. **Present climate (2004–2023):** driven by surrogate winds from present-day MPI-ESM under SSP5-8.5, with observed sea ice included in WAM1.0NA and present-day sea level incorporated into SWAN.

2. **Future climate (2081–2100):** driven by future MPI-ESM surrogate winds under SSP5-8.5, with sea ice set to zero and projected sea level rise incorporated into SWAN simulations.

Table 4.4: Overview of wave model simulations conducted using the nested WAM–SWAN framework.

Simulation	Period	Wind Forcing	Sea Ice	Sea Level
Present climate	2004–2023	MPI-ESM present (SSP5-8.5)	MPI-ESM present	Present-day
Future climate	2081–2100	MPI-ESM future (SSP5-8.5)	Set to zero	Projected SLR (SSP5-8.5)

Table 4.5: Computational resources used for wave model simulations on the Levante supercomputer at DKRZ (Project ID: uo1075).

Model	Run Mode	Nodes	CPUs	Peak Memory	Per Simulated Day
WAM1.0NA	MPI parallel	5	15	∼147 MB	∼42 sec
WAM0.5NEA	MPI parallel	5	15	∼155 MB	∼44 sec
SWAN0.025	OpenMP parallel	1	20	∼2.1 GB	∼4.9 min

4.7 Wave projections in the Northeast Atlantic

The present (2004–2023) and future (2081–2100) wave climate simulations were conducted as described in Section 4.6, using surrogate winds generated under the SSP5-8.5 high-emissions scenario. Spatial and seasonal changes in significant wave height between the two periods are analysed in the following sections.

4.7.1 Spatial variation of wave height for Northeast Atlantic

The analysis of H_s differences between future and present conditions, based on a 20-year mean and seasonal averages, reveals notable spatial variations across the NEA under high emissions scenario. These variations can be directly related to the projected changes in wind patterns, which are the primary drivers of wave dynamics.

The spatial variation of 20-year mean H_s differences (Figure 4.6) indicates a significant increase in wave heights in the northern part of the domain, mainly in the northwest of Scotland and the west of Ireland. This is likely driven by stronger and more persistent westerly winds associated with a general poleward shift in storm tracks and intensified mid-latitude cyclones (Gentile et al., 2023; Pinto et al., 2013).

In contrast, a reduction in H_s is observed primarily in the central part of the domain, particularly in the mid-latitudes of the NEA. These areas show a broad but moderate decrease in wave heights, which may be attributed to a shift in storm trajectories. The Iberian Peninsula exhibits relatively stable conditions, with minimal change in H_s compared to the present, indicating little impact from projected wind changes in this region. The semi enclosed seas such as the Irish Sea and the English Channel show a slight reduction in H_s. The change in this area is smaller than in the central open ocean, possibly due to the influence of local wind dynamics and the sheltering effect of surrounding landmasses. Earlier studies have shown that the NEA is a region with strong seasonal variations in H_s (Gallagher et al., 2016a; Tiron et al., 2013). Our analysis also reveals pronounced seasonal differences under future climate conditions: winter and summer show increased H_s, spring shows only minor changes, and autumn shows a marked reduction in H_s. Quantitatively, the largest seasonal increase reaches up to 22 cm in winter and the strongest decrease of about 26 cm in autumn. Figure 4.7 illustrates these seasonal differences and highlights the associated spatial patterns across the NEA domain.

During winter, a pronounced increase in H_s is visible across the northern and western parts of the domain, indicating stronger wave conditions likely associated with intense and frequent winter storms. The region around Ireland, shows a widespread increase in H_s under future conditions. Additionally, the Irish sea shows noticeable increase in H_s, suggesting enhanced local wind forcing or greater wave penetration from the adjacent open Atlantic. In spring, the changes are minimal. Most areas are showing weak positive or negative differences. This suggests that spring will bring relatively stable

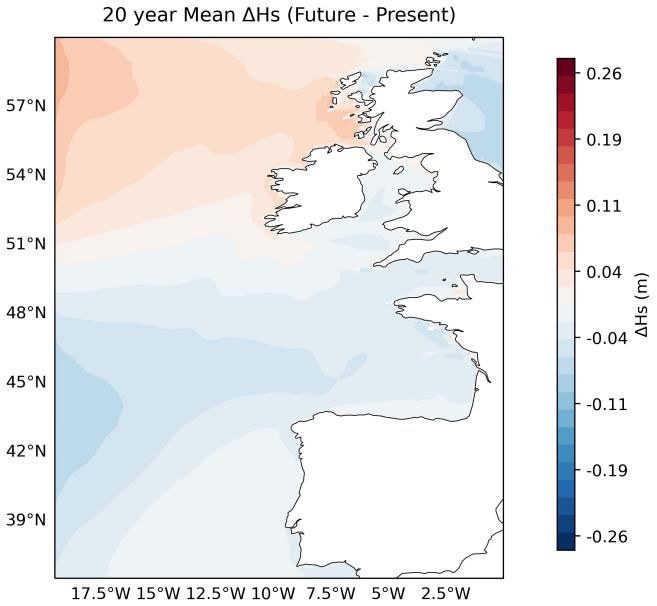

Figure 4.6: Spatial difference in the 20 year mean significant wave height (H_s) for the Northeast Atlantic between future (2081–2100) and present (2004–2023) conditions. Positive values (red) indicate an increase in wave height, while negative values (blue) indicate a decrease, highlighting regional variability in projected wave climate changes

wave conditions in the future. Summer shows a moderate increase in H_s in the northern and southern parts of the NEA, while the central part shows reduction. Notably, the western Iberian Peninsula, the area near the northern Ireland, and waters west of the outer Hebrides experience higher H_s increases in summer than in winter. This highlights the influence of seasonal wind shifts or persistent local wind forcing during this time. In contrast, autumn shows a widespread and significant decrease in H_s, especially across the central and southern parts of the domain, including the area of west of the Iberian Peninsula and the Bay of Biscay. This is the only season showing a strong and consistent negative anomaly across a broad area, suggesting a notable weakening of wave-generating conditions during this period compared to other seasons.

4.7.2 Localized changes in wave height along the west coast of Ireland

To understand how wave height distributions change locally, I compare the distributions of H_s at the locations where the M3 (southwest of Ireland) and M4 (northwest of Ireland) buoys are deployed (hereafter $M3_L$ and $M4_L$ will be used to represent the locations where

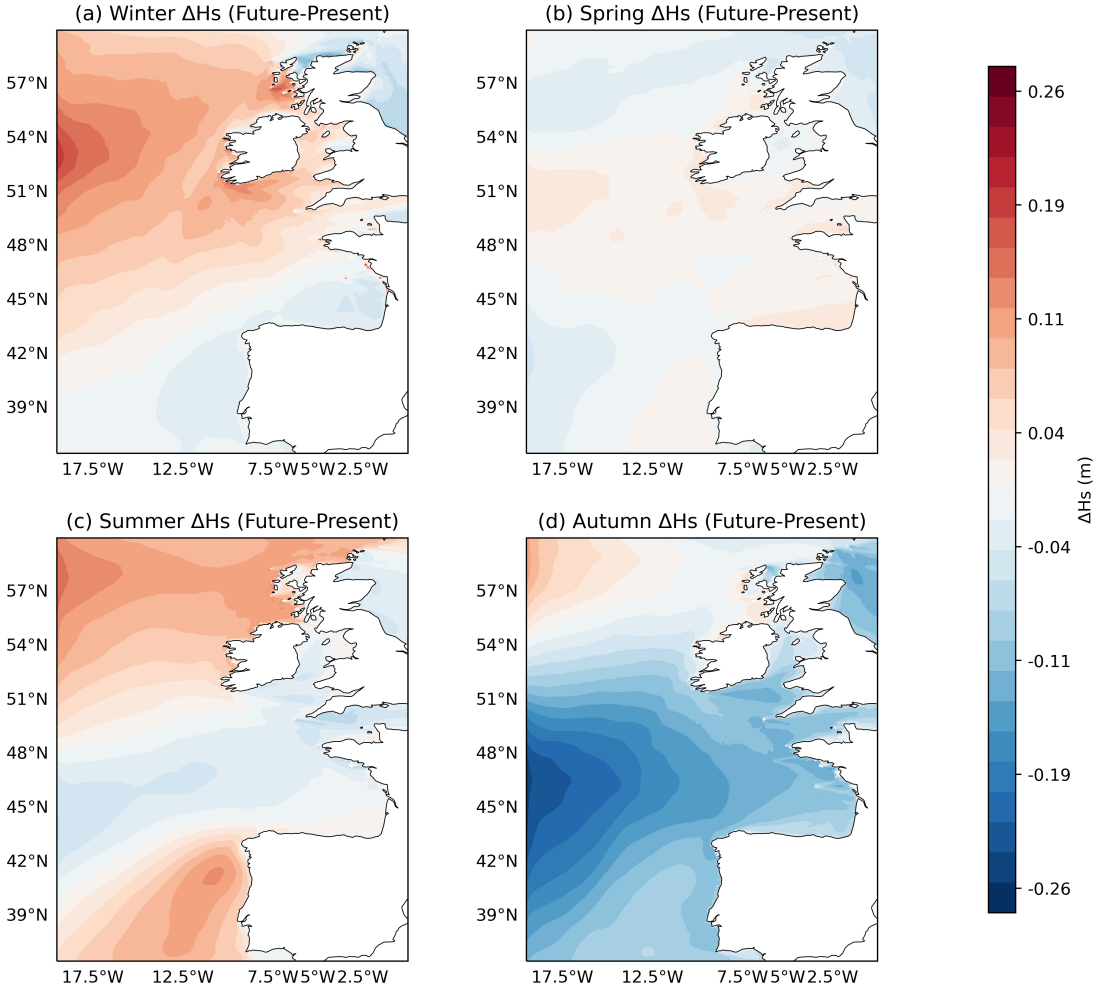

Figure 4.7: Seasonal differences in the mean significant wave height (H_s) between future (2081–2100) and present (2004–2023) conditions for the Northeast Atlantic. Each panel represents a season (a - Winter, b - Spring, c - Summer, d - Autumn), with positive values (red) indicating an increase and negative values (blue) indicating a decrease in H_s. The plots highlight the seasonal variability in projected wave climate changes

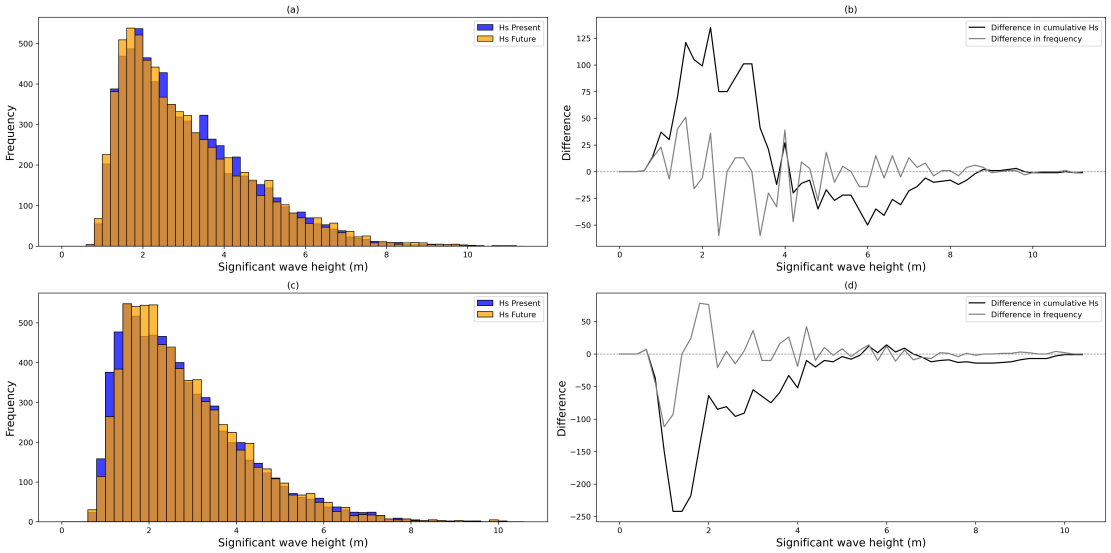

Figure 4.8: Distribution of H_s and comparison of future and present H_s at $M3_L$ and $M4_L$. The histogram plot (a) shows the comparison of H_s at $M3_L$ for present (blue) and future (orange), while in (b) grey line represent the difference (Future - Present) in bin frequencies of H_s and black line represent the difference in cumulative sum of H_s. Like wise histogram plot (c) shows the comparison of H_s at $M4_L$ for present (blue) and future (orange), while in (d) grey line represent the difference (Future - Present) in H_s and black line represent the difference in cumulative sum of H_s.

the M3 and M4 buoys are deployed). The analysis compares the present and future H_s, using histograms to examine the wave height distribution and to analyse the differences in bin frequencies and cumulative sum of H_s. This comparison provides insights into shifts in wave height characteristics such as whether future conditions involve more frequent high waves, changes in moderate wave occurrences or shifts in calm conditions. The climate change evaluation shown in Figure 4.8 and 4.9 is based on the full 20-year simulation periods, covering 2004–2023 for the present climate and 2081–2100 for the future climate. The analysis focuses on the locations in the west, $M3_L$ and $M4_L$, as the west coast of Ireland is the primary focus of this study due to its direct exposure to North Atlantic swell. Locations in the east, $M2_L$ and $M5_L$, located in the Irish Sea, are dominated by local wind-sea conditions and represent a fundamentally different wave climate regime, and are therefore not directly comparable to the swell-dominated western stations in the context of this climate assessment.

The analysis of wave height distributions at the $M3_L$ and $M4_L$ shows notable differences between present (2004–2023) and future (2081–2100). Histograms at both locations (see

Figure 4.8(a), for $M3_L$ and Figure 4.8(c) for $M4_L$) reveal contrasting trends. At $M3_L$, the orange bars (future H_s) are generally taller than the blue bars (present H_s) for $H_s <$ 2 m, while blue bars are mostly taller for moderate waves (2-4 m). But for high waves, from 4 to 8 m, the number of alternating blue and orange bars is roughly equal, making it difficult to identify a clear pattern within that range. A few orange bars appear for $H_s >$ 8m at $M3_L$. In contrast, at $M4_L$, blue bars are taller than orange bars below 1.5 m, while from 1.5 to 4 m, the orange bars gradually increase and become taller. For higher waves, $M4_L$ shows a pattern similar to that observed at $M3_L$, and above 8 m, orange bars are present but shorter than blue bars.

It is important to note here that the increase and decrease in each bin are not entirely consistent within a given range. The trend described for each range is based on the majority of bins being taller in either the present or future distribution, rather than every single bin within that interval. While the histograms provide a visual summary of these differences, they do not capture the full picture. The grey lines in Figure 4.8(b) and 4.8(d) which represents the bin to bin frequency differences capture these fluctuations; however, these are often noisy and difficult to interpret. To better highlight the overall shift between present and future distributions, the black cumulative sum difference line was included.

At $M3_L$ (Figure 4.8b), there is a net positive shift below 2 m confirming that calm conditions are projected to become more frequent. A dip across the 2-4 m waves indicates a net reduction in moderate wave heights except around 3 m, where the dip is less pronounced. Interestingly, the black line also reveals a distinct pattern for higher waves at $M3_L$ that was not easily visible in the histogram plot. The line shows a decline from 4 to 6 m followed by a rise from 6 to 8 m suggesting a redistribution within the higher wave categories. The curve then flattens after 8 m, highlighting slightly increased extremes.

At $M4_L$ (Figure 4.8d), the cumulative curve shows a sharp decline for calm conditions and a steady increase for H_s in the moderate range. While the curve drops below zero, this does not indicate that wave heights are decreasing overall. Instead, it shows that the future has fewer calm wave events compared to the present. For $H_s >$ 2 m, the curve starts to rise, meaning that moderate waves become more frequent in the future. Overall, the plot reflects a shift in the distribution, where calmer conditions reduce, and moderate wave activity increases. More flatten curve afterwards confirms that extreme conditions remain stable or slightly decrease.

Altogether, at $M3_L$, wave conditions are shifting towards both calmer and more energetic extremes with a reduction of moderate waves. $M4_L$ shows fewer calm states and modest

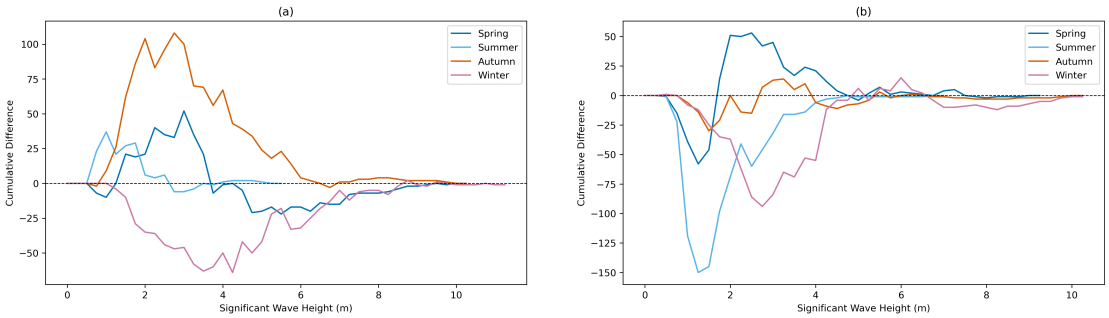

Figure 4.9: Seasonal difference in cumulative H_s between future and present scenarios at locations $M3_L$ (a) and $M4_L$ (b). The blue line represent spring, sky blue line represent summer, the orange line represent autumn and the pink line represent winter.

increase in moderate waves and stable extreme wave frequencies in future. The shifts towards moderate to high waves at $M4_L$ and those towards calm waves at $M3_L$ is in line with the 20-year mean H_s difference, which clearly shows greater wave activity in the northwest of Ireland compared to the southwest. Expanding on the histogram-based analysis, the seasonal cumulative differences at $M3_L$ and $M4_L$ provide a detailed view of how wave height distributions vary across different seasons. The seasonal cumulative differences of H_s between future and present conditions at $M3_L$ (Figure 4.9a) and $M4_L$ (Figure 4.9b) reveal distinct patterns in wave height distribution. At $M3_L$, calmer waves ($H_s < 2$ m) are more frequent in the future, while moderate waves (2-4 m) show a decline, and those between 4 and 6 m (high waves) remain relatively stable in summer. No extreme waves are observed in summer at $M3_L$. During autumn, there is an increase in waves between 1 and 3 m, indicating a shift to calmer, rather than moderate conditions. However, the difference decreases between 3 and 6 m, while higher waves (above 6m) show very less increase in the future, with the presence of extreme waves (> 8 m). In spring, a similar pattern to that of autumn is observed, with an increase between 1 and 3 m, followed by a decline up to 6 m. However, the magnitude of these changes is less pronounced. Unlike in autumn, high waves above 6 m are expected to be more frequent in spring. Winter, in contrast to other seasons, shows a negative cumulative difference for calm to moderate waves, indicating a reduced frequency of these events, while the occurrence of higher and extreme waves (> 6 m) increases. This suggests a shift toward more energetic wave events during winter at $M3_L$.

At $M4_L$, small waves are projected to decrease in all seasons. In autumn, minimal changes are seen across all wave heights marking a contrast to autumn at $M3_L$, except for extreme waves, which will remain similar to present conditions. Moderate waves

become more frequent in spring, with higher and extreme waves showing little change compared to present. Summer at $M4_L$ shows an opposite trend to that at $M3_L$, with a sharp increase in moderate waves and some high waves up to ~ 7 m, suggesting more energetic conditions. Winter indicates an increase in moderate waves, as well as a rise in the occurrence of high waves and some extreme events in the 8-10 m range.
The seasonal cumulative differences at $M3_L$ and $M4_L$ can be further related to the seasonal spatial patterns of wave height change across the NEA domain. In winter, the spatial maps (Figure 4.7) indicate increased wave activity along the west coast of Ireland, which is reflected in the increased frequency of high waves ($H_s > 4$ m) at both $M3_L$ and $M4_L$. In spring, the spatial maps show relatively stable or modest increases in H_s along the west coast, consistent with the local distributions showing an increase in moderate waves (1-3 m) at both locations and a decline in the 3-6 m range, alongside some increase in high waves. In summer, the spatial maps show contrasting behaviour between the southwest and northwest coasts, with increased wave activity at $M4_L$ but reduced activity at $M3_L$. This is reflected in the local distributions, where $M3_L$ shows an increase in calm states with no extreme waves, while $M4_L$ exhibits higher wave activity including waves up to approximately 7 m. In autumn, the spatial maps indicate a general decline in wave height across the region, broadly consistent with the local results at $M4_L$, which shows more frequent calm waves and a decline in higher waves. However, $M3_L$ shows a comparatively different response during autumn, with wave conditions remaining more similar to present conditions. This contrasting behaviour between $M3_L$ and $M4_L$ during autumn may be associated with the poleward shift of the North Atlantic storm track during the transition from autumn to winter, which could differentially affect the southwest and northwest coasts of Ireland. However, this interpretation requires further investigation.

4.8 Discussions

4.8.1 Surrogate data as an efficient downscaling alternative

Understanding future wave changes is crucial for long-term coastal planning and management. Global climate models (GCMs), serve as the primary source of future atmospheric forcing. However, because of their coarse spatial resolution (typically ranging from 100 to 250 km grid spacing), traditional GCMs, like MPI-ESM, have difficulty

in adequately representing small-scale wind variability. To address this, various downscaling approaches, such as dynamical downscaling, statistical downscaling, and, more recently, machine learning-based methods have been developed.

Dynamical downscaling offers detailed physical representations. However, it is computationally intensive, requiring significant storage and long simulation times (Rozoff and Alessandrini, 2022). In contrast, statistical methods are computationally efficient but rely on predefined relationships, which may limit their ability to capture complex, non-linear interactions between variables (Rozoff and Alessandrini, 2022). According to Zhang et al. (2024), machine learning-based approach models intricate, non-linear relationships and effectively handle high-dimensional datasets. However, they demand significant computational resources, large training datasets, and domain expertise, which can pose challenges for practical implementation (Getter et al., 2024).

This study employs an analogue-based approach as a simpler and more resource-efficient alternative. By selecting analogue days based on the average vector difference with MPI-ESM winds and rearranging high-resolution ERA5 data, the surrogate wind dataset preserves the temporal evolution of the climate model while achieving both spatial and temporal coherence with ERA5. In addition, this method captures the non-linear dynamics in the observational dataset and preserves the physical realism. The method therefore overcomes the limitation of traditional statistical methods that often rely on empirical fits or treat grid points independently. Furthermore, by using existing datasets and rearranging them based on identified analogues, rather than generating new data through complex simulations or extensive model training, this method aligns with the principles of surrogate modelling – a concept commonly used in machine learning (Bocquet, 2023). Surrogate models simplify complex systems, enabling faster predictions without the need for full simulations (Bocquet, 2023). Similarly, the analogue approach effectively generates high-resolution surrogate data using statistical techniques. Thus, the method avoids the computational demands of dynamical downscaling and machine learning while providing reliable inputs for wave climate analysis. Furthermore, considering that machine learning methods often fail to outperform simpler interpolation techniques, such as bicubic interpolation, in reconstructing extreme wind conditions (Rezvov et al., 2022), the analogue-based approach provides a computationally efficient and reliable solution for downscaling winds for nearshore wave modelling.

4.8.2 Methodological considerations

The sensitivity of SWAN to the temporal resolution of ERA5 wind forcing underscores the importance of high-frequency wind data for accurate wave simulations. The significant deviations observed with 6-hourly and daily wind forcings highlight the inability to resolve the temporal variability needed for reproducing moderate and frequent waves. This finding aligns with the study by Bauer and Weisse (2000), which demonstrated that wave models driven by coarser winds (temporal resolution) significantly underestimate significant wave height. EMD values computed in this study further strengthen this. The model performance with 1-hourly and 3-hourly wind forcings aligns with the previous studies, reinforcing the decision to use 3-hourly wind data for surrogate wind generation. This decision balances computational efficiency and model accuracy which are critical for long-term simulations.

The choice of spatial domain is an important part of the surrogate data generation process, as it affects how well the selected analogues represent the target conditions. The domain should be chosen based on the specific goals of the study. In this study, the surrogate wind data are used to drive wave models. So, it is important to make sure that the selected domain captures the wind patterns that generate waves affecting the region of interest.

Even when the analogue selection was based on a smaller region around Ireland, the resulting surrogate winds were created by shuffling ERA5 data covering the full NA, using the selected time indices. Since the prevailing winds reaching Ireland are westerlies, the regional domain inherently reflects large-scale atmospheric patterns over the NA. This means that even though the analogue selection is performed from a smaller area, the chosen time indices can reflect the larger weather patterns. Preserving large-scale wind effects is crucial for simulating waves near Ireland, as swells significantly shape the Irish wave climate (Gaughan and Fitzgerald, 2020; Gallagher et al., 2016b). The good agreement (low EMD value) achieved by SWAN model nested in WAM forced by same surrogate winds suggests that the surrogate data not only reproduced the local wind conditions but effectively captured the large-scale wind patterns over the NA basin, which are also responsible for the waves along the Irish coast.

The Euclidean distance between MPI-ESM and ERA5 wind fields computed using the vector components of wind allowed to incorporate both wind speed and direction in similarity assessment. For each day in MPI-ESM, the analogue was identified as the day in ERA5 with the minimum spatially averaged vector difference. Following this, the 3-hourly wind data were rearranged according to the new time sequence derived from

the comparison.

4.8.3 Key findings

Model validation, sensitivity analysis, and projected wave height changes provide a detailed understanding of the wave climate in the study area under the current and future scenarios. Validation of the models against buoy observations confirms that both WAM (WAM0.5NEA) and SWAN (SWAN0.025) adequately capture wave conditions, but their performance varies depending on location. The WAM model was effective in capturing wave dynamics in open waters and its limitations nearshore underscore the need for models like SWAN to resolve fine-scale features. The accuracy of SWAN in representing nearshore wave characteristics further reinforces its suitability for coastal applications, especially in regions having complex geomorphology like the Irish coast.

The future projections show noticeable spatial variations in wave height changes across the NEA under the RCP8.5 scenario. An intensification of wave activity is observed in the northern parts of the domain, while the southern and eastern regions experience a reduction in wave heights. These changes can be linked to the influence of shifting wind patterns. The NEA region around Ireland exhibits contrasting trends, with the west coast showing an increase in mean significant wave height, while the east coast remains more stable. Seasonal variations in wave height changes provide additional insights, with the most pronounced increases occurring in winter (up to 22 cm) and summer (up to 15 cm), while autumn exhibits the largest decrease in wave height (up to 26 cm).

However, these findings contrast with those of Gallagher et al. (2016a) and Gallagher et al. (2016b), which projected an overall decrease in H_s, with the greatest reductions occurring in winter and summer under the RCP8.5 scenario near Ireland. Gallagher et al. (2016a) conducted a 30-year future projection compared with a 30 year hindcast of wind-waves using WW3 and wind data from the EC-Earth global climate model. In contrast, the present study focuses on a 20-year comparison of future projections with present conditions, incorporating present and future sea level rise scenarios.

The seasonal variations in wave heights follow a pattern similar to the seasonal differences in 20-year mean wind patterns between the future and present from surrogate data (refer Figure A.9). This similarity confirms that NEA waves are predominantly wind-driven. However, in spring, the H_s pattern does not directly mirror the wind speed changes, which show weak and spatially mixed signals across the domain. This can be attributed to the transitional nature of spring, where wave conditions retain the memory of the preceding winter storm activity while simultaneously experiencing the onset of

the less active summer circulation, where the expanding Azores High begins to suppress westerly winds across the NEA. The combination of these competing influences, residual winter wave energy and emerging summer suppression, results in a spring wave height pattern that does not directly reflect the concurrent wind forcing, but rather represents a transition between the energetic winter and calmer summer wave regimes.

Despite the resolution difference between the raw MPI-ESM winds (1.8°) and the surrogate winds (0.25°), the seasonal difference patterns show broad agreement in their spatial structure across all seasons (refer Appendix A.8 and A.9). This agreement confirms that the surrogate method successfully captures the large-scale climate change signal projected by MPI-ESM, while simultaneously providing a higher resolution and more physically realistic representation of the wind field over the ocean. The winter differences between the two patterns, where the MPI-ESM signal appears displaced toward coastal grid points, are attributed to the known equatorward bias of the North Atlantic storm track in coarse-resolution CMIP models (Harvey et al., 2020). As the surrogate method selects high-resolution ERA5 days based on their synoptic similarity to MPI-ESM patterns, the resulting surrogate wind fields inherit the higher spatial resolution of ERA5, which may partially reduce the influence of this bias over ocean grid points. The overall consistency between the MPI-ESM and surrogate seasonal wind patterns nonetheless provides confidence that the surrogate method successfully captures the large-scale climate change signal projected by MPI-ESM.

While future projections indicate an increase in mean wave heights over the northern NEA, the regional variability in wave climate needs to be carefully analysed. This need is reinforced by the contrasting trends observed at locations $M3_L$ and $M4_L$. At $M4_L$, a decline in calm sea states along with an increase in moderate and higher wave heights indicates a transition toward more energetic and active wave conditions. The H_s distribution at $M3_L$ reflects a shift in waves where moderate waves become less frequent, while both calm and high waves are becoming more dominant. A potential increase in high wave events at $M4_L$ (located NW of Ireland) could be attributed to its exposure to the poleward shifting storm tracks. Projected higher waves and stable extreme waves at both locations may reflect increased storm severity or regional response of the wave climate under future conditions.

The seasonal spatial plots show that autumn experiences the greatest overall reduction in H_s and winter showing an increase in H_s across the NEA domain; the location specific analysis at $M3_L$ and $M4_L$ further validates this trend. In autumn, $M3_L$ shows a shift towards calmer waves and $M4_L$ exhibits stable conditions across all H_s ranges. Both

findings support the broader regional signal of declining wave activity in autumn. In winter, when increased H_s is observed along the west coast of Ireland, both locations show an increase in moderate to very high waves. However, extreme wave events continue to occur at both sites across both seasons, emphasizing that while regional trends are useful, location-specific assessments are essential to capture the full range of wave height behaviour.

The significant increase in extreme waves during winter at both $M3_L$ and $M4_L$ highlights the elevated risks associated with winter storms in future scenarios. Conversely, summer month H_s are less influenced by extreme events, making summer more suitable for activities like sailing. At $M3_L$, the increase in calm conditions across most seasons, except winter, suggests that spring, summer, and autumn offer suitable windows for marine operations. At $M4_L$, autumn appears to be the most favourable period as it remains relatively stable across all wave height ranges.

4.9 Study specific limitations

The same reference period (2004–2023) is used to generate surrogates for both present and future scenarios, since ERA5 data are only available up to the present. However, this does not imply that the same wind represent both time periods. Instead, ERA5 days were selected based on their similarity to MPI-ESM wind patterns for the present and future, allowing the surrogate wind fields to reflect the projected climate signal while maintaining high-resolution physical realism.

This study relies on a single ensemble member of MPI-ESM under the SSP5-8.5 scenario. Even under the same emissions scenario, the climate in 2081–2100 can evolve differently depending on the model used and its internal variability which refers to the natural random fluctuations within the climate system that are not driven by external forcing (Wu et al., 2022; Morim et al., 2019). The use of a single ensemble member means that the projected wave climate changes presented here represent one plausible future scenario. Other ensemble members of the same model, or different climate models entirely, may produce somewhat different projections in terms of the magnitude and spatial pattern of wind and wave height changes. The results should therefore be interpreted with this uncertainty in mind. A multi-model or multi-member ensemble approach would provide a more robust assessment of the uncertainty in future wave climate projections and is recommended for future work .

The MPI-ESM simulations used in this study project generally lower or comparable wind

magnitudes in the future relative to the present. Figure A.10(a-d) shows that MPI-ESM projects a notable decrease in both the 95^{th} percentile and maximum wind speeds in the future, especially over the NA storm track region. As future wind magnitudes are generally lower than or comparable to those already captured in ERA5, this reinforces that ERA5 remains a valid and appropriate source for analogue selection under projected future conditions.

Furthermore, Figure A.10 (e) and (f) show that ERA5 includes a broad range of wind conditions, including extreme values exceeding 30 m/s. This confirms that ERA5 provides a sufficiently wide and realistic pool of wind events for analogue selection, even when generating surrogate data for future conditions.

In the NEA, where the prevailing winds are predominantly westerlies, surrogate winds generated through the analogue method effectively captured the seasonal variations in wind seen in MPI-ESM. The resemblance of seasonal wave patterns with those of wind variations also demonstrates the robustness of the approach in regions with relatively consistent wind regimes. However, in more complex environments like the Indian Ocean, where wind patterns exhibit significant seasonal and spatial variability due to phenomena such as monsoons, the domain selection for the surrogate data generation method requires careful evaluation.

Thus, the method of surrogate generation has certain limitations that did not significantly affect the study. However, it should be carefully used when applied to extreme events or to regions with projected increases in wind or highly complex wind regimes.

While this study focuses on significant wave height (H_s) as the primary parameter for climate change assessment, wave peak period (T_p), mean period (T_m), spectral moments and wave direction are also important parameters for coastal protection design and seabed erosion studies. These parameters are available as standard outputs from both the WAM and SWAN simulations.

Explicit tidal forcing was not applied in the wave simulations. Instead, projected sea level rise from IPCC AR6 and the storm surge anomaly from UKCP18 were incorporated as sea level inputs into SWAN, accounting for the mean change in water depth under both present and future climate conditions. Generating consistent tidal forcing fields for the full 20-year present and future simulation periods would require a dedicated tidal modelling exercise, which was beyond the scope of this study. The exclusion of tidal forcing is acknowledged as a limitation, and its inclusion is recommended for future work focused on nearshore wave processes

Another important aspect concerns sea level rise. Although sea level rise consistent with

the high emissions scenario (RCP8.5) was incorporated in the wave model, its influence on wave simulations was not explicitly analysed in this chapter. The impact of sea level rise are most pronounced in the coastal areas, where even small increases in water level significantly amplify the coastal wave impacts leading to flooding and erosion (van de Wal et al., 2023). Understanding the combined effect of sea level rise and waves are important for evaluating the potential climate change impacts on the coast and remains an important area of research. The detailed analysis of the combined effect sea level rise with coastal waves and their impacts are presented in the following chapter.

4.10 Conclusion

In this study, the robust wave modelling framework developed includes finer resolution models for the NEA and the Irish coastal waters. The models driven by high-resolution surrogate winds were able to capture the spatiotemporal variability of the wave climate which is predominantly wind driven. The analogue method was more efficient in terms of computational time and expenses compared to common downscaling techniques which made the surrogate data a practical resource for long-term assessments of wave climate. The findings provide a reliable foundation for understanding wave dynamics and supporting coastal management under future climate scenarios.

CHAPTER 5

Translating Offshore Waves to Coastal Wave Impact Assessment: Wave Run-up on Galway Bay

The previous chapter explored offshore wave dynamics using WAM and SWAN, providing a detailed understanding of wave conditions in the deep and nearshore waters of the NEA region around Ireland. However, they do not directly capture the impacts of wave events on the coast. In this chapter, the focus shifts towards assessing impacts by analysing wave-driven run-up, a key indicator of the potential coastal flooding and erosion. Both the magnitude and frequency of high run-up events are evaluated under present and future climate conditions. This approach enables a more impact oriented analysis of how changing wave climates and sea level rise may affect coastal risk at Fanore Beach.

5.1 Introduction

Regional wave climate projections are essential for understanding large-scale oceanographic changes, yet they cannot directly inform coastal management decisions or infrastructure design (Guisado-Pintado and Jackson, 2019). The projected wave height changes observed across Irish waters, as established in the previous Chapter 4, carry

significant implications for Ireland's maritime planning and regional risk assessments. However, such regional-scale informations provides little guidance for coastal engineers determining heights of sea walls, for flood risk managers planning evacuation routes, or for local authorities assessing vulnerable communities. This highlights a critical gap: the need to translate these offshore wave climate projections into quantifiable coastal impacts. In particular, an open question remains - how do changing offshore wave conditions manifest as run-up elevations at a specific coastal location?

Wave run-up is the final stage of wave energy transformation as waves propagate from deep to shallow water environments (Brocchini and Baldock, 2008). In deep water, waves travel unaffected by the sea bed. However, when waves enter shallow water (typically defined as depths less than half of the wavelength; Simmonds et al., 1996), they begin interacting with the bottom bathymetry. This interaction creates bottom friction that slows the lower part of the wave while the upper part continues at its original speed, resulting in steepening and eventually breaking. After breaking in the surf zone, waves continue into the swash zone, where uprush on the beach face or coastal structure is observed as run-up (Brocchini and Baldock, 2008).

Numerous definitions of wave run-up exist. In this study, run-up is defined following Van der Meer (2017), as the vertical height from the still water level to the maximum uprush on a beach or coastal structure (see Figure 5.1). This process depends on both offshore wave conditions and local coastal morphology (Dodet et al., 2018), making it a complex but critical parameter for coastal impact assessment.

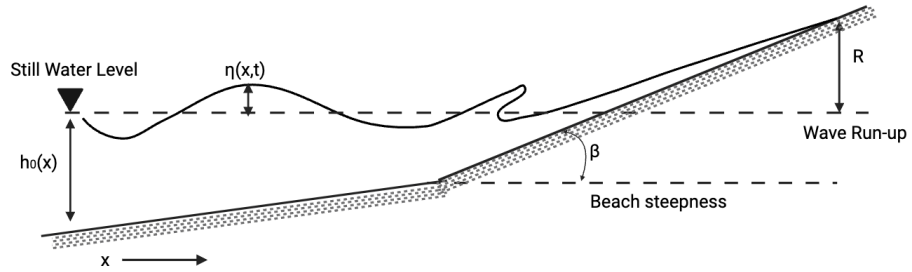

Figure 5.1: Conceptual schematic of wave run-up (adapted from; Villarroel-Lamb and Williams, 2022). The dashed line below the black arrow represents the still water level. Wave run-up, R, is the maximum vertical elevation reached by waves from the still water level across beach profile having steepness β.

Wave run-up is a driving force for coastal processes, such as sediment transport, including beach erosion and coastal flooding. It also plays a central role in swash zone sediment transport through the uprush and backwash cycle, with wide-ranging implications for both engineering applications and coastal dynamics (Lerma et al., 2017; Zijlema and Stelling, 2008). It influences the design of protection structures, beach nourishment projects, and flood mitigation strategies (Solano et al., 2025; Senechal et al., 2011). Under high-energy conditions, run-up plays a central role in coastal erosion and flooding (Lee et al., 2024; Li et al., 2021; Earlie et al., 2018; Dewey and Ryan, 2017; Wahl et al., 2016). Run-up levels are also a major factor in overtopping, as uprush exceeding the crest of sea walls or revetments can allow water to pass landward, leading to flooding and damage to coastal structures (Solano et al., 2025; Pullen et al., 2007). In addition, run-up governs the extent of coastal inundation, an impact expected to intensify under projected sea level rise and posing risks to low-lying communities and infrastructure (Senechal et al., 2011). Large run-up events also pose direct safety risks, such as those documented along the Pacific Northwest coast of the United States, where they contribute to fatalities and severe beach hazards (García-Medina et al., 2017).

Ireland's exposure to the energetic NA wave climate makes run-up assessment crucial for coastal protection and flood risk management. Irish coastal research has provided valuable insights into run-up impacts during storm events, yet dedicated quantitative run-up studies remain limited. For example, a study by Guisado-Pintado and Jackson (2019), on Ireland's northwest coast demonstrated that the coincidence of energetic wave conditions with favourable hydrographic conditions – particularly higher water levels – matters more for coastal impact than wave energy alone. When high waves arrive at high tide, the elevated water depth allows waves to propagate further into the nearshore zone before breaking, delivering more energy directly to the beach face and producing greater run-up heights. Their study at Five Finger Strand, County Donegal, compared two storms: Storm Ophelia (2017) and Storm Hector (2018). Despite Storm Hector having lower wave energy than Ophelia, it caused more dune erosion because its wave run-up occurred during high tide, allowing waves to reach and damage the dune. This study aligns with Cooper et al. (2004), who found that Ireland's west coast beaches are normally protected by their wide, energy-dissipating surf zones. However, they become vulnerable when severe waves coincide with high tide, enabling wave run-up to reach dune face. Numerical studies suggest significant run-up amplification is possible under certain wave and bathymetric conditions (Herterich and Dias, 2017). However, comprehensive run-up quantification remains limited for Irish coastal environments.

To address this limitation, I developed a one-dimensional numerical model for wave run-up, SWARM-1D: Shallow WAter WAve Run-up Model in 1 Dimension. Existing models for simulating nearshore processes like XBeach (Smit et al., 2010), SWASH (Zijlema et al., 2011), or OpenFOAM (Jasak et al., 2007) are powerful but computationally demanding and require substantial resources to operate at high resolution over long simulation periods. The motivation for developing a one-dimensional model is to create a tool that can run efficiently on modest computational resources while still resolving the key physics of wave run-up.
SWARM-1D is based on the first order finite difference solution of the non-linear shallow water equations (NSWE). The model is used to compute wave run-up along a representative coastal profile at the entrance of Galway Bay, using the wave boundary conditions from SWAN simulations (from Chapter 4). This framework enables the quantification of present and future run-up levels, including the effect of sea level rise (SLR).

5.2 Site description

Galway Bay (see Figure 5.2 b), is a large semi-enclosed marine embayment located on the central west coast of Ireland. The bay is partially sheltered from direct Atlantic exposure, though significant wave energy still enters through the North and South Sounds, particularly during storm events (Calvino, 2021; Bento et al., 2018). The bay is approximately 62 km long and 30 km wide, with depth varying from 70 m (outer bay) to 30 m (inner bay) (Calvino, 2021; McCullagh et al., 2020). It also experiences significant tidal variation ranging from 2 to 5 m (Calvino, 2021).
Galway Bay is one of the most severely wave-impacted regions in the western Ireland (Scheffers et al., 2009). The bay's exposure to wave energy is evidenced by coastal boulder deposit with individual boulders exceeding 50 tons found at least 15 m above the coastal mean high water (Erdmann et al., 2017). The region also faces increasing coastal flood risk, with Galway County identifying severe storm events as the most significant climate hazard during the period 1973–2022 (GCC, 2024). Galway City Council's (GCC) first Climate Action Plan (GCC, 2024) indicates a sea level rise up to 24 cm by 2050, which will increase the frequency of coastal inundation. The significance of these coastal risks is amplified by the region's substantial population exposure, with Galway County home to approximately 193,000 inhabitants, of which 43% live in Galway city (CSO, 2022). These concerns have led Galway City Council and the Office of Public Works (OPW) to identify the area as requiring detailed wave climate assessment for coastal

flood risk management (Neill, 2021).

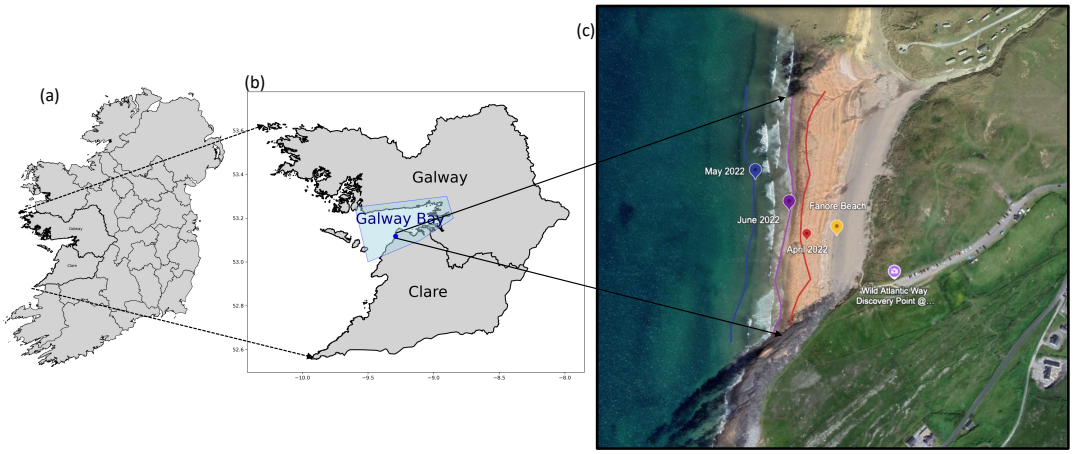

Figure 5.2: Study site location and boundary setup for SWARM-1D simulations. (a) Map of Ireland with Counties Galway and Clare highlighted. (b) Zoomed in view of Galway Bay (shaded in blue). The red dot marks the Fanore Beach. (c) Google Earth image of Fanore Beach, with shorelines extracted for three consecutive months in 2022 illustrating the dynamic nature of the beach (The map includes data from: Data SIO, NOAA, U.S. Navy, NGA, GEBCOMaxar TechnologiesAirbus; Google Earth, 2025).

Fanore Beach, located at Galway Bay's southern entrance, was selected as the specific case study location for wave run-up analysis. Visual analysis of shoreline change illustrated in Figure 5.2(c) using Google Earth satellite imagery, demonstrates the dynamic nature of the beach. Being a sandy beach within Galway Bay (Erdmann et al., 2017), Fanore provides an ideal setting to investigate wave run-up processes on dissipative beach profiles typical of Ireland's Atlantic coast. The location combines extreme wave exposure with representative coastal morphology, making it suitable for examining run-up dynamics under both current and projected climate conditions.

Though Fanore beach is situated along the County Clare coast, it serves as the primary passage through which the NA wave energy entering the bay. Despite being located in County Clare, this entrance point directly influences wave conditions throughout Galway Bay and the flood risks identified by the GCC and the OPW.

5.3 Model development choices

The development of one-dimensional model began with the aim of creating a stable and computationally efficient numerical model for simulating wave transformation near the shore. Initially, higher-order Boussinesq type equations following the approach of Liang et al. (2013) were considered to better represent the dispersive effects of waves. Preliminary tests showed that these equations could successfully propagate solitary waves over flat bathymetry. However, when applied to sloping bathymetry, an essential feature for nearshore wave transformation and run-up studies, the formulation showed numerical instabilities and accuracy issues. Developing a robust and stable Boussinesq solver capable of handling variable bathymetry was beyond the practical scope of my research. Consequently, the decision was made to adapt an existing shallow water model, by extending it with first-order non-linear terms, to provide a computationally effective and stable framework for predicting wave run-up.

As a result, I revisited work undertaken during my model development training, where I developed a one-dimensional shallow water model based on the approach of Kämpf (2009). In that exercise, tsunami waves propagating over an island were simulated using the shallow water equations. It successfully captured how waves deform as they travel over varying bathymetry. While testing the model, I recognised that the same physics applies to waves approaching a beach; this framework was adapted to study wave run-up on a sloping coastal profile.

The main modification in the present work is the inclusion of non-linear advection and flux terms in the governing equations, thus extending the linear shallow water into a fully non-linear form. These additions enable the model to capture essential nearshore processes of wave shoaling, wave steepening, and wave run-up to the beach (Zijlema and Stelling, 2008). The resulting one-dimensional framework was then discretised using explicit finite difference methods, which form the basis of the SWARM-1D. Overall, the model maintained numerical stability and computational efficiency which were one of the main objectives of developing a model rather than using an existing one.

Furthermore, the NSWE have been successfully employed by numerous researchers for modelling nearshore wave transformation (Noor et al., 2024; Fatihah and Loy, 2023; Harris et al., 2015; Kuiry et al., 2012; Brocchini and Dodd, 2008; Zijlema and Stelling, 2008), demonstrating their ability to capture the dynamics of waves near the shore.

5.4 SWARM-1D: Numerical approach

In this section I am presenting the mathematical formulation and numerical implementation of the SWARM-1D model. The model solves the NSWE in one dimension using finite difference methods with the explicit time-stepping and upwind spatial discretisation. The foundational numerical approach is based on the work by Kämpf (2009), but extends it through the inclusion of the advection and flux terms, thereby making the model fully non-linear.

Spatial discretisation employs a mixed finite difference scheme, combining forward differencing with an upwind approach to ensure stability and accurate momentum transport. The use of the upwind scheme for non-linear terms was independently developed during this study (in 2023) and later found to be consistent with the approach by Noor et al. (2024).

5.4.1 Governing equation : NSWE

The classic NSWE (Mousa, 2018; Gedik et al., 2005) are:

$$\frac{\partial \eta_{(x,t)}}{\partial t} + \frac{\partial (uh)_{(x,t)}}{\partial x} = 0, \tag{5.1}$$

$$\frac{\partial u_{(x,t)}}{\partial t} + u_{(x,t)} \frac{\partial u_{(x,t)}}{\partial x} = -g \frac{\partial \eta_{(x,t)}}{\partial x} \tag{5.2}$$

where η denotes the water surface elevation above the still water level, u is depth-averaged horizontal velocity, and $h = h_0 + \eta$ is the total water depth. The variable g is the acceleration due to gravity, x is the horizontal coordinate, and t is time.

For clarity, the spatial and temporal dependencies (x, t) of variables are shown only once here and are omitted in the following equations.

In Eq. 5.1, which is the conservation of mass (continuity equation), $\frac{\partial \eta}{\partial t}$ represents the rate of water level, that is, change that is how quickly the water surface is rising or falling at a point. In addition, $\frac{\partial (uh)}{\partial x}$ is the flux gradient, which shows how the flow rate changes over time.

Eq. 5.2 is the momentum conservation equation, $\frac{\partial u}{\partial t}$, is actually the acceleration term representing how quickly the water velocity is changing at a point (for example there might be a sudden acceleration if a tsunami arrives), $u\frac{\partial u}{\partial x}$ is the advection term (transport of momentum by flow), and $\frac{\partial \eta}{\partial x}$ is the slope of the water surface showing the surface elevation changing over distance.

5.4.2 Numerical discretization

The model implements an explicit finite difference scheme to solve the coupled system of the NSWE. It involves the sequential updates of momentum and mass conservation at each time step.

The numerical implementation of model employs a forward Euler scheme for temporal discretization, providing an explicit time-stepping approach. Spatial discretization is carried out using a mixed finite-difference (forward difference and upwind scheme) approach to ensure numerical stability.

The computational domain is divided into N_x grid points with uniform spacing Δx,

$$x_i = x_{min} + (i-1)\Delta x, i = 1, 2, ..., N_x \tag{5.3}$$

where i is the grid index and x_{min} is minimum distance.

Time is discretised as follows:

$$t^n = n\Delta t, i = 1, 2, ..., N_t \tag{5.4}$$

where Δt is the time step, N_t is total number of time steps, n is the time index.

The NSWE are discretised as follows:

$$u_i^{n+1} = u_i^n + \Delta t \ [-g\frac{\eta_{i+1}^n - \eta_i^n}{\Delta x} - (u\frac{\partial u}{\partial x})_i^n] = 0 \tag{5.5}$$

$$\eta_i^{n+1} = \eta_i^n + \frac{\Delta t}{\Delta x}(F_{i+\frac{1}{2}}^{n+1} - F_{i-\frac{1}{2}}^{n+1})) = 0 \tag{5.6}$$

where $F_{i+\frac{1}{2}} = (uh)_{i+\frac{1}{2}}$ represents the mass flux at the cell interface.

The subscripts and superscripts used in these equations are numerical indices rather than mathematical powers. This notation is standard in finite-difference schemes. The subscript i refers to the spatial grid point, while the superscript n indicates the discrete time level. For example, η_i^n represents the water surface elevation at grid point i and time step n; η_i^{n+1} corresponds to the next time step; and η_{i+1}^{n+1} refers to the elevation at the neighbouring grid point at the next time step.

It should be noted that the advection term in Eq. 5.6 is retained in differential notation in Eq. 5.8 because its discretized form is conditional on the local flow direction. Depending on the sign of the velocity, two different differencing stencils are applied following the upwind scheme, and the conditional discretisation of this term is therefore presented separately in Eq. 5.8.

5.4.2.1 Spatial discretization

The pressure gradient term in the momentum equation employs a forward difference scheme:

$$\left.\frac{\partial \eta}{\partial x}\right|_i \approx \frac{\eta_{i+1}^n - \eta_i^n}{\Delta x} \tag{5.7}$$

The approach evaluates the gradient using the current and downstream points, ensuring that the pressure forcing is aligned with the shoreward direction of wave propagation. While the non-linear advection term $u\frac{\partial u}{x}$ utilises a first order upwind scheme that adapts the differencing method based on local flow conditions:

$$u\left.\frac{\partial u}{\partial x}\right|_i \approx \begin{cases} u_i^n \dfrac{u_i^n - u_{i-1}^n}{\Delta x}, & \text{if } u_i^n \geq 0 \\ u_i^n \dfrac{u_{i+1}^n - u_i^n}{\Delta x}, & \text{if } u_i^n < 0 \end{cases} \tag{5.8}$$

The method selects the derivative based on the sign of the velocity. When the flow is directed onshore (u>0), the backward-difference form is used, while offshore directed flow (u<0) is resolved using forward differencing. This ensures that the information always propagates from the upstream side.

The continuity equation employs a conservative control volume approach to ensure mass conservation. The numerical flux (in Eq. 5.6) at cell interfaces is computed using an upwind scheme as follows:

$$F_{i+1/2} = \begin{cases} u_i^{n+1} H_i^n & \text{if } u_{i+1/2} \geq 0 \\ u_{i+1}^{n+1} H_{i+1}^n & \text{if } u_{i+1/2} < 0 \end{cases} \tag{5.9}$$

$$F_{i-1/2} = \begin{cases} u_{i-1}^{n+1} H_{i-1}^n & \text{if } u_{i-1/2} \geq 0 \\ u_i^{n+1} H_i^n & \text{if } u_{i-1/2} < 0 \end{cases} \tag{5.10}$$

where $u_{i+\frac{1}{2}} = \frac{1}{2}(u_i^{n+1} + u_{i+1}^{n+1})$ and $u_{i-\frac{1}{2}} = \frac{1}{2}(u_{i-1}^{n+1} + u_i^{n+1})$.

In Equations 5.9 and 5.10, if the velocity at the interface is positive, the flux is taken from the left (upstream) cell, whereas if the velocity is negative, flux is taken from the right cell. This guarantees that volume transport is always resolved according to flow direction, preventing non-physical oscillations and thus preserving stability.

5.4.3 Temporal discretization

The model is implemented using explicit forward Euler time integration for both momentum and continuity equations. Explicit forward Euler is a time-stepping method in

which new values, at n+1, are calculated directly using known values, at n (Rapp, 2016). It is simple to implement but requires small time steps for stability.

5.4.4 Stability criterion

The explicit time approach requires satisfying stability criterion for the above equations, known as the Courant-Friedrichs-Lewy condition or the CFL condition (Courant et al., 1928)

$$\Delta t \leq \frac{\Delta x}{\sqrt{g h_{max}}}, \tag{5.11}$$

where h_{max} is the maximum water depth. This constraint ensures that the fastest wave cannot propagate more than one grid cell per time step. The model implements automatic CFL checking and terminates execution if the condition is violated.

5.4.5 Numerical filtering

To suppress the high-frequency numerical oscillations that often arise in finite-difference schemes, a selective Shapiro filter is applied to the water surface elevation.

$$\tilde{\eta}_i = (1 - \varepsilon W_i)\eta_i^{n+1} + \frac{\varepsilon W_i}{2}(\eta_{i+1}^{n+1} + \eta_{i-1}^{n+1}) \tag{5.12}$$

The filter acts by replacing the raw water level at a grid point with a weighted average of its own value and those of its two nearest neighbours. The weighing parameter, ε, controls the amount of smoothing applied. In this study, $\varepsilon = 0.2$ was selected based on sensitivity tests that confirmed this value suppresses spurious oscillations without significantly damping the physical wave signal. Values of ε between 0.1 and 0.5 are commonly used in shallow water models (Kämpf, 2009). $\varepsilon = 0.2$ was found to provide the best balance between numerical stability and wave amplitude preservation for the grid resolution and wave conditions used here.

The wet cell indicator, W_i, ensures that filtering is performed only in wet computational cells. A cell is classified as wet when $W_i = 1$ (i.e., when the total water depth $h \geq H_{min}$), and as dry when $W_i = 0$.. Filtering is applied only to wet cells to avoid unphysical smoothing near the wet/dry interface.

After this step, the water surface elevation at the new time level (n+1) is updated with the filtered elevation, i.e., $\eta_i^{n+1} = \tilde{\eta}_i$

5.4.6 Wetting and Drying algorithm

The wetting-drying algorithm provides a simple but robust way to represent the moving shoreline in the 1D model. This algorithm addresses the fundamental challenge of shallow water equation becoming mathematically singular (becoming unstable due to division by 0) as water depth approaches zero.

At each time step, every computational cell is checked against a minimum water depth (H_{min}). If the total water depth, h, in a cell is greater than or equal to this threshold, the cell is classified as wet ($W_i = 1$). The full NSWE are applied in wet cells. If the depth is smaller, the cell is classified as dry ($W_i = 0$) and is treated with a simplified momentum condition that prevents the unrealistic velocities from developing in near dry regions. The unrealistic flow is prevented by setting velocities to zero and only allowing momentum changes when water is being pushed into the dry cell from adjacent wet areas.

As water moves shoreward, cells that were initially dry may become wet when local water depth exceeds the threshold. These newly wet cells are initialised with appropriate water surface elevation and velocity, making them part of full dynamics of the flow. When water retreats and the depth in a wet cell drops below the threshold, the cell transitions into dry state. Its velocity is set to zero and its depth is fixed at the minimum value to avoid negative depth, thereby preserving mass conservation.

Thus SWARM-1D naturally captures the advance and retreat of the shoreline through dynamic switching of wet and dry states. The maximum landward extent of wet cells therefore corresponds to the run-up distance. In practice, the model records the index of the last wet cell at each time step and determines the run-up position relative to the still-water line. The vertical run-up or run-up height is computed as the elevation of this shoreline point above the still-water line.

5.4.7 Boundary conditions

5.4.7.1 Offshore wave generation

Time-varying wave conditions are applied at the offshore boundary using wave data from SWAN simulations:

$$\eta_1^{n+1} = A(t)sin(\omega(t)t) \tag{5.13}$$

$$u_1^{n+1} = \eta_1^{n+1}\sqrt{\frac{g}{h_{0,1}}}, \tag{5.14}$$

where

$$A(t) = \frac{H_s(t)}{2} \tag{5.15}$$

$$\omega(t) = \frac{2\pi}{T_p(t)}. \tag{5.16}$$

$A(t)$ is the time varying wave amplitude, H_s is the wave height, and $\omega(t)$ is the angular frequency, T_p is the wave period, and $\pi = 3.14$

5.4.7.2 Onshore boundary condition

At the onshore boundary, a zero-gradient (Neumann) boundary is applied to prevent the artificial inflow from the landward side (Kämpf, 2009). In this method, the free surface elevation and velocity at the boundary cell are set equal to those of the adjacent interior cell:

$$\eta_{N_x}^{n+1} = \eta_{N_x-1}^{n+1} \tag{5.17}$$

$$u_{N_x}^{n+1} = u_{N_x-1}^{n+1} \tag{5.18}$$

The wetting-drying algorithm controls the movement of the shoreline within the computational domain. This naturally stops the inland propagation of momentum once a cell becomes dry, thereby representing the run-up limit within the grid. However, the numerical scheme also requires a boundary condition at the fixed landward edge of the domain. Without such a condition, the finite-difference stencil would attempt to access points outside the grid. This can lead to numerical instabilities or spurious wave signals. Reflective boundary is implemented to avoid these spurious oscillations, effectively acting as a solid wall that prevents artificial inflow or outflow.

5.5 Model run-up comparison against empirical run-up

To evaluate the performance of SWARM-1D, a comparison test was carried out using an idealised sloping beach with a uniform slope of 1:10 and a maximum depth of 18 m. The choice of 18 m was made to match the conditions of Holman (1986), whose empirical formula was derived using field data collected at Duck, NC, with a wave height measured in 18 m water depth. A sinusoidal boundary condition was prescribed at the offshore boundary with $H_s = 4m$ and $T_p = 10s$. Waves were propagated across the profile under these forcing conditions.

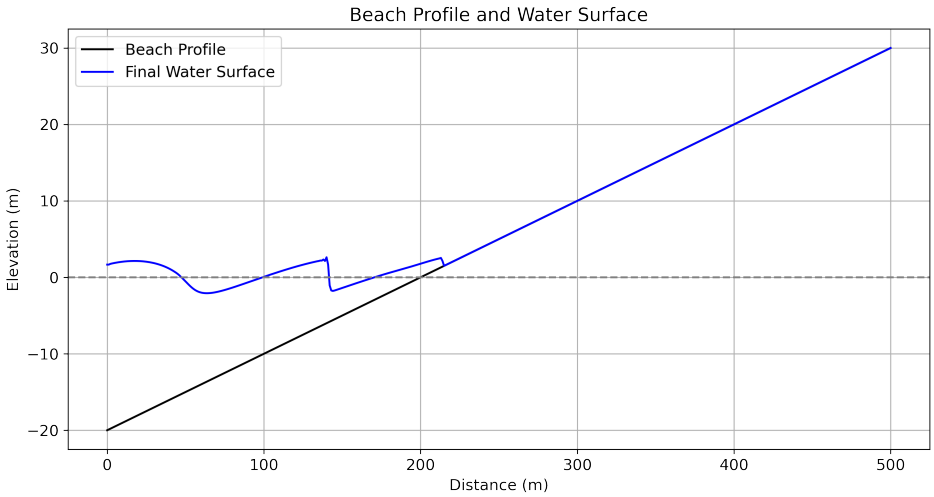

Figure 5.3: Simulated wave run-up on an idealised 1:10 sloping beach profile with a maximum offshore depth of 18 m. The black line shows the beach profile, the dashed line indicates the still water level, and the blue line represents the final simulated water surface after wave propagation.

Figure 5.3 shows the simulated water surface elevation after a representative time step. The beach profile is shown in black, still-water level is indicated by the dashed line and the computed free surface is plotted in blue. It can be seen that the blue line extends over the beach face and continues upward to the top of the profile. This extension is purely a feature of the visual representation, as the free surface η was initialised along the full domain for plotting. In the numerical model, values of η in dry cells are excluded from the computation, and the shoreline position is determined solely by the wetting-drying algorithm. Thus, the apparent overshoot of the blue line on land has no influence on the simulated dynamics or the calculated run-up height.

It can be seen from the figure that waves, on approaching the shore, they shoal (shows a slight increase in height) and steepen due to decreasing depth. Finally runs up to the beach. The resulting run-up height was computed using the wetting-drying algorithm as described in Section 5.4.6.

For comparison, the run-up height from the model was evaluated against the empirical predictor of Holman (1986), which relates the 2% exceedance value of run-up height ($R_{2\%}$) to the offshore wave height and the Iribarren number (or surf similarity parameter,

ξ_0):

$$R_{2\%} = H_s(0.83\xi_0 + 0.2) \tag{5.19}$$

with H_s measured at 18m depth. The numerical simulation produced a maximum run-up of 3.10 m, while the empirical formula predicted 2.87 m under the same input conditions. This close agreement demonstrates that SWARM-1D predicts run-up dynamics with good accuracy. This also provided confidence in applying it for studying run-up in a selected profile on the west coast of Ireland under both present and future conditions. The Holman (1986) formula was selected for this comparison because the validation test was deliberately configured to replicate the exact observational conditions from which the empirical formula was derived. The most widely used Stockdon-type empirical models (Stockdon et al., 2006), are derived from a broader range of spectral wave conditions and beach types. Applying them to a monochromatic, single-slope validation case would introduce inconsistencies between the model forcing and the empirical derivation conditions. The Holman (1986) model therefore represents the most consistent and physically appropriate benchmark for this specific validation configuration.

5.6 Model set up: Application on Fanore beach

Following the comparison, the SWARM-1D model was applied to a real-world site at Fanore beach on the west coast of Ireland. A one-dimensional cross-shore profile of approximately 3 km was selected, extending from offshore to a maximum depth of 30 m. The profile was extracted from the EMODnet dataset (EMODnet, 2024). The data was then interpolated to a uniform computational grid with $\Delta x = 5m$, providing high-resolution representation of the coastal profile (refer Figure 5.4)

The model was forced with H_s and T_p obtained from SWAN simulations for both present and future conditions. The model time step was set to $\Delta t = 0.1s$, ensuring numerical stability. The wetting-drying algorithm was configured with a minimum water depth threshold of $H_{min} = 0.1m$, while the Shapiro filter smoothing parameter was set to $\varepsilon = 0.2$

The offshore wave conditions from SWAN simulations were applied at daily resolution. These values were used as constant boundary conditions for each 24-hour SWARM-1D simulation. Although this approach does not capture the sub-daily variability in the offshore wave climate, it provides a computationally efficient method for assessing the daily maximum run-up under representative forcing conditions, which is appropriate for the long-term climate-scale objectives of this study. The aim of this study is to assess

long-term climate-driven changes in run-up statistics, rather than to simulate individual storm events, for which daily resolution is sufficient. In addition, the daily mean values are derived from SWAN simulations that resolve the full North Atlantic storm climatology, and therefore reflect the statistical influence of storm activity on the long-term wave climate.

Under these conditions, the shoreline evolution was tracked dynamically, and the maximum daily run-up was recorded and written to file for subsequent analysis. An illustration of SWARM-1D capturing the basic shallow water wave propagation and run-up to shore is provided in Appendix A.12.

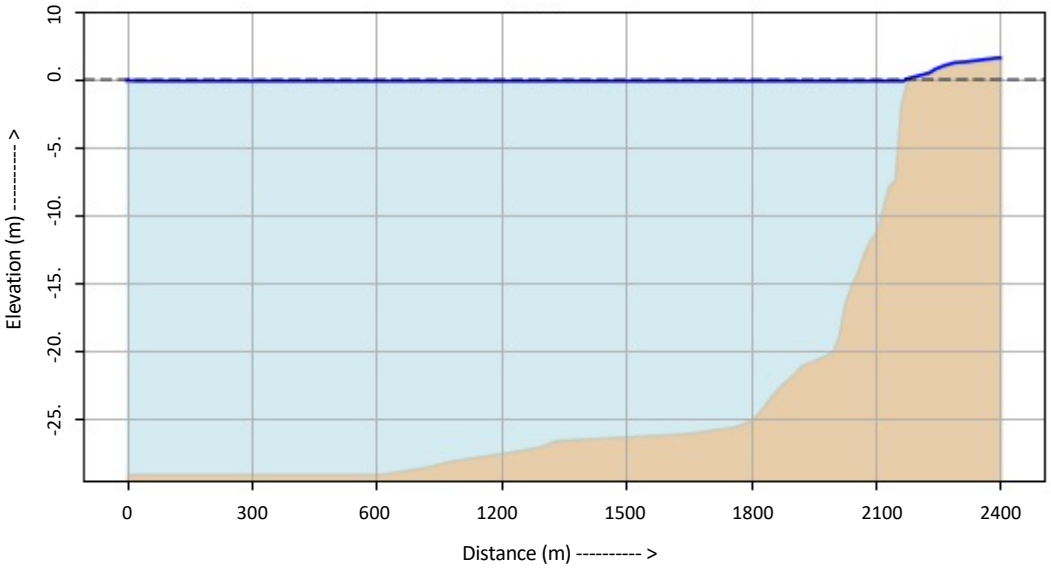

Figure 5.4: Cross-shore profile at Fanore Beach extracted from EMODnet. The brown shading represents the seabed, light blue the water column, and the solid blue line the initial water surface at $t = 0$, where t is the time. The water surface is extended along the topography for visual clarity only, this has no effect on the model computations. The horizontal dotted line indicates the still water level (SWL).

5.7 Results

Run-up events at Fanore Beach were analysed under three scenarios: the present climate (2004-2023), a future climate scenario (2081-2100) based on the projected wave conditions, and a future + SLR scenario, in which still-water levels were uniformly increased by 0.70 m to represent long-term SLR. The analysis was carried out in two stages: a return-level analysis using annual maxima and a seasonal exceedance frequency analysis.

Together, these approaches provide insights into both the magnitude and the frequency of hazardous run-up events, and how they are expected to evolve under changing climate.

5.7.1 Return period using annual maximum run-up

A return-level analysis was carried out using the Generalised Extreme Value (GEV) distribution fitted to annual maximum run-up values. Annual maximum run-up values were ranked in ascending order and assigned empirical return periods using the formula $T = \frac{N+1}{m}$, where N is the total number of years and m is the rank (Makkonen, 2006). The GEV distribution was then fitted to these annual maxima using maximum likelihood estimation, providing a theoretical framework for extrapolation to longer return periods (Rydén, 2024).

To account for uncertainty in the fitted return levels, a bootstrap resampling approach was used. For each scenario, the annual maxima were resampled 1000 times, the return levels were recalculated, and the GEV fit was repeated. The shaded regions in Figure 5.5 represent the 95% range (2.5^{th}-97.5^{th} percentiles) of these return-level estimates, providing a measure of the spread in possible run-up values for each return period.

The GEV fitted curves in Figure 5.5 show a steep initial section for return period approximately below $T = 1.1$, where no model data (annual maximum values) are present. With 20 years of simulated data, the smallest observed annual maximum of run-up corresponds to return period of approximately $T = \frac{20+1}{20} = 1.05$years. Therefore, the GEV fitted curve extrapolates downward to T=1 year to estimate the theoretical location parameter. As shown in Figure 5.5 that the empirical data points (triangles and dots) and the associated uncertainty bands begin above 1.05 years. The curves are also extrapolated beyond $T = 20$ to estimate the return levels of rare events (up to 30 years). Although this extrapolation is a standard feature of GEV analysis, it should be interpreted with caution as it extends beyond the actual available data (Charras-Garrido and Lezaud, 2013).

The fitted return-level curves in Figure 5.5 show a clear upward shift in run-up magnitude under future conditions when sea level (Future+SLR) was included. For example, a 10-year return-level increases from approximately 3.32 m in the present to over 3.6 m in the Future+SLR scenario. Similarly, the return period associated with a 3.30 m shortens. The occurrence of 3.30 m once every in 2.5 to 3 years in present has shortened to once in every 1 to 1.3 years in the future with increased SLR.

It is important to note here that the run-up values in this study are measured above the still-water level, representing the vertical elevation of the water surface above the

still-water level for each scenario. Therefore, the higher run-up values observed in the Future+SLR scenario represent run-up above an elevated baseline, not just the effect of higher water level.

In the Future+SLR scenario, the highest run-up each year is always greater than 3.30 m. This means that 3.30 m is expected to be exceeded annually in the future as sea levels rise. Based on this, a run-up threshold of 3.30 m was selected as a critical impact level for the seasonal exceedance analysis.

The uncertainty patterns in the GEV fitted return-level curves reveal important characteristics about the reliability of extreme run-up value predictions. The uncertainty at shorter return periods (1–5 years) is narrower and indicates greater statistical reliability of the GEV model for predicting frequently occurring events. All three scenarios consistently show higher run-up magnitudes with increasing return periods. However uncertainty bands widen for longer return periods (20–30 years). This indicates increased variability and less confidence in predicting the magnitude of very rare run-up events, especially under the Future + SLR scenario. This is expected, as extreme events become harder to estimate accurately due to fewer data points in the tail.

The Future+SLR uncertainty bands are clearly separated from the other two scenarios showing that SLR consistently produces higher run-up estimates across all bootstrap samples. This separation indicates that the higher run-up under sea level rise is a reliable finding, it appears in all 1000 bootstrap samples, not just one of them.

In contrast, only minor differences were observed between the present and future (without SLR) scenarios. The return-level curves for these two cases are closely aligned across all return periods, with differences (e.g., at the 10-year return level) falling well within the bootstrap uncertainty range. This suggests that projected changes in wave climate alone result in limited increases in extreme run-up magnitudes and that SLR is a major factor in predicting future run-up.

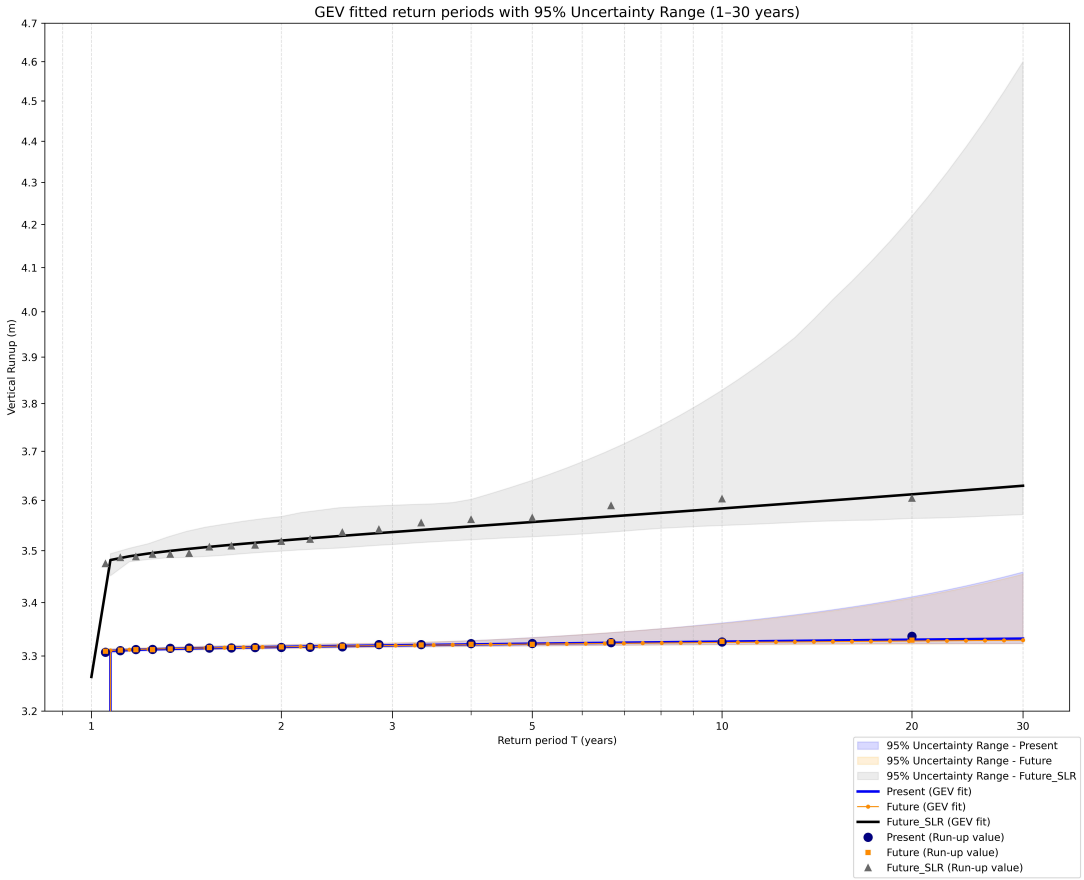

Figure 5.5: Return level plots fitted with GEV distribution for annual maximum under Present, Future and Future + Sea Level Rise (SLR) scenarios. The curve shows the estimated run-up heights (m) corresponding to return periods ranging from 1 to 30 years. Shaded area represent the 95% uncertainty range from bootstrapped samples of annual maximum run-up. Markers indicate observed annual maxima: circles for Present, squares for Future, and triangles for Future + SLR.

5.7.2 Seasonal exceedence frequency

To understand how the frequency of run-up events may change throughout the year, a seasonal analysis was carried out. This focused on how often the run-up exceeded the critical threshold of 3.30 m during each season. The approach used was the Peaks Over Threshold (POT) method. This method identifies and counts every instance (or data point) where the run-up exceeds the chosen threshold (Bommier, 2014). The average number of such exceedances was calculated for each season and scenario, providing a measure of how frequently events occur at each time of the year. This frequency is

expressed as Λ, or the average number of events per season.

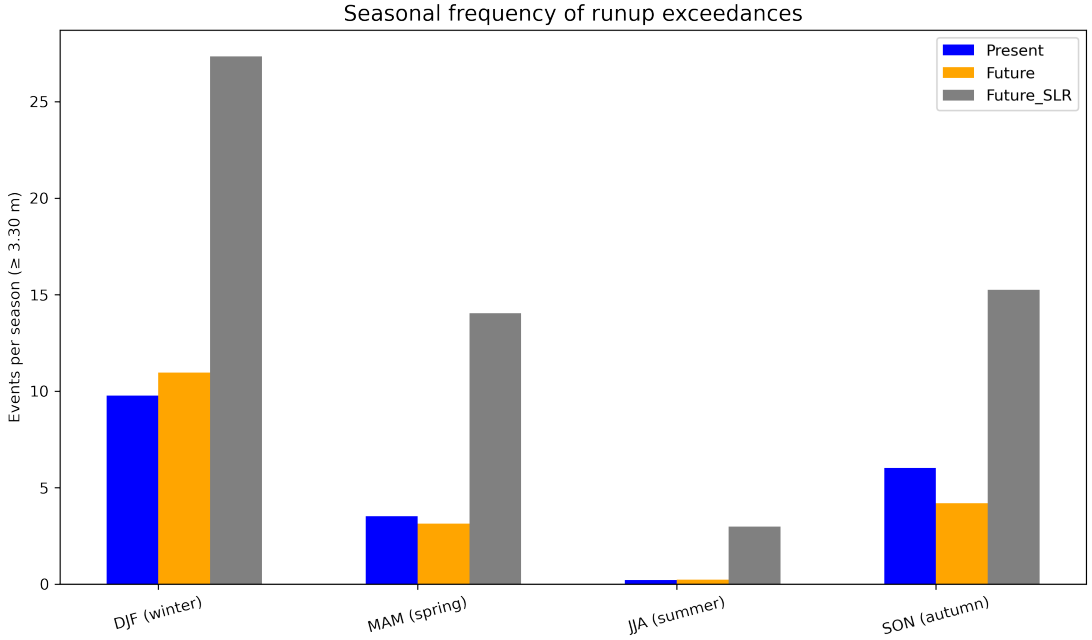

Figure 5.6: Average number of run-up exceedence events per season (Λ) exceeding 3.30m, based on daily run-up data for Present, Future, and Future + SLR scenarios. Seasons are defined as: DJF (Winter), MAM (Spring), JJA (Summer), and SON (Autumn).

As illustrated in Figure 5.6, under present-day conditions, run-up events exceeding 3.30 m occur most frequently in winter and autumn, with average rates of 9.76 and 6.01 events per season. Spring shows moderate exceedance rates at 3.52 events per season, while summer experiences the fewest, with only 0.20 events per season.
In the future scenario without sea-level rise, the seasonal frequencies change only slightly compared to the present. Winter (+12%) and summer (+15%) show minor increases, while spring (-11%) and autumn (-30%) show small decreases. The overall seasonal pattern remains similar to the present. This further confirms that wave climate changes alone are not sufficient to produce large shifts in seasonal hazard.
The percentage change was calculated using the formula:

$$\%\ Change = \frac{\Lambda_{Future} - \Lambda_{Present}}{\Lambda_{Present}} \times 100 \tag{5.20}$$

where $\Lambda_{Present}$ and Λ_{Future} are the average number of exceedances for present and future.

However, when SLR is included in the future scenario, all four seasons exhibit dramatic increases in the frequency of exceedance events. In winter, the number of events rises from 9.76 to 27.43 events per season with a relative increase of 181%. In spring, the frequency increases from 3.52 to 14.03 events per season, marking a 298% increase. The most extreme relative increase is observed in summer, where events rise from just 0.20 to 2.98 per season, representing a +1360% relative change. In autumn, events increase from 6.01 to 15.24 resulting in a relative increase of 253%.
Together, these results indicate that the impact of SLR on run-up exceedance frequency is not only substantial but also seasonally widespread. Although the present-day hazard is mostly concentrated in winter and autumn, the future scenario with SLR shows that every season is affected, and that the window of hazardous conditions will extend throughout the year.

5.8 Discussion

The extreme value analysis of SWARM-1D results revealed the role of SLR in amplifying the extreme coastal run-up at the selected location on Fanore beach. Present and future wave climate scenarios without SLR produced only minor differences in both return levels and seasonal exceedance frequencies. In contrast, the inclusion of a uniform 0.70 m sea level rise led to an increase in run-up magnitude, frequency, and variability. A 70 cm rise elevated extreme run-up values by about 30 cm relative to the present, representing approximately 42% of the imposed SLR. Seasonal analysis further showed that present-day hazards are concentrated in winter and autumn, with calm spring and summer months. However, SLR extends the hazard window across all seasons in the future.
In this section, I discuss the findings in the context of existing literature, considers methodological strengths and limitations, and their implications for future coastal risk assessment and management.

5.8.1 Role of SLR

The finding that sea level amplifying wave run-up is consistent with previous studies that highlight the role of elevated water level leading to increased wave run-up (Almar et al., 2021; Liu et al., 2020; Kim and Suh, 2018; Arns et al., 2017; Chini et al., 2010). As sea level increases, waves are no longer constrained to break as far offshore, allowing long-period and higher-amplitude waves to propagate closer to the shoreline before losing energy (Arns et al., 2017). As a result, waves that previously dissipated much of

their energy in deeper water will increasingly reach coastal defences directly producing higher run-up heights (Chini et al., 2010). More broadly, elevated water levels delay depth-induced breaking and reduce bottom friction, which enhances the energy transferred to the shoreline (Dean and Dalrymple, 2004).

Medellín et al. (2021) assessed the effects of climate change on coastal flooding in the southeastern coast of Gulf of Mexico by analysing wave run-up and storm impacts under RCP8.5 scenario. Their model results showed no significant increase in storm impact between present and future conditions unless sea level was included. This outcome is consistent with the findings of the present study, where run-up extremes at Fanore beach showed little difference between present and future wave climates alone, but increased substantially when a uniform +0.70 m SLR was imposed.

A potential concern is whether including SLR in both SWAN and SWARM-1D models might lead to double-counting of its effect. However, the SWARM-1D wave boundary conditions are largely unaffected by SLR (refer Figure A.11, where the percentile distributions of H_s and T_p from SWAN simulations confirm that present and future scenarios show minor differences in offshore conditions). This is consistent with the finding of Chini et al. (2010), who demonstrated that SLR has minimal influence on the offshore wave climate. Thus, the inclusion of SLR within SWAN does not significantly affect the offshore wave parameters used as boundary conditions for SWARM-1D.

The addition of 0.70 m SLR in SWARM-1D captures the critical nearshore processes that are strongly affected by water depth. The observed amplification in run-up can be attributed to the delayed depth-induced breaking and longer period waves propagating closer to the shoreline due to elevated still water levels. This distinction explains why the present and future scenarios in SWARM-1D (same offshore waves, unchanged nearshore depth) produced nearly identical extreme run-up results, while the Future+SLR scenario (same offshore waves, but deeper nearshore water) resulted in substantially higher extreme values.

When comparing the seasonal exceedance of run-up events in the future (without SLR) with the present, a shift in the seasonal pattern is observed. Winter and summer showed a relative increase in extreme run-up whereas spring and autumn showed a decrease. This pattern is consistent with the projected significant wave height climatologies for the NEA, where future scenarios suggest enhanced wave activity in winter and summer but reduced activity during spring and autumn.

However, once SLR is included, all four seasons show increases in exceedance frequency. Winter remains the most hazardous season in both scenarios, while summer, which was a

low-risk season, experiences more than a tenfold increase when SLR was included. This demonstrates that the effect of SLR on nearshore waves can transform seasons that are currently considered low risk into periods of significant coastal hazard, extending the window of exposure across the entire year.

5.8.2 Methodological limitations and scope

The use of NSWE for simulating wave run-up is well established in the literature. For example, Noor et al. (2024) developed a finite difference scheme incorporating an upwind scheme for non-linear terms to predict run-up at Canti Beach in South Lampung. Harris et al. (2015) applied a one-dimensional analytical approach based on averaged NSWE to investigate long wave run-up in trapezoidal bays. Fatihah and Loy (2023) solved the NSWE using a fourth-order Runge-Kutta method for time integration and a second-order central difference scheme for spatial discretisation. Furthermore, Kuiry et al. (2012) implemented a high-resolution finite-volume model with a Godunov-type scheme and HLL Riemann solver to achieve second-order accuracy. More advanced formulations have coupled NSWE with dispersive Boussinesq-type terms, as in the hybrid model of Orszaghova et al. (2010), or used high-resolution shock-capturing methods such as the TVD-WAF (Total Variation Diminishing version of Weighted Average Flux) scheme with approximate Riemann solvers (Mahdavi and Talebbeydokhti, 2009).

Although these approaches demonstrate the ability of higher-order or Boussinesq-type schemes to be less diffusive, more accurate, and better at capturing dispersive processes, the main objective of my study was to develop a computationally efficient (the model runs quickly on a local computer), stable and easy to implement scheme for long-term climate-scale simulations. The primary test results show that SWARM-1D reproduces the key nearshore physics of wave shoaling, steepening, and run-up. Thus the model developed provides a robust basis for assessing present and future changes in run-up, including the influence of SLR.

Despite these strengths, SWARM-1D has several limitations that must be acknowledged. The one-dimensional framework represents wave transformation and run-up along a single cross shore transect. It neglects alongshore variability, oblique wave incidence and complex wave interactions that may influence wave run-up in morphologically complex coasts (Harris et al., 2015; Bradford and Sanders, 2002). However, this approach is suited to Fanore beach, which exhibits a relatively straight shoreline orientation. For straight geometries, cross shore processes typically dominate the run-up magnitude (Guza and Feddersen, 2012; Harley et al., 2011). Thus, the approach of 1D simulations is appro-

priate for assessing climate-driven changes in extreme wave events in the selected profile while maintaining computational efficiency for long-term analysis.

The one-dimensional framework does not resolve longshore wave dynamics or wave refraction, assuming an idealised coastal geometry in which the model axis is oriented perpendicular to the shoreline, an assumption that is satisfied at Fanore Beach but limits applicability elsewhere. The absence of directional spread in the monochromatic boundary forcing, unlike models such as XBeach, may lead to an overestimation of wave run-up compared to more realistic spectral wave conditions. Furthermore, SWARM-1D solves the non-dispersive shallow-water equations, whereas the SWAN model that provides the boundary conditions is dispersive. The further offshore the SWARM-1D domain boundary is positioned, the greater the accumulated error from missing wave dispersion; sensitivity tests with different domain lengths would help quantify this effect. Finally, applying both H_s and T_p at the offshore boundary may introduce an inconsistency when swell energy is present, as the swell component of H_s would be propagated using the wind-sea peak period and frequency rather than its own, potentially misrepresenting the spectral energy distribution at the boundary.

Furthermore, SWARM-1D framework is not suitable for modelling wave run-up on rocky beaches, due to the fundamentally different wave interaction processes involved, including high wave reflection from impermeable rock surfaces, the absence of wave energy dissipation through infiltration, abrupt surging/collapsing wave breaking on steep rock faces, and spatially variable bed roughness from irregular rock topography, which are not represented in the shallow water equation framework. The model presented in this chapter is applicable only to the assessment of sandy beaches like Fanore beach.

SWARM-1D uses a single sinusoidal wave at the boundary which simplifies the complex spectral nature of real wave behaviour. The approach of using a sinusoidal boundary is widely accepted in coastal engineering, as Dean and Dalrymple (1991) showed that a single sinusoidal wave provides reasonable accuracy for run-up studies. Recent work by Noor et al. (2024) successfully applied the same approach for run-up analysis at Canti Beach. This simplification captures the essential wave energy needed for run-up prediction while enabling efficient long-term climate analysis.

A further limitation concerns the temporal resolution of the offshore wave forcing. Wave conditions derived from SWAN simulations were applied at daily resolution, with each daily mean H_s and T_p used as a constant boundary condition for a 24-hour simulation. Although this approach does not capture sub-daily variability in the offshore wave climate, it provides a computationally efficient method for assessing the daily maximum

run-up under representative forcing, which is appropriate for the long-term climate-scale objectives of this study.

However, it should be noted that daily averaging smooths the sub-daily variability within individual storm events. While the daily mean H_s reflects the statistical presence of storms in the long-term wave climate, it does not capture the peak wave conditions that typically occur over only a few hours at the height of a storm. As a result, the model outputs represent the daily maximum run-up under average daily forcing rather than the absolute extremes driven by peak storm conditions. In addition, storm surge contributions to sea level, which are also short-duration phenomena, are not accounted for. Furthermore, if future climate change leads to more intense individual storm peaks rather than simply more frequent storms, this would not be fully reflected in the daily mean boundary conditions, and its influence on future run-up extremes would therefore be underestimated.

These limitations may influence the results in Figures 5.5 and 5.6, where SLR is identified as the dominant driver of future changes in extreme run-up. However, the relative dominance of SLR, which raises the still-water level uniformly across all wave conditions, would likely be preserved even if sub-daily storm peaks were included, as demonstrated by Medellín et al. (2021), who reached the same conclusion using a different model and forcing approach.

The first-order finite-difference solution with explicit time-stepping and upwind flux schemes introduces numerical diffusion (Toro, 2013; Hecht et al., 1995). That is, it may reduce the peak wave amplitudes during propagation and may lead to underestimation of maximum run-up. However, this creates a conservative bias generally favourable for hazard assessments (**?**Burguete and Navarro, 2000). Additional stabilisation algorithms (Shapiro filtering and the wetting-drying algorithm) introduce further approximations but are necessary for numerical stability. The comparison of model run-up with empirical predictions (over estimation by 8%) suggests these effects remain within acceptable bounds.

Validation of SWARM-1D was constrained to comparison with an empirical relationship due to the absence of site-specific observational data. While model reproduced results consistent with the theoretical expectations, its output should be interpreted as a representative estimate of climate driven changes in run-up at Fanore beach. The results are appropriate for climate impact assessment, relative risk evaluation, and preliminary hazard analysis, though more detailed site-specific studies with observational validation would be required for precise engineering design.

5.8.3 Future work and applications

While this study provides a first step in quantifying wave run-up under SLR on a simplified cross shore profile, it also opens several doors for future development. The current implementation of SWARM-1D is in one-dimension and uses daily wave boundary conditions, which are appropriate for climate-scale assessments but do not resolve alongshore variability or capture coastal responses from short-term storm dynamics. The framework already includes features such as the Manning's friction formula, but this was kept inactive in the current study. Activating and calibrating this component along with incorporating tides and storm surges would allow assessment of compound flooding events and site-specific extremes. Higher resolution forcing, including sub-daily wave conditions, storm surge, and climate-driven changes in storm intensity, would provide a more complete assessment of future run-up extremes. Validation against field observations would further enhance confidence in the model projections. Additionally, testing multiple SLR scenarios (e.g., 0.5 m and 1.0 m) would provide a more comprehensive picture of the coastal risk envelope under different sea level rise trajectories.

Traditionally, climate effects in coastal engineering have been addressed by simply raising the height of coastal defences by the projected amount of SLR (Hunter, 2010). This method neglects the fact that elevated water levels also modify wave characteristics and nearshore processes. A recent study by Arns et al. (2017) shows that sea-level-driven changes in waves and to a lesser extent tides can amplify design heights by 48-56% beyond what is explained by SLR alone. The results from this study reinforce this point: a +0.70 m rise in sea level produced an increase of approximately 0.30 m in extreme run-up, equivalent to about 42% of the imposed rise. In this way, SWARM-1D can provide engineers with quantitative estimates of how SLR translates into additional run-up, offering more robust guidance than simply adding projected SLR to the design coastal structures.

In future developments, implementing higher-order numerical schemes that reduce numerical diffusion and capture dispersive effects would extend the applicability of SWARM-1D beyond climate-scale assessments. Such improvements would make the model suitable for detailed engineering applications, including the design and optimisation of coastal structures, more accurate estimation of run-up heights, and the evaluation of overtopping rates under extreme conditions.

5.9 Conclusion

In conclusion, this chapter presents the development and application of SWARM-1D, a fast and computationally efficient run-up model based on first-order numerical schemes. The model results were used to investigate how SLR modifies wave impacts at the coast through extreme value analysis of annual maxima. Seasonal exceedance analysis further revealed that higher run-up events, currently concentrated in winter and autumn, are projected to extend into spring and summer under Future+SLR conditions, transforming the calmer seasons into periods of frequent hazardous run-up. Overall, the study shows that a fast and efficient one dimensional modelling framework can be used to assess long-term climate impacts and that SLR is the one of the factors driving future increases in coastal run-up risk.

CHAPTER 6

Conclusions

This chapter summarises the main findings of the thesis and explains how they address the research questions set out at the beginning of the study. It then highlights the contributions the research made to the field and identifies the groups who can benefit from these findings. Finally, the chapter discusses possible further developments and directions of research.

6.1 Thesis overview

Ireland's position on the eastern NA edge makes it directly exposed to energetic surface waves. These waves are not only a feature of the Irish maritime environment, but also a source of growing risk to the coastal communities.

Thus the thesis tries to answer a broad question: *how can the wave climate around Ireland be better understood, both for present and future, and how can large-scale wave forcing be linked to the impacts felt along the coast?*.

To answer this question, the research follows three main parts. Firstly, the influence of remotely generated swells on the Irish coast was identified through statistical analysis. Secondly, surrogate wind data was developed to drive high-resolution wave models, along with other climate drivers (sea ice and sea level). Finally, a one-dimensional model was designed to predict wave run-up at the selected beach on the west coast of Ireland. Together, these strands represent a journey from large-scale processes down to localised coastal impacts at the shoreline.

6.2 Linking North Atlantic swells and shoreline impacts

The research progressed from large-scale climatological analysis to regional wave simulations and finally to coastal-scale modelling with each stage providing the foundation for the next. This progression helped to answer the three research questions set out in Chapter 1.

6.2.1 Understanding swell influence on the Irish wave climate

Many previous studies have highlighted the influence of remotely generated NA swells on the Irish wave climate (Shanahan and Fitzgerald, 2025; Nic Guidhir et al., 2022; Gaughan and Fitzgerald, 2020; Scott et al., 2021; Gallagher et al., 2014; Fusco et al., 2010). However, the specific source regions contributing to Ireland's wave climate and the variability in their influence had not been systematically quantified. It was therefore important in my study to identify the regions of the NA that strongly affect Ireland and to establish broader climatological context by identifying the origins, variability and travel times of swell reaching the Irish west coast.
In Chapter 3, I tried to address this by selecting seven source regions across the NA and correlating the swell period from each source region to a target region in the west of Ireland. A lagged cross correlation method was applied to determine the dominant swell sources and their travel time to the target. Additionally, a block bootstrapping resampling was done for each source-target pair to quantify the uncertainty. This statistical analysis using 20-year swell period data from ERA5 helped me to address the first research question,

- Which are the dominant North Atlantic swell source regions influencing the west of Ireland, and how does their influence vary with season?

The analysis revealed that multiple regions across the NA contribute to Ireland's wave climate. The source regions in the extra-tropical NA showed the strongest and most consistent correlations with swell conditions along the west of Ireland. The results also indicated clear seasonal variations in the influence of different NA sources, with winter months showing the most pronounced and widespread swell activity. Interannual variability was also evident, which can be linked to large-scale atmospheric conditions such

as the NAO. For example, different NAO phases can modulate the strength of winds across the basin (Iversen and Burningham, 2015; Phillips et al., 2013), which in turn can affect swell generation and propagation in regions under its direct influence.
Thus the results from swell analysis reveal that Ireland's wave climate is driven by large-scale atmospheric systems and westerly winds over the NA. These strong winds transfer energy to the ocean surface, generating long-period swells (Hell et al., 2021). These swells travel thousands of kilometres to reach the Irish coast, demonstrating that Ireland's wave conditions are strongly connected to atmospheric activity over distant regions. Seasonal differences in swell reflect changes in storm intensity and position, which are largely controlled by the NAO and associated shifts in wind patterns. This finding is consistent with studies showing that NA swells can transport energy across the basin and shape coastal wave climates far from their generation zones (Alves, 2006). In simple terms, the waves that we see along the Irish west coast are part of large-scale atmospheric systems that occur far out in the NA. These distant weather systems generate swells that carry energy across the ocean and play a major role in shaping Ireland's wave climate. The analysis further confirmed that Ireland's wave climate cannot be fully understood without considering large-scale processes of the NA. This established the first link in the physical chain from atmospheric to coastal processes.

6.2.2 Exploring present and future wave climate around Ireland

After identifying the dominant swell generating regions and recognising the influence of large-scale NA atmospheric processes on the Irish wave climate, the next step was to generate waves from atmospheric forcing and transform the deep-water waves to the nearshore. Thus, a nested wave modelling framework is developed to simulate wave conditions from the deep NA waters to Irish waters.
Extending the analysis to future projections required the use of wind fields from climate models, as they are the only available source of wind projections. However, the coarse-resolution of these models limits their ability to capture the spatio-temporal variability of wind patterns relevant for regional wave generation. Therefore, instead of adopting computationally demanding dynamical downscaling or complex statistical and machine learning approaches, an analogue method was implemented to downscale the MPI-ESM wind data. The surrogate winds generated from the analogue method provided physically consistent and fine-scale wind forcing to drive the nested wave model and aided in

answering the second main research question,

- Is it possible to predict wave climate around Ireland using WAM–SWAN modelling system driven by statistically generated surrogate wind data over multi-year periods representative of climatological scales? What are the projected changes in wave heights under future high-emission climate scenario (SSP5-8.5)?

To answer this, I used a nested modelling framework consisting of WAM models for the NA and the NEA and a high-resolution SWAN model for Irish waters in Chapter 4. The models were driven by surrogate winds generated for both present (2004 to 2023) and future periods (2081 to 2100), providing realistic atmospheric forcing representative of climatological conditions. In addition to wind forcing, the simulations incorporated the effects of sea level and sea ice, not for separate analysis, but to ensure that their physical influence on wave generation and propagation is appropriately represented in the models.

The WAM-SWAN modelling system, driven by surrogate winds, successfully reproduced Ireland's observed wave climate at climatological timescales during the present period, providing a physically credible basis for projecting future wave conditions under the SSP5-8.5 scenario. Surrogate winds generated from ERA data reproduced observed wave statistics (detailed in Section 4.5.3) and captured the variability of climate model outputs (refer Figure A.8 and A.9 which show a similar seasonal pattern) while maintaining physical realism. Furthermore, the surrogate approach provided a computationally efficient alternative to the conventional downscaling methods of wind in wave modelling purposes.

Under the high emission scenario, projected changes in H_s in the NEA domain show strong spatial and seasonal variability. Northern parts of the NEA are projected to experience an increase, particularly in winter (up to 22 cm); while central and southern regions may see a decrease, most pronounced in autumn (up to 26 cm). Local wave height assessments revealed contrasting trends. Southwestern Ireland is projected to experience more calm conditions, while the northwestern area is expected to experience fewer calm conditions and a modest increase in moderate waves. These findings demonstrate that Ireland's future wave climate will not change uniformly but will reflect complex regional patterns.

The projected H_s change in the NEA represents the redistribution of wind energy associated with large-scale atmospheric circulation shifts. The increased wave height in

the northern NEA can be linked to intensified and poleward-shifting NA storm tracks that enhance westerly winds in the northern regions of the domain (Gentile et al., 2023; Pinto et al., 2013). On the other hand, the reduction in H_s in the southern region can be because of the weakening of subtropical pressure gradients (Lemos et al., 2021). Location-specific results further support this pattern: the northwest location is projected to experience fewer calm waves and an increased frequency of moderate to high waves, consistent with the location's exposure to the shifting storm track corridor. Meanwhile, the relative stability of extremes at northwest and southwest locations may reflect compensating regional effects where enhanced storm activity is balanced by local winds or bathymetry influence. These findings align with studies showing that poleward migration of storm activity alters the regional balance between wind-sea generation and swell propagation (Woollings et al., 2012). Overall, the modelling results illustrate how projected changes in the large-scale wind and pressure patterns over the NA can modify the spatial and location-specific distribution of wave heights across the NEA and ultimately influence Ireland.

6.2.3 From deep water to the shoreline: Understanding coastal responses

The large-scale simulations from the previous section capture the oceanographic response to climate forcing. Their relevance to coastal communities depends on how these offshore waves transform as they reach shore. Waves undergo processes such as shoaling, refraction, and breaking, which redistribute their energy across the surf zone. It is these nearshore transformations that finally determine the intensity of coastal hazards such as overtopping and flooding (Lemos et al., 2024). Understanding this translation from offshore to the coast is therefore essential for linking large-scale wave climate projections with real-world coastal impacts and adaptation purposes. Recent studies have shown that the relationship between offshore wave changes and coastal impacts is not linear and is mediated by complex nearshore processes. For example, d'Anna et al. (2025), showed that even if projected deep water wave changes do not directly intensify flooding risks, their indirect effects on nearshore processes, such as mud-bank dynamics, can strongly influence future coastal evolution.

To understand how the offshore wave height variations observed from wave simulations in Chapter 4 impact the coast, I developed a one-dimensional model: SWARM-1D (Shallow Water Wave Run-up Model in 1 Dimension), to answer the final research question,

- How do waves transform in the nearshore surf zone under future conditions, and what are the implications for coastal impacts such as run-up?

SWARM-1D is based on the non-linear shallow water equations. As a case study, SWARM-1D was used to predict coastal wave run-up at Fanore Beach in the west coast of Ireland. Offshore wave conditions from SWAN were taken as boundary input for present and future climates with and without sea level rise.
The extreme value analysis from the SWARM-1D model outputs in Chapter 5 revealed that future offshore wave changes alone produced minimal changes in run-up values. However, when sea level was increased by 0.7 m in future scenario, a clear increase in extreme run-up was observed. A similar trend was also observed in the seasonal exceedance analysis. Under present conditions, hazardous run-up events (exceeding 3.30 m) occur primarily in winter and autumn, with minimal summer occurrences. Future wave changes alone produced only minor shifts in this seasonal pattern. However, incorporating SLR dramatically increased exceedance frequencies across all seasons, with summer experiencing the most striking relative increase, transforming historically low-risk periods into potentially hazardous times of year.
These results highlight the critical importance of considering multiple climate drivers when assessing coastal risk, as the wave changes and SLR have compound effects on shoreline impacts.
The amplification of run-up when sea level was increased in the model simulations arises from fundamental nearshore processes. As sea level rises, waves shoal and break closer to shore, experiencing reduced bottom friction and delayed energy dissipation (Dean and Dalrymple, 2004). This allows long-period waves to retain energy as they approach the beach, leading to greater run-up heights (Arns et al., 2017).
Together, these findings confirm that the integrated multi-scale approach successfully linked large-scale atmospheric forcing with regional wave climate and local coastal impacts, providing a comprehensive framework for understanding Ireland's wave climate and coastal vulnerability under changing climate.

6.3 Thesis contributions

The thesis makes several important contributions to the study of Irish wave climate and to the wider coastal research field.
The first contribution is the swell analysis, which establishes a baseline understanding of Ireland's swell climatology that had not been previously done. This study represents

the first systematic investigation of the influence of NA swells on the Irish coast. The analysis quantified the travel times of remotely generated distant swells to Ireland and provided robust estimates of uncertainty through the use of block bootstrap resampling. A second major contribution is the development of surrogate winds through an analogue-based method. This is an innovative approach in the wave modelling field. The technique preserves the statistical properties of climate model winds while making use of the high spatial and temporal resolution of reanalysis data. It provides a computationally efficient method to generate high-resolution wind fields for driving wave models, thereby reducing the resource demands associated with general downscaling methods.

In addition, the analysis of wave model output in this thesis focuses on the full distribution of wave heights rather than only extreme events. This perspective allowed a more comprehensive characterisation of wave climate variability. By shifting the emphasis from extremes to the broader distribution, the study contributes to a more balanced understanding of how wave climates evolve.

The thesis also contributes an integrated multi-scale modelling framework that connects offshore climate forcing to local coastal impacts. By combining nested WAM and SWAN models with the newly developed SWARM-1D coastal model, the research established a scalable system for translating deep-water waves into shoreline responses. Furthermore, by demonstrating how offshore conditions can be translated into coastal impact assessments, the study provides a template that can be adapted to other coastal regions facing similar risk.

Finally, the research enhances understanding of the drivers of future coastal risk. The extreme value analysis shows that SLR, rather than changes in wave climate alone, is likely to dominate the future extremes of run-up along the Irish coast. The seasonal exceedance analysis further revealed that future hazards are expected to extend into periods that historically carried lower risk, thereby altering the temporal patterns of coastal vulnerability. These findings highlight how climate change will alter not only the magnitude but also the timing of coastal vulnerability around Ireland.

6.4 Beneficiaries of the thesis

The findings of this thesis are highly relevant to a wide range of stakeholders. When most people think of ‘climate’, they usually associate it with the atmospheric factors such as temperature, rainfall, wind or storms (Bramante, 2017). Stocker et al. (2013) defines climate in a narrow sense as the ‘average weather’ typically described through

variables such as temperature, precipitation, and wind. These variables receive most attention because of their immediate and direct influence on daily life.

Less widely recognised, but equally important for coastal regions, is the wave climate. Its variability across seasons to decades strongly affects coastal flooding, erosion and infrastructure exposure (Méndez and Rueda, 2020). Coastal communities benefit most directly from advances in understanding wave climate. In Ireland, where around 50% of the population lives within 15 km of the coast (Devoy, 2009), waves influence daily life as much as atmospheric weather. Large waves can disrupt marine transport, making fishing and ferry operations unsafe, and generate run-up that increases flooding risk (Li et al., 2022a; Bramante, 2017). Improved knowledge of wave run-up, such as that provided by SWARM-1D simulations, can provide critical information for improving early warning systems and disaster preparedness (Huang et al., 2020). At the same time, local systems and national governments can use the results to inform coastal zone management, infrastructure planning and long-term climate change adaptation strategies, especially in vulnerable cities like Galway, Cork, and Dublin.

The offshore renewable energy sector also benefits significantly. Accurate wave conditions including spatial and seasonal variability are essential for the safe operation and maintenance of offshore wind and wave energy installations (Ambarita et al., 2023; O'Connell et al., 2020). Understanding calm windows and high energy periods allows for better scheduling of deployment and repairs, improving safety, and reducing costs. These windows can also be used for planning maritime activities such as shipping and fishing, where the sea conditions play a critical role in operational success and safety.

The insights on swell variability, projected changes in wave climate, and shoreline response support the development of coastal adaptation strategies. This information is particularly important for prioritising coastal protection investments and long-term spatial planning in vulnerable regions. The modelling framework and projections can inform the design and maintenance of coastal defences, ports, and offshore renewable energy facilities, ensuring that these structures remain resilient under changing climate conditions.

From a scientific perspective, this study supports advancements in climate-scale wave modelling by offering a computationally efficient surrogate based approach. It also demonstrates its applications from offshore to nearshore scales. Coastal engineers, planners and researchers can use the methods and datasets developed here to simulate wave-driven impacts under future climate scenarios.

Beyond infrastructure, energy planning and scientific knowledge, this research holds deep societal and emotional significance. Coasts are more than just physical spaces. People

form strong connections with coasts over time, not just because they are inhabitants but the coast offer space for relaxation, beauty and emotional or even spiritual experiences (Hubbard, 2012; Kellert, 2005). However, these emotional ties can be disrupted by environmental degradation. Albrecht et al. (2007) introduced a term "*solastalgia*" to describe the distress people feel when familiar landscapes undergo unwanted changes. Coastal erosion and extreme events can spoil the natural character of coast, eroding not just land but also people's emotional connections. Satariano (2021) highlighted that contact with the sea can promote mental health and therapeutic recovery, underscoring the importance of protecting coastal environments not only for physical safety but also for psychological well-being.

By contributing to better coastal hazard assessment and informing sustainable coastal management under climate change, this thesis indirectly supports the preservation of coastal ecosystems and cultural values. The wave run-up analysis also supports long-term planning to safeguard these socially and emotionally significant spaces. In doing so, this research helps to protect the coast as a shared public space, a source of livelihood, and a place of personal and cultural meaning.

6.5 Overall framework limitation

While limitations specific to each methodological component have been discussed within their respective chapters, it is important to reflect on the constraints of the overall modelling framework, as these shape how the findings should be interpreted and define the boundaries within which the conclusions can be generalised.

The most significant framework level limitation concerns the reliance on a single ensemble member of MPI-ESM under the SSP5-8.5 scenario as the upstream climate forcing. Internal climate variability, the natural, unforced fluctuations within the climate system, means that even under identical emissions forcing, different ensemble members of the same model can produce meaningfully different regional wind and wave patterns. The findings presented here therefore represent one plausible future pathway rather than a definitive projection. Whether the same direction and magnitude of wave climate change would emerge under a different global climate model, or across a broader multi-model ensemble, remains an open question and it also carries practical importance for coastal adaptation planning.

Closely related to this is the cascade of uncertainty that propagates through the multi-scale modelling chain adopted in this thesis. Outputs from the global climate model

inform surrogate wind generation, which forces the regional wave model, whose outputs in turn drive the one-dimensional run-up model. Each step introduces its own sources of uncertainty, in climate model structure, in the analogue selection method, in wave model physics, and in the simplified nearshore representation, and these uncertainties interact and compound in ways that are difficult to fully characterise from a single model configuration. The consequence is that uncertainty in the final run-up projections is likely larger than any individual component suggests in isolation. A multi-model or multi-member ensemble approach applied consistently across the chain would be needed to quantify the uncertainty.

The surrogate wind methodology, while well suited to the relatively stable westerly wind regime of the North East Atlantic, has not been tested against alternative reanalysis products or under scenarios where projected future winds diverge substantially from the historical ERA5 envelope. The robustness of the analogue selection approach therefore remains to be established across a wider range of forcing conditions and ocean basins. Similarly, the swell analysis in Chapter 3 relies on fixed source regions and temporally averaged time series, which may not capture shifts in storm track behaviour or swell generation areas that could emerge under future climate change, meaning that the climatological patterns identified here may evolve in ways the current framework cannot resolve. The wave and run-up simulations focus on a single location and a single high-emission scenario, limiting the generalisability of the quantitative results to other Irish coastal sites or alternative emissions pathways.

Finally, the absence of dynamic tidal forcing and storm surge coupling across the wave and run-up simulations introduces uncertainty in the magnitude of projected coastal impacts. This is particularly important when extreme events where tidal phase and surge contribute meaningfully to total water level. These simplifications were necessary given the computational scope of the study, but they define an important boundary on the precision of the nearshore projections.

Taken together, these framework-level limitations do not undermine the core conclusions of the thesis. The approach provides a physically coherent and computationally tractable pathway from large-scale climate forcing to local coastal wave impacts. However, robustness testing against alternative climate models, ensemble spread, and additional coastal sites remains a priority before the framework is adopted with confidence for operational coastal planning or engineering design.

6.6 Future directions

While the study achieved its primary objectives, the limitations acknowledged across each chapter and at the overall framework level highlight clear directions for future research. The following recommendations are offered to guide work that builds on this thesis. In terms of extending the swell analysis, future work could:

- Incorporate directional wave spectra and energy-based parameters into the correlation framework, moving beyond swell period alone and enabling direct linkage to energy flux and coastal hazard assessments.
- Allow source regions to be defined dynamically rather than as fixed boxes, so that shifts in storm track and swell generation areas associated with climate variability can be captured.
- Examine teleconnections between swell variability and large-scale atmospheric modes, particularly the North Atlantic Oscillation, using longer observational records or reanalysis ensembles.
- Validate statistically estimated lag times against observed buoy records or spectral tracking methods to establish the physical accuracy of the propagation signals identified.

Regarding the wave projection framework, priority areas include:

- Applying the surrogate wind methodology with multiple reanalysis products to assess sensitivity to the choice of historical wind source, and testing robustness under alternative emissions scenarios such as SSP2-4.5.
- Extending to a multi-model or large ensemble configuration to quantify the range of uncertainty in projected wave climate changes and to place the findings in the context of a wider spread of climate model responses.
- Coupling the wave modelling framework with regional ocean and atmospheric models to allow a more physically consistent treatment of wave-atmosphere-ocean interactions, which would improve the realism of future projections at the cost of greater computational demand.

For the coastal run-up model, the most valuable next steps would be:

- Extending SWARM-1D to other sandy beach sites around Ireland to test the generalisability of the projections and, where field observations are available, to validate the model against measured run-up.
- Incorporating sub-daily wave forcing, dynamic storm surge, and tidal modulation to capture peak storm conditions that are smoothed by the current daily mean boundary approach.
- Testing multiple sea level rise scenarios to define the full coastal risk envelope rather than a single future state, and expanding the framework into two or three dimensions to resolve longshore variability and morphodynamic feedbacks at more complex coastal sites.

At a broader level, future work should also address two wider priorities: conducting a formal uncertainty analysis using multi-model and multi-member ensembles to quantify how uncertainty accumulates across each step of the modelling chain, and linking wave climate projections with socio-economic exposure data to translate the physical findings into actionable guidance for coastal adaptation planning.

6.7 Final reflections

This thesis has demonstrated that Ireland's wave climate is strongly shaped by North Atlantic swells and is likely to undergo significant changes under future climate scenarios. By integrating statistical methods, surrogate data generation, and multi-scale modelling, it has bridged the gap between large-scale climate drivers and local coastal impacts. This integrated ocean-to-regional-to-coast approach demonstrates that Ireland's coastal hazards are closely connected to large-scale North Atlantic processes and local changes. Future changes in storm tracks, wind fields, and sea level rise will act together to reshape the spatial and temporal patterns of coastal vulnerability. This further reinforces the need for multi-scale approaches that couple atmospheric, oceanic, and coastal processes in both scientific research and practical adaptation strategies. The methodological advances and findings contribute to both scientific understanding and practical coastal risk assessment. As climate change continues to reshape oceanic and atmospheric systems, approaches of this kind will be essential in guiding the sustainable management of vulnerable coastlines.

APPENDIX A

Appendix

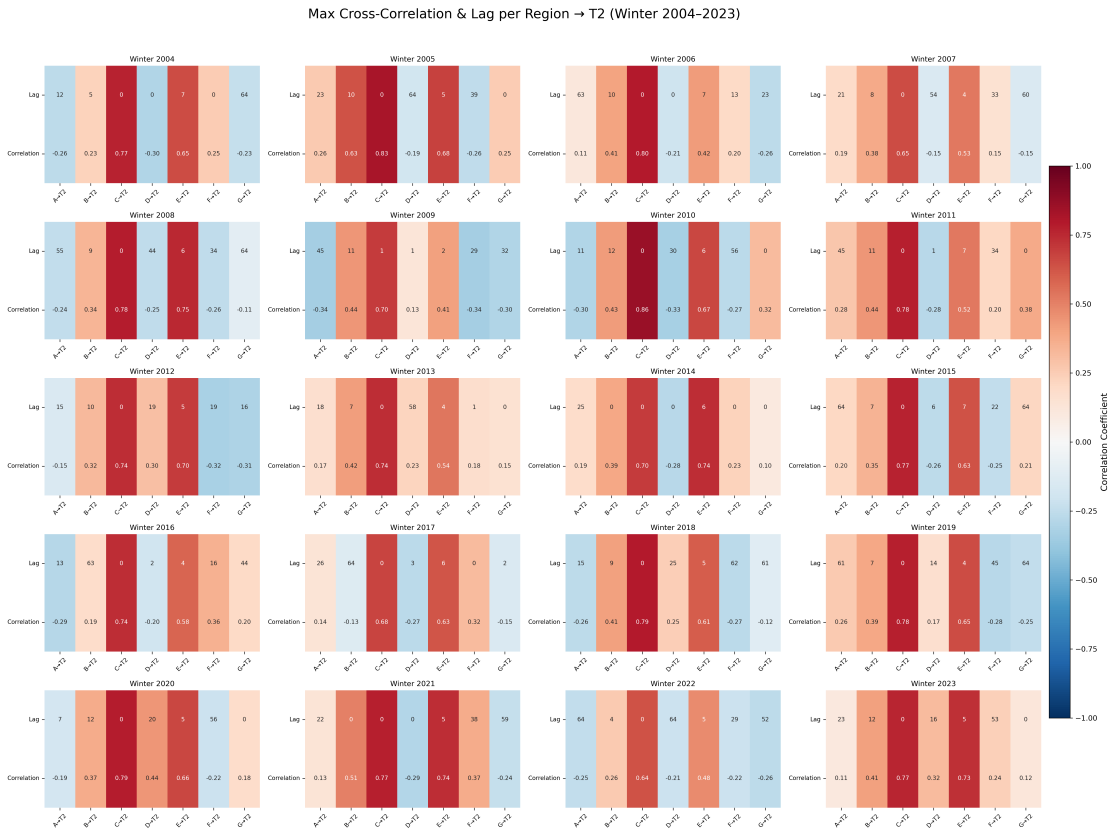

Figure A.1: Summary of lag at which maximum correlation occurred between source and target and the corresponding correlation values for Winter

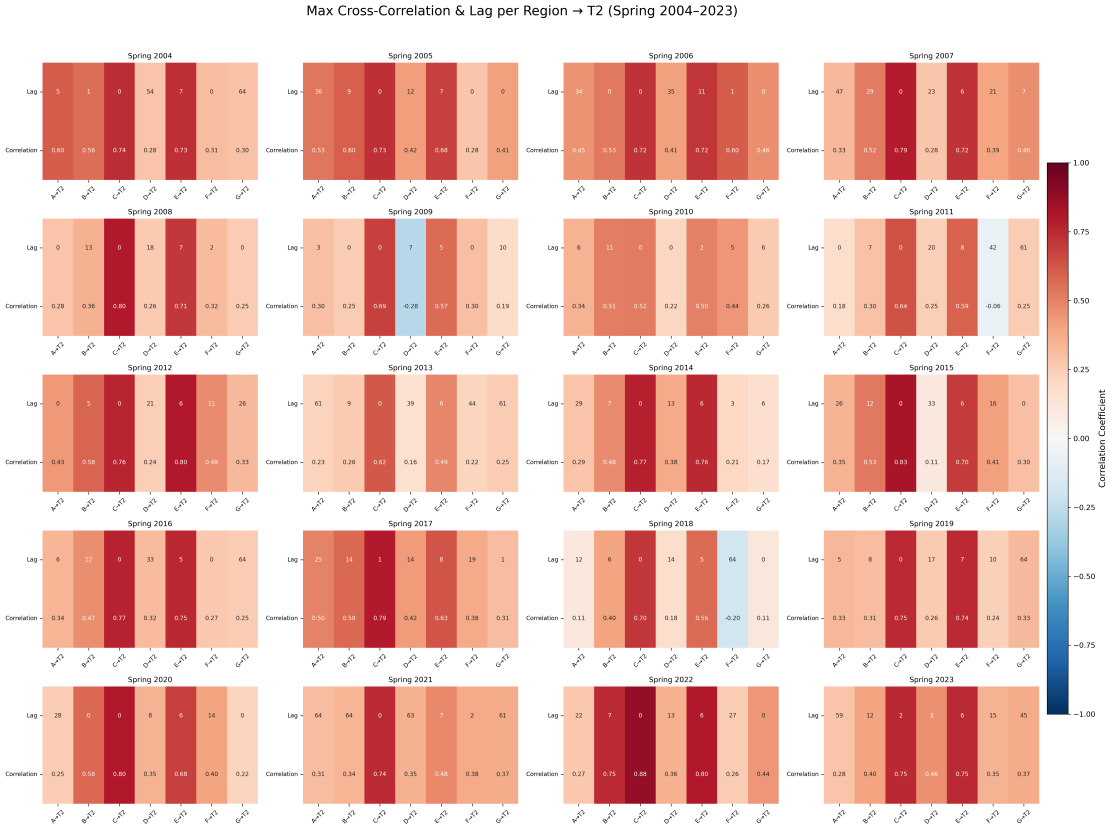

Figure A.2: Summary of lag at which maximum correlation occurred between source and target and the corresponding correlation values for Spring

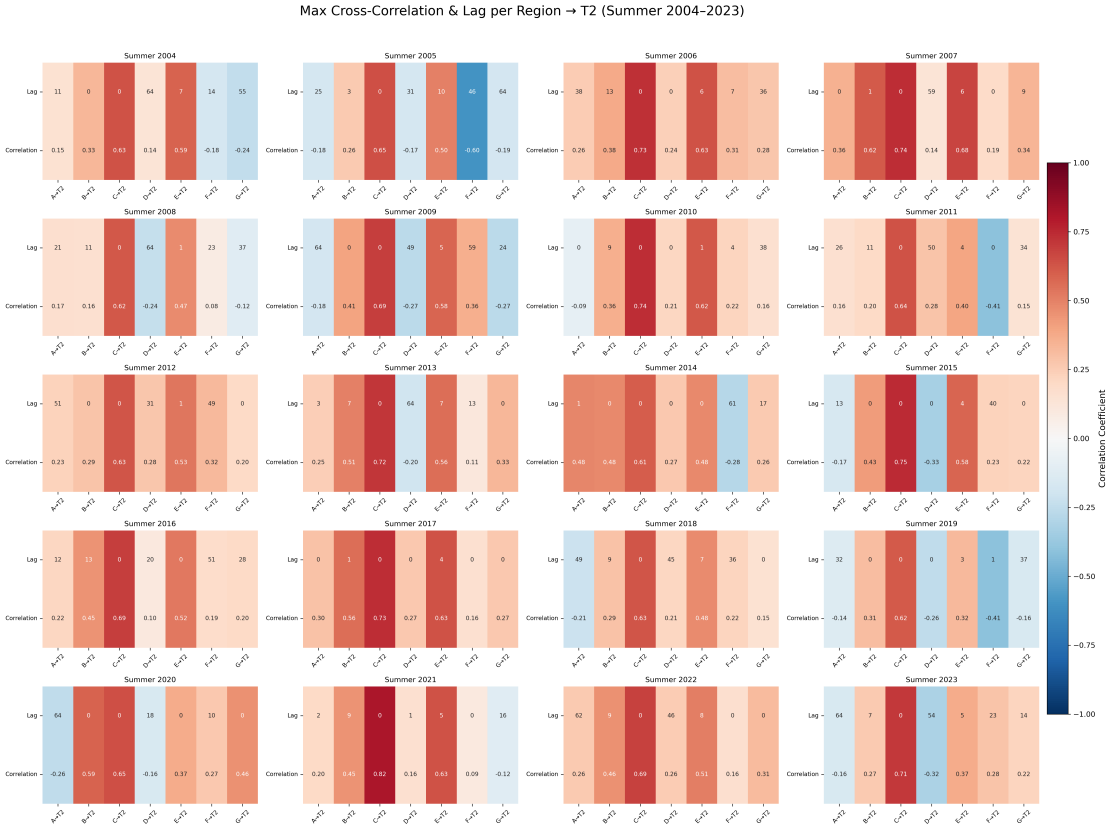

Figure A.3: Summary of lag at which maximum correlation occurred between source and target and the corresponding correlation values for Summer

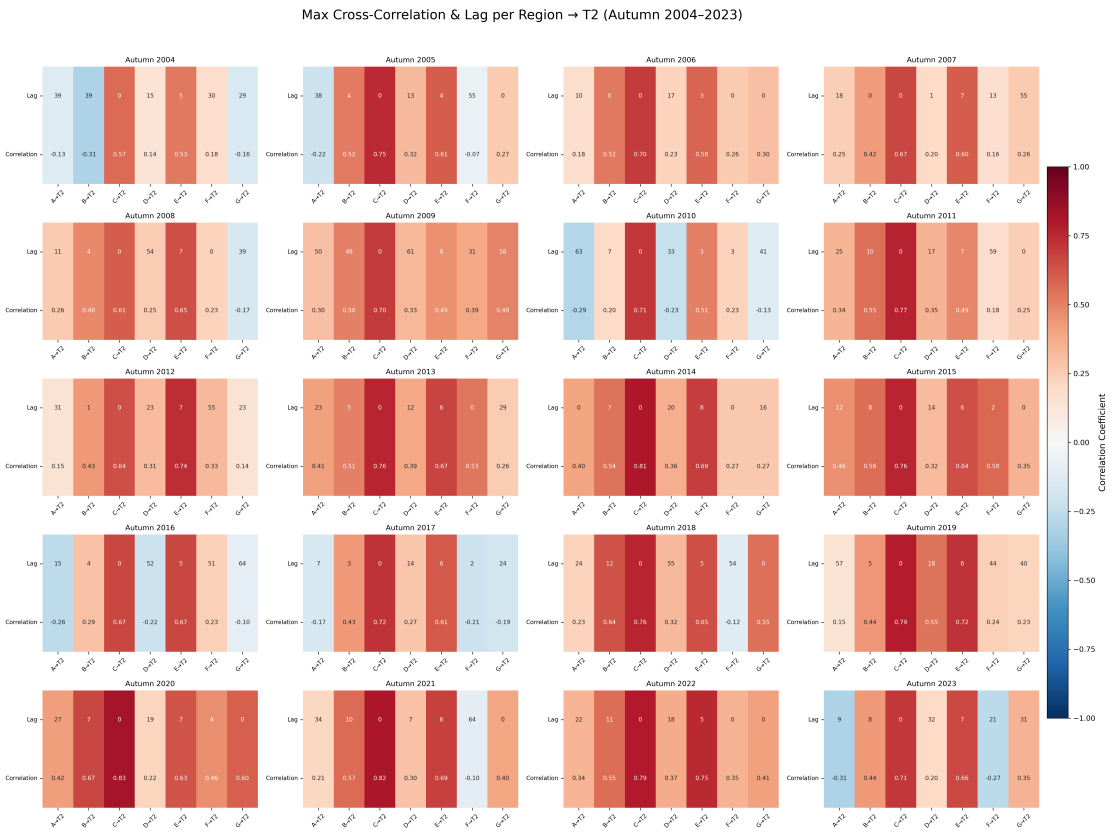

Figure A.4: Summary of lag at which maximum correlation occurred between source and target and the corresponding correlation values for Autumn

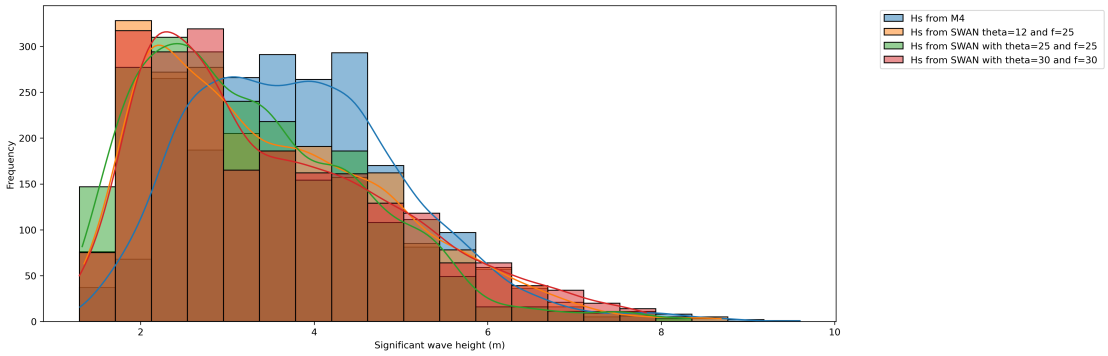

Figure A.5: Sensitivity of significant wave height (H_s) distributions from SWAN to directional and frequency resolution, compared against Hs observations from buoy M4. Three SWAN configurations are tested: 12 directional bins with 25 frequency bins ($\theta = 12, f = 25$); 25 directional bins with 25 frequency bins ($\theta = 25, f = 25$); and 30 directional bins with 30 frequency bins ($\theta = 30, f = 30$)

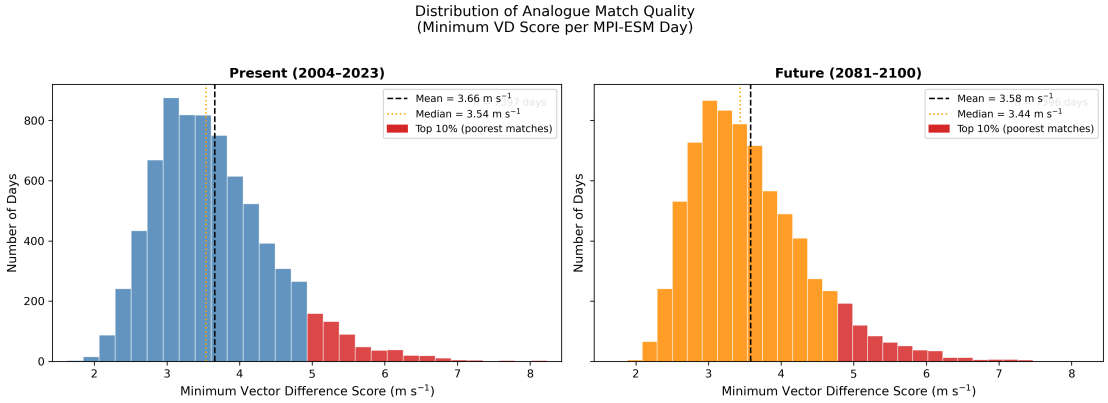

Figure A.6: Distribution of minimum Vector Difference (VD) scores for analogue selections across the present (2004-2023, blue) and future (2081-2100, orange) periods. Red bars indicate the top 10% of poorest matches. Dashed and dotted lines show the mean and median respectively.

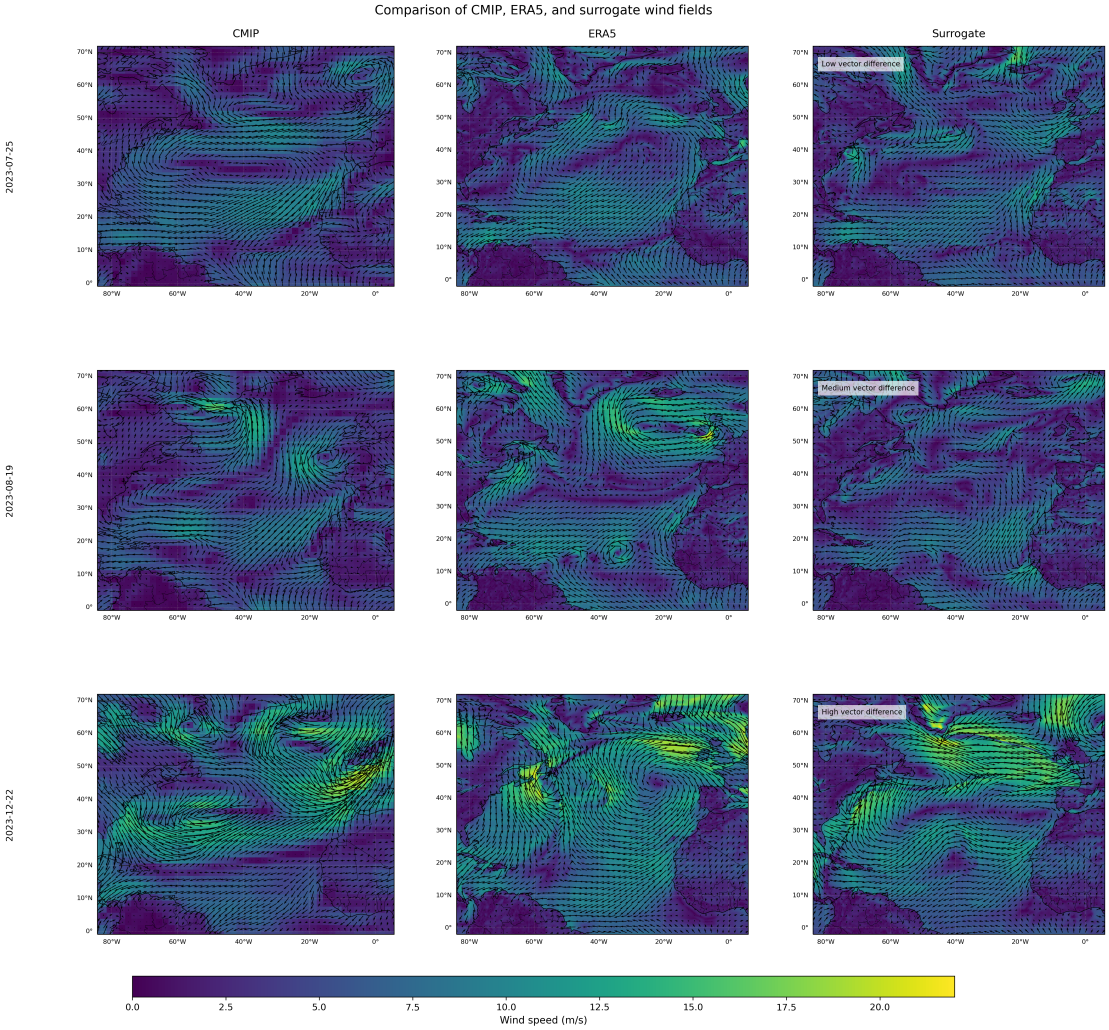

Figure A.7: Comparison of MPI-ESM (CMIP), ERA5 and surrogate wind fields for three example days representing different analogue match qualities. Top row: low VD score (2.4 m/s), MPI-ESM day 2023-07-25, best ERA5 analogue from 2009-07-24. Middle row: medium VD score (3.5 m/s), MPI-ESM day 2023-08-19, best ERA5 analogue from 2022-08-13. Bottom row: high VD score (7.9 m/s), MPI-ESM day 2023-12-22, best ERA5 analogue from 2017-12-10. Wind speed (m/s) and direction (arrows) are shown across the North Atlantic domain. Despite the range of VD scores, the surrogate wind fields successfully reproduce the dominant large-scale circulation patterns of MPI-ESM across all three cases, confirming the robustness of the analogue selection method.

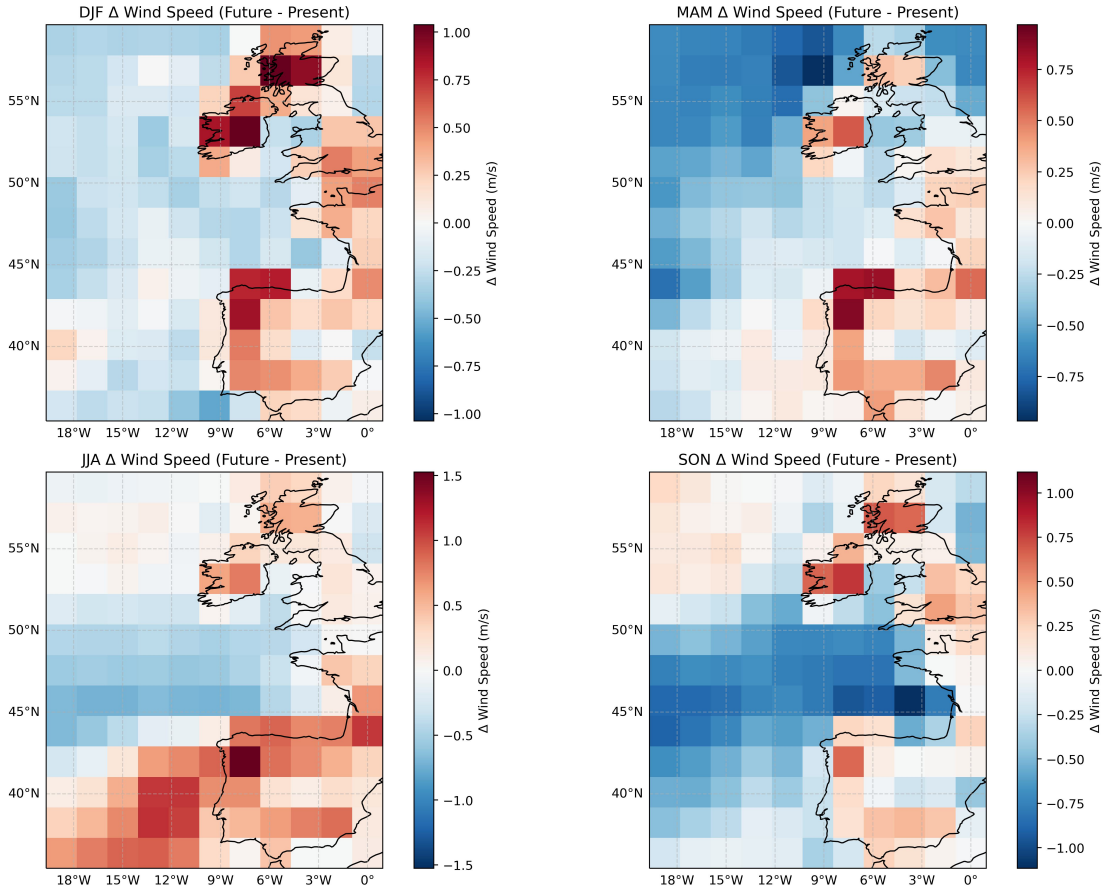

Figure A.8: Seasonal differences in 10 m wind speed (future: 2081–2100 minus present: 2004–2023) from MPI-ESM for the Northeast Atlantic. Positive values (red) indicate stronger winds in the future, while negative values (blue) indicate weaker winds.

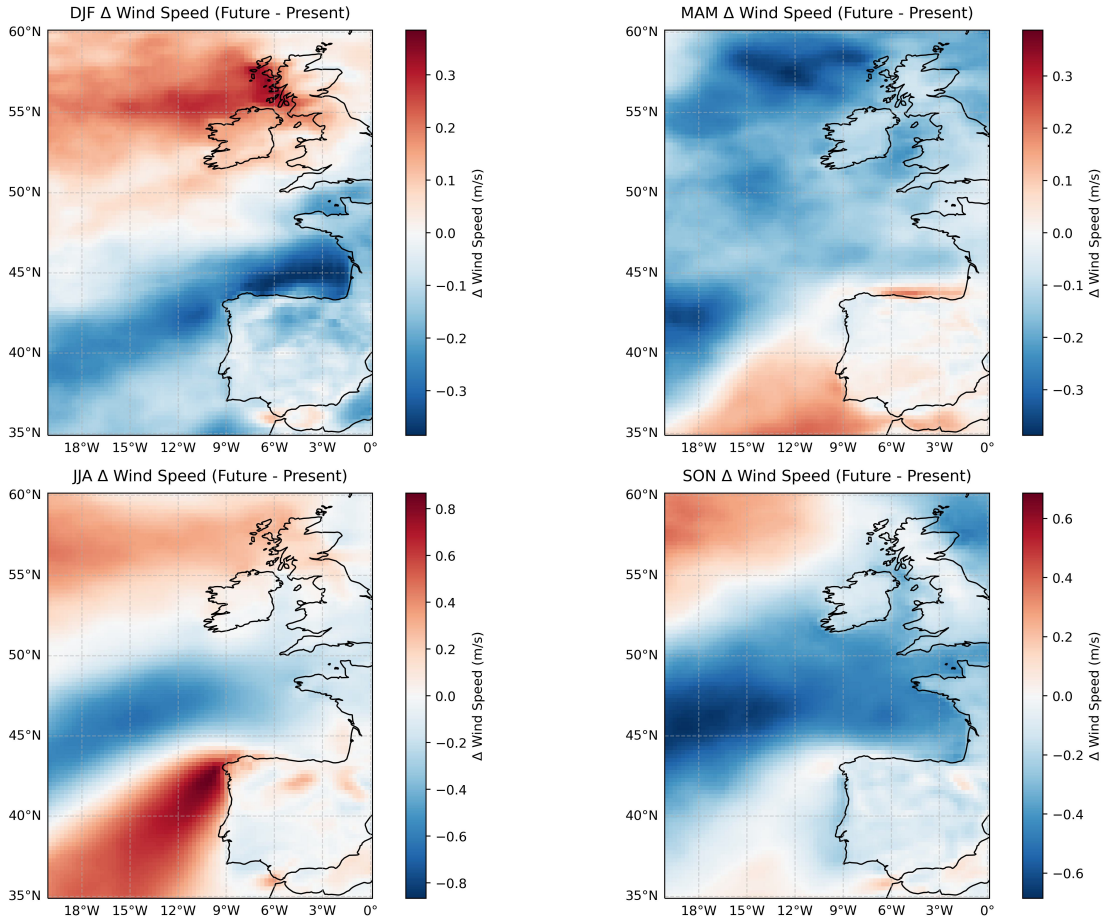

Figure A.9: Seasonal differences in 10 m wind speed (future: 2081–2100 minus present: 2004–2023) from surrogate data for the Northeast Atlantic. Positive values (red) indicate stronger winds in the future, while negative values (blue) indicate weaker winds.

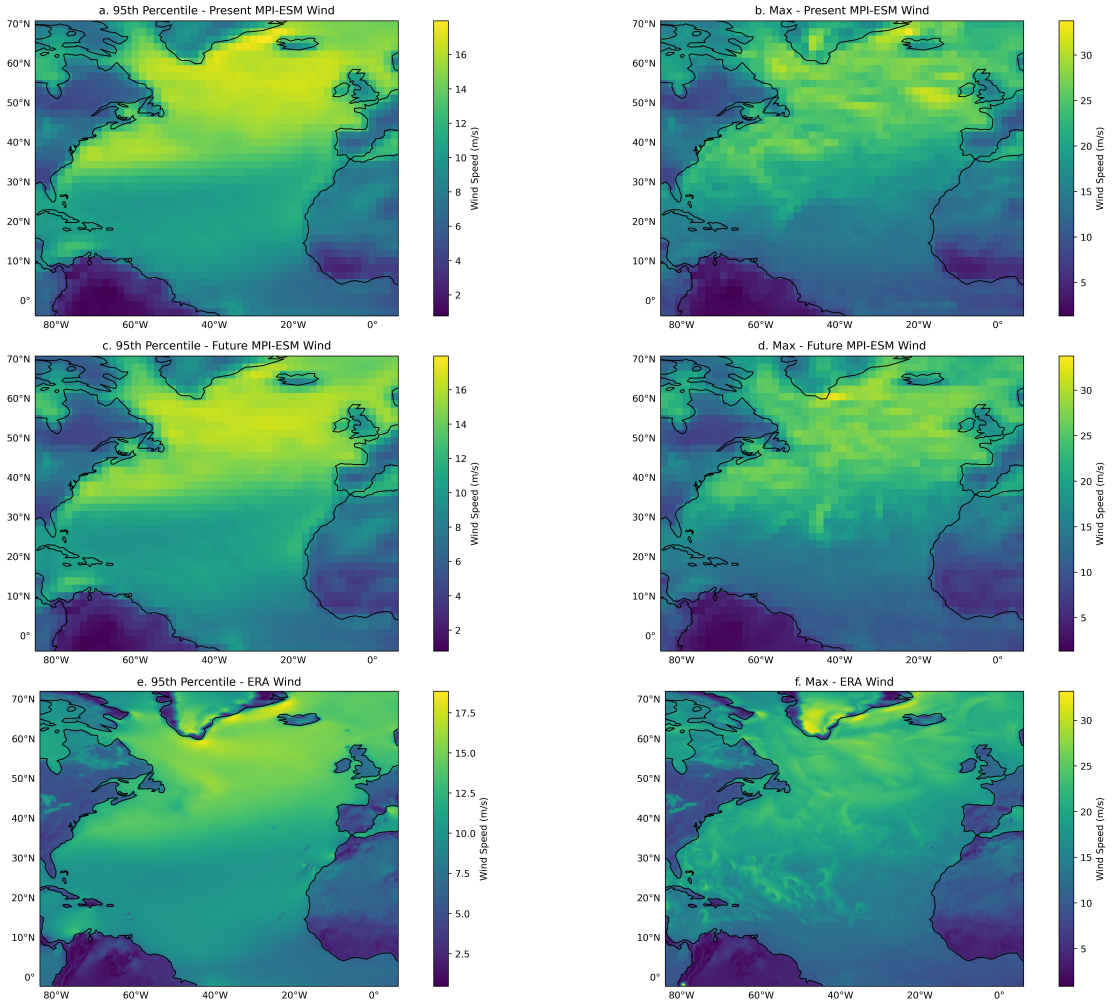

Figure A.10: Extreme wind statistics from ERA5 (historical) and MPI-ESM (present and future).

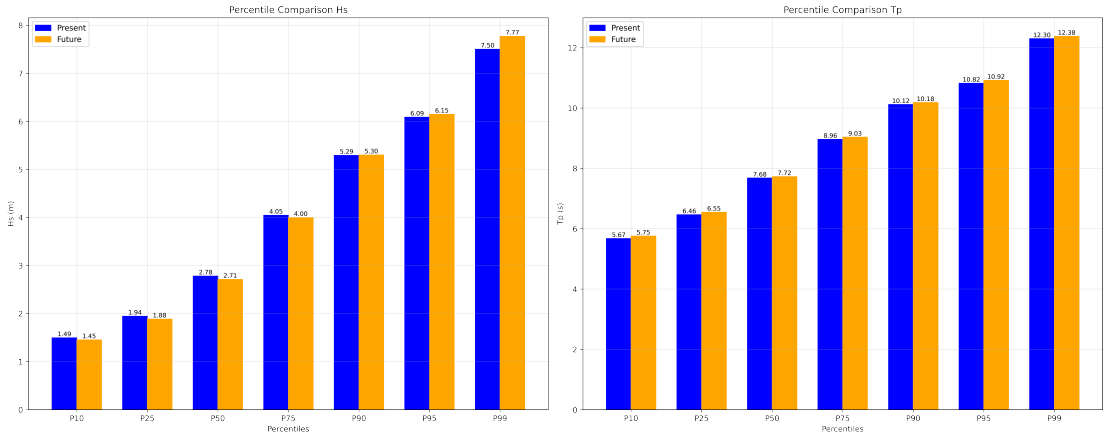

Figure A.11: Percentile distribution of Significant wave height (H_s) and peak period (T_p) at the offshore boundary location near the entrance to Galway Bay, for present (blue) and future (orange) conditions. Percentiles indicate the proportion of values below a given threshold (e.g., P_{10} = 1.49m for H_s means that 10% pf wave heights are below 1.49m, while 90% are higher). The close alignment of present and future values across all percentiles show that the offshore wave conditions at selected location change very little under future climate projections.

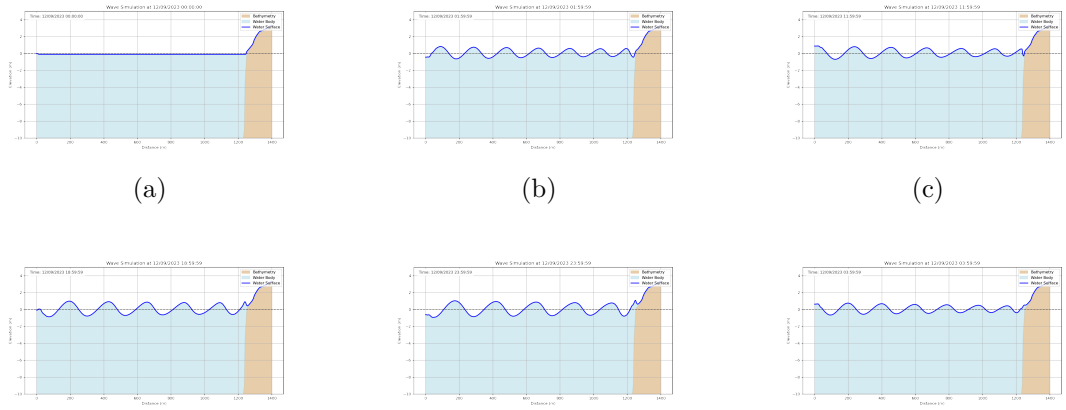

(a) (b) (c)

(d) (e) (f)

Figure A.12: Illustration of wave propagation and run-up simulated with SWARM-1D at successive time steps. (a) initial condition, (b) wave propagation begins with noticeable transformation near the coast, (c) wave steepening as it shoals in shallow water, and (d–e) wave run-up onto the beach. The sequence demonstrates that SWARM-1D reproduces the fundamental physics of wave propagation, shoaling, and run-up.

Maynooth University
National University of Ireland Maynooth

Maynooth University
Department of Geography

This form is to accompany the submission of a PhD that contains research reported in published or unpublished work. **Please include one copy of this form for each co-authored work.** This form along with the published work should, under normal circumstances, appear in an Appendix.

Authorship Declaration Form

Publication Details:

Thesis Chapter/Pages	Chapter 4
Publication title	Wave projections for Northeast Atlantic using High Resolution Surrogate winds.
Publication status	Submitted (Under Review/Preprint)
Type of publication	Journal
Publication citation	Ashly Kalayil Uthaman, Tomasz Dabrowski, Gerard Daniel McCarthy, et al. Wave Projections for the Northeast Atlantic using High Resolution Surrogate winds. *ESS Open Archive* . March 18, 2025. DOI: 10.22541/essoar.174231789.91051332/v1

Nature/extent of my contribution to the work detailed above is as follows:

Nature/Extent of Contribution	**Lead author**
For this paper, I contributed to the conceptualization and design of the study, performed the model simulations, conducted the analysis of model outputs, and writing the manuscript.	☐ Yes ✓ ☐ No

The following co-authors contributed to the work (all contributing co-authors):

Name	**Nature of contribution**
Tomasz Dabrowski	Concept and design, proof reading, edits to original text.
Gerard McCarthy	Concept and design, proof reading, edits to original text.
André Düsterhus	Concept and design, proof reading, edits to original text.

The undersigned hereby certify that the above declaration correctly reflects the nature and extent of the student's and co-author's contribution to this work

	Name	**Signature**	**Date**
Student	Ashly Kalayil Uthaman		**07/10/2025**
Co-author 1	Tomasz Dabrowski	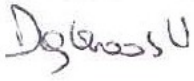	**10/10/2025**

Co-author 2	Gerard McCarthy		**8/10/2025**
Co-author 3	André Düsterhus		**09/10/2025**

Wave Projections for the Northeast Atlantic using High Resolution Surrogate winds

Ashly Kalayil Uthaman[1],Tomasz Dabrowski[2,], Gerard D. McCarthy[1], and André Düsterhus[1,3*]

[1]Irish Climate Analysis and Research Units (ICARUS), Department of Geography, Maynooth University, Maynooth, Ireland
[2]Ocean Science and Information Services Marine Institute Headquarters, Galway, Ireland
[3]National Centre for Climate Research (NCKF), Danish Meteorological Institute, Copenhagen, Denmark

Key Points:

- We developed a statistical-dynamical modelling framework to investigate wave climate in the North Atlantic.
- An analogue method is employed to generate high resolution surrogates as wind boundary condition
- Wave height distribution shows seasonal trends, with future wave activity increasing in all seasons except autumn along Ireland's west coast

*Now at Danish Meteorological Institute, Denmark.

Corresponding author: Ashly Kalayil Uthaman, ashly.uthaman.2022@mumail.ie

Abstract

Understanding projected changes in wave heights influenced by climate-driven factors, such as wind, sea ice, and sea level are essential for mitigating risks and ensuring sustainable use of marine and coastal resources, especially in a highly energetic wave region like the Northeast Atlantic (NEA). With a particular focus on Ireland, wave climate in Northeast Atlantic region is investigated using wave models, WAM (WAve Model) and SWAN (Simulating WAves Nearshore). These are driven by high-resolution surrogate winds, incorporating sea ice and sea level as additional inputs. The surrogate wind data is created by an analogue method using high-resolution wind data of the ECMWF atmospheric reanalysis dataset to downscale data from the low-resolution Max-Planck Institute of Earth System Model (MPI-ESM-LR). This statistical approach provide computationally efficient and reliable wind inputs for wave modelling while capturing the temporal and spatial variability of present and future wind patterns.

While the spatial distribution of significant wave height differences shows a north-south gradient, with an increase in the northern Northeast Atlantic and decrease in the south, regional variability is evident. Seasonal analysis indicate pronounced increases in wave heights during winter and summer, with the largest decrease observed in autumn. This study demonstrates the efficiency of surrogate wind data for downscaling climate model outputs to support nearshore wave modelling. The findings underscore the importance of considering both regional and seasonal variability in wave climate assessments for proper coastal planning and adaptation strategies under changing climatic conditions.

Plain Language Summary

Deeper insights on how waves behave are necessary for coastal communities, maritime activities and climate adaptation planning. Our study investigates wave height changes in the Northeast Atlantic under the influence of climate driven factors like wind, sea level, and sea ice. Accurate representation of wind fields are necessary for wave simulations. We address the limitation of coarse resolution wind data from climate models for wave modelling, by implementing a method of generating high resolution surrogates from observations. Surrogates are data behaving similar to original dataset. For the current study we are using high resolution fifth generation atmospheric reanalysis data as reference for generating surrogates for wind from a climate model.

While overall wave heights are projected to increase in the northern NEA, it's important to carefully assess local variations. Instead of focusing only on extreme waves or specific events, our study looks at the full distribution of wave heights, offering valuable insights for better planning and adaptation strategies. For instance, some seasons may offer calmer and more stable conditions that are suitable for marine activities, while others see rise in more high waves, depending on the location.

1 Introduction

Wind-generated surface waves are a significant renewable energy source (Farrok et al., 2024), and are important for many coastal processes, including erosion (Palermo et al., 2024; Scott et al., 2019) and the modulation of local trends of sea level (Dodet et al., 2019; Melet et al., 2018; Vousdoukas et al., 2017). This interaction between the wind and ocean surface wave is a fundamental component of the Earth system, with significant implications for climate modeling, coastal processes, and marine operations. These waves are not just surface phenomena but critical components of complex Earth system interactions, influencing everything from marine ecosystem to global climate patterns (Cavaleri et al., 2012). Understanding wave climate variability is particularly important in dynamic regions like the Northeast Atlantic (NEA), where the wave climate is significantly influenced by atmospheric patterns (Morales-Márquez et al., 2020), climate change and sea-

sonal patterns (Bitner-Gregersen et al., 2022; Morales-Márquez et al., 2020; Markina et al., 2019).

In addition to the broader climatic importance, ocean waves have significant societal implications for coastal regions. This is particularly relevant for Ireland, where the coastline is directly exposed to energetic North Atlantic wave conditions (Tiron et al., 2013). During storm events, high energy waves can accelerate coastal erosion and contribute to overtopping of coastal defences, with flooding further exacerbated by storm surges that pose a major risk to low lying regions in terms of economic damage and casualties (Paranunzio et al., 2022). For example, during the exceptionally stormy winter of 2013-2014, a sequence of intense storms caused widespread coastal erosion and infrastructure damage exceeding €110 million along the south and west coasts of Ireland (Kandrot et al., 2016). More recently, during Storm Éowyn in January 2025, Galway city narrowly avoided severe flooding when a 2.6m storm surge coincided with mid-tide conditions, highlighting vulnerability of Irish coastlines (Madden et al., 2025). Furthermore, the economic implications of coastal flooding are expected to increase substantially under future sea level rise scenarios. De Bruin and Kyei (2024) estimate that without additional mitigation measures, the cost of a 0.56 m sea level rise is projected to reach approximately €3 billion by 2100 in Ireland, with potential GDP losses of up to 2.6 % by 2030 in the absence of adaptation measures (De Bruin & Kyei, 2024). These costs are further compounded when extreme waves coincide with storm surges and elevated sea levels. Robust projections of future wave climates are therefore essential for coastal flood risk assessment and long-term adaptation planning.

The general concept of wave generation, propagation, and the transition from the deep ocean to the coastal environment involves downscaling the wave processes from the oceanic scale to the regional and coastal scales. Various state-of-the-art wave models such as WAM (WAve Model; WAMdi Group, 1988), WW3 (WaveWatchIII; Tolman, 1989), and SWAN (Simulating WAves Nearshore; Booij et al., 1999) are implemented on nested grids to achieve fine-resolution wave simulation. For instance, Brown et al. (2010) and Pilar et al. (2008) effectively demonstrated that a North Atlantic (NA) domain, when used with a nested WAM model, is sufficient to capture swells influencing wave conditions in the NEA. In contrast, Calvino et al. (2022) employed a nested WW3 model with larger outer domain covering the entire Atlantic to investigate the large scale processes, such as NA current, on wave propagation.

WAM considers problems on oceanic scales and it uses the explicit schemes in space so that it requires small grid size in shallow water, thus making it unsuitable to coastal applications (Bingölbali et al., 2019). SWAN, specifically designed for shallow water processes, is more suitable to simulate wave conditions nearshore in NEA (Neill, 2024; Zed et al., 2022; Anton & Nash, 2020; Guisado-Pintado, 2020; Reduan Atan & Goggins, 2017; Atan et al., 2016; Bento et al., 2016; Bento. et al., 2011) Nesting SWAN within large - scale models such as WAM and WW3 is a common practice. Swain et al. (2019) demonstrated that SWAN hindcasts using WAM boundary conditions generally showed a 5–15% error compared to deep-water models, yet provided more reliable nearshore wave predictions at buoy locations in the North Indian Ocean, compared to SWAN hindcasts using WW3 boundary conditions. Additionally, the nested WAM-SWAN approach by Lalbeharry and Ritchie (2009) demonstrated that coarse grid (0.5°) WAM outputs can provide effective boundary conditions for SWAN, enabling accurate simulation of wave transformation from deep to shallow waters. These studies collectively support the nesting approach employed in the present study, which uses WAM and SWAN to capture the full wave spectrum, from the swell generation in the open ocean to the wave transformation in shallow coastal waters.

Accurate wave predictions rely heavily on high-resolution wind forcing, as wind serves as the primary mechanism for wave generation (Barbariol et al., 2022; Baordo et al., 2020). The generation of such high resolution wind data at regional scales typically involves downscaling techniques. Dynamical downscaling employs atmospheric models to enhance the spatial and temporal resolution of wind fields, providing more robust solutions for wave

modelling. For instance, Markina et al. (2018), utilized the WRF model to downscale wind fields in the NA, achieving a 14 km resolution to improve wave prediction accuracy in this region. Similarly, HARMONIE meso-scale model was used to dynamically downscale ERA-Interim reanalysis data to 2.5 km resolution for wave hindcasts in Ireland (Gallagher, Tiron, et al., 2016). In Galway bay (west coast of Ireland), regional weather model, WRF, provided atmospheric forcing for SWAN, further demonstrating the effectiveness of localized wind inputs for wave simulations (Ana Rute Bento & Soares, 2018). While these dynamical approaches significantly enhance the accuracy of wave predictions, their computational demands and resource intensity is still a challenge. On the other hand, statistical downscaling methods have been widely utilised to refine coarse global climate model (GCM) outputs for wave studies. For instance, Weibull based downscaling techniques (Alizadeh et al., 2020) and multi step statistical algorithms (Towe et al., 2017) have been applied to improve wind fields for wave climate analysis in the Persian Gulf and the North Sea. However, statistical downscaling often assumes stationary relationships between large scale predictors and local scale predictands, which may limit its applicability under changing climate conditions (Alizadeh et al., 2020).

This paper aims to overcome the limitations associated with low-resolution climate model data and the challenges in downscaling methods by using wind data for wave modelling. For this we implement an analogue approach to generate surrogate wind data for the MPI-ESM (Max Plank Institute of Earth System Model) climate model, utilising high resolution ERA5 reanalysis data. The surrogate wind data is used to drive SWAN and WAM wave models in the NEA, with a particular emphasis on Ireland, to explore the wave dynamics for present and future. This approach aims to provide a computationally efficient and accurate framework for studying wave climate variability in dynamic and high-energy coastal regions.

The paper begins with the introduction of the NEA, the primary area of interest (Section 2). To analyse the behavior of waves in this area, wave models are driven by regionally appropriate input data(Section 3). A key aspect of this research is the generation of surrogate wind data to ensure high resolution wind for wave models (Section 4). The performance of the model is assessed by comparing model results with observational data and sensitivity analyses (Section 5). From this foundation, the research examines the projections of waves both spatially and seasonally with a specific focus on the west coast of Ireland (Section 6). The results are then fully discussed with implications and limitations in Section 7.

2 Study region

The wind-wave dynamics of NEA are driven predominantly by westerly and south westerly winds blowing over the NA ocean (Gleeson et al., 2019; Gallagher et al., 2014; Bertin et al., 2013). Figure 1(a) illustrates the mean ERA5 wind speed and direction for 2018 for the NA domain, highlighting that most of the wind in the NEA (shown in the red box), particularly around Ireland, is predominantly westerlies. NA swells influenced by wind patterns and mid-latitude cyclones, significantly affect the wave climate around Ireland (Loureiro & Cooper, 2019; Gallagher, Gleeson, et al., 2016a). These swells propagates eastward play a critical role in shaping nearshore wave characteristics of Ireland, including significant wave heights and the occurence of extreme wave events (Gallagher, Gleeson, et al., 2016b). Analysis of nearshore waves during major storm events in 2015 - 2017 highlights how these swells contribute to high energy waves in NEA, particularly along Ireland's Atlantic coast (Fedele et al., 2019). These waves are further influenced by the complex geomorphology of the Irish coast (O'Brien et al., 2013) and climate phenomena such as the North Atlantic Oscillation (NAO). During positive NAO phase, stronger westerly winds intensify wave heights and increase the frequency of storm events making the region highly energetic and dynamic (Dodet et al., 2010). Projections using global climate models such as EC-Earth, indicate a potential decrease in wind speeds over NA by upto 3.5% by the end of the century, which may reduce swell generation and signif-

icant wave heights near Ireland (upto 15% in some seasons; Gallagher, Gleeson, et al., 2016a). Similarly, WW3 model predicts decline in both mean and extreme wave heights, with the most pronounced reductions occuring in winter and summer around Ireland (Gallagher, Gleeson, et al., 2016b). Despite these projected decreases, the variability in wave conditions remains significant. This is due to the regions sensitivity to NAO phase and interactions between local wind patterns and the Irish coastlines geomorphology. The western Irish coast, directly exposed to NA weather systems, experiences a wave climate dominated by long-period swells superimposed with locally generated wind waves (Gaughan & Fitzgerald, 2020). This combination, along with the influence of climatic drivers and the extensive fetch of the Atlantic, underscores the importance for understanding wave climate dynamics in the region and its implications for natural and socio-economic systems, particularly in the context of future climate change.

3 Wave Model and Data

3.1 WAM Model

WAM (Günther et al., 1992) is a third generation model that describes the evolution of wave spectrum by solving wave energy equation. WAM, which is used here with its latest version Cycle 6, is an open-source code developed by the WAMD Group and maintained by the German Institute HZG (Helmholtz-Zentrum Geesthacht; Baordo et al., 2020).

A domain covering the entire NA was chosen to capture the swell waves generated in mid-latitudes. The WAM model, with a spatial resolution of $1.0^\circ \times 1.0^\circ$ (WAM1.0NA), simulates large-scale wave generation and propagation across the Atlantic basin (refer Figure 1.b). This model serves as the outer boundary for subsequent nested models, enabling the transition of oceanic waves into more detailed regional and coastal simulations. Daily sea ice concentration was incorporated into WAM1.0NA simulations. As highlighted by Tuomi et al. (2019), the choice of sea ice data source significantly influences the results, irrespective of the method employed. For current model setup, grid points with an ice concentration exceeding 30% were excluded from model computations. To provide higher-resolution boundary conditions for coastal modelling, one way nesting technique is applied in the WAM model. A finer-resolution WAM model with spatial resolution of 0.5° (WAM0.5NEA) was set up for the NEA, refining the wave field for regional analysis (black box in Figure 1.b represents the WAM0.5NEA domain). This domain covers the waters surrounding Ireland and accounts for the wave transformations that occur as waves propagate from the deeper NA towards the continental shelf. Wave boundary conditions for this domain are supplied by the coarser NA WAM model. However, sea ice was excluded from the WAM0.5NEA simulations, as it was observed only in the Northwest Atlantic, outside the primary domain of interest.

Both WAM models were implemented with 12 directional bins and 25 frequency bands, with the energy balance equation integrated using a propagation time step of 10 minutes. The lowest frequency resolved is 0.0418 Hz and all other settings were kept to default values. The WAM model simulations were conducted using default ECMWF Cycle 45R1 physics for input and open ocean dissipation (IPHYS set to 0). Wave breaking (BREAK) and the Phillips source function (PHILL) were both set to 0 as the focus was on large-scale wave simulations, these process are less critical. Depth scaling of the source function (ISLN) was set to 0 making it suitable for deep water conditions (Janssen & Bidlot, 2003).

3.2 SWAN Model

Another third-generation spectral wave model SWAN is used to simulate wave climates around Ireland. Though WAM and SWAN have the same scientific principle, SWAN has some additional formulation for shallow water simulations (Lemos et al., 2023; Rusu

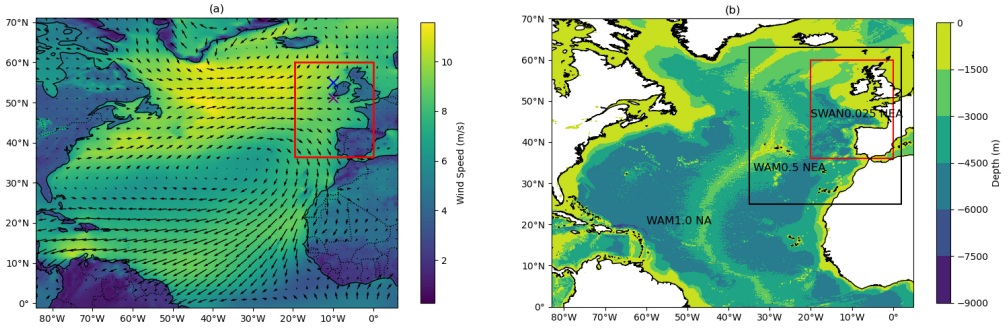

Figure 1. a. Study region in the North Atlantic, illustrating the mean wind speed (color shading) and direction (black arrows) for 2018 based on ERA5 data. The red box highlights the main area of interest of this study. The blue cross denotes the location of the M4 buoy, while the purple cross represents the M3 buoy. b. Spatial map of the model domains used in the study. The entire domain represents the WAM1.0NA (North Atlantic) domain, with the black box representing WAM0.5NEA (Northeast Atlantic) domain and the red box representing SWAN0.025 domain. The color shading shows GEBCO bathymetry for the entire region, highlighting variations in seafloor depth.

et al., 2008). SWAN Cycle III 41.45 version is used to set up the regional model for NEA. The current method uses one-way nesting, where WAM0.5NEA model provides wave boundary conditions to the finer SWAN model. This ensures that large-scale wave processes are accurately represented in the coastal model, allowing the high-resolution SWAN model to simulate local wave conditions without feedback loops that would increase computational complexity. The nesting approach dynamically downscales the wave field, ensuring that swell generated in the open ocean is transferred effectively to the regional and coastal models. The SWAN model, with a spatial resolution of $0.025° \times 0.025°$ (SWAN0.025), provides detailed simulations of the wave climate around the Irish coast (red box in Figure 1 b represents the SWAN domain). The geographical extent of WAM and SWAN domains along with grid information and inputs used are provided in Table 1. The model captures the wave transformation processes as waves move into shallow coastal waters, influenced by local bathymetry and coastline features.

SWAN was configured with the same directional discretisation as WAM (12 bins), and sensitivity tests showed only minor differences when using higher spectral resolution. So the current SWAN set up consists of 12 uniformly distributed directions and 25 frequencies, which are logarithmically spaced from 0.046 Hz to 1.0 Hz. The SWAN model simulations are run with a non-stationary mode with a 30-minute time step. SWAN was run in third-generation mode, incorporating the WESTH (nonlinear saturation-based white capping combined with wind input; SWAN Team (2023)) formulation for wind-driven wave growth, the BSBT (Backward Space Backward Time) scheme for wave propagation, and both triad and quadruplet wave–wave interactions. The model included white-capping and bottom friction to account for wave energy dissipation, and wave breaking was enabled to capture nearshore wave transformations. SWAN default formulations and coefficients were used for all of the physical processes.

Table 1. Computational Grids and Inputs used for Model Simulations

Grids	**Geographical Extent**				**Spatial resolution**		**Inputs**			
	North	South	West	East	$\Delta x \times \Delta y$	$nx \times ny = N$	Wave	Wind	Sea ice	Sea level
WAM1.0NA	69°	0°	-82°	4°	$1° \times 1°$	$70 \times 87 = 6090$	-	×	×	-
WAM0.5NEA	63°	25°	-35°	2°	$0.5° \times 0.5°$	$77 \times 75 = 5775$	×	×	-	-
SWAN0.025	60°	36.5°	-19.5°	0°	$0.025° \times 0.025°$	$780 \times 940 = 733200$	×	×	-	×

Δx: spatial resolution in x direction
Δy: spatial resolution in y direction
nx: number of grid points in x direction
ny: number of grid points in y direction.

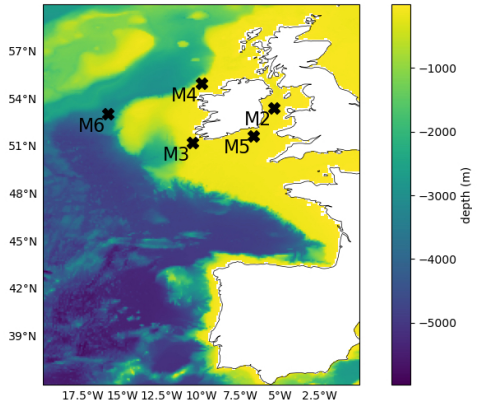

Figure 2. Domain covering SWAN0.025 grid, showing high-resolution bathymetry used for SWAN model set up. The bathymetry is derived from combination of INFOMAR and GEBCO datasets. The locations of Irish observational buoys used for validation are marked (cross) within the domain.

3.3 Data

3.3.1 Bathymetry

Two datasets were used for model bathymetry development. GEBCO_2023 (General Bathymetric Chart of the Oceans_2023) grid is a global model for ocean and land that provides elevation data which is available on 15 arc seconds interval grid (GEBCO Bathymetric Compilation Group, 2023). Both WAM models use GEBCO bathymetry interpolated to a 0.5° grid. INFOMAR (Integrated Mapping for the Sustainable Development of Ireland's Marine Resources) maps Irish coastal and offshore waters at resolution ranging from 500 m to 2 m and is managed by Geological Survey of Ireland (GSI) and the Marine Institute (Sheehan, Kevin and INFOMAR Survey Team, 2021). To obtain high resolution bathymetry near the shore, SWAN uses INFORMAR and GEBCO bathymetry interpolated to a grid of 0.025° resolution.

3.3.2 Wind

The study utilizes two distinct wind datasets: the low-resolution MPI-ESM (Max-Planck Institute of Earth System Model) wind data from CMIP6 ensemble and the high resolution ERA5 reanalysis data. To mitigate the limitations associated with the coarse resolution wind data for wave modelling, we employed ERA5 data as a high-resolution reference for generating surrogates for MPI-ESM wind. This is explained in detail in Section 4.

ERA5 is the fifth generation of ECMWF atmospheric reanalysis of the global climate (ECMWF, 2019) which delivers atmospheric, land surface, and ocean wind wave data. Wind components are available at 0.25° (31km) grid spacing and at an hourly frequency (Hersbach et al., 2023; ECMWF, 2016). This work utilizes 10 m u (u10) and v (v10) components of wind spanning from period 2004 to 2023.

MPI-ESM is a comprehensive climate model used for simulating Earth's climate system and developed by Max-Plank Institute of Meteorology, Hamburg, Germany (Garcia-Pereira et al., 2023). It couples different components of Earth system including the atmosphere - ECHAM6 (Stevens et al., 2013), ocean dynamics and sea ice - MPIOM (Jungclaus

et al., 2013), land surface processes - JSBACH (Reick et al., 2013) and marine biogeochemistry - HAMOCC (Ilyina et al., 2013).

The 10m u (uas) and v (vas) components of wind used in this study is obtained from first realisation (r1i1p1f1) model simulation of CMIP6 version of Max Planck Institute Grand Ensemble (MPI-GE CMIP6) which is based on the MPI-ESM version 1.201p7 (Olonscheck et al., 2023). The model includes simulations under five emission scenarios and the data used in the current study corresponds to SSP5-8.5. The low-resolution (LR) configuration, MPI–ESM LR, has a horizontal atmospheric resolution of 1.875° (200 km) and includes 47 vertical layers (Düsterhus & Brune, 2024). For the present study, MPI-ESM LR wind from 2004 to 2023 (representing the present climate) and 2081 to 2100 (representing future climate projections) were used.

3.3.3 Sea ice

The sea ice model is integrated within the ocean general circulation model MPIOM. It provides daily sea ice concentration on a bipolar grid with nominal resolution of 1.5° (Jungclaus et al., 2013). To make the sea ice data compatible with the wave models, the data was interpolated to a regular grid of resolution 0.5°. According to recent studies, Arctic sea ice is projected to experience a significant decline by 2100 (Ivanov & Repina, 2018), with the oldest ice potentially disappearing around mid-century (Chen et al., 2021). Chen et al. (2021), further indicate that sea ice thickness is anticipated to decrease at an average rate of 0.22 m per decade after September 2060, accompanied by a comprehensive decline in sea ice concentration and volume. Similarly, Dauner et al. (2024), highlights a long-term decline in sea ice extent in the Greenland and NA sector based on historical data, model simulations, and proxy-based reconstructions, which consistently predict significant reductions in sea ice. Considering these projections, the presence of sea ice in the study region was neglected for the future.

3.3.4 Sea level

Regional sea level data from the IPCC 6th Assessment Report (AR6) (Fox-Kemper et al., 2021). SSP5-8.5 scenario is used for the present study. Data is available from 2020 to 2150 along with how these projections differ depending on future scenarios (Kopp et al., 2023). To account for the effects of tide and storm surges, the tide surge anomaly (tideSurgeAnom) from UK climate Projections 2018 (UKCP18), based on RCP8.5, was added to the regional sea level projection, creating a combined dataset that was used in wave modelling. UKCP18 offers updated observations and climate change projections extending to 2100 in the UK and globally (Lowe et al., 2018). Since the UKCP18 data is available on an irregular grid, it was interpolated to a 0.5° regular grid before being integrated with the sea level projections.

3.3.5 Wave buoy data

Wave height data from observational buoys (M2-M6) are used to validate the models. These buoys form part of the Irish Marine Data Buoy Observation Network (IMDBON), which is managed by the Marine Institute, Met Éireann, funded by the Department of Agriculture, Food and the Marine (Marine Institute, 2022). IMDBON provides hourly weather measurements as well as wave height and wave period since 2001.

The locations of the wave buoys are shown in Figure 2 and the distance from shore along with latitude and longitude values are provided in Table 2. Buoy M6, situated off the west coast of Ireland in deep water, was used to validate significant wave height (Hs) outputs from the WAM0.5NA model. The other buoys, M2 to M5, are located closer to the shore and were employed for validating the SWAN model. Among these, buoys M3 and M4, positioned along the west coast of Ireland, were of particular interest as this re-

gion is directly influenced by NA swells. For further details on the validation process, refer to Section 5.

4 Downscaling wind via surrogate data generation

Dynamical downscaling of winds, which uses regional weather models to drive wave simulations (Markina et al., 2018) or coupling them with wave models (Bento et al., 2016) is a common approach in wave modelling. Instead we use an analogue method to downscale the climate model output. High-resolution ERA5 reanalysis data is used to generate surrogate winds for low resolution MPI-ESM. The surrogate winds follow daily evolution of MPI-ESM and preserves its large scale spatio-temporal characteristics, while providing realistic high resolution representation through selected ERA fields. This ensures temporal and spatial consistency between the coarse resolution driving model and the high-resolution surrogate data.

4.1 Analogue method for surrogate data generation

The analogue approach used here involves finding analogues or similar instances in a reference dataset that match certain characteristics of the target dataset. This method relies on identifying the instances from the reference dataset that closely resemble the conditions observed in the target dataset. Then use the corresponding values from the reference dataset as surrogates for the target dataset.

In this study, the analogue approach is applied to generate surrogate wind data for both present and future MPI-ESM simulations using the ERA5 as reference. The goal is to construct surrogates that retains large-scale structure and long term trends of MPI-ESM wind while retaining the resolution (both in time and space) of ERA5.

To ensure a consistent comparison during analogue selection, it is necessary to bring both datasets to same spatial and temporal resolution. Accordingly, the ERA5 data, available at 0.25° is first spatially regridded to match the coarser MPI-ESM grid (1.8°). Then daily averages of the u10 and v10 are computed from ERA5. This preprocessing ensures that both datasets are aligned in space and time, enabling a direct comparison of wind conditions over a defined spatial domain.

The choice of this spatial domain is a key aspect of the surrogate generation process, as it strongly influences the ability of the selected analogues to reproduce relevant physical conditions. In particular, the spatial domain determines which atmospheric features are prioritized when computing similarity between the target and candidate wind fields. A larger domain may emphasize large-scale wind patterns, while a smaller, regional domain focuses the comparison on localized wind conditions. A detailed discussion on the sensitivity to domain size is provided in the section 5.3.

To identify analogues, the daily wind fields from MPI-ESM are compared with daily averaged wind fields from ERA5. For each target day in MPI-ESM (M_{ref}), a search window of ±14 days around the same calendar day is applied to each year in the ERA5 dataset spanning from 2004 to 2023. This rolling 29 day window across 20 years resulted in a candidate pool of 580 ERA5 days (E_n, n = 1, 2, ..., N; N is total number of candidates) for each M_{ref}. This approach balances the need for seasonal consistency with sufficient variability in candidate patterns.

The similarity between M_{ref} and E_n was quantified using vector difference (VD) in wind components. Specifically, the Euclidean distance (Senter & Lupo, 2024) between the wind vectors was computed at each grid point using the formula:

$$VD_n = \sqrt{(M_{ref_u} - E_{n_u})^2 + (M_{ref_v} - E_{n_v})^2}, \quad n = 1, 2, \ldots, N$$

where N=580, depending on data availability (eg: leap year).

The VD field then quantifies the difference between MPI-ESM and ERA wind vectors at each grid point. The VD field is then spatially averaged over the domain to obtain a single similarity score for each candidate day. The ERA5 day with the minimum

spatially averaged VD is selected as the best analogue for the corresponding M_{ref}. The schematic diagram Figure 3 illustrates the process of analogue selection for MPI-ESM surrogate generation. An advantage of using the vector difference as the similarity metric is that it inherently captures both wind speed and wind direction differences, thereby simplifying the similarity assessment while still retaining the full vector characteristics of the wind field.

Once the best analogue day is identified for each MPI-ESM day, the corresponding high resolution wind fields from ERA5 (u10 and v10) were extracted. These extracted wind fields are then connected in temporal order to construct a continuous high-resolution surrogate wind time series. As the analogue days are selected based on daily similarity to MPI-ESM wind fields, the resulting sequence of surrogate days reflects the trends and variability embedded in the original MPI-ESM simulations, while attaining spatial and temporal resolution of ERA5.

As an example, consider January 18, 2081, from the MPI-ESM simulation. A ± 14 day search window is applied around this date, spanning from January 4 to February 1. All dates within this window are extracted from each of the 20 years in the regridded ERA5 record (2004 to 2023), resulting in a total of 580 candidate days. For each candidate day, the spatially distributed vector difference between the MPI-ESM and ERA5 wind components is computed, and the mean VD over the domain is calculated. Suppose January 22, 2007, is identified as the day with the minimum spatially averaged VD; this day is then selected as the best analogue for January 18, 2081.

If 3-hourly ERA5 wind data are used as the high-resolution reference, then the full 3-hourly wind fields from the selected analogue day (in this case, January 22, 2007) are used as the surrogate wind input for the MPI-ESM target day. This process is repeated for each day in the MPI-ESM time series, resulting in a surrogate dataset with the resolution of ERA5 and the large-scale variability of the MPI-ESM simulation.

Using the same ERA5 dataset for both present and future scenarios offers a consistent baseline, reducing the risk of introducing biases that could arise from using different datasets. While this method assumes that present-day ERA5 variability is a reasonable proxy for the structure of future variability, it is a standard and robust approach in climate modelling, especially when high-resolution observational datasets for the future are unavailable. A similar approach was employed by Noël et al. (2021), who performed statistical downscaling of CMIP5 projections using ERA5 as a reference dataset. In their study, they statistically downscaled historical data, validated it against ERA5, and used the identified biases to correct the projected downscaled data. This demonstrates the viability of using ERA5 as a reliable baseline for generating high-resolution data and correcting model biases, further supporting the assumption that present-day ERA5 variability can serve as a reasonable proxy for future scenarios in surrogate data generation.

5 Model Validation and Sensitivity Analysis

In this section, the two experiments-validation and temporal sensitivity analysis-are conducted using real wind data from ERA5 to assess the model's ability to represent current conditions. The validation involves computing the statistical matrices of model outputs driven by high-resolution ERA5 winds against observed data. Following this, a sensitivity analysis examines the impact of wind data resolution by comparing model performance using high to low-resolution wind inputs. Based on the conclusions drawn from this analysis, a second sensitivity experiment is carried out using surrogate winds generated by selecting different domain for computing VD between climate model and reanalysis data.

5.1 Model Validation against Observational buoys

The study area chosen benefits from a dense network of in-situ buoy observations (refer Figure 2 for locations). The validation period from 21 September 2023 to 10 Oc-

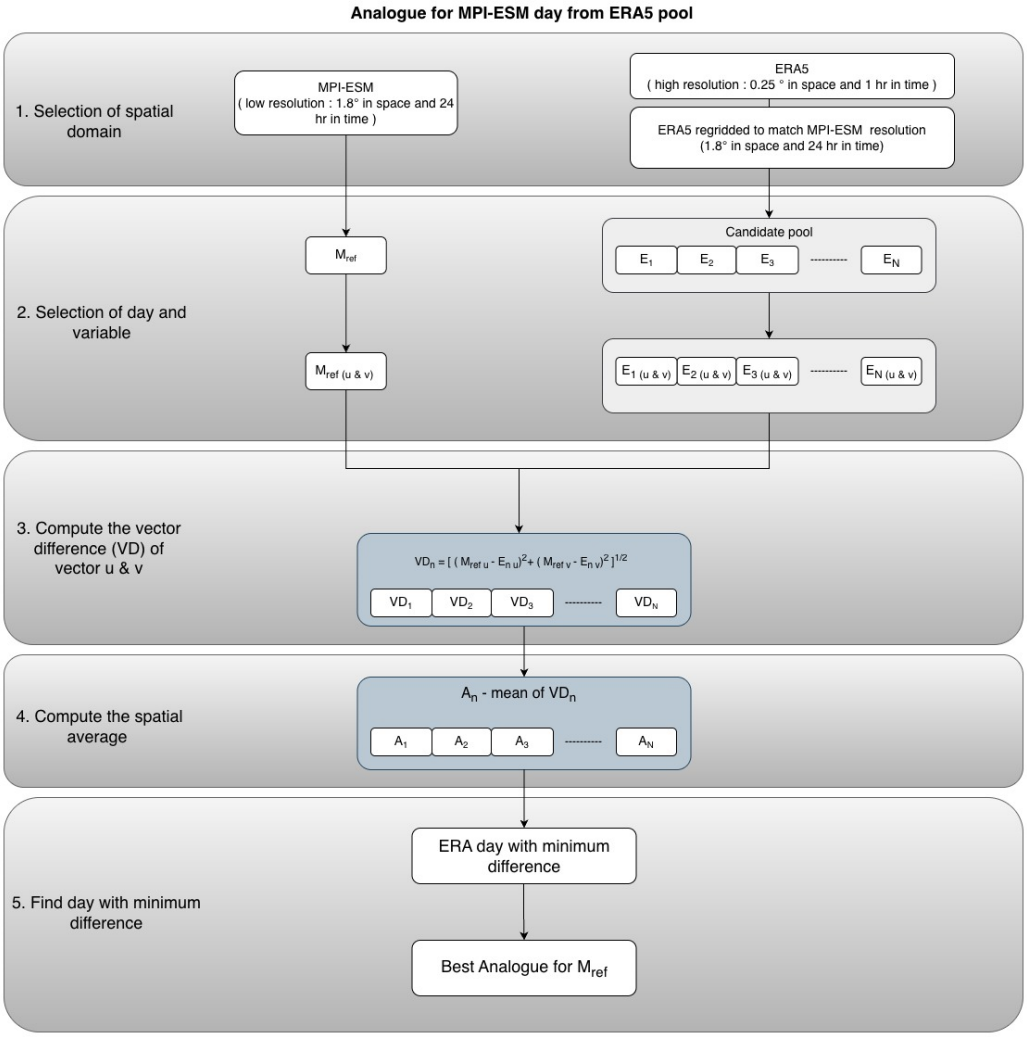

Figure 3. Schematic representation of analogue finding for the surrogate wind data generation. The method integrates coarser MPI-ESM and fine ERA5 data. The process begins with selecting the spatial domain, after which datasets are regridded and resampled to ensure consistent spatial and temporal resolution. For selected day in MPI-ESM (M_{ref}), the vector difference (VD_n) between ERA5 ($E_{n(u\&v)}$) and MPI-ESM ($M_{ref(u\&v)}$) wind components is computed over the selected domain. The spatially averaged vector difference (A_n) is then used to identify the ERA day with minimum difference, which is selected as best analogue.

tober 2023 was carefully chosen, to ensure the availability of continuous-error free observational data, thereby eliminating potential uncertainties associated with data gaps or inaccuracies. For this simulation period, model outputs were saved at hourly intervals to allow for detailed temporal comparison with observation.

Statistical validation of modelled Hs against buoy observation was undertaken to understand the skill of models WAM0.5NEA and SWAN0.025. The computed statistics of Hs (refer Table 2) are mean of measurements (Bm) and model simulations (Sm), the bias, root mean square error (RMSE), scatter index (SI) and the Pearson's Correlation Coefficient (r).

The locations in west coast of Ireland (M6, M3 and M4), directly influenced by NA swells, exhibit higher mean Hs than the locations in the east coast of Ireland (M2 and M5) during the validation period. In contrast, M2 and M5, which are sheltered from direct influence of swells and dominated by wind-sea conditions, has different statistical characteristics than M6, M4, and M3. Negative bias across all locations suggest that model tend to underpredict the Hs than the observations, with higher bias in the west coast locations where the influence of swell is stronger. RMSE follows similar pattern with higher values in west coast. The lower bias and RMSE in the east coast reflects the dominance of local wind driven waves. Conversely, the lower scatter index (SI) in the west coast indicates that the model predictions are more consistent for swell-dominated locations but show greater variability (high SI in east coast) in regions where wind-driven waves dominate.

Correlation coefficients (r) further support these findings, with the highest correlations observed in the east coast (M5: 0.922, M2: 0.899) and slightly lower values in the west (M3: 0.871, M4: 0.867, M6: 0.766). The strong correlation across all locations suggests that the model successfully captures temporal variations in wave height.

5.2 Sensitivity to temporal resolution of ERA5 wind forcing

Simulations, similar to the validation period, were conducted by driving WAM-SWAN setup using ERA5 wind data at different temporal resolutions–1 hour, 3 hours, 6 hours, and 24 hours–to assess the influence of wind forcing on wave model performance. Most of the studies focus on the matching of waves and extreme events. However, our focus is on the full distribution of wave heights along the Irish coast, as it provides valuable insights for adaptation strategies. The Hs distribution from SWAN0.025 simulations, driven by ERA5 winds, was compared to observations from the M4 buoy. The results, as illustrated in Figure 4, indicated good alignment of distribution curve of Hs from model (blue lines) with observations (orange lines) for 1-hourly and 3-hourly wind data, while significant deviations were noted with 6-hourly and daily forcings. Also, the models successfully reproduced the frequent waves with heights ranging between 2.5 and 4 m when driven by hourly and three-hourly wind forcing. However, this was not achieved with six-hourly and daily wind forcing.

To quantitatively assess the similarity between modelled and observed wave height distributions, the Earth Mover's Distance (EMD) was computed for model Hs from each wind forcing cases with the buoy Hs. EMD is a metric used to compare two distributions (Düsterhus & Hense, 2012; Luzia et al., 2022). It measures the effort required to transform one distribution into another by considering the amount and distance of "mass" that must be shifted (Luzia et al., 2022). The results provided in Phase I of Table 3 revealed that 3-hourly forcing produced lower EMD value (0.38), indicating closest match to the observed distribution. Although, model results from the 1 hour wind forcing appeared visually similar to observation, it has higher EMD than 3 hourly wind forcing because the metric captures even small shifts across full distribution. The 6-hourly and 24-hourly wind forcing produced higher EMD values (1.44 and 1.08), reflecting their inability to reproduce the observed Hs distribution accurately. Considering these findings, along with computational and storage requirements, we selected 3-hourly ERA5 data for generating surrogate winds for MPI–ESM simulations.

Table 2. Statistical results of Hs at each locations

	Lat	Lon	Distance from Irish shore	Bm	**Hs from WAM0.5NEA**				
	(°)	(°)	(km)		Sm	Bias	RMSE	SI	r
M6	52.986	-15.866	389	3.912	3.514	-0.397	0.768	0.196	0.766
	Lat	Lon	Distance from shore	Bm	**Hs from SWAN0.025**				
	(°)	(°)	(km)		Sm	Bias	RMSE	SI	r
M3	51.217	-10.550	56	3.656	3.427	-0.229	0.627	0.171	0.871
M4	55.000	-10.000	83	3.742	3.519	-0.223	0.528	0.146	0.867
M2	53.480	-5.425	37	1.671	1.527	-0.143	0.419	0.250	0.899
M5	51.690	-6.704	56	2.717	2.552	-0.165	0.570	0.209	0.922

Bm: mean Hs from buoy, Sm: mean Hs from model simulations

RMSE: root mean square error, SI: scatter index

r: Pearson's Correlation Coefficient.

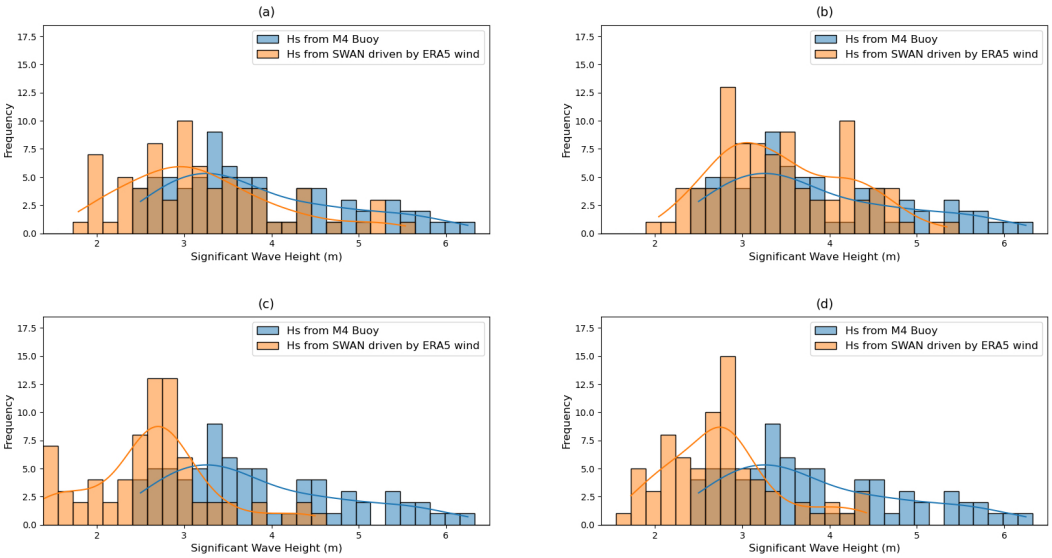

Figure 4. Comparison of Hs distribution from SWAN driven by ERA5 winds having temporal resolution of 1 hour (a), 3 hours (b), 6 hours (c) and 24 hours (d) with significant wave height from M4 buoy. The blue line represents the distribution curve of Hs from M4 buoy, while the orange line represent the distribution curve of Hs from SWAN0.025 model. The blue bars indicate the wave height distribution derived from M4 buoy while the orange bars indicate the wave height distribution derived from the model simulations.

5.3 Sensitivity to spatial domain selection for surrogate winds

To investigate the influence of spatial domain selection (represented as the first step in schematic diagram Figure 3) on surrogate wind quality on wave model performance, surrogate datasets were generated using three different domains: the full NA, the NEA region consistent with the WAM0.5NEA domain and the region around Ireland matching SWAN0.025 model. In all cases the high resolution surrogate wind fields were generated by rearranging 3-hourly ERA5 wind data from the entire NA, based on time indices identified through analogue matching. The resulting surrogate wind forcing was then used to drive the nested model system to simulate wave conditions for the year 2023. The modelled daily Hs from each experiment is compared against observations from the M3 and M4 buoys. Model performance was also evaluated by calculating the EMD between the modelled and observed Hs distribution at both locations.

The wave height distribution curves as shown in Figure 5 from three different model simulations appear to be similar to observations. However the surrogate wind generated using the domain around Ireland resulted in closest match. This is further supported by the EMD values, which were lowest at both buoy locations (0.09 at M3 and 0.1 at M4) when the wave models were driven by VD-Ireland wind field. These results highlight that selecting analogues based on local wind conditions can significantly improve model performance in nearshore region around Ireland.

The experiments described above determine the final model set up in this study. Using ERA5 winds, the validation against buoy observations demonstrates that the nested WAM-SWAN framework can reproduce observed wave conditions in the Irish waters with reasonable accuracy. The sensitivity analyses further indicate that 3-hourly wind forcing provides the best representation of the full distribution of significant wave heights, and that selecting analogues based on the Ireland domain produces surrogate wind fields that generate realistic wave conditions. Based on these findings, 3-hourly wind data and

Table 3. Summary of data inputs for wave simulations, resolution of input data, and agreement of model Hs with observations

	Input data	Temporal resolution (hr)	Spatial resolution (°)	Buoy used for comparison	EMD (buoy vs model Hs)
Phase I	ERA5	1	0.25	M4	0.656
	ERA5	3	0.25	M4	0.386
	ERA5	6	0.25	M4	1.449
	ERA5	24	0.25	M4	1.083
Phase II	VD-NA	3	0.25	M3	0.156
	VD-NEA	3	0.25	M3	0.146
	VD-Ireland	3	0.25	M3	0.091
	VD-NA	3	0.25	M4	0.173
	VD-NEA	3	0.25	M4	0.129
	VD-Ireland	3	0.25	M4	0.103

Notes: In Phase I, 3-hourly ERA5 (highlighted in grey) wind was chosen for surrogate wind data generation in Phase II.
In Phase II, the model was driven using surrogate winds generated using different domains selected for computing vector difference, and model performance was compared. VD-Ireland (grey rows) was selected for our study.
VD-NA: Surrogate data generated by computing vector difference between MPI-ESM and ERA5 winds over the North Atlantic.
VD-NEA: Surrogate data generated by computing vector difference over the Northeast Atlantic.
VD-Ireland: Surrogate data generated by computing vector difference over a domain around Ireland.

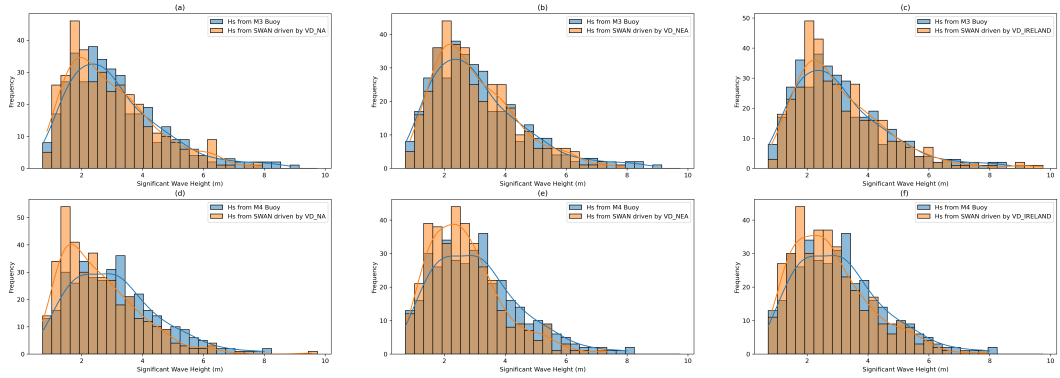

Figure 5. Comparison of significant wave height distribution from SWAN driven by surrogate winds generated through selecting different domain with significant wave height from M4 and M4 buoy. The blue line represents the distribution curve of Hs from buoy and the orange line represent the distribution curve of Hs from SWAN0.025 model driven by VD-NA winds (a and d), VD-NEA winds (b and e), and VD-Ireland winds (c and f). The top three plots represent comparison of model Hs with M3 buoy and bottom three for that with M4 buoy. The bars indicate the histogram of wave heights from buoy and model.

the Ireland domain were selected for generating surrogate winds. These surrogate winds, derived from climate model data, are used to simulate wave conditions to examine the present and future wave climate around Ireland. While biases exist in climate model winds, the focus of this study is the relative differences between present and future simulations, rather than the absolute magnitude of wave heights.

6 Wave projections in the Northeast Atlantic

A 20-year simulation (2004-2023) was conducted to represent the present wave conditions, using surrogate data generated under high-emission scenario (RCP8.5). Sea ice was included in NA (WAM1.0NA) model to capture its influence on wave propagation to inner domain, and sea level, consistent with same emission scenario, was incorporated into the SWAN model to account for its effects. To evaluate changes in the wave climate, the present simulation was compared with a 20-year projection (2081-2100), also under RCP8.5. The surrogate wind data generated for the future scenario was used to drive the wave models. In the present condition, sea ice was only observed only in the northwest Atlantic within the WAM1.0NA domain. Considering the projections from previous studies (Dauner et al., 2024; Chen et al., 2021), sea ice was set to zero in the future simulations to reflect its expected absence under future climate conditions, while projected sea level was included in SWAN simulations.

6.1 Spatial variation of wave height for Northeast Atlantic

The analysis of Hs differences between future and present conditions, based on a 20-year mean and seasonal averages, reveals notable spatial variations across the NEA under high emission scenario. These variations can be directly related to the projected changes in wind patterns, which are the primary drivers of wave dynamics.

The spatial variation of 20-year mean Hs differences (Figure 6) indicates a significant increase in wave heights in the northern part of domain, mainly in the northwest of Scotland and west of Ireland. This is likely driven by stronger and more persistent

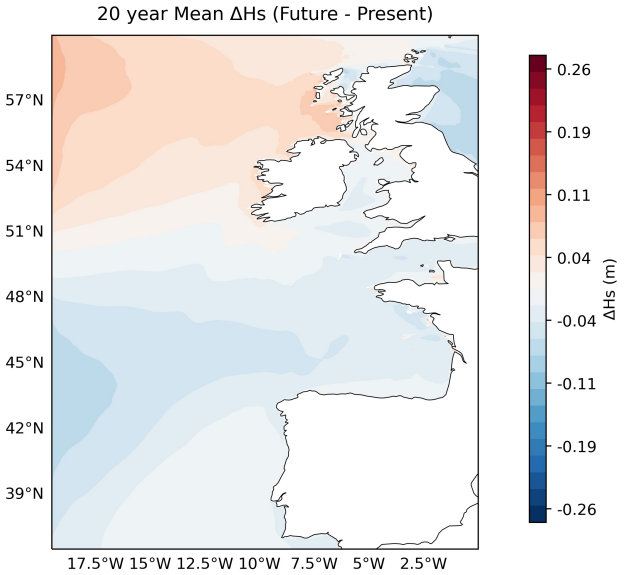

Figure 6. Spatial difference in the 20-year mean significant wave height (Hs) for the North-east Atlantic between future (2081-2100) and present (2004-2023) conditions. Positive values (red) indicate an increase in wave height, while negative values (blue) indicate a decrease, highlighting regional variability in projected wave climate changes

westerly winds associated with general poleward shift in storm tracks and intensified mid-latitude cyclones (Gentile et al., 2023; Pinto et al., 2013).

In contrast, a reduction in Hs is observed primarily in the central part of the domain, particularly in the mid-latitudes of the NEA. These areas show a broad but moderate decrease in wave heights, which may be attributed to shift in storm trajectories. The Iberian Peninsula exhibits relatively stable conditions, with minimal change in Hs compared to the present, indicating little impact from projected wind changes in this region. While the semi enclosed seas such as the Irish Sea and the English Channel show a slight reduction in Hs. The change in this area is smaller than in the central open ocean, possibly due to the influence of local wind dynamics and the sheltering effect of surrounding landmasses.

Earlier studies have shown that the NEA is a region with strong seasonal variations in Hs (Gallagher, Gleeson, et al., 2016a; Tiron et al., 2013). Our analysis also reveals pronounced seasonal difference under future climate conditions: winter and summer show increased Hs, spring shows only minor changes, and autumn shows a marked reduction in Hs. Quantitatively, the largest seasonal increase reaches up to 22 cm in winter and the strongest decrease of about 26 cm in autumn. Figure 7 illustrates these seasonal differences and highlights the associated spatial patterns across the NEA domain.

During winter, a pronounced increase in Hs is visible across the northern and western parts of domain, indicating stronger wave conditions likely associated with intense and frequent winter storms. The region around Ireland, shows widespread increase in Hs under future conditions. Additionally, the Irish sea shows noticeable increase in Hs, suggesting enhanced local wind forcing or greater wave penetration from the adjacent open Atlantic. In spring, the changes are minimal. Most areas are showing weak positive or negative differences. This suggests spring will bring relatively stable wave conditions in the future. Summer shows a moderate increase in Hs in the northern and southern parts of NEA, while the central part shows reduction. Notably, the western Iberian Peninsula, the area near the norther Ireland, and waters west of the outer Hebrides ex-

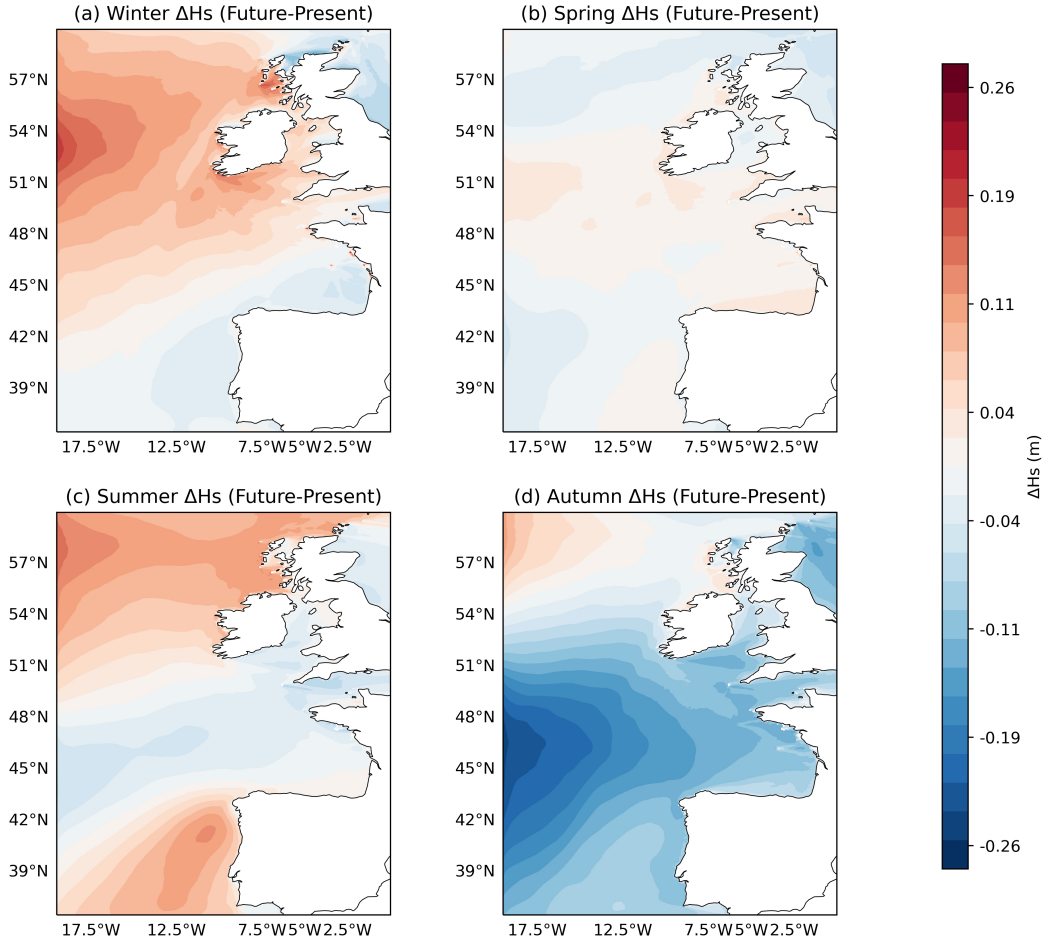

Figure 7. Seasonal differences in the mean significant wave height (Hs) between future (2081-2100) and present (2004-2023) conditions for the Northeast Atlantic. Each panel represents a season (a - Winter, b - Spring, c - Summer, d - Autumn), with positive values (red) indicating an increase and negative values (blue) indicating a decrease in Hs. The plots highlight the seasonal variability in projected wave climate changes

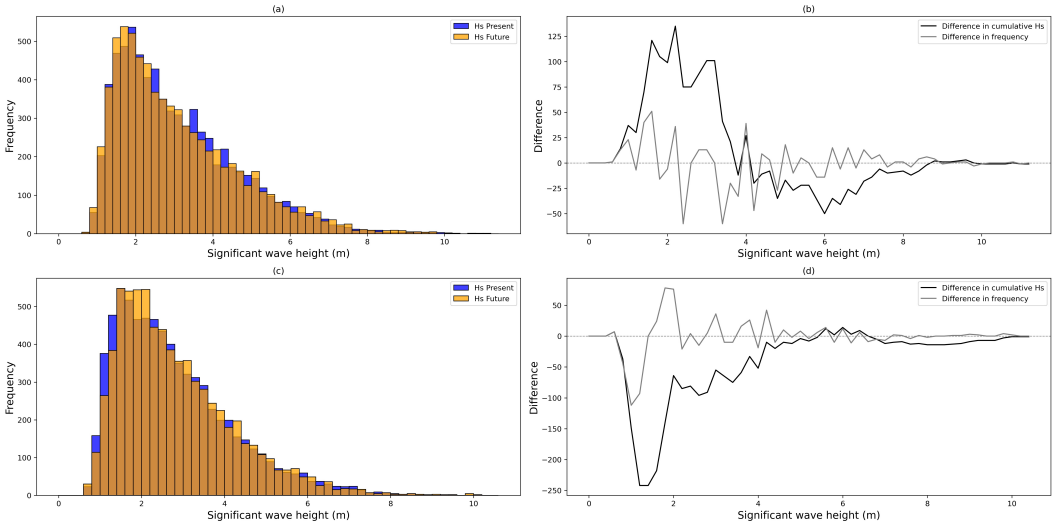

Figure 8. Distribution of Hs and comparison of future and present Hs at $M3_L$ and $M4_L$. The histogram plot (a) shows the comparison of Hs at $M3_L$ for present (blue) and future (orange), while in (b) grey line represent the difference (Future - Present) in bin frequencies of Hs and black line represent the difference in cumulative sum of Hs. Like wise histogram plot (c) shows the comparison of Hs at $M4_L$ for present (blue) and future (orange), while in (d) grey line represent the difference (Future - Present) in Hs and black line represent the difference in cumulative sum of Hs.

perience higher Hs increases in summer than in winter, highlighting the influence of seasonal wind shifts or persistent local wind forcing during this time. In contrast, autumn shows a widespread and significant decrease in Hs, especially across the central and southern parts of the domain, including west of the Iberian Peninsula and the Bay of Biscay. This is the only season showing a strong and consistent negative anomaly across a broad area, suggesting a notable weakening of wave-generating conditions during this period.

6.2 Localized changes in wave height along the west coast of Ireland

To understand how wave height distributions change locally, we compare the distributions of Hs at the locations where the M3 (southwest of Ireland) and M4 (northwest of Ireland) buoys are deployed (hereafter $M3_L$ and $M4_L$ will be used to represent location where M3 and M4 buoy is deployed). The analysis compares the present and future Hs, using histograms to examine the wave height distribution and analysing the differences in bin frequencies and cumulative sum of Hs to provide insights to shifts in wave height characteristics. This helps to identify whether future conditions involve more frequent high waves, changes in moderate wave occurences or shifts in calm conditions.

The analysis of wave height distributions at the $M3_L$ and $M4_L$ shows notable differences between present (2004-2023) and future (2081-2100). Histograms at both locations (refer Figure 8a, for $M3_L$ and Figure 8c for $M4_L$) reveal contrasting trends. At $M3_L$, the orange bars (future Hs) are generally taller than the blue bars (present Hs) for Hs < 2 m, while blue bars are mostly taller for moderate waves (2-4 m). But for high waves, from 4 to 8 m, the number of blue and orange bars alternating each other is roughly equal, making it difficult to identify a clear pattern within that range. Few orange bars appear above for Hs $>$ 8m at $M3_L$. In contrast, at $M4_L$, blue bars are taller than orange bars below 1.5 m, while from 1.5 to 4 m, the orange bars gradually increase and

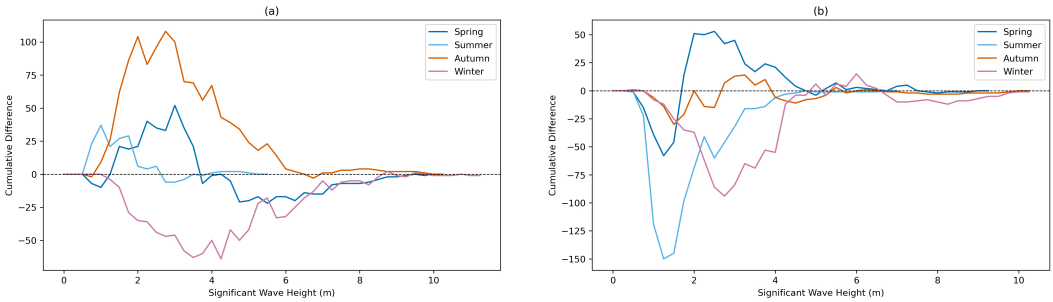

Figure 9. Seasonal difference in cumulative Hs between future and present scenarios at locations $M3_L$ (a) and $M4_L$ (b). The blue line represent spring, sky blue line represent summer, the orange line represent autumn and the pink line represent winter.

become taller. For higher waves, $M4_L$ shows a pattern similar to what is observed at $M3_L$, and above 8m, orange bars are present but shorter than blue bars.

It is important to note here that the increase and decrease in each bin is not entirely consistent within a given range. The trend described for each range is based on the majority of bins being taller in either the present or future distribution, rather than every single bin within that interval. While the histograms provide visual summary of these differences, it do not capture the full picture. The grey lines in Figure 8b and 8d which represents the bin to bin frequency differences capture these fluctuations, they are often noisy and difficult to interpret. To better highlight the overall shift between present and future distribution, the black cumulative sum difference line was included.

At $M3_L$ (Figure 8b), there is a net positive shift below 2m confirming that calm conditions are projected to become more frequent. A dip across the 2-4 m waves indicates a net reduction in moderate wave heights except around 3m, where the dip is less pronounced. Interestingly, the black line also reveal a distinct pattern for higher waves at $M3_L$ that was not easily visible in histogram plot. The line shows a decline from 4 to 6 m followed by a rise from 6 to 8m suggesting a redistribution within higher wave categories. The curve then flattens after 8m, highlighting a slightly increased extremes.

At $M4_L$ (Figure 8d), the cumulative curve shows sharp decline for calm conditions , a steady increase for the moderate range. While the curve drops below zero, this does not indicate that wave heights are decreasing overall. Instead, it shows that the future has fewer calm wave events compared to the present. As we move from Hs $>$ 2m, the curve starts to rise, meaning that moderate waves become more frequent in the future. Overall, the plot reflects a shift in the distribution, where calmer conditions reduce, and moderate wave activity increases. More flatten curve afterwards confirms that extreme conditions remain stable or slightly decrease.

Altogether, at $M3_L$, wave conditions are shifting towards both calmer and more energetic extremes with a reduction of moderate waves. $M4_L$ shows fewer calm states and modest increase in moderate waves and stable extreme wave frequencies in future. The shifts towards moderate to high waves at $M4_L$ and that towards calm waves at $M3_L$ is in line with the 20 year mean Hs difference, which clearly shows greater wave activity in the northwest of Ireland compared to the southwest.

Expanding on the histogram-based analysis, the seasonal cumulative differences at $M3_L$ and $M4_L$ provide a detailed view of how wave height distributions vary across different seasons. The seasonal cumulative differences of Hs between future and present conditions at $M3_L$ (Figure 9a) and $M4_L$ (Figure 9b) reveal distinct patterns in wave height distribution. At $M3_L$, seasonal cumulative differences reveal distinct patterns across wave height ranges. In summer, calmer waves (Hs $<$ 2 m) are more frequent in future, while moderate waves (2 - 4 m) show a decline, and those between 4 and 6 m (high waves) re-

main relatively stable. No extreme waves are observed in summer at $M3_L$. During autumn, there is an increase in waves between 1 and 3 m, indicating a shift to calmer than moderate conditions. However the difference decreases between 3 and 6 m, while higher waves (above 6m) shows very less increase in future, with the present of extreme waves (> 8 m). In spring, a similar pattern to autumn is observed, with an increase between 1 and 3 m , followed by a decline up to 6 m. However, the magnitude of these changes are less pronounced. Unlike in autumn, high waves above 6 m are expected to be more frequent in spring. Winter, in contrast to other seasons, shows a negative cumulative difference for calm to moderate waves, indicating reduced frequency of these events, while occurence of higher and extreme waves (> 6 m) increases. This suggest a shift toward more energetic wave events during winter at $M3_L$.

At $M4_L$, small waves are projected to decrease in all seasons. In autumn, minimal changes are seen across all wave heights marking a contrast to autumn at $M3_L$, except for extreme waves, which will remain similar to present conditions. Moderate waves becomes frequent in spring, with higher and extreme waves showing little changes than present. Summer at $M4_L$ shows an opposite trend to $M3_L$, with a sharp increase in moderate waves and some high waves up to ~ 7 m, suggesting more energetic conditions. Winter indicates an increase in moderate waves, as well as rise in occurrence of high waves and some extreme events in the 8 - 10 m range.

7 Discussion

Understanding future wave changes is crucial for long-term coastal planning and management. Global climate models (GCMs), serve as primary source of future atmospheric forcing. However, because of their coarse spatial resolution (typically ranging from 100 to 250 km grid scales), traditional GCMs, like MPI-ESM, have difficulty in adequately representing small scale wind variability. To address this, various downscaling approaches, such as dynamical downscaling, statistical downscaling, and, more recently, machine learning-based methods, have been developed.

Dynamical downscaling offers detailed physical representations. But it is computationally intensive, requiring significant storage and long simulation times (Rozoff & Alessandrini, 2022). In contrast, statistical methods are computationally efficient but rely on predefined relationships, which may limit their ability to capture complex, non-linear interactions between variables (Rozoff & Alessandrini, 2022). According to Zhang et al. (2024), machine learning-based approach models intricate, non-linear relationships and effectively handle high-dimensional dataset. However, they demand significant computational resources, large training datasets, and domain expertise, which can pose challenges for practical implementation (Getter et al., 2024).

This study employs an analogue-based approach as a simpler and more resource-efficient alternative. By selecting analogue days based on average vector difference with MPI-ESM wind and rearranging high-resolution ERA5 data, the surrogate wind dataset preserves the temporal evolution of the climate model while achieving both spatial and temporal coherence of ERA5. In addition, this method captures the non-linear dynamics in the observational dataset and preserves the physical realism. Hence, the method adopted overcome the limitation of traditional statistical methods that often rely on empirical fits or treat grid points independently. Additionally, by using existing datasets and rearranging them based on identified analogs, rather than generating new data through complex simulations or extensive model training, this method aligns with the principles of surrogate modeling - a concept commonly used in machine learning (Bocquet, 2023). Surrogate models simplify complex systems, enabling faster predictions without the need for full simulations (Bocquet, 2023). Similarly, the analogue approach effectively generates high-resolution surrogate data using statistical techniques. Thus the method avoids the computational demands of dynamical downscaling and machine learning while providing reliable inputs for wave climate analysis. Furthermore, considering that machine learning methods often fail to outperform simpler interpolation techniques, such as bicu-

bic interpolation, in reconstructing extreme wind conditions (Rezvov et al., 2022), the analogue-based approach provides a computationally efficient and reliable solution for downscaling winds for nearshore wave modelling.

Model validation, sensitivity analysis, and projected wave height changes provide a detailed understanding of the wave climate in the study area under the current and future scenarios. Validation of models against buoy observations confirms that both WAM (WAM0.5NAE) and SWAN (SWAN0.025) adequately capture wave, but their performance varies depending on the locations. WAM model was effective in capturing wave dynamics in open waters, its limitations nearshore underscore the need for models like SWAN to resolve fine-scale features. The accuracy of SWAN in representing nearshore wave characteristics further reinforces its suitability for coastal applications, especially in regions having complex geomorphology like the Irish coast. Consistent with this, the comparisons between WAM and SWAN simulations showed that SWAN reproduces wave height variability more accurately at locations closer the the Irish shelf (e.g., M3 and M4) while differences between the two models are smaller at the more offshore location M6.

The sensitivity of SWAN to the temporal resolution of ERA5 wind forcing underscores the importance of high-frequency wind data for accurate wave simulations. The significant deviations observed with 6-hourly and daily wind forcings highlight the inability to resolve the temporal variability needed for reproducing moderate and frequent waves. This finding aligns with the study by (Bauer & Weisse, 2000), which demonstrated that wave models driven by coarser winds (temporal resolution) significantly underestimates significant wave height. EMD values computed in this study further strengthen this. The model performance with 1-hourly and 3-hourly wind forcings align with the previous studies, reinforcing the decision to use 3-hourly wind data for surrogate wind generation. This decision balances computational efficiency and model accuracy, critical for long-term simulations.

The choice of spatial domain is an important part of the surrogate data generation process, as it affects how well the selected analogues represent the target conditions. The domain should be chosen based on the specific goals of the study. In this study, the surrogate wind data are used to drive wave models. So, it is important to make sure that the selected domain captures the wind patterns that generate waves affecting the region of interest.

Even when the analogue selection was based on a smaller region around Ireland, the resulting surrogate winds were created by shuffling ERA5 data covering the full NA, using the selected time indices. Since the prevailing winds reaching Ireland are westerlies, the regional domain inherently reflects large scale atmospheric patterns over NA. This means that even though the analogue selection is done from smaller area, the chosen time indices can reflect the larger weather patterns. Preserving large-scale wind effects is crucial for simulating waves near Ireland, as swells significantly shape the Irish wave climate (Gaughan & Fitzgerald, 2020; Gallagher, Gleeson, et al., 2016b). The good agreement (low EMD value) achieved by SWAN model nested in WAM forced by same surrogate wind suggests that the surrogate data not only reproduced the local wind condition but effectively captured the large-scale wind pattern over NA basin, which are also responsible for the waves in Irish coast.

The euclidean distance between MPI-ESM and EAR5 wind fields computed using the vector components of wind allowed to incorporate both wind speed and direction in similarity assessment. For each day in MPI-ESM, the analogue was identified as the day in ERA5 having minimum spatially averaged vector difference. Following this, the 3-hourly wind data were rearranged according to the new time sequence derived from the comparison.

Since ERA5 data are only available up to the present, we used the same reference period (2004-2023) to generate surrogates for both present and future scenarios. However, this does not imply that the same wind represent both time periods. Instead, ERA5 days were selected based on their similarity to MPI-ESM wind patterns for the present and future, allowing the surrogate wind fields to reflect the projected climate signal while

maintaining high-resolution physical realism. Furthermore, the MPI-ESM simulations used in this study project generally lower or comparable wind magnitudes in the future relative to the present. This reinforces that ERA5 provides a sufficiently broad range of wind events and remains a valid and appropriate source for analogue selection under projected future conditions.

The future projections show noticeable spatial variations in wave height changes across the NEA under the RCP8.5 scenario. An intensification of wave activity is observed in the northern parts of domain, while the southern and eastern regions experience a reduction in wave heights. These changes can be linked to the influence of shifting wind patterns. The NEA region around Ireland exhibits contrasting trends, with the west coast showing an increase in mean significant wave height, while the east coast remains more stable. Seasonal variations in wave height changes provide additional insights, with the most pronounced increases occurring in winter (up to 22 cm) and summer (up to 15 cm), while autumn exhibits the largest decrease in wave height (up to 26 cm).

However, these findings contrast with those of Gallagher, Gleeson, et al. (2016a) and Gallagher, Gleeson, et al. (2016b), which projected an overall decrease in Hs, with the greatest reductions occurring in winter and summer under the RCP8.5 scenario near Ireland. Gallagher, Gleeson, et al. (2016a) conducted a 30-year future projection compared with a 30-year hindcast of wind-waves using WAVEWATCH III (WW3) and wind data from the EC-Earth global climate model. In contrast, our study focuses on a 20-year comparison of future projections with present conditions, incorporating present and future sea level rise scenarios. The seasonal variations in wave heights follow a pattern similar to the seasonal differences in 20-year mean wind patterns between the future and present from surrogate data. This similarity confirms that NEA waves are predominantly wind-driven.

In the NEA, where the prevailing winds are predominantly westerlies, surrogate winds generated through analogue method effectively captured the seasonal variations in wind seen in MPI-ESM. The resemblance of seasonal wave patterns with wind variations also demonstrates the robustness of the approach in regions with relatively consistent wind regimes. However, in more complex environments like the Indian Ocean, where wind patterns exhibit significant seasonal and spatial variability due to phenomena such as monsoons, the domain selection for surrogate data generation method requires careful evaluation.

Another important aspect concerns sea level rise. Although sea level rise consistent with the high emission scenario (RCP8.5) was incorporated in wave model, its influence on wave simulations was not explicitly analysed, as it was not the focus of the study. The impact of sea level rise are most pronounced in the coastal areas, where even small increase in water level significantly amplify the coastal wave impacts leading to flooding and erosion (van de Wal et al., 2023). Understanding the combined effect of sea level rise and waves are important for evaluating the potential climate change impacts on the coast and remains important area for future research.

While future projections indicate an increase in mean wave heights over northern NEA, the regional variability in wave climate need to be carefully analysed. This need is reinforced by the contrasting trends observed at locations $M3_L$ and $M4_L$. At $M4_L$, decline in calm sea states along with an increase in moderate and higher wave heights indicates a transition toward more energetic and active wave conditions. Hs distribution at $M3_L$ reflects a shift in waves where moderate waves becomes less frequent, while both calm and high waves are becoming more dominant. A potential increase of high wave events at $M4_L$ (located NW of Ireland) could be its exposure to the poleward shifting storm tracks. While projected higher waves and stable extreme waves at both locations may reflect the increased storm severity or regional response of the wave climate under future conditions.

The seasonal spatial plot shows that autumn experiences the greatest overall reduction in Hs and winter showing increase in Hs across NEA domain, the location specific analysis at $M3_L$ and $M4_L$ further validates this trend. In autumn, $M3_L$ shows shift

towards calmer waves and $M4_L$ exhibits stable conditions across all Hs ranges. Both findings supports the broader regional signal of declining wave activity in autumn. In winter, when increased Hs is observed along west coast of Ireland, both locations show as increase in moderate to very high waves. However, extreme wave events continue to occur at both sites across both seasons, emphasizing that while regional trends are useful, location-specific assessments are essential to capture the full range of wave height behavior.

The significant increase in extreme waves during winter at both $M3_L$ and $M4_L$ highlights the elevated risks associated with winter storms in future scenarios. Conversely, summer months are less influenced by extreme events, making it more suitable for activities like sailing. At $M3_L$, the increase in calm conditions across most seasons, except winter, suggests that spring, summer, and autumn offer suitable windows for marine operations. While at $M4_L$, autumn appears to be most favourable period as it remains relatively stable across all wave height ranges.

The methodology, together with the findings demonstrates an efficient and physically realistic mean of simulating waves in the NEA. By analyzing the full distributions of wave heights, this study provides detailed insights into spatial and temporal patterns of wave climate, offering a deeper understanding of wave behavior beyond mean values. The findings highlight the critical importance of incorporating both regional and seasonal variability into wave climate assessments which are essential for developing effective mitigation and adaptation strategies under a changing climate.

8 Conclusion

In this study, we developed a robust wave modelling framework that includes finer resolution models for NEA and Irish coastal waters. The models driven by high resolution surrogate winds were able to capture the spatiotemporal variability of the wave climate which is predominantly wind driven. The analogue method was more efficient in terms of time and computational expenses compared to the common downscaling techniques which made surrogate data a practical resource for long term assessments of wave climates. The findings provide a reliable foundation for understanding wave dynamics and supporting coastal management under future climate scenarios.

Acknowledgments

The study is conducted as part of PhD work funded by Marine Institute, Galway, Ireland under the project "Decadal Wave Prediction of Irish coast" *(MI/CS/20/111)*.

AD received funding from the Danish state through the National Centre for Climate Research (NCKF).

This work used resources of the Deutsches Klimarechen-zentrum (DKRZ) granted by its Scientific Steering Committee (WLA) under project ID uo1075. We thank DKRZ Helpdesk for their technical support.

We, also, acknowledge Dr. Mikhail Dobrynin, Dr. Sebastian Brune and Kieran Lyons, for their insightful discussions and valuable input, which greatly contributed to the progress of this work.

Conflict of Interest Statement

The authors have no conflicts of interest to disclose.

Data Availability statement

The ERA5 wind data on single levels were obtained through the Copernicus Climate Change Service (C3S), available at `https://www.ecmwf.int/en/forecasts/dataset/ecmwf-reanalysis-v5` (Hersbach et al., 2023).

Daily MPI-ESM wind and Sea ice concentration was accessed via Levante and is publicly available through the ESGF archive `https://esgf-data.dkrz.de/search/cmip6-dkrz/` (Eyring et al., 2016). Sea level data were sourced from UKCP18 `http://catalogue.ceda.ac.uk/uuid/5fcae68057ea43259d0a4530d34e4ba5` (Met Office Hadley Centre, 2018) and IPCC AR6 sea-level projections (Garner et al., 2021)

The wave models used, SWAN which can be downloaded from `http://swanmodel.sourceforge.net/` (SWAN Team, 2023) and WAM, available via `https://github.com/mywave/WAM` (Baordo et al., 2020), are open-source models.

Bathymetric data, combining GEBCO and INFOMAR, were provided by the Marine Institute. GEBCO data is publicly available through GEBCO Bathymetric Compilation Group (2023), and INFOMAR data can be accessed via `https://www.infomar.ie/data`

In situ wave data for model validation were also provided by the Marine Institute and are publicly available via the ERDDAP data server (`https://erddap.marine.ie/erddap/index.html`).

Plots presented in this study were generated using Jupyter Notebooks running on JupyterHub, hosted on the Levante HPC system at the German Climate Computing Center (DKRZ).

References

Alizadeh, M. J., Kavianpour, M. R., Kamranzad, B., & Etemad-Shahidi, A. (2020). A distributed wind downscaling technique for wave climate modeling under future scenarios. , *145*, 101513. Retrieved from `https://www.sciencedirect.com/science/article/pii/S1463500318304062` doi: https://doi.org/10.1016/j.ocemod.2019.101513

Ana Rute Bento, N. S., & Soares, C. G. (2018). Validation of a wave forecast system for galway bay. , *11*(2), 112–124. Retrieved from `https://doi.org/10.1080/1755876X.2018.1470454` (Publisher: Taylor & Francis _eprint: https://doi.org/10.1080/1755876X.2018.1470454) doi: 10.1080/1755876X.2018.1470454

Anton, I., & Nash, S. (2020). Application of the IEC technical specification for assessment of wave energy resource: A case study from the west coast of ireland.

Atan, R., Goggins, J., & Nash, S. (2016). Development of a high resolution wave model at AMETS using SWAN. In *Proceedings of the civil engineering research in ireland (CERI) conference, galway, ireland* (pp. 29–30).

Baordo, F., Clementi, E., Iovino, D., & Masina, S. (2020). Intercomparison and assessement of wave models at global scale [Software].

Barbariol, F., Pezzutto, P., Davison, S., Bertotti, L., Cavaleri, L., Papa, A., ... Benetazzo, A. (2022). Wind-wave forecasting in enclosed basins using statistically downscaled global wind forcing. , *9*. Retrieved from `https://www.frontiersin.org/journals/marine-science/articles/10.3389/fmars.2022.1002786` doi: 10.3389/fmars.2022.1002786

Bauer, E., & Weisse, R. (2000). Determination of high-frequency wind variability from observations and application to north atlantic wave modeling. , *105*, 26179–26190. Retrieved from `https://agupubs.onlinelibrary.wiley.com/doi/abs/10.1029/1999JC000066` (_eprint: https://agupubs.onlinelibrary.wiley.com/doi/pdf/10.1029/1999JC000066) doi: https://doi.org/10.1029/1999JC000066

Bento, A., Gonçalves, M., Campos, R., & Guedes Soares, C. (2016). Comparison between two forecast systems implemented with WAM and WaveWatch 3 for the north atlantic. In (p. V003T02A035). doi: 10.1115/OMAE2016-54464

Bento., A. R., Martinho, P., Campos, R., & Guedes Soares, C. (2011). Modelling wave energy resources in the irish west coast. In *International conference on offshore mechanics and arctic engineering* (Vol. 44373, pp. 945–953).

Bertin, X., Prouteau, E., & Letetrel, C. (2013). A significant increase in wave height in the north atlantic ocean over the 20th century. , *106*, 77–83. Retrieved from https://www.sciencedirect.com/science/article/pii/S092181811300088X doi: https://doi.org/10.1016/j.gloplacha.2013.03.009

Bingölbali, B., Akpınar, A., Jafali, H., & Vledder, G. P. V. (2019). Downscaling of wave climate in the western black sea. , *172*, 31–45. Retrieved from https://www.sciencedirect.com/science/article/pii/S0029801818321139 doi: https://doi.org/10.1016/j.oceaneng.2018.11.042

Bitner-Gregersen, E. M., Waseda, T., Parunov, J., Yim, S., Hirdaris, S., Ma, N., & Soares, C. G. (2022). Uncertainties in long-term wave modelling. , *84*, 103217. Retrieved from https://www.sciencedirect.com/science/article/pii/S0951833922000569 doi: https://doi.org/10.1016/j.marstruc.2022.103217

Bocquet, M. (2023). Surrogate modeling for the climate sciences dynamics with machine learning and data assimilation. , *9*, 1133226. doi: 10.3389/fams.2023.1133226

Booij, N., Ris, R. C., & Holthuijsen, L. H. (1999). A third-generation wave model for coastal regions: 1. model description and validation. , *104*, 7649–7666. Retrieved from https://agupubs.onlinelibrary.wiley.com/doi/abs/10.1029/98JC02622 (_eprint: https://agupubs.onlinelibrary.wiley.com/doi/pdf/10.1029/98JC02622) doi: https://doi.org/10.1029/98JC02622

Brown, J. M., Souza, A. J., & Wolf, J. (2010). An 11-year validation of wave-surge modelling in the irish sea, using a nested POLCOMS–WAM modelling system. , *33*(1), 118–128. Retrieved from https://www.sciencedirect.com/science/article/pii/S146350030900239X doi: https://doi.org/10.1016/j.ocemod.2009.12.006

Calvino, C., Dabrowski, T., & Dias, F. (2022). Current interaction in large-scale wave models with an application to ireland. , *245*, 104798. Retrieved from https://www.sciencedirect.com/science/article/pii/S0278434322001510 doi: https://doi.org/10.1016/j.csr.2022.104798

Cavaleri, L., Fox-Kemper, B., & Hemer, M. (2012). Wind waves in the coupled climate system. , *93*(11), 1651 – 1661. Retrieved from https://journals.ametsoc.org/view/journals/bams/93/11/bams-d-11-00170.1.xml (Place: Boston MA, USA Publisher: American Meteorological Society) doi: 10.1175/BAMS-D-11-00170.1

Chen, J., Kang, S., Du, W., Guo, J., Xu, M., Zhang, Y., ... Chen, J. (2021). Perspectives on future sea ice and navigability in the arctic. , *15*(12), 5473–5482. Retrieved from https://tc.copernicus.org/articles/15/5473/2021/ doi: 10.5194/tc-15-5473-2021

Dauner, A. L. L., Schenk, F., Power, K. E., & Heikkilä, M. (2024). Sea-ice variations and trends during the common era in the atlantic sector of the arctic ocean. , *18*(3), 1399–1418. Retrieved from https://tc.copernicus.org/articles/18/1399/2024/ doi: 10.5194/tc-18-1399-2024

De Bruin, K. C., & Kyei, C. K. (2024). *Climate change adaptation options and their associated costs and benefits in ireland* (Tech. Rep.). ESRI Working Paper.

Dodet, G., Bertin, X., & Taborda, R. (2010). Wave climate variability in the north-east atlantic ocean over the last six decades. , *31*(3), 120–131. Retrieved from https://www.sciencedirect.com/science/article/pii/S1463500309002066 doi: https://doi.org/10.1016/j.ocemod.2009.10.010

Dodet, G., Melet, A., Ardhuin, F., Bertin, X., Idier, D., & Almar, R. (2019). The contribution of wind-generated waves to coastal sea-level changes. , *40*(6), 1563–1601. Retrieved from https://doi.org/10.1007/s10712-019-09557-5 (Type: Article) doi: 10.1007/s10712-019-09557-5

Düsterhus, A., & Hense, A. (2012). Advanced information criterion for environmental data quality assurance. *Advances in Science and Research*, *8*(1), 99–104.

Retrieved from https://asr.copernicus.org/articles/8/99/2012/ doi: 10.5194/asr-8-99-2012

Düsterhus, A., & Brune, S. (2024). Decadal predictability of seasonal temperature distributions. , *51*(11), e2023GL107838. Retrieved from https://agupubs.onlinelibrary.wiley.com/doi/abs/10.1029/2023GL107838 (_eprint: https://agupubs.onlinelibrary.wiley.com/doi/pdf/10.1029/2023GL107838) doi: https://doi.org/10.1029/2023GL107838

ECMWF. (2016). IFS documentation CY41r2. (Publisher: ECMWF Reading, UK)

ECMWF. (2019). *ERA5 reanalysis (0.25 degree latitude-longitude grid).* Research Data Archive at the National Center for Atmospheric Research, Computational and Information Systems Laboratory. Retrieved from https://rda.ucar.edu/datasets/dsd633000/ (Place: Boulder CO)

Eyring, V., Bony, S., Meehl, G. A., Senior, C. A., Stevens, B., Stouffer, R. J., & Taylor, K. E. (2016). Overview of the coupled model intercomparison project phase 6 (cmip6) experimental design and organization [Dataset]. *Geoscientific Model Development*, *9*(5), 1937–1958.

Farrok, O., Farah, M. M., & Islam, M. R. (2024). Introduction to the principles of wave energy conversion. In O. Farrok & M. R. Islam (Eds.), *Oceanic wave energy conversion: Advancement of electrical generators* (pp. 1–15). Springer Nature Singapore. Retrieved from https://doi.org/10.1007/978-981-99-9814-2_1 doi: 10.1007/978-981-99-9814-2_1

Fedele, F., Herterich, J., Tayfun, A., & Dias, F. (2019). Large nearshore storm waves off the irish coast. , *9*(1), 15406. Retrieved from https://doi.org/10.1038/s41598-019-51706-8 doi: 10.1038/s41598-019-51706-8

Fox-Kemper, B., Hewitt, H. T., Xiao, C., G., A., Drijfhout, S. S., Edwards, T. L., ... Yu, Y. (2021). Ocean, cryosphere and sea level change. In V. Masson-Delmotte et al. (Eds.), *Climate change 2021: The physical science basis. contribution of working group i to the sixth assessment report of the intergovernmental panel on climate change* (pp. 1211–1362). Cambridge, United Kingdom and New York, NY, USA: Cambridge University Press. Retrieved from https://doi.org/10.1017/9781009157896.011 doi: 10.1017/9781009157896.011

Gallagher, S., Gleeson, E., Tiron, R., McGrath, R., & Dias, F. (2016a). Twenty-first century wave climate projections for ireland and surface winds in the north atlantic ocean. , *13*, 75–80. Retrieved from https://asr.copernicus.org/articles/13/75/2016/ doi: 10.5194/asr-13-75-2016

Gallagher, S., Gleeson, E., Tiron, R., McGrath, R., & Dias, F. (2016b). Wave climate projections for ireland for the end of the 21st century including analysis of EC-earth winds over the north atlantic ocean. , *36*(14), 4592–4607. Retrieved from https://rmets.onlinelibrary.wiley.com/doi/abs/10.1002/joc.4656 (_eprint: https://rmets.onlinelibrary.wiley.com/doi/pdf/10.1002/joc.4656) doi: https://doi.org/10.1002/joc.4656

Gallagher, S., Tiron, R., & Dias, F. (2014). A long-term nearshore wave hindcast for ireland: Atlantic and irish sea coasts (1979–2012). , *64*(8), 1163–1180. Retrieved from https://doi.org/10.1007/s10236-014-0728-3 doi: 10.1007/s10236-014-0728-3

Gallagher, S., Tiron, R., Whelan, E., Gleeson, E., Dias, F., & McGrath, R. (2016). The nearshore wind and wave energy potential of ireland: A high resolution assessment of availability and accessibility. , *88*, 494–516. Retrieved from https://www.sciencedirect.com/science/article/pii/S0960148115304304 doi: https://doi.org/10.1016/j.renene.2015.11.010

Garcia-Pereira, F., González-Rouco, J. F., & Johann, J. (2023). *MPI-ESM1.2-LR p2k+ with a deep version of JSBACH (MPI-ESM p2k+d).* doi: 10.5281/

ZENODO.10364950

Garner, G. G., Hermans, T., Kopp, R. E., Slangen, A. B. A., Edwards, T. L., Levermann, A., ... Pearson, B. (2021). *IPCC AR6 Sea Level Projections [Dataset].* Zenodo. Retrieved from https://doi.org/10.5281/zenodo.5914709 (Dataset accessed: 2025-02-23) doi: 10.5281/zenodo.5914709

Gaughan, E., & Fitzgerald, B. (2020). An assessment of the potential for co-located offshore wind and wave farms in ireland. , *200*, 117526. Retrieved from https://www.sciencedirect.com/science/article/pii/S0360544220306332 doi: https://doi.org/10.1016/j.energy.2020.117526

GEBCO Bathymetric Compilation Group. (2023). *The GEBCO_2023 grid - a continuous terrain model of the global oceans and land [Dataset].* NERC EDS British Oceanographic Data Centre NOC. Retrieved from https://www.gebco.net/data_and_products/gridded_bathymetry_data/ doi: 10.5285/f98b053b-0cbc-6c23-e053-6c86abc0af7b

Gentile, E. S., Zhao, M., & Hodges, K. (2023). Poleward intensification of midlatitude extreme winds under warmer climate. , *6*(1), 219. Retrieved from https://doi.org/10.1038/s41612-023-00540-x doi: 10.1038/s41612-023-00540-x

Getter, D., Bessac, J., Rudi, J., & Feng, Y. (2024). Statistical treatment of convolutional neural network superresolution of inland surface wind for subgrid-scale variability quantification. , *3*(1), e230009. Retrieved from https://journals.ametsoc.org/view/journals/aies/3/1/AIES-D-23-0009.1.xml (Place: Boston MA, USA Publisher: American Meteorological Society) doi: 10.1175/AIES-D-23-0009.1

Gleeson, E., Clancy, C., Zubiate, L., Janjić, J., Gallagher, S., & Dias, F. (2019). Teleconnections and extreme ocean states in the northeast atlantic ocean. , *16*, 11–29. Retrieved from https://asr.copernicus.org/articles/16/11/2019/ doi: 10.5194/asr-16-11-2019

Guisado-Pintado, E. (2020). *Shallow water wave modelling in the nearshore (SWAN).* (Publication Title: Sandy Beach Morphodynamics) doi: 10.1016/B978-0-08-102927-5.00017-5

Günther, H., Hasselmann, S., & Janssen, P. A. (1992). The WAM model cycle 4 (revised version).
(Publisher: Deutsches KlimaRechenZentrum)

Hersbach, H., Bell, B., Berrisford, P., Biavati, G., Horányi, A., Muñoz Sabater, J., ... Thépaut, J.-N. (2023). *ERA5 hourly data on single levels from 1940 to present [Dataset].* Copernicus Climate Change Service (C3S) Climate Data Store (CDS). Retrieved from https://doi.org/10.24381/cds.adbb2d47 doi: 10.24381/cds.adbb2d47

Ilyina, T., Six, K. D., Segschneider, J., Maier-Reimer, E., Li, H., & Nunez-Riboni, I. (2013). Global ocean biogeochemistry model HAMOCC: Model architecture and performance as component of the MPI-earth system model in different CMIP5 experimental realizations. , *5*(2), 287–315. doi: 10.1029/2012MS000178

Ivanov, V. V., & Repina, I. A. (2018). The effect of seasonal variability of atlantic water on the arctic sea ice cover. , *54*(1), 65–72. Retrieved from https://doi.org/10.1134/S0001433818010061 doi: 10.1134/S0001433818010061

Janssen, P., & Bidlot, J.-R. (2003). Part vii: Ecmwf wave-model documentation. *IFS Documentation Cycle CY23R4, ECMWF*, *46*.

Jungclaus, J. H., Fischer, N., Haak, H., Lohmann, K., Marotzke, J., Matei, D., ... von Storch, J. S. (2013). Characteristics of the ocean simulations in the max planck institute ocean model (MPIOM) the ocean component of the MPI-earth system model. , *5*(2), 422–446. Retrieved from https://agupubs.onlinelibrary.wiley.com/doi/abs/10.1002/jame.20023 (_eprint: https://agupubs.onlinelibrary.wiley.com/doi/pdf/10.1002/jame.20023)

doi: https://doi.org/10.1002/jame.20023

Kandrot, S., Farrell, E., & Devoy, R. (2016). The morphological response of foredunes at a breached barrier system to winter 2013/2014 storms on the southwest coast of ireland. *Earth Surface Processes and Landforms*, *41*(14), 2123–2136.

Kopp, R. E., Garner, G. G., Hermans, T. H. J., Jha, S., Kumar, P., Reedy, A., ... Smith, C. (2023). The framework for assessing changes to sea-level (FACTS) v1.0: A platform for characterizing parametric and structural uncertainty in future global, relative, and extreme sea-level change. *Geoscientific Model Development*, *16*, 7461–7489. Retrieved from https://doi.org/10.5194/gmd-16-7461-2023 doi: 10.5194/gmd-16-7461-2023

Lalbeharry, R., & Ritchie, H. (2009). Wave simulation using SWAN in nested and unnested mode applications..

Lemos, G., Semedo, A., Kumar, R., Dobrynin, M., Akpinar, A., Kamranzad, B., ... Lobeto, H. (2023). Performance evaluation of a global CMIP6 single forcing, multi wave model ensemble of wave climate simulations. , *184*, 102237. Retrieved from https://www.sciencedirect.com/science/article/pii/S1463500323000781 doi: https://doi.org/10.1016/j.ocemod.2023.102237

Loureiro, C., & Cooper, A. (2019). Temporal variability in winter wave conditions and storminess in the northwest of ireland. , *51*(2), 155–170. Retrieved from https://irishgeography.ie/index.php/irishgeography/article/view/1369 (Section: Articles) doi: 10.55650/igj.2018.1369

Lowe, J. A., Bernie, D., Bett, P., Bricheno, L., Brown, S., Calvert, D., ... Fosser, G. (2018). UKCP18 science overview report. , 1–73.

Luzia, G., Hahmann, A., & Koivisto, M. (2022, November). Evaluating the mesoscale spatio-temporal variability in simulated wind speed time series over northern Europe. *Wind Energy Science*, *7*, 2255–2270. doi: 10.5194/wes-7-2255-2022

Madden, N., Olbert, I., & Shchepetkin, A. (2025). *Tidal research reveals power of storm Éowyn and unfathomable near-miss.* https://www.universityofgalway.ie/about-us/news-and-events/news-archive/2025/april/tidal-research-reveals-power-of-storm-eowyn-and-unfathomable-near-miss--.html. (University of Galway news article. Accessed: 6 March 2026)

Marine Institute. (2022). *Irish marine data buoy observation network.* Retrieved from https://www.marine.ie/site-area/infrastructure-facilities/marine-research-infrastructures/irish-marine-data-buoy

Markina, M., Gavrikov, A., Gulev, S., & Barnier, B. (2018). Developing configuration of WRF model for long-term high-resolution wind wave hindcast over the north atlantic with WAVEWATCH III. , *68*(11), 1593–1604. Retrieved from https://doi.org/10.1007/s10236-018-1215-z doi: 10.1007/s10236-018-1215-z

Markina, M., Studholme, J. H. P., & Gulev, S. K. (2019). Ocean wind wave climate responses to wintertime north atlantic atmospheric transient eddies and low-frequency flow. , *32*(17), 5619 – 5638. Retrieved from https://journals.ametsoc.org/view/journals/clim/32/17/jcli-d-18-0595.1.xml (Place: Boston MA, USA Publisher: American Meteorological Society) doi: 10.1175/JCLI-D-18-0595.1

Melet, A., Meyssignac, B., Almar, R., & Le Cozannet, G. (2018). Underestimated wave contribution to coastal sea-level rise. , *8*(3), 234–239. Retrieved from https://doi.org/10.1038/s41558-018-0088-y doi: 10.1038/s41558-018-0088-y

Met Office Hadley Centre. (2018). *UKCP18 simulations of sea surface elevation for uk waters [Dataset].* Centre for Environmental Data Analysis. Retrieved from http://catalogue.ceda.ac.uk/uuid/5fcae68057ea43259d0a4530d34e4ba5 (Accessed: 2025-02-21)

Morales-Márquez, V., Orfila, A., Simarro, G., & Marcos, M. (2020). Extreme waves and climatic patterns of variability in the eastern north atlantic and mediterranean basins. , *16*(6), 1385–1398. Retrieved from https://os.copernicus.org/articles/16/1385/2020/ doi: 10.5194/os-16-1385-2020

Neill, S. P. (2024). Wave resource characterization and co-location with offshore wind in the irish sea. , *222*, 119902. Retrieved from https://www.sciencedirect.com/science/article/pii/S0960148123018177 doi: https://doi.org/10.1016/j.renene.2023.119902

Noël, T., Loukos, H., Defrance, D., Vrac, M., & Levavasseur, G. (2021). A high-resolution downscaled CMIP5 projections dataset of essential surface climate variables over the globe coherent with the ERA5 reanalysis for climate change impact assessments. , *35*, 106900. Retrieved from https://www.sciencedirect.com/science/article/pii/S2352340921001840 doi: https://doi.org/10.1016/j.dib.2021.106900

O'Brien, L., Dudley, J. M., & Dias, F. (2013). Extreme wave events in ireland: 14 680 BP–2012. , *13*(3), 625–648. Retrieved from https://nhess.copernicus.org/articles/13/625/2013/ doi: 10.5194/nhess-13-625-2013

Olonscheck, D., Suarez-Gutierrez, L., Milinski, S., Beobide-Arsuaga, G., Baehr, J., Fröb, F., ... Brune, S. (2023). The new max planck institute grand ensemble with CMIP6 forcing and high-frequency model output. , *15*(10), e2023MS003790. Retrieved from https://agupubs.onlinelibrary.wiley.com/doi/abs/10.1029/2023MS003790 (_eprint: https://agupubs.onlinelibrary.wiley.com/doi/pdf/10.1029/2023MS003790) doi: https://doi.org/10.1029/2023MS003790

Palermo, R. V., Perron, J. T., Soderblom, J. M., Birch, S. P. D., Hayes, A. G., & Ashton, A. D. (2024). NEWTS1.0: Numerical model of coastal erosion by waves and transgressive scarps. , *17*(8), 3433–3445. Retrieved from https://gmd.copernicus.org/articles/17/3433/2024/ doi: 10.5194/gmd-17-3433-2024

Paranunzio, R., Guerrini, M., Dwyer, E., Alexander, P. J., & O'Dwyer, B. (2022). Assessing coastal flood risk in a changing climate for dublin, ireland. *Journal of Marine Science and Engineering*, *10*(11), 1715.

Pilar, P., Soares, C. G., & Carretero, J. C. (2008). 44-year wave hindcast for the north east atlantic european coast. , *55*(11), 861–871. Retrieved from https://www.sciencedirect.com/science/article/pii/S0378383908000458 doi: https://doi.org/10.1016/j.coastaleng.2008.02.027

Pinto, J. G., Bellenbaum, N., Karremann, M. K., & Della-Marta, P. M. (2013). Serial clustering of extratropical cyclones over the north atlantic and europe under recent and future climate conditions. , *118*(22), 12,476–12,485. Retrieved from https://agupubs.onlinelibrary.wiley.com/doi/abs/10.1002/2013JD020564 (_eprint: https://agupubs.onlinelibrary.wiley.com/doi/pdf/10.1002/2013JD020564) doi: https://doi.org/10.1002/2013JD020564

Reduan Atan, S. N., & Goggins, J. (2017). Development of a nested local scale wave model for a 1/4 scale wave energy test site using SWAN. , *10*(1), 59–78. Retrieved from https://doi.org/10.1080/1755876X.2016.1275495 (Publisher: Taylor & Francis _eprint: https://doi.org/10.1080/1755876X.2016.1275495) doi: 10.1080/1755876X.2016.1275495

Reick, C. H., Raddatz, T., Brovkin, V., & Gayler, V. (2013). Representation of natural and anthropogenic land cover change in MPI-ESM. , *5*(3), 459–482. doi: 10.1002/jame.20022

Rezvov, V., Krinitskiy, M., & Gulev, S. (2022). Approximation of high-resolution surface wind speed in the north atlantic using discriminative and generative neural models based on RAS-NAAD 40-year hindcast. In (p. 023). doi: 10.22323/1.429.0023

Rozoff, C. M., & Alessandrini, S. (2022). A comparison between analog ensemble and convolutional neural network empirical-statistical downscaling techniques for reconstructing high-resolution near-surface wind. , *15*(5). Retrieved from https://www.mdpi.com/1996-1073/15/5/1718 doi: 10.3390/en15051718

Rusu, L., Pilar, P., & Guedes Soares, C. (2008). Hindcast of the wave conditions along the west iberian coast. , *55*, 906–919. doi: 10.1016/j.coastaleng.2008.02.029

Scott, T., Wiggins, M., Masselink, G., Castelle, B., Dodet, G., & SAULTER, A. (2019). ATMOSPHERIC CLIMATE CONTROL OF DIRECTIONAL WAVES IN THE UNITED KINGDOM AND IRELAND. In (pp. 708–721). doi: 10.1142/9789811204487_0063

Senter, J., & Lupo, A. (2024). *A euclidean distance diagnostic of north atlantic basin activity.* doi: 10.21203/rs.3.rs-3869007/v1

Sheehan, Kevin and INFOMAR Survey Team. (2021). *CV20_02 INFOMAR survey report.* Retrieved from http://hdl.handle.net/10793/1733

Stevens, B., Giorgetta, M., Esch, M., Mauritsen, T., Crueger, T., Rast, S., ... Roeckner, E. (2013). Atmospheric component of the MPI-m earth system model: ECHAM6. , *5*(2), 146–172. Retrieved from https://agupubs.onlinelibrary.wiley.com/doi/abs/10.1002/jame.20015 (_eprint: https://agupubs.onlinelibrary.wiley.com/doi/pdf/10.1002/jame.20015) doi: https://doi.org/10.1002/jame.20015

Swain, J., Umesh, P., & Balchand, A. (2019). WAM and WAVEWATCH-III intercomparison studies in the north indian ocean using oceansat-2 scatterometer winds. , *9*, 2516019219866569. Retrieved from https://doi.org/10.1177/2516019219866569 (Publisher: SAGE Publications Ltd STM) doi: 10.1177/2516019219866569

SWAN Team. (2023). *Swan - scientific and technical documentation [Software].* Retrieved from http://www.swan.tudelft.nl (Version 41.45)

Tiron, R., Gallagher, S., Gleeson, E., Dias, F., & McGrath, R. (2013). The future wave climate of ireland: From averages to extremes. , *17*. doi: 10.1016/j.piutam.2015.06.007

Tolman, H. L. (1989). The numerical model WAVEWATCH: a third generation model for hindcasting of wind waves on tides in shelf seas.

Towe, R., Eastoe, E., Tawn, J., & Jonathan, P. (2017). Statistical downscaling for future extreme wave heights in the north sea. , *11*(4), 2375 – 2403. Retrieved from https://doi.org/10.1214/17-AOAS1084 (Publisher: Institute of Mathematical Statistics) doi: 10.1214/17-AOAS1084

Tuomi, L., Kanarik, H., Björkqvist, J.-V., Marjamaa, R., Vainio, J., Hordoir, R., ... Kahma, K. K. (2019). Impact of ice data quality and treatment on wave hindcast statistics in seasonally ice-covered seas. , *7*. Retrieved from https://www.frontiersin.org/journals/earth-science/articles/10.3389/feart.2019.00166 doi: 10.3389/feart.2019.00166

van de Wal, R. S., Melet, A., Bellafiore, D., Vousdoukas, M., Camus, P., Ferrarin, C., ... others (2023). Sea level rise in europe: Impacts and consequences. *State of the Planet Discussions*, *2023*, 1–65.

Vousdoukas, M. I., Mentaschi, L., Voukouvalas, E., Verlaan, M., & Feyen, L. (2017). Extreme sea levels on the rise along europe's coasts. , *5*(3), 304–323. Retrieved from https://agupubs.onlinelibrary.wiley.com/doi/abs/10.1002/2016EF000505 (_eprint: https://agupubs.onlinelibrary.wiley.com/doi/pdf/10.1002/2016EF000505) doi: https://doi.org/10.1002/2016EF000505

WAMdi Group. (1988). The WAM model—a third generation ocean wave prediction model. , *18*(12), 1775–1810. Retrieved from https://journals.ametsoc.org/view/journals/phoc/18/12/1520-0485_1988_018_1775_twmtgo_2_0_co_2.xml (Place: Boston MA, USA Publisher: American Meteorological Society) doi: 10

.1175/1520-0485(1988)018⟨1775:TWMTGO⟩2.0.CO;2

Zed, A. A. A., Kansoh, R. M., Iskander, M. M., & Elkholy, M. (2022). Wind and wave climate southeastern of the mediterranean sea based on a high-resolution SWAN model. , *99*, 101311. Retrieved from `https :// www .sciencedirect .com / science / article / pii / S0377026522000306` doi: https://doi.org/10.1016/j.dynatmoce.2022.101311

Zhang, D., Tang, N., Dong, W., & Zhao, L. (2024). Machine learning-based financial big data analysis and forecasting: From preprocessing to deep learning models. , *116*, 143–149. doi: 10.54254/2755-2721/116/20251731

Bibliography

Aarnes, O. J., Reistad, M., Breivik, Ø., Bitner-Gregersen, E., Ingolf Eide, L., Gramstad, O., Magnusson, A. K., Natvig, B., and Vanem, E. (2017). Projected changes in significant wave height toward the end of the 21st century: Northeast a tlantic. *Journal of Geophysical Research: Oceans*, 122(4):3394–3403. 17, 18, 20, 29, 30, 70

Albrecht, G., Sartore, G.-M., Connor, L., Higginbotham, N., Freeman, S., Kelly, B., Stain, H., Tonna, A., and Pollard, G. (2007). Solastalgia: the distress caused by environmental change. *Australasian psychiatry*, 15(sup1):S95–S98. 138

Alizadeh, M. J., Kavianpour, M. R., Kamranzad, B., and Etemad-Shahidi, A. (2020). A distributed wind downscaling technique for wave climate modeling under future scenarios. *Ocean Modelling*, 145:101513. 69

Allan, R. P., Arias, P. A., Berger, S., Canadell, J. G., Cassou, C., Chen, D., Cherchi, A., Connors, S. L., Coppola, E., Cruz, F. A., et al. (2023). Intergovernmental panel on climate change (ipcc). summary for policymakers. In *Climate change 2021: The physical science basis. Contribution of working group I to the sixth assessment report of the intergovernmental panel on climate change*, pages 3–32. Cambridge University Press. 3, 29

Almar, R., Ranasinghe, R., Bergsma, E. W., Diaz, H., Melet, A., Papa, F., Vousdoukas, M., Athanasiou, P., Dada, O., Almeida, L. P., et al. (2021). A global analysis of extreme coastal water levels with implications for potential coastal overtopping. *Nature communications*, 12(1):3775. 123

Alonso, R. and Solari, S. (2021). Automatic calibration and uncertainty quantification in waves dynamical downscaling. *Coastal Engineering*, 169:103944. 31

Alves, J.-H. G. (2006). Numerical modeling of ocean swell contributions to the global wind-wave climate. *Ocean Modelling*, 11(1-2):98–122. 34, 35, 36, 37, 63, 132

Ambarita, E. E., Karlsen, A., Osen, O., and Hasan, A. (2023). Towards fully autonomous floating offshore wind farm operation & maintenance. 9:103–108. 15, 137

Amores, A. and Marcos, M. (2020). Ocean Swells along the Global Coastlines and Their Climate Projections for the Twenty-First Century. *Journal of Climate*, 33(1):185 – 199. Place: Boston MA, USA Publisher: American Meteorological Society. 34

Ana Rute Bento, N. S. and Soares, C. G. (2018). Validation of a wave forecast system for galway bay. 11(2):112–124. Publisher: Taylor & Francis _eprint: https://doi.org/10.1080/1755876X.2018.1470454. 68

Annau, N. J., Cannon, A. J., and Monahan, A. H. (2023). Algorithmic Hallucinations of Near-Surface Winds: Statistical Downscaling with Generative Adversarial Networks to Convection-Permitting Scales. *Artificial Intelligence for the Earth Systems*, 2(4):e230015. Place: Boston MA, USA Publisher: American Meteorological Society. 5

Anton, I. and Nash, S. (2020). Application of the IEC technical specification for assessment of wave energy resource: A case study from the west coast of ireland. 23

Ardhuin, F., Bertotti, L., Bidlot, J.-R., Cavaleri, L., Filipetto, V., Lefevre, J.-M., and Wittmann, P. (2007). Comparison of wind and wave measurements and models in the Western Mediterranean Sea. *Ocean Engineering*, 34(3):526–541. 1

Ardhuin, F., Chapron, B., and Collard, F. (2009). Observation of swell dissipation across oceans. *Geophysical Research Letters*, 36(6). _eprint: https://agupubs.onlinelibrary.wiley.com/doi/pdf/10.1029/2008GL037030. 27, 37, 40, 65

Ardhuin, F., O'Reilly, W. C., Herbers, T. H. C., and Jessen, P. F. (2002). Spectral evolution of swell across the continental shelf. pages 744 – 753. 34

Arinaga, R. A. and Cheung, K. F. (2012). Atlas of global wave energy from 10 years of reanalysis and hindcast data. *Renewable Energy*, 39(1):49–64. 63

Arns, A., Dangendorf, S., Jensen, J., Talke, S., Bender, J., and Pattiaratchi, C. (2017). Sea-level rise induced amplification of coastal protection design heights. *Scientific reports*, 7(1):40171. 3, 24, 25, 123, 128, 135

Atan, R., Goggins, J., and Nash, S. (2016). Development of a high resolution wave model at AMETS using SWAN. In *Proceedings of the Civil Engineering Research in Ireland (CERI) Conference, Galway, Ireland*, pages 29–30. 23

Atkinson, J., Smith, J., and Bender, C. (2013). Sea Level Rise Effects on Storm Surge and Nearshore Waves on the Texas Coast: Influence of Landscape and Storm Characteristics. *Journal of Waterway Port Coastal and Ocean Engineering*, 139:98–117. 5

B. Kinsman (1965). Wind Waves. 33

Babanin, A. V. and Jiang, H. (2017). Ocean swell: how much do we know. In *International conference on offshore mechanics and arctic engineering*, volume 57656, page V03AT02A010. American Society of Mechanical Engineers. 65

Baordo, F., Clementi, E., Iovino, D., and Masina, S. (2020). Intercomparison and assessement of wave models at global scale. 68, 71

Barbariol, F., Pezzutto, P., Davison, S., Bertotti, L., Cavaleri, L., Papa, A., Favaro, M., Sambo, E., and Benetazzo, A. (2022). Wind-wave forecasting in enclosed basins using statistically downscaled global wind forcing. 9. 68

Barber, N. F. and Ursell, F. (1948). The generation and propagation of ocean waves and swell. i. wave periods and velocities. *Philosophical Transactions of the Royal Society of London. Series A, Mathematical and Physical Sciences*, 240(824):527–560. 12, 27

Battjes, J. and Beji, S. (1992). Breaking waves propagating over a shoal. In *Coastal Engineering 1992*, pages 41–50. 21

Bauer, E. and Weisse, R. (2000). Determination of high-frequency wind variability from observations and application to north atlantic wave modeling. 105:26179–26190. _eprint: https://agupubs.onlinelibrary.wiley.com/doi/pdf/10.1029/1999JC000066. 98

Bellomo, K., Clement, A., Mauritsen, T., Rädel, G., and Stevens, B. (2014). Simulating the Role of Subtropical Stratocumulus Clouds in Driving Pacific Climate Variability. *Journal of Climate*, 27:5119–5131. 40

Bento, A., Gonçalves, M., Campos, R., and Guedes Soares, C. (2016). Comparison between two forecast systems implemented with WAM and WaveWatch 3 for the north atlantic. page V003T02A035. 23, 77

Bento., A. R., Martinho, P., Campos, R., and Guedes Soares, C. (2011). Modelling wave energy resources in the irish west coast. In *International Conference on Offshore Mechanics and Arctic Engineering*, volume 44373, pages 945–953. 15, 23

Bento, A. R., Salvação, N., and Guedes Soares, C. (2018). Validation of a wave forecast system for Galway Bay. *Journal of Operational Oceanography*, 11(2):112–124. Publisher: Taylor & Francis. 1, 4, 107

Benton, B., Buster, G., Pinchuk, P., Glaws, A., King, R., Maclaurin, G., and Chernyakhovskiy, I. (2024). *Super Resolution for Renewable Energy Resource Data With Wind From Reanalysis Data (Sup3rWind) and Application to Ukraine*. 5

Bernardino, M., Goncalves, M., and Guedes Soares, C. (2021). Marine climate projections toward the end of the twenty-first century in the north atlantic. *Journal of Offshore Mechanics and Arctic Engineering*, 143(6):061201. 18, 70

Bernardino, M. and Guedes Soares, C. (2016). A climatological analysis of storms in the north atlantic. *Maritime Technology and Engineering*, 3:1021–1026. 19

Bertin, X., Prouteau, E., and Letetrel, C. (2013). A significant increase in wave height in the north atlantic ocean over the 20th century. *Global and Planetary Change*, 106:77–83. 18, 69

Bhowmick, S. A., Kumar, R., Chaudhuri, S., and Sarkar, A. (2011). Swell propagation over indian ocean region. *The International Journal of Ocean and Climate Systems*, 2(2):87–99. 63

Bingölbali, B., Akpınar, A., Jafali, H., and Vledder, G. P. V. (2019). Downscaling of wave climate in the western black sea. 172:31–45. 23

Bitner-Gregersen, E. M., Waseda, T., Parunov, J., Yim, S., Hirdaris, S., Ma, N., and Soares, C. G. (2022). Uncertainties in long-term wave modelling. 84:103217. 20

Bocquet, M. (2023). Surrogate modeling for the climate sciences dynamics with machine learning and data assimilation. 9:1133226. 97

Bommier, E. (2014). Peaks-over-threshold modelling of environmental data. 121

Booij, N., Ris, R. C., and Holthuijsen, L. H. (1999). A third-generation wave model for coastal regions: 1. Model description and validation. *Journal of Geophysical Research: Oceans*, 104(C4):7649–7666. _eprint: https://agupubs.onlinelibrary.wiley.com/doi/pdf/10.1029/98JC02622. 4, 21, 22, 23

Borzi, L., Marino, M., Stagnitti, M., Di Stefano, A., Sciandrello, S., Cavallaro, L., Foti, E., and Musumeci, R. E. (2025). Impact of coastal land use on long-term shoreline change. *Ocean & Coastal Management*, 262:107583. 2

Bradford, S. F. and Sanders, B. F. (2002). Modeling flows with moving boundaries due to flooding, recession, and wave run-up. In *Estuarine and Coastal Modeling (2001)*, pages 695–708. 125

Bradley, S. L., Ely, J. C., Clark, C. D., Edwards, R. J., and Shennan, I. (2023). Reconstruction of the palaeo-sea level of britain and ireland arising from empirical constraints of ice extent: implications for regional sea level forecasts and north american ice sheet volume. *Journal of Quaternary Science*, 38(6):791–805. 25

Bramante, J. (2017). Why is wave climate important. *Woods Hole Oceanographic Institution.(September 4th, 2017)*. 14, 136, 137

Bricheno, L., Amies, J., Chowdhury, P., Woolf, D., and Timmermans, B. (2023). Climate Change Impacts on Storms and Waves Relevant to the UK and Ireland, MCCIP Science Review 2023. page 20pp. 2, 27

Bricheno, L. M. and Wolf, J. (2018). Future wave conditions of europe, in response to high-end climate change scenarios. *Journal of Geophysical Research: Oceans*, 123(12):8762–8791. 17, 70

Brocchini, M. and Baldock, T. (2008). Recent advances in modeling swash zone dynamics: Influence of surf-swash interaction on nearshore hydrodynamics and morphodynamics. *Reviews of Geophysics*, 46(3). 3, 105

Brocchini, M. and Dodd, N. (2008). Nonlinear shallow water equation modeling for coastal engineering. *Journal of waterway, port, coastal, and ocean engineering*, 134(2):104–120. 109

Brown, J. M., Souza, A. J., and Wolf, J. (2010). An 11-year validation of wave-surge modelling in the irish sea, using a nested POLCOMS–WAM modelling system. 33(1):118–128. 4, 68

Bruno, M. F., Molfetta, M. G., Totaro, V., and Mossa, M. (2020). Performance Assessment of ERA5 Wave Data in a Swell Dominated Region. *Journal of Marine Science and Engineering*, 8(3). 37

Brus, S. R., Wolfram, P. J., Van Roekel, L. P., and Meixner, J. D. (2021). Unstructured global to coastal wave modeling for the energy exascale earth system model using wavewatch iii version 6.07. *Geoscientific Model Development*, 14(5):2917–2938. 12

Burguete, J. and Navarro, P. G. (2000). An upwind conservative treatment of source terms in shallow water equations. In *European Congress on Computational Methods in Applied Sciences and Engineering, Eccomas 2000, Barcelona (Spain)*. 127

Calvino, C. (2021). *Coupled wave-ocean models: An application to Galway Bay*. PhD thesis, UCD. 107

Calvino, C., Dabrowski, T., and Dias, F. (2022). Current interaction in large-scale wave models with an application to ireland. 245:104798. 4, 23, 29, 68

Camps-Valls, G., Fernández-Torres, M.-A., Cohrs, K.-H., H'ohl, A., Castelletti, A., Pacal, A., Robin, C., Martinuzzi, F., Papoutsis, I., Prapas, I., Pérez-Aracil, J., Weigel, K., Gonzalez-Calabuig, M., Reichstein, M., Rabel, M., Giuliani, M., Mahecha, M. D., Popescu, O.-I., Pellicer-Valero, O. J., Ouala, S., Salcedo-Sanz, S., Sippel, S., Kondylatos, S., Happé, T., and Williams, T. (2025). Artificial intelligence for modeling and understanding extreme weather and climate events. *Nature Communications*, 16(1):1919. 5

Cardone, V. and Greenwood, J. (1986). Ocean surface wave prediction,-current trends and future prospects. In *OCEANS'86*, pages 1372–1378. IEEE. 22

Casas-Prat, M., Hemer, M. A., Dodet, G., Morim, J., Wang, X. L., Mori, N., Young, I., Erikson, L., Kamranzad, B., Kumar, P., et al. (2024). Wind-wave climate changes

and their impacts. *Nature Reviews Earth & Environment*, 5(1):23–42. 14, 15, 16, 18, 27

Cavaleri, L., Fox-Kemper, B., and Hemer, M. (2012). Wind waves in the coupled climate system. *Bulletin of the American Meteorological Society*, 93(11):1651–1661. 14, 65

Charles, E., Idier, D., Thiébot, J., Le Cozannet, G., Pedreros, R., Ardhuin, F., and Planton, S. (2012). Present wave climate in the bay of biscay: spatiotemporal variability and trends from 1958 to 2001. *Journal of Climate*, 25(6):2020–2039. 19, 20

Charras-Garrido, M. and Lezaud, P. (2013). Extreme value analysis: an introduction. *Journal de la société française de statistique*, 154(2):66–97. 119

Chen, G., Chapron, B., Ezraty, R., and Vandemark, D. (2002). A Global View of Swell and Wind Sea Climate in the Ocean by Satellite Altimeter and Scatterometer. *Journal of Atmospheric and Oceanic Technology*, 19(11):1849–1859. Place: Boston MA, USA Publisher: American Meteorological Society. 34

Chen, J., Kang, S., Du, W., Guo, J., Xu, M., Zhang, Y., Zhong, X., Zhang, W., and Chen, J. (2021). Perspectives on future sea ice and navigability in the arctic. *The Cryosphere*, 15(12):5473–5482. 15, 28, 76

Chen, W.-B. (2024). Analysing seven decades of global wave power trends: The impact of prolonged ocean warming. *Applied Energy*, 356:122440. 15

Chini, N., Stansby, P., Leake, J., Wolf, J., Roberts-Jones, J., and Lowe, J. (2010). The impact of sea level rise and climate change on inshore wave climate: A case study for east anglia (uk). *Coastal Engineering*, 57(11-12):973–984. 24, 123, 124

Christakos, K., Lavidas, G., Gao, Z., and Björkqvist, J.-V. (2024). Long-term assessment of wave conditions and wave energy resource in the arctic ocean. *Renewable Energy*, 220:119678. 28

Collard, F., Ardhuin, F., and Chapron, B. (2009). Monitoring and analysis of ocean swell fields from space: New methods for routine observations. *Journal of Geophysical Research: Oceans*, 114(C7). Publisher: John Wiley & Sons, Ltd. 34

Colosi, L. V., Villas Bôas, A. B., and Gille, S. T. (2021). The seasonal cycle of significant wave height in the ocean: Local versus remote forcing. *Journal of Geophysical Research: Oceans*, 126(8):e2021JC017198. 63

Cooper, J., Jackson, D., Navas, F., McKenna, J., and Malvárez, G. (2004). Identifying storm impacts on an embayed, high-energy coastline: examples from western ireland. *Marine Geology*, 210(1-4):261–280. 106

Courant, R., Friedrichs, K., and Lewy, H. (1928). Über die partiellen differenzengleichungen der mathematischen physik. *Mathematische annalen*, 100(1):32–74. 113

CSO (2022). Census of Population 2022 – Preliminary Results. Press Statement, Central Statistics Office (CSO). Accessed: 2025-09-03. 107

Dabrowski, T., Nagy, H., McGovern, J., Gallagher, S., Nic Guidhir, M., and Olbert, A. I. (2023). Regional and local downscaled models. Technical report, Marine Institute. 20

d'Anna, M., Vedie, L., Belmadani, A., Idier, D., Thieblemont, R., Palany, P., and Longueville, F. (2025). Wave climate projections off coastal french guiana based on high-resolution modelling over the atlantic ocean. *Ocean Modelling*, 194:102468. 134

Dauner, A. L. L., Schenk, F., Power, K. E., and Heikkilä, M. (2024). Sea-ice variations and trends during the common era in the atlantic sector of the arctic ocean. *The Cryosphere*, 18(3):1399–1418. 76

Deacon, G. E. R. (1946). Ocean waves and swell. *The International Hydrographic Review*. 23

Dean, R. G. and Dalrymple, R. A. (1991). *Water wave mechanics for engineers and scientists*, volume 2. world scientific publishing company. 126

Dean, R. G. and Dalrymple, R. A. (2004). *Coastal processes with engineering applications*. Cambridge University Press. 124, 135

Delpey, M. T., Ardhuin, F., Collard, F., and Chapron, B. (2010). Space-time structure of long ocean swell fields. *Journal of Geophysical Research: Oceans*, 115(C12). 40

Devoy, R. (2009). Coastal Vulnerability and the Implications of Sea-Level Rise for Ireland. *Journal of Coastal Research*, 24:325–341. 1, 2, 137

Dewey, J. F. and Ryan, P. D. (2017). Storm, rogue wave, or tsunami origin for megaclast deposits in western ireland and north island, new zealand? *Proceedings of the National Academy of Sciences*, 114(50):E10639–E10647. 106

Dobrynin, M., Kleine, T., Düsterhus, A., and Baehr, J. (2019). Skilful seasonal prediction of ocean surface waves in the atlantic ocean. *Geophysical Research Letters*, 46(3):1731–1739. 17, 18, 19, 27, 30

Dobrynin, M., Murawski, J., Baehr, J., and Ilyina, T. (2015). Detection and attribution of climate change signal in ocean wind waves. *Journal of Climate*, 28(4):1578–1591. 18

Dodet, G., Bertin, X., and Taborda, R. (2010). Wave climate variability in the north-east atlantic ocean over the last six decades. 31(3):120–131. 18, 20, 70

Dodet, G., Leckler, F., Sous, D., Ardhuin, F., Filipot, J. F., and Suanez, S. (2018). Wave runup over steep rocky cliffs. *Journal of Geophysical Research: Oceans*, 123(10):7185–7205. 3, 105

Dodet, G., Melet, A., Ardhuin, F., Bertin, X., Idier, D., and Almar, R. (2019). The Contribution of Wind-Generated Waves to Coastal Sea-Level Changes. *Surveys In Geophysics*, 40(6):1563–1601. Type: Article. 5, 14

Donn, W. L. (1949). Studies of waves and swell in the western north atlantic. *Eos, Transactions American Geophysical Union*, 30(4):507–516. 37, 63

Düsterhus, A. and Brune, S. (2024). Decadal predictability of seasonal temperature distributions. *Geophysical Research Letters*, 51(11):e2023GL107838. 76

Düsterhus, A. and Hense, A. (2012). Advanced information criterion for environmental data quality assurance. *Advances in Science and Research*, 8(1):99–104. 83

Earlie, C., Masselink, G., and Russell, P. (2018). The role of beach morphology on coastal cliff erosion under extreme waves. *Earth Surface Processes and Landforms*, 43(6):1213–1228. 106

Eastman, R., Wood, R., and Bretherton, C. S. (2016). Time scales of clouds and cloud-controlling variables in subtropical stratocumulus from a lagrangian perspective. *Journal of the Atmospheric Sciences*, 73(8):3079 – 3091. 40

ECMWF (2016). IFS documentation CY41r2. Publisher: ECMWF Reading, UK. 4, 75

ECMWF (2019). ERA5 reanalysis (0.25 degree latitude-longitude grid). Place: Boulder CO. 75

Efron, B. (1992). Bootstrap methods: another look at the jackknife. In *Breakthroughs in statistics: Methodology and distribution*, pages 569–593. Springer. 40

EMODnet (2024). EMODnet Digital Bathymetry (DTM 2024). 117

Erdmann, W., Kelletat, D., and Kuckuck, M. (2017). Boulder ridges and washover features in galway bay, western ireland. *Journal of Coastal Research*, 33(5):997–1021. 107, 108

Fan, Y., Lin, S.-J., Griffies, S. M., and Hemer, M. A. (2014). Simulated global swell and wind-sea climate and their responses to anthropogenic climate change at the end of the twenty-first century. *Journal of Climate*, 27(10):3516–3536. 64

Farrok, O., Farah, M. M., and Islam, M. R. (2024). Introduction to the principles of wave energy conversion. In Farrok, O. and Islam, M. R., editors, *Oceanic Wave Energy Conversion: Advancement of Electrical Generators*, pages 1–15. Springer Nature Singapore. 14

Fatihah, M. P. N. and Loy, K. (2023). On efficient fourth-order runge-kutta-central schemes for modeling tsunami propagation and run-up prediction. In *AIP Conference Proceedings*, volume 2484, page 030006. AIP Publishing LLC. 109, 125

Fedele, F., Herterich, J., Tayfun, A., and Dias, F. (2019). Large nearshore storm waves off the irish coast. 9(1):15406. 69

Feser, F., Barcikowska, M., Krueger, O., Schenk, F., Weisse, R., and Xia, L. (2015). Storminess over the north atlantic and northwestern europe—a review. *Quarterly Journal of the Royal Meteorological Society*, 141(687):350–382. 20

Forbes, D., Taylor, R., Orford, J., Carter, R., and Shaw, J. (1991). Gravel-barrier migration and overstepping. *Marine Geology*, 97(3-4):305–313. 2

Forristall, G. Z. and Reece, A. M. (1985). Measurements of wave attenuation due to a soft bottom: the swamp experiment. *Journal of Geophysical Research: Oceans*, 90(C2):3367–3380. 22

Fox-Kemper, B. (2021). Ocean, cryosphere and sea level change. In *AGU fall meeting abstracts*, volume 2021, pages U13B–09. 15, 16, 24, 29, 76

Fusco, F., Nolan, G., and Ringwood, J. V. (2010). Variability reduction through optimal combination of wind/wave resources–an irish case study. *Energy*, 35(1):314–325. 2, 35, 131

Gaffet, A., Bertin, X., Sous, D., Michaud, H., Roland, A., and Cordier, E. (2025). A new global high-resolution wave model for the tropical ocean using WAVEWATCH III version 7.14. *Geoscientific Model Development*, 18(6):1929–1946. 3, 4, 15

Gallagher, S., Gleeson, E., Tiron, R., McGrath, R., and Dias, F. (2016a). Twenty-first century wave climate projections for ireland and surface winds in the north atlantic ocean. *Advances in Science and Research*, 13:75–80. 18, 29, 30, 69, 70, 90, 99

Gallagher, S., Gleeson, E., Tiron, R., McGrath, R., and Dias, F. (2016b). Wave climate projections for ireland for the end of the 21st century including analysis of EC-earth winds over the north atlantic ocean. 36(14):4592–4607. _eprint: https://rmets.onlinelibrary.wiley.com/doi/pdf/10.1002/joc.4656. 25, 69, 70, 98, 99

Gallagher, S., Tiron, R., and Dias, F. (2014). A long-term nearshore wave hindcast for Ireland: Atlantic and Irish Sea coasts (1979–2012). *Ocean Dynamics*, 64(8):1163–1180. 2, 27, 35, 69, 131

Gallagher, S., Tiron, R., Whelan, E., Gleeson, E., Dias, F., and McGrath, R. (2016c). The nearshore wind and wave energy potential of Ireland: A high resolution assessment of availability and accessibility. *Renewable Energy*, 88:494–516. 1, 3, 68

García-Medina, G., Özkan-Haller, H. T., Holman, R. A., and Ruggiero, P. (2017). Large runup controls on a gently sloping dissipative beach. *Journal of Geophysical Research: Oceans*, 122(7):5998–6010. 106

Garcia-Pereira, F., González-Rouco, J. F., and Johann, J. (2023). MPI-ESM1.2-LR p2k+ with a deep version of JSBACH (MPI-ESM p2k+d). 75

Gaughan, E. and Fitzgerald, B. (2020). An assessment of the potential for Co-located offshore wind and wave farms in Ireland. *Energy*, 200:117526. 2, 35, 70, 98, 131

GCC (2024). Chapter 2: Climate Change Overview of the local authority climate action plan 2024–2029. Web page, Galway County Council Consultation Portal. Accessed: 2025-09-03. 107

GEBCO Bathymetric Compilation Group (2023). The GEBCO_2023 grid - a continuous terrain model of the global oceans and land. 75

Gedik, N., İrtem, E., and Kabdasli, S. (2005). Laboratory investigation on tsunami run-up. *Ocean Engineering*, 32(5-6):513–528. 110

Gentil, E., Lorenzzetti, J., and Chapron, B. (2012). Swell and Wind-Sea Distributions over the Mid-Latitude and Tropical North Atlantic for the Period 2002–2008. *International Journal of Oceanography*, 2012. 34

Gentile, E. S., Zhao, M., and Hodges, K. (2023). Poleward intensification of midlatitude extreme winds under warmer climate. *npj Climate and Atmospheric Science*, 6(1):219. 90, 134

Gerber, E. P., Voronin, S., and Polvani, L. M. (2008). Testing the annular mode autocorrelation time scale in simple atmospheric general circulation models. *Monthly Weather Review*, 136(4):1523 – 1536. 40

Getter, D., Bessac, J., Rudi, J., and Feng, Y. (2024). Statistical treatment of convolutional neural network superresolution of inland surface wind for subgrid-scale variability quantification. 3(1):e230009. Place: Boston MA, USA Publisher: American Meteorological Society. 97

Gleeson, E., Clancy, C., Zubiate, L., Janjić, J., Gallagher, S., and Dias, F. (2019). Teleconnections and extreme ocean states in the northeast atlantic ocean. *Advances in Science and Research*, 16:11–29. 69, 70

Google Earth (2025). Satellite image of galway, ireland. Imagery ©2025 Maxar Technologies. Google Earth. Accessed September 17, 2025. 108

Guenther, Reading (United Kingdom)], H. E. C. f. M. R. W. F. E., "[GKSS-Forschungszentrum Geesthacht GmbH (Germany)]", "Hasselmann, Hamburg (Germany)]", S. M.-P.-I. f. M., and "Janssen, De Bilt (Netherlands)]", P. A. K. N. M. I. (1992). The WAM model cycle 4. Technical report, Germany. Journal Abbreviation: [] Publication Title: []. 4

Guisado-Pintado, E. (2020). *Shallow water wave modelling in the nearshore (SWAN)*. Publication Title: Sandy Beach Morphodynamics. 22, 23

Guisado-Pintado, E. and Jackson, D. W. (2019). Coastal impact from high-energy events and the importance of concurrent forcing parameters: The cases of storm ophelia (2017) and storm hector (2018) in nw ireland. *Frontiers in Earth Science*, 7:190. 2, 14, 104, 106

Gulev, S. K. and Grigorieva, V. (2006). Variability of the Winter Wind Waves and Swell in the North Atlantic and North Pacific as Revealed by the Voluntary Observing Ship Data. *Journal of Climate*, 19(21):5667 – 5685. Place: Boston MA, USA Publisher: American Meteorological Society. 26, 34

Guza, R. and Feddersen, F. (2012). Effect of wave frequency and directional spread on shoreline runup. *Geophysical Research Letters*, 39(11). 125

Günther, H., Hasselmann, S., and Janssen, P. A. (1992). The WAM model cycle 4 (revised version). Publisher: Deutsches KlimaRechenZentrum. 71

Hall, P., Horowitz, J. L., and Jing, B.-Y. (1995). On blocking rules for the bootstrap with dependent data. *Biometrika*, 82(3):561–574. 40

Han, Z. and Li, S. (2018). Precursor role of winter sea-ice in the Labrador Sea for following-spring precipitation over southeastern North America and western Europe. *Adv. Atmos. Sci.*, 35(1):65–74. 62

Harley, M., Turner, I., Kinsela, M., Middleton, J., Mumford, P., Splinter, K., Phillips, M., Simmons, J., Hanslow, D., and Short, A. (2017). Extreme coastal erosion enhanced by anomalous extratropical storm wave direction. sci rep 7: 1–9. 65

Harley, M. D., Turner, I., Short, A., and Ranasinghe, R. (2011). A reevaluation of coastal embayment rotation: The dominance of cross-shore versus alongshore sediment transport processes, collaroy-narrabeen beach, southeast australia. *Journal of Geophysical Research: Earth Surface*, 116(F4). 125

Harris, M., Nicolsky, D., Pelinovsky, E., and Rybkin, A. (2015). Runup of nonlinear long waves in trapezoidal bays: 1-d analytical theory and 2-d numerical computations. *Pure and Applied Geophysics*, 172(3):885–899. 109, 125

Harvey, B., Cook, P., Shaffrey, L., and Schiemann, R. (2020). The response of the northern hemisphere storm tracks and jet streams to climate change in the cmip3, cmip5, and cmip6 climate models. *Journal of Geophysical Research: Atmospheres*, 125(23):e2020JD032701. 100

Hasselmann, K., Barnett, T. P., Bouws, E., Carlson, H., Cartwright, D. E., Enke, K., Ewing, J., Gienapp, A., Hasselmann, D., Kruseman, P., et al. (1973). Measurements of wind-wave growth and swell decay during the joint north sea wave project (jonswap). *Ergaenzungsheft zur Deutschen Hydrographischen Zeitschrift, Reihe A*. 10, 11, 12

Hecht, M. W., Holland, W. R., and Rasch, P. J. (1995). Upwind-weighted advection schemes for ocean tracer transport: An evaluation in a passive tracer context. *Journal of Geophysical Research: Oceans*, 100(C10):20763–20778. 127

Hell, M. C., Ayet, A., and Chapron, B. (2021). Swell generation under extra-tropical storms. *Journal of Geophysical Research: Oceans*, 126(9):e2021JC017637. 132

Hemer, M. A., Fan, Y., Mori, N., Semedo, A., and Wang, X. L. (2013). Projected changes in wave climate from a multi-model ensemble. *Nature climate change*, 3(5):471–476. 15, 18, 30, 31

Hersbach, H., Bell, B., Berrisford, P., Biavati, G., Horányi, A., Muñoz Sabater, J., Nicolas, J., Peubey, C., Radu, R., Rozum, I., Schepers, D., Simmons, A., Soci, C., Dee, D., and Thépaut, J.-N. (2023). ERA5 hourly data on single levels from 1940 to present. 75

Hersbach, H., Bell, B., Berrisford, P., Hirahara, S., Horányi, A., Muñoz-Sabater, J., Nicolas, J., Peubey, C., Radu, R., Schepers, D., Simmons, A., Soci, C., Abdalla, S., Abellan, X., Balsamo, G., Bechtold, P., Biavati, G., Bidlot, J., Bonavita, M., De Chiara, G., Dahlgren, P., Dee, D., Diamantakis, M., Dragani, R., Flemming, J., Forbes, R., Fuentes, M., Geer, A., Haimberger, L., Healy, S., Hogan, R. J., Hólm, E., Janisková, M., Keeley, S., Laloyaux, P., Lopez, P., Lupu, C., Radnoti, G., de Rosnay, P., Rozum, I., Vamborg, F., Villaume, S., and Thépaut, J.-N. (2020). The ERA5 global reanalysis. 146(730):1999–2049. _eprint: https://rmets.onlinelibrary.wiley.com/doi/pdf/10.1002/qj.3803. 26, 27, 37

Herterich, J. G. and Dias, F. (2017). Wave breaking and runup of long waves approaching a cliff over a variable bathymetry. *Procedia IUTAM*, 25:18–27. 106

Holman, R. A. (1986). Extreme value statistics for wave run-up on a natural beach. *Coastal Engineering*, 9(6):527–544. 115, 116, 117

Holthuijsen, L. (2007). Waves in Oceanic and Coastal Waters. *Waves in Oceanic and Coastal Waters, by Leo H. Holthuijsen, pp. 404. Cambridge University Press, January 2007. ISBN-10: . ISBN-13:.* 4, 13, 34, 37

Horrillo-Caraballo, J. M., Yin, Y., Fairley, I., Karunarathna, H., Masters, I., and Reeve, D. E. (2021). A comprehensive study of the tides around the Welsh coastal waters. *Estuarine, Coastal and Shelf Science*, 254:107326. 35

Huang, C.-J., Chang, Y.-C., Tai, S.-C., Lin, C.-Y., Lin, Y.-P., Fan, Y.-M., Chiu, C.-M., and Wu, L.-C. (2020). Operational monitoring and forecasting of wave run-up on seawalls. *Coastal Engineering*, 161:103750. 137

Huang, J., Ji, M.-X., Kaz, H., and Shabbar, A. (2006). Temporal structures of the north atlantic oscillation and its impact on the regional climate variability. *Advances in Atmospheric Sciences*, 23:23 – 32. 46

Hubbard, P. (2012). Thinking spaces, differently? *Dialogues in Human Geography*, 2(1):23–26. 138

Hughes, M. (2016). Coastal waves, water levels, beach dynamics and climate change. *Coast Adapt, National Climate Change Adaptation Research Facility, Gold Coast.* 23

Hunter, J. (2010). Estimating sea-level extremes under conditions of uncertain sea-level rise. *Climatic change*, 99(3):331–350. 128

Hurrell, J. (2001). North atlantic oscillation (nao)*. In Steele, J. H., editor, *Encyclopedia of Ocean Sciences (Second Edition)*, pages 65–72. Academic Press, Oxford, second edition edition. 18, 19, 46

Ilyina, T., Six, K. D., Segschneider, J., Maier-Reimer, E., Li, H., and Nunez-Riboni, I. (2013). Global ocean biogeochemistry model HAMOCC: Model architecture and performance as component of the MPI-earth system model in different CMIP5 experimental realizations. 5(2):287–315. 75

Islek, F., Yuksel, Y., and Sahin, C. (2022). Evaluation of regional climate models and future wave characteristics in an enclosed sea: A case study of the Black Sea. *Ocean Engineering*, 262:112220. 4

Ivanov, V. and Repina, I. (2018). The effect of seasonal variability of atlantic water on the arctic sea ice cover. *Izvestiya, Atmospheric and Oceanic Physics*, 54(1):65–72. 76

Iversen, E. and Burningham, H. (2015). Relationship between NAO and wind climate over Norway. *Clim. Res.*, 63(2):115–134. 62, 132

Izaguirre, C., Méndez, F. J., Menéndez, M., and Losada, I. J. (2011). Global extreme wave height variability based on satellite data. *Geophysical Research Letters*, 38(10). 19

Izaguirre Lasa, C., Méndez Incera, F. J., Menéndez García, M., Luceño Vázquez, A., Losada Rodríguez, I., et al. (2010). Extreme wave climate variability in southern europe using satellite data. 19

Janssen, P. and Bidlot, J.-R. (2003). Part vii: Ecmwf wave-model documentation. *IFS Documentation Cycle CY23R4, ECMWF*, 46. 12, 37, 72

Janssen, P. A. (1991). Quasi-linear theory of wind-wave generation applied to wave forecasting. *Journal of physical oceanography*, 21(11):1631–1642. 11

Janssen, P. A. (2008). Progress in ocean wave forecasting. *Journal of Computational Physics*, 227(7):3572–3594. 21

Jasak, H., Jemcov, A., Tukovic, Z., et al. (2007). Openfoam: A c++ library for complex physics simulations. In *International workshop on coupled methods in numerical dynamics*, volume 1000, pages 1–20. Dubrovnik, Croatia). 107

Jenkins, A. D., Paskyabi, M. B., Fer, I., Gupta, A., and Adakudlu, M. (2012). Modelling the effect of ocean waves on the atmospheric and ocean boundary layers. *Energy Procedia*, 24:166–175. 14

Jungclaus, J. H., Fischer, N., Haak, H., Lohmann, K., Marotzke, J., Matei, D., Mikolajewicz, U., Notz, D., and von Storch, J. S. (2013). Characteristics of the ocean simulations in the max planck institute ocean model (MPIOM) the ocean component of the MPI-earth system model. 5(2):422–446. _eprint: https://agupubs.onlinelibrary.wiley.com/doi/pdf/10.1002/jame.20023. 75, 76

Kämpf, J. (2009). *Ocean modelling for beginners: using open-source software*. Springer Science & Business Media. 109, 110, 113, 115

Kandrot, S., Farrell, E., and Devoy, R. (2016). The morphological response of foredunes at a breached barrier system to winter 2013/2014 storms on the southwest coast of ireland. *Earth Surface Processes and Landforms*, 41(14):2123–2136. 2

Kellert, S. R. (2005). Coastal values and a sense of place. *America's changing coasts: Private rights and public trust*, pages 13–25. 138

Kim, I.-C. and Suh, K.-D. (2018). Effect of sea level rise and offshore wave height change on nearshore waves and coastal structures. *Journal of marine science and application*, 17(2):192–207. 123

Kirby, J. T., Wei, G., Chen, Q., Kennedy, A. B., and Dalrymple, R. A. (1998). Funwave 1.0: fully nonlinear boussinesq wave model-documentation and user's manual. Technical report, University of Delaware. 5

Klotzbach, P. J. (2011). The influence of el nino-southern oscillation and the atlantic multidecadal oscillation on caribbean tropical cyclone activity. *Journal of Climate*, 24:721 – 731. 63

Komen, G. J., Cavaleri, L., Donelan, M., Hasselmann, K., Hasselmann, S., Janssen, P., et al. (1994). *Dynamics and modelling of ocean waves*, volume 532. Cambridge university press UK. 11, 12, 21, 22

Kopp, R. E., Garner, G. G., Hermans, T. H., Jha, S., Kumar, P., Reedy, A., Slangen, A. B., Turilli, M., Edwards, T. L., Gregory, J. M., et al. (2023). The framework for assessing changes to sea-level (facts) v1. 0: a platform for characterizing parametric and structural uncertainty in future global, relative, and extreme sea-level change. *Geoscientific Model Development*, 16(24):7461–7489. 76

Kuiry, S. N., Wu, W., and Ding, Y. (2012). A one-dimensional shock-capturing model for long wave run-up on sloping beaches. *ISH Journal of Hydraulic Engineering*, 18(2):65–79. 109, 125

Kumar, A. and Hayatdavoodi, M. (2023). On wave–current interaction in deep and finite water depths. *Journal of Ocean Engineering and Marine Energy*, 9(3):455–475. 15, 29

Kumar, R., Lemos, G., Semedo, A., and Li, J.-G. (2025). A global high-resolution cmip6 ensemble of wave climate simulations and projections using a coastal multigrid: configuration and performance evaluation. *Ocean Modelling*, page 102566. 16

Künsch, H. R. (1989). The jackknife and the bootstrap for general stationary observations. *The annals of Statistics*, pages 1217–1241. 40

Lalbeharry, R. and Ritchie, H. (2009). Wave simulation using SWAN in nested and unnested mode applications. 68

Lara, J., Losada, I., Del Jesus, M., Barajas, G., and Guanche, R. (2010). Ih-3vof: A three-dimensional navier-stokes model for wave and structure interaction. *COASTAL ENGINEERING*, page 2. 5

Leach, C., Hague, B. S., Kennedy, D. M., Carvalho, R. C., and Ierodiaconou, D. (2021). Identifying oceanographic conditions conducive to coastal impacts on temperate open coastal beaches. *Natural Hazards*, 109(1):499–521. 14

Lee, E., Van Dang, H., Shin, S., Yoo, J., and Park, H. (2024). Observations of wave run-up affected by dune scarp during storm conditions: a two dimensional large-scaled movable bed experiment. *Frontiers in Marine Science*, 11:1369418. 106

Lefèvre, J.-M. (2009). High swell warnings in the caribbean islands during march 2008. *Natural hazards*, 49(2):361–370. 65

Lemos, G., Bosnic, I., Antunes, C., Vousdoukas, M., Mentaschi, L., Santo, M., Ferreira, V., and Soares, P. M. (2024). The future of the portuguese most vulnerable coastal areas under climate change–shoreline evolution and future extreme coastal flooding from downscaled bias corrected ensembles. Technical report, Copernicus Meetings. 134

Lemos, G., Menendez, M., Semedo, A., Camus, P., Hemer, M., Dobrynin, M., and Miranda, P. M. (2020). On the need of bias correction methods for wave climate projections. *Global and Planetary Change*, 186:103109. 18, 30

Lemos, G., Menendez, M., Semedo, A., Miranda, P. M., and Hemer, M. (2021). On the decreases in north atlantic significant wave heights from climate projections. *Climate Dynamics*, 57(9):2301–2324. 29, 70, 134

Lemos, G., Semedo, A., Dobrynin, M., Behrens, A., Staneva, J., Bidlot, J.-R., and Miranda, P. M. (2019). Mid-twenty-first century global wave climate projections: Results from a dynamic cmip5 based ensemble. *Global and planetary change*, 172:69–87. 18, 30

Lemos, G., Semedo, A., Kumar, R., Dobrynin, M., Akpinar, A., Kamranzad, B., Bidlot, J., and Lobeto, H. (2023). Performance evaluation of a global CMIP6 single forcing, multi wave model ensemble of wave climate simulations. 184:102237. 72

Lerma, A. N., Pedreros, R., Robinet, A., and Sénéchal, N. (2017). Simulating wave setup and runup during storm conditions on a complex barred beach. *Coastal Engineering*, 123:29–41. 106

Lewis, J. (2001). Fast Normalized Cross-Correlation. *Ind. Light Magic*, 10. 38

Li, C., Özkan-Haller, H. T., García-Medina, G., Holman, R. A., Ruggiero, P., Jensen, T. M., Elson, D. B., and Schneider, W. R. (2021). Observations of extreme wave runup events on the us pacific northwest coast. *Natural Hazards and Earth System Sciences Discussions*, 2021:1–26. 106

Li, C., Özkan-Haller, H. T., Lomonaco, P., Maddux, T. B., and García-Medina, G. (2022a). Experimental study of wave runup variability on a dissipative beach. *Journal of Geophysical Research: Oceans*, 127(6):e2022JC018418. 137

Li, D., Feng, J., Zhu, Y., Staneva, J., Qi, J., Behrens, A., Lee, D., Min, S.-K., and Yin, B. (2022b). Dynamical projections of the mean and extreme wave climate in the bohai sea, yellow sea and east china sea. *Frontiers in Marine Science*, 9:844113. 17

Li, X.-M. (2016). A new insight from space into swell propagation and crossing in the global oceans. *Geophysical Research Letters*, 43(10):5202–5209. 34

Liang, D., Liu, H., Tang, H., and Rana, R. (2013). Comparison between boussinesq and shallow-water models in predicting solitary wave runup on plane beaches. *Coastal engineering journal*, 55(04):1350014. 109

Liu, W.-j., Shao, K.-q., Ning, Y., and Zhao, X.-z. (2020). Numerical study of the impact of climate change on irregular wave run-up over reef-fringed coasts. *China Ocean Engineering*, 34(2):162–171. 123

Loarca, A. L., Cobos, M., Besio, G., and Baquerizo, A. (2021). Projected wave climate temporal variability due to climate change. *Stochastic Environmental Research and Risk Assessment*, 35(9):1741–1757. 16

Lobeto, H., Menendez, M., and Losada, I. J. (2021). Future behavior of wind wave extremes due to climate change. *Scientific Reports*, 11(1):7869. 3, 15, 16, 70

Lobeto, H., Semedo, A., Menendez, M., Lemos, G., Kumar, R., Akpinar, A., Dobrynin, M., and Kamranzad, B. (2023). On the assessment of the wave modeling uncertainty in wave climate projections. *Environmental Research Letters*, 18(12):124006. 17

Longuet-Higgins, M. S. (1953). On the statistical distribution of the heights of sea waves. 13

Lopez, H., Lee, S.-K., West, R., Kim, D., Foltz, G. R., Alaka Jr, G. J., and Murakami, H. (2024). Projected increase in the frequency of extremely active atlantic hurricane seasons. *Science Advances*, 10(46):eadq7856. 3

Loureiro, C. and Cooper, A. (2019). Temporal variability in winter wave conditions and storminess in the northwest of ireland. 51(2):155–170. Section: Articles. 69

Lowe, J. A., Bernie, D., Bett, P., Bricheno, L., Brown, S., Calvert, D., Clark, R., Eagle, K., Edwards, T., Fosser, G., et al. (2018). Ukcp18 science overview report. *Met Office Hadley Centre: Exeter, UK*, pages 1–73. 76

Lowe, R. J., Buckley, M. L., Altomare, C., Rijnsdorp, D. P., Yao, Y., Suzuki, T., and Bricker, J. (2019). Numerical simulations of surf zone wave dynamics using smoothed particle hydrodynamics. *Ocean Modelling*, 144:101481. 21

Luo, W. and Flather, R. (1997). Nesting a nearshore wave model (swan) into an ocean wave model (wam) with application to the southern north sea. *WIT Transactions on The Built Environment*, 30. 23

Luzia, G., Hahmann, A. N., and Koivisto, M. J. (2022). Evaluating the mesoscale spatio-temporal variability in simulated wind speed time series over northern europe. *Wind Energy Science*, 7(6):2255–2270. 83

Mahdavi, A. and Talebbeydokhti, N. (2009). Modeling of non-breaking and breaking solitary wave run-up using force-muscl scheme. *Journal of hydraulic research*, 47(4):476–485. 125

Maia, N., Almeida, L. P., Emmendorfer, L., Nicolodi, J. L., and Calliari, L. (2022). Wave climate trends and breakpoints during the Atlantic Multidecadal Oscillation (AMO) in southern Brazil. *Coastal Management*, 70:22027. 3, 15

Makkonen, L. (2006). Plotting positions in extreme value analysis. *Journal of Applied Meteorology and Climatology*, 45(2):334–340. 119

Marine Institute (2022). Irish marine data buoy observation network. 30, 77

Markina, M., Gavrikov, A., Gulev, S., and Barnier, B. (2018). Developing configuration of WRF model for long-term high-resolution wind wave hindcast over the North Atlantic with WAVEWATCH III. *Ocean Dynamics*, 68(11):1593–1604. 4, 27, 33, 34, 68, 77

Markina, M., Studholme, J. H. P., and Gulev, S. K. (2019). Ocean wind wave climate responses to wintertime north atlantic atmospheric transient eddies and low-frequency flow. 32(17):5619 – 5638. Place: Boston MA, USA Publisher: American Meteorological Society. 20

Marshall, J., Kushnir, Y., Battisti, D., Chang, P., Czaja, A., Dickson, R., Hurrell, J., McCartney, M., Saravanan, R., and Visbeck, M. (2001). North atlantic climate variability: phenomena, impacts and mechanisms. *International Journal of Climatology: A Journal of the Royal Meteorological Society*, 21(15):1863–1898. 18

Martínez-Asensio, A., Tsimplis, M. N., Marcos, M., Feng, X., Gomis, D., Jordà, G., and Josey, S. A. (2016). Response of the north atlantic wave climate to atmospheric modes of variability. *International Journal of Climatology*, 36(3). 17, 18, 19

Massel, S. R. (2017). *Ocean surface waves: their physics and prediction*, volume 45. World scientific. 13

Mauritsen, T., Bader, J., Becker, T., Behrens, J., Bittner, M., Brokopf, R., Brovkin, V., Claussen, M., Crueger, T., Esch, M., Fast, I., Fiedler, S., Fläschner, D., Gayler, V., Giorgetta, M., Goll, D. S., Haak, H., Hagemann, S., Hedemann, C., Hohenegger, C., Ilyina, T., Jahns, T., Jimenéz-de-la Cuesta, D., Jungclaus, J., Kleinen, T., Kloster, S., Kracher, D., Kinne, S., Kleberg, D., Lasslop, G., Kornblueh, L., Marotzke, J., Matei, D., Meraner, K., Mikolajewicz, U., Modali, K., Möbis, B., Müller, W. A., Nabel, J. E. M. S., Nam, C. C. W., Notz, D., Nyawira, S.-S., Paulsen, H., Peters, K., Pincus, R., Pohlmann, H., Pongratz, J., Popp, M., Raddatz, T. J., Rast, S., Redler, R., Reick, C. H., Rohrschneider, T., Schemann, V., Schmidt, H., Schnur, R., Schulzweida, U., Six, K. D., Stein, L., Stemmler, I., Stevens, B., von Storch, J.-S., Tian, F., Voigt, A., Vrese, P., Wieners, K.-H., Wilkenskjeld, S., Winkler, A., and Roeckner, E. (2019). Developments in the MPI-m earth system model version 1.2 (MPI-ESM1.2) and its response to increasing CO2. 11(4):998–1038. _eprint: https://agupubs.onlinelibrary.wiley.com/doi/pdf/10.1029/2018MS001400. 27

McCullagh, D., Benetti, S., Plets, R., Sacchetti, F., O'keeffe, E., and Lyons, K. (2020). Geomorphology and substrate of galway bay, western ireland. *Journal of Maps*, 16(2):166–178. 107

McGrath, R., Lynch, P., Dunne, S., Hanafin, J., Nishimura, E., Nolan, P., Venkata Ratnam, J., Semmler, T., Sweeney, C., Varghese, S., et al. (2008). Ireland in a warmer world: scientific predictions of the irish climate in the twenty-first century. 3, 25

McGrath, R., Nishimura, E., Nolan, P., Semmler, T., Sweeney, C., and Wang, S. (2005). *Climate change: Regional climate model predictions for Ireland*. Environmental Protection Agency Dublin. 3

Medellín, G., Mayor, M., Appendini, C. M., Cerezo-Mota, R., and Jiménez, J. A. (2021). The role of beach morphology and mid-century climate change effects on wave runup and storm impact on the northern yucatan coast. *Journal of Marine Science and Engineering*, 9(5):518. 124, 127

Melet, A., Meyssignac, B., Almar, R., and Le Cozannet, G. (2018). Under-estimated wave contribution to coastal sea-level rise. *Nature Climate Change*, 8(3):234–239. 5, 14, 15, 25, 29

Méndez, F. J. and Rueda, A. (2020). Wave climates: deep water to shoaling zone. In *Sandy Beach Morphodynamics*, pages 39–59. Elsevier. 11, 14, 137

Meucci, A., Young, I. R., Hemer, M., Kirezci, E., and Ranasinghe, R. (2020). Projected 21st century changes in extreme wind-wave events. *Science advances*, 6(24):eaaz7295. 31

Meucci, A., Young, I. R., Trenham, C., and Hemer, M. (2024). An 8-model ensemble of cmip6-derived ocean surface wave climate. *Scientific Data*, 11(1):100. 16, 18, 28, 31

Miles, J. W. (1957). On the generation of surface waves by shear flows. *Journal of Fluid Mechanics*, 3(2):185–204. 10, 11

Mora-Escalante, R. E., Osuna, P., Ocampo-Torres, F. J., Villarreal-Olavarrieta, C. E., and Babanin, A. V. (2025). High-frequency wave dynamics in mixed seas: The influence of swells on wind waves characteristics. *Ocean Modelling*, 196:102523. 12

Morales-Márquez, V., Orfila, A., Simarro, G., and Marcos, M. (2020). Extreme waves and climatic patterns of variability in the eastern north atlantic and mediterranean basins. 16(6):1385–1398. 18, 19, 20, 30

Morim, J., Hemer, M., Wang, X. L., Cartwright, N., Trenham, C., Semedo, A., Young, I., Bricheno, L., Camus, P., Casas-Prat, M., et al. (2019). Robustness and uncertainties in global multivariate wind-wave climate projections. *Nature Climate Change*, 9(9):711–718. 15, 17, 18, 20, 30, 31, 101

Morim, J., Vitousek, S., Hemer, M., Reguero, B., Erikson, L., Casas-Prat, M., Wang, X. L., Semedo, A., Mori, N., Shimura, T., et al. (2021). Global-scale changes to extreme ocean wave events due to anthropogenic warming. *Environmental Research Letters*, 16(7):074056. 17

Mousa, M. M. (2018). Efficient numerical scheme based on the method of lines for the shallow water equations. *Journal of Ocean Engineering and Science*, 3(4):303–309. 110

Murphy, C., Heaphy, L., Quinn, T., O'Brien, E., and Nolan, P. (2023). Ireland's Climate Change Assessment. Volume 3: Being Prepared for Ireland's Future Climate. Publisher: Environmental Protection Agency Ireland (EPA). 2

Neill, C. (2021). Galway City Coastal Wave and Water Level Modelling Study 2020. Technical Report IBE1703 CWWS, Office of Public Works. Accessed: 2025-09-03. 108

Neill, S. P. (2024). Wave resource characterization and co-location with offshore wind in the irish sea. 222:119902. 23

Nic Guidhir, M., Kennedy, D., Berry, A., Christy, B., Clancy, C., Creamer, C., Westbrook, G., and Gallagher, S. (2022). Irish Wave Data—Rogues, Analysis and Continuity. *Journal of Marine Science and Engineering*, 10(8). 2, 27, 35, 131

NOAA Ocean Service (2024). What causes waves in the ocean? Accessed: 2025-07-15. 4

Noël, T., Loukos, H., Defrance, D., Vrac, M., and Levavasseur, G. (2021). A high-resolution downscaled cmip5 projections dataset of essential surface climate variables over the globe coherent with the era5 reanalysis for climate change impact assessments. *Data in Brief*, 35:106900. 79

Noone, C., McClean, D., Gallagher, D., and Thorne, P. (2024). Ireland's climate change assessment 2023. volume 1: Climate science-ireland in a changing world. summary of policymakers. 16, 25

Noor, D. M. M., Faiqoh, M. H., and Fauzi, R. (2024). Numerical simulation of run-up wave using nonlinear shallow water equations with staggered grid at canti beach, south lampung. *Sainmatika: Jurnal Ilmiah Matematika dan Ilmu Pengetahuan Alam*, 21(2):161–169. 109, 110, 125, 126

Nwogu, O. G. and Demirbilek, Z. (2001). Bouss-2d: A boussinesq wave model for coastal regions and harbors. *(No Title)*. 21

O'Brien, L., Dudley, J. M., and Dias, F. (2013). Extreme wave events in ireland: 14 680 BP–2012. 13(3):625–648. 2, 69

O'Brien, L., Renzi, E., Dudley, J., Clancy, C., and Dias, F. (2018). Catalogue of extreme wave events in Ireland: revised and updated for 14 680 BP to 2017. *Natural Hazards and Earth System Sciences*, 18:729–758. 2

O'Connell, R., Montera, L. d., Peters, J. L., and Horion, S. (2020). An updated assessment of Ireland's wave energy resource using satellite data assimilation and a revised wave period ratio. *Renewable Energy*, 160:1431–1444. 15, 137

Olbert, A. I., Dabrowski, T., Nash, S., and Hartnett, M. (2012). Regional modelling of the 21st century climate changes in the irish sea. *Continental Shelf Research*, 41:48–60. 3

Olonscheck, D., Suarez-Gutierrez, L., Milinski, S., Beobide-Arsuaga, G., Baehr, J., Fröb, F., Ilyina, T., Kadow, C., Krieger, D., Li, H., et al. (2023). The new max planck institute grand ensemble with cmip6 forcing and high-frequency model output. *Journal of Advances in Modeling Earth Systems*, 15(10):e2023MS003790. 27, 76

Orford, J. D. and Carter, R. (1982). Crestal overtop and washover sedimentation on a fringing sandy gravel barrier coast, carnsore point, southeast ireland. *Journal of Sedimentary Research*, 52(1):265–278. 2

Orszaghova, J., Borthwick, A. G., and Taylor, P. (2010). Boussinesq modelling of solitary wave propagation, breaking, runup and overtopping. In *32nd International Conference on Coastal Engineering (ICCE2010), Shanghai, China, 2010.* 125

Palermo, R. V., Perron, J. T., Soderblom, J. M., Birch, S. P. D., Hayes, A. G., and Ashton, A. D. (2024). NEWTS1.0: Numerical model of coastal erosion by waves and transgressive scarps. 17(8):3433–3445. 14

Palmer, T., Nicholls, R., Wells, N., Saulter, A., and Mason, T. (2014). Identification of 'energetic'swell waves in a tidal strait. *Continental Shelf Research*, 88:203–215. 65

Patra, A., Dodet, G., Min, S.-k., and Hochet, A. (2024). Quantifying anthropogenic influences on global wave height trend during 1961–2020 with focus on polar ocean. *Geophysical Research Letters*, 51(6):e2023GL106544. 31

Patra, A., Min, S.-K., Kumar, P., and Wang, X. L. (2021). Changes in extreme ocean wave heights under 1.5 c, 2 c, and 3 c global warming. *Weather and Climate Extremes*, 33:100358. 16

Phillips, M., Rees, E., and Thomas, T. (2013). Winds, sea levels and North Atlantic Oscillation (NAO) influences: An evaluation. *Global and Planetary Change*, 100:145–152. 62, 132

Phillips, O. M. (1957). On the generation of waves by turbulent wind. *Journal of fluid mechanics*, 2(5):417–445. 10, 11

Pierson, Jr., W. J. and Moskowitz, L. (1964). A Proposed Spectral Form for Fully Developed Wind Seas Based on the Similarity Theory of S. A. Kitaigorodskii. *\jgr*, 69(24):5181–5190. 34

Pierson Jr, W. J. (1955). Wind generated gravity waves. In *Advances in geophysics*, volume 2, pages 93–178. Elsevier. 12

Pierson Jr, W. J. and Moskowitz, L. (1964). A proposed spectral form for fully developed wind seas based on the similarity theory of sa kitaigorodskii. *Journal of geophysical research*, 69(24):5181–5190. 12

Pilar, P., Soares, C. G., and Carretero, J. C. (2008). 44-year wave hindcast for the north east atlantic european coast. 55(11):861–871. 4, 68

Piles, M., Muñoz, J., Guerrero-Curieses, A., Camps-Valls, G., and Rojo-Álvarez, J. L. (2021). Autocorrelation metrics to estimate soil moisture persistence from satellite time series: Application to semiarid regions. 40

Pinto, J. G., Bellenbaum, N., Karremann, M. K., and Della-Marta, P. M. (2013). Serial clustering of extratropical cyclones over the north atlantic and europe under recent and future climate conditions. *Journal of geophysical research: Atmospheres*, 118(22):12–476. 90, 134

Ponce de León, S., Restano, M., and Benveniste, J. (2023). Assessment of wave power density using sea state climate change initiative database in the french façade. *Journal of Marine Science and Engineering*, 11(10):1970. 63

Portilla, J., Ocampo-Torres, F. J., and Monbaliu, J. (2009). Spectral partitioning and identification of wind sea and swell. *Journal of atmospheric and oceanic technology*, 26(1):107–122. 63

Portilla-Yandún, J. (2018). The global signature of ocean wave spectra. *Geophysical Research Letters*, 45(1):267–276. 12

Prestes, Y. O., da Silva, A. C., Marquez, A. L., Gomes Junior, G. D., and Hernandez, F. (2025). Climate variability and atlantic surface gravity wave variability based on reanalysis data. *Journal of Marine Science and Engineering*, 13(8):1536. 17

Pugh, D. T., Bridge, E., Edwards, R., Hogarth, P., Westbrook, G., Woodworth, P. L., and McCarthy, G. D. (2021). Mean sea level and tidal change in ireland since 1842: a case study of cork. *Ocean Science*, 17(6):1623–1637. 25

Pullen, T., Allsop, N., Bruce, T., Kortenhaus, A., Schüttrumpf, H., and Van der Meer, J. (2007). Eurotop wave overtopping of sea defences and related structures: assessment manual. *Die Küste*. 106

Rapp, B. E. (2016). *Microfluidics: modeling, mechanics and mathematics*. William Andrew. 113

Rasmussen, T., Thomsen, E., and Moros, M. (2016). North atlantic warming during dansgaard-oeschger events synchronous with antarctic warming and out-of-phase with greenland climate. *Scientific Reports*, 6:20535. 62

Reduan Atan, S. N. and Goggins, J. (2017). Development of a nested local scale wave model for a 1/4 scale wave energy test site using SWAN. 10(1):59–78. Publisher: Taylor & Francis _eprint: https://doi.org/10.1080/1755876X.2016.1275495. 23

Reguero, B. G., Losada, I. J., and Méndez, F. J. (2019). A recent increase in global wave power as a consequence of oceanic warming. *Nature communications*, 10(1):205. 15

Reick, C. H., Raddatz, T., Brovkin, V., and Gayler, V. (2013). Representation of natural and anthropogenic land cover change in MPI-ESM. 5(3):459–482. 75

Rezvov, V., Krinitskiy, M., and Gulev, S. (2022). Approximation of high-resolution surface wind speed in the north atlantic using discriminative and generative neural models based on RAS-NAAD 40-year hindcast. page 023. 97

Ribal, A., Babanin, A. V., Zieger, S., and Liu, Q. (2020). A high-resolution wave energy resource assessment of indonesia. *Renewable Energy*, 160:1349–1363. 15

Rogers, W. E. (2020). Phase-averaged wave models. In *Ocean Wave Dynamics*, pages 163–204. World Scientific. 21

Rozoff, C. M. and Alessandrini, S. (2022). A comparison between analog ensemble and convolutional neural network empirical-statistical downscaling techniques for reconstructing high-resolution near-surface wind. *Energies*, 15(5):1718. 97

Ruiz-Barradas, A., Nigam, S., and Kavvada, A. (2013). The atlantic multidecadal oscillation in twentieth century climate simulations: Uneven progress from cmip3 to cmip5. *Climate Dynamics*, 41. 40

Rusu, L., Pilar, P., and Guedes Soares, C. (2008). Hindcast of the wave conditions along the west iberian coast. 55:906–919. 72

Rydén, J. (2024). Estimation of return levels with long return periods for extreme sea levels by the average conditional exceedance rate method. *GeoHazards*, 5(1):166–175. 119

Sabique, L., Annapurnaiah, K., Nair, T. B., and Srinivas, K. (2012). Contribution of southern indian ocean swells on the wave heights in the northern indian ocean—a modeling study. *Ocean Engineering*, 43:113–120. 63

Santo, H., Taylor, P., and Gibson, R. (2016). Decadal variability of extreme wave height representing storm severity in the northeast atlantic and north sea since the foundation of the royal society. *Proceedings of the Royal Society A: Mathematical, Physical and Engineering Sciences*, 472(2193):20160376. 19

Satariano, B. (2021). The therapeutic value of the sea and its impact on health and wellbeing. 138

Scheffers, A., Scheffers, S., Kelletat, D., and Browne, T. (2009). Wave-emplaced coarse debris and megaclasts in ireland and scotland: boulder transport in a high-energy littoral environment. *The Journal of Geology*, 117(5):553–573. 107

Scott, T., McCarroll, R. J., Masselink, G., Castelle, B., Dodet, G., Saulter, A., Scaife, A. A., and Dunstone, N. (2021). Role of Atmospheric Indices in Describing Inshore Directional Wave Climate in the United Kingdom and Ireland. *Earth's Future*, 9(5):e2020EF001625. _eprint: https://agupubs.onlinelibrary.wiley.com/doi/pdf/10.1029/2020EF001625. 19, 35, 131

Scott, T., Wiggins, M., Masselink, G., Castelle, B., Dodet, G., and SAULTER, A. (2019). ATMOSPHERIC CLIMATE CONTROL OF DIRECTIONAL WAVES IN THE UNITED KINGDOM AND IRELAND. pages 708–721. 14

Seibert, S. L., Degenhardt, J., Ahrens, J., Reckhardt, A., Schwalfenberg, K., and Waska, H. (2020). Investigating the Land-Sea Transition Zone. In Jungblut, S., Liebich, V., and Bode-Dalby, M., editors, *YOUMARES 9 - The Oceans: Our Research, Our Future: Proceedings of the 2018 conference for YOUng MArine RESearcher in Oldenburg, Germany*, pages 225–242. Springer International Publishing, Cham. 1

Semedo, A. (2005). The north atlantic oscillation influence on the wave regime in portugal: An extreme wave event analysis. page 106. 46, 61

Semedo, A., Sušelj, K., Rutgersson, A., and Sterl, A. (2011). A global view on the wind sea and swell climate and variability from era-40. *Journal of Climate*, 24(5):1461 – 1479. 26, 34, 63, 65

Semedo, A., Vettor, R., Breivik, Ø., Sterl, A., Reistad, M., Soares, C. G., and Lima, D. (2015). The wind sea and swell waves climate in the Nordic seas. *Ocean Dynamics*, 65(2):223–240. 33

Semedo, A., Weisse, R., Behrens, A., Sterl, A., Bengtsson, L., and Günther, H. (2012). Projection of global wave climate change toward the end of the twenty-first century. *Journal of Climate*, 26(21):8269–8288. 18

Senechal, N., Coco, G., Bryan, K. R., and Holman, R. A. (2011). Wave runup during extreme storm conditions. *Journal of Geophysical Research: Oceans*, 116(C7). 106

Seneviratne, S. I., Zhang, X., Adnan, M., Badi, W., Dereczynski, C., Luca, A. D., Ghosh, S., Iskandar, I., Kossin, J., Lewis, S., et al. (2021). Weather and climate extreme events in a changing climate. 3

Senter, J. and Lupo, A. (2024). *A Euclidean Distance Diagnostic of North Atlantic Basin Activity*. 78

Shanahan, T. and Fitzgerald, B. (2025). Wind–wave misalignment in irish waters and its impact on floating offshore wind turbines. *Energies*, 18(2):372. 2, 35, 131

Sharmar, V., Markina, M. Y., and Gulev, S. (2021). Global ocean wind-wave model hindcasts forced by different reanalyzes: A comparative assessment. *Journal of Geophysical Research: Oceans*, 126(1):e2020JC016710. 27

Sheehan, Kevin and INFOMAR Survey Team (2021). CV20_02 INFOMAR survey report. 75

Shimura, T., Mori, N., and Mase, H. (2013). Ocean waves and teleconnection patterns in the northern hemisphere. *Journal of Climate*, 26(21):8654–8670. 19

Shoari Nejad, A., Parnell, A. C., Greene, A., Thorne, P., Kelleher, B. P., Devoy, R. J. N., and McCarthy, G. (2022). A newly reconciled dataset for identifying sea level rise and variability in Dublin Bay. *Ocean Science*, 18(2):511–522. 3, 25

Siegelman, M. N., O'Reilly, W. C., Becker, J., Young, R., Olfe, C., Colin, P. L., Terrill, E., and Merrifield, S. (2025). Spectral refraction modeling of waves around the steep reef at palau. *Journal of Geophysical Research: Oceans*, 130(10):e2025JC022391. 17

Simmonds, J., Brampton, A., Beech, N., and Brooke, J. (1996). *Beach management manual*, volume 153. Construction Industry Research and Information Association. 105

Slangen, A. B., Carson, M., Katsman, C. A., Van de Wal, R. S., Köhl, A., Vermeersen, L., and Stammer, D. (2014). Projecting twenty-first century regional sea-level changes. *Climatic Change*, 124(1):317–332. 25

Smit, P., Stelling, G., Roelvink, J., Van Thiel de Vries, J., McCall, R., Van Dongeren, A., Zwinkels, C., and Jacobs, R. (2010). Xbeach: Non-hydrostatic model: Validation, verification and model description, delft univ. *Technol., Delft.* 5, 107

Snodgrass, F., Hasselmann, K., Miller, G., Munk, W. H., and Powers, W. (1966). Propagation of ocean swell across the pacific. *Philosophical Transactions of the Royal Society of London. Series A, Mathematical and Physical Sciences*, 259(1103):431–497. 34

Snyder, A., Prime, N., Tebaldi, C., and Dorheim, K. (2024). Uncertainty-informed selection of cmip6 earth system model subsets for use in multisectoral and impact models. *Earth System Dynamics*, 15(5):1301–1318. 17

Soci, C., Hersbach, H., Simmons, A., Poli, P., Bell, B., Berrisford, P., Horányi, A., Muñoz-Sabater, J., Nicolas, J., Radu, R., et al. (2024). The era5 global reanalysis from 1940 to 2022. *Quarterly Journal of the Royal Meteorological Society*, 150(764):4014–4048. 26

Solano, C. L., Turki, E. I., Barceló, Á. D. G., Selvam, H., Mendoza, E. T., Costa, S., Salameh, E., Migaud, A., and Lafite, R. (2025). Modelling of wave run–up on a macrotidal beach for assessing coastal flooding. *Results in engineering*, 25:104379. 106

Sreelakshmi, S. and Bhaskaran, P. K. (2022). Extreme swell wave energy and its directional characteristics in the indian ocean. *Climate Dynamics*, 58(9):2193–2212. 63

Stelling, G. and Zijlema, M. (2009). Numerical modeling of wave propagation, breaking and run-up on a beach. In *Advanced computational methods in science and engineering*, pages 373–401. Springer. 23, 24

Stevens, B., Giorgetta, M., Esch, M., Mauritsen, T., Crueger, T., Rast, S., Salzmann, M., Schmidt, H., Bader, J., Block, K., Brokopf, R., Fast, I., Kinne, S., Kornblueh, L., Lohmann, U., Pincus, R., Reichler, T., and Roeckner, E. (2013). Atmospheric component of the MPI-m earth system model: ECHAM6. 5(2):146–172. _eprint: https://agupubs.onlinelibrary.wiley.com/doi/pdf/10.1002/jame.20015. 75

Stockdon, H. F., Holman, R. A., Howd, P. A., and Sallenger Jr, A. H. (2006). Empirical parameterization of setup, swash, and runup. *Coastal engineering*, 53(7):573–588. 117

Stocker, T. F., Qin, D., Plattner, G.-K., Alexander, L. V., Allen, S. K., Bindoff, N. L., Bréon, F.-M., Church, J. A., Cubasch, U., Emori, S., et al. (2013). Technical summary. In *Climate change 2013: the physical science basis. Contribution of Working Group I to the Fifth Assessment Report of the Intergovernmental Panel on Climate Change*, pages 33–115. Cambridge University Press. 136

Sverdrup, H. U. and Munk, W. H. (1947). *Wind, sea and swell: Theory of relations for forecasting*. Number 601. Hydrographic Office. 12

Swain, J., Umesh, P., and Balchand, A. (2019). WAM and WAVEWATCH-III intercomparison studies in the north indian ocean using oceansat-2 scatterometer winds. 9:2516019219866569. Publisher: SAGE Publications Ltd STM. 23, 68

SWAN Team (2023). *SWAN – Scientific and Technical Documentation*. Version 41.45. 12, 73

Tao, J. (2020). Numerical simulation of wave run-up and breaking on beach. In *Numerical Simulation of Water Waves*, pages 185–209. Springer. 24

Thomas, T. J. and Dwarakish, G. (2015). Numerical wave modelling–a review. *Aquatic procedia*, 4:443–448. 5, 20, 21

Tiron, R., Gallagher, S., Gleeson, E., Dias, F., and McGrath, R. (2013). The future wave climate of ireland: From averages to extremes. 17. 90

Tiron, R., Gallagher, S., Gleeson, E., Dias, F., and McGrath, R. (2015). The Future Wave Climate of Ireland: From Averages to Extremes. *Procedia IUTAM*, 17:40–46. 1, 4

Tolman, H. (1989). The numerical model WAVEWATCH. Publisher: TU Delft. 4, 22

Toro, E. F. (2013). *Riemann solvers and numerical methods for fluid dynamics: a practical introduction*. Springer Science & Business Media. 127

Towe, R., Eastoe, E., Tawn, J., and Jonathan, P. (2017). Statistical downscaling for future extreme wave heights in the north sea. 11(4):2375 – 2403. Publisher: Institute of Mathematical Statistics. 69

Trindade, A., Portabella, M., Stoffelen, A., Lin, W., and Verhoef, A. (2019). ERAstar: A High-Resolution Ocean Forcing Product. *IEEE Transactions on Geoscience and Remote Sensing*, PP:1–11. 5

Tuomi, L., Kanarik, H., Björkqvist, J.-V., Marjamaa, R., Vainio, J., Hordoir, R., Höglund, A., and Kahma, K. K. (2019). Impact of ice data quality and treatment on wave hindcast statistics in seasonally ice-covered seas. 7. 71

van de Wal, R. S., Melet, A., Bellafiore, D., Vousdoukas, M., Camus, P., Ferrarin, C., Oude Essink, G., Haigh, I. D., Lionello, P., Luijendijk, A., et al. (2023). Sea level rise in europe: Impacts and consequences. *State of the Planet Discussions*, 2023:1–65. 103

Van der Meer, J. W. (2017). Wave run-up and overtopping. In *Dikes and revetments*, pages 145–160. Routledge. 3, 105

Van Der Meer, J. W., Allsop, N., Bruce, T., De Rouck, J., Kortenhaus, A., Pullen, T., Schüttrumpf, H., Troch, P., Zanuttigh, B., et al. (2016). Eurotop-manual on wave overtopping of sea defences and related structures. an overtopping manual largely based on european research, but for worldwide application. 21

van Ormondt, M., Leijnse, T., de Goede, R., Nederhoff, K., and van Dongeren, A. (2025). Subgrid corrections for the linear inertial equations of a compound flood model–a case study using sfincs 2.1. 1 dollerup release. *Geoscientific Model Development*, 18(3):843–861. 5

Villarroel-Lamb, D. and Williams, A. H. (2022). Quantifying wave runup in data-sparse locations for planning. *West Indian Journal of Engineering*, pages 58–69. 105

Viñes, M., Mösso, C., Calderón-Vega, F., Calvillo, B., Mestres, M., and Sánchez-Arcilla, A. (2026). Long-term variability and trends in extreme wave climate along the bay of biscay. *Journal of Marine Science and Engineering*, 14(7):646. 19, 30

Vousdoukas, M. I., Mentaschi, L., Voukouvalas, E., Verlaan, M., and Feyen, L. (2017). Extreme sea levels on the rise along Europe's coasts. *Earth's Future*, 5(3):304–323. _eprint: https://agupubs.onlinelibrary.wiley.com/doi/pdf/10.1002/2016EF000505. 3, 14

Wahl, T., Plant, N. G., and Long, J. W. (2016). Probabilistic assessment of erosion and flooding risk in the northern gulf of mexico. *Journal of Geophysical Research: Oceans*, 121(5):3029–3043. 106

Walker, G. T. (1924). Correlations in seasonal variations of weather. viii, a further study of world weather. *Men. Indian Meteor. Dept.*, 24:275–332. 46

Wallace, J. M. and Gutzler, D. S. (1981). Teleconnections in the geopotential height field during the northern hemisphere winter. *Monthly weather review*, 109(4):784–812. 18

Wamdi Group (1988). The WAM Model—A Third Generation Ocean Wave Prediction Model. *Journal of Physical Oceanography*, 18(12):1775–1810. Place: Boston MA, USA Publisher: American Meteorological Society. 4, 10, 12, 21, 22

Wang, X., Jiang, H., Chen, G., and Yu, F. (2016). Identifying storm-induced wave origins using sar wave mode data. *Science China Earth Sciences*, 59(10):1971–1980. 65

Warren, I. and Bach, H. (1992). Mike 21: a modelling system for estuaries, coastal waters and seas. *Environmental software*, 7(4):229–240. 5

Webb, P. (2021). *Introduction to oceanography*. Roger Williams University. 5

Whitehouse, P. L. (2018). Glacial isostatic adjustment modelling: historical perspectives, recent advances, and future directions. *Earth surface dynamics*, 6(2):401–429. 25

Wittmann, P. A. and Farrar, P. D. (1997). Global, regional and coastal wave prediction. *Marine Technology Society. Marine Technology Society Journal*, 31(1):76. 23

Wolf, J. (2009). Coastal flooding: impacts of coupled wave–surge–tide models. *Natural Hazards*, 49(2):241–260. 24

Wolf, J., Woolf, D., and Bricheno, L. (2020). Impacts of climate change on storms and waves relevant to the coastal and marine environment around the uk. *MCCIP Science Review*, 2020:132–157. 70

Woolf, D. K., Challenor, P., and Cotton, P. (2002). Variability and predictability of the north atlantic wave climate. *Journal of Geophysical Research: Oceans*, 107(C10):9–1. 17, 18, 19

Woollings, T., Gregory, J. M., Pinto, J. G., Reyers, M., and Brayshaw, D. J. (2012). Response of the north atlantic storm track to climate change shaped by ocean–atmosphere coupling. *Nature Geoscience*, 5(5):313–317. 134

Wu, H., Yan, J., and Cao, W. (2024a). Methodologies on spatial and temporal correlation analysis between regional neighboring sites. pages 1 – 4. 39

Wu, L., Sahlée, E., Nilsson, E., and Rutgersson, A. (2024b). A review of surface swell waves and their role in air–sea interactions. *Ocean Modelling*, 190:102397. 34

Wu, Y., Miao, C., Fan, X., Gou, J., Zhang, Q., and Zheng, H. (2022). Quantifying the uncertainty sources of future climate projections and narrowing uncertainties with bias correction techniques. *Earth's Future*, 10(11):e2022EF002963. 101

Young, I. (1999a). Seasonal variability of the global ocean wind and wave climate. *International Journal of Climatology*, 19:931 – 950. 34

Young, I. R. (1999b). *Wind generated ocean waves*, volume 2. Elsevier. 11, 13

Yuan, Y., Yu, F., Chen, Z., Li, X., Hou, F., Gao, Y., Gao, Z., and Pang, R. (2024). Towards a real-time modeling of global ocean waves by the fully gpu-accelerated spectral wave model wam6-gpu. *EGUsphere*, 2024:1–20. 23

Zed, A. A. A., Kansoh, R. M., Iskander, M. M., and Elkholy, M. (2022). Wind and wave climate southeastern of the mediterranean sea based on a high-resolution SWAN model. 99:101311. 23

Zhang, D., Tang, N., Dong, W., and Zhao, L. (2024). Machine learning-based financial big data analysis and forecasting: From preprocessing to deep learning models. 116:143–149. 97

Zhang, X., Wu, K., Li, R., Li, D., Zhang, S., Zhang, R., Li, S., and Dong, X. (2023). Analysis of the Interannual Variability of Pacific Swell Pools. *Journal of Marine Science and Engineering*, 11(10). 34

Zheng, C. W., Li, C. Y., and Pan, J. (2018). Propagation Route and Speed of Swell in the Indian Ocean. *Journal of Geophysical Research: Oceans*, 123(1):8–21. _eprint: https://agupubs.onlinelibrary.wiley.com/doi/pdf/10.1002/2016JC012585. 35, 37, 38, 39, 64

Zheng, C.-w., Wu, D., Wu, H.-l., Guo, J., Shen, C., Tian, C., Tian, X.-l., Xiao, Z.-n., Zhou, W., and Li, C.-y. (2022). Propagation and attenuation of swell energy in the Pacific Ocean. *Renewable Energy*, 188:750–764. 35, 37, 38, 39

Zijlema, M. and Stelling, G. (2008). Efficient computation of surf zone waves using the nonlinear shallow water equations with non-hydrostatic pressure. *Coastal Engineering*, 55(10):780–790. 106, 109

Zijlema, M., Stelling, G., and Smit, P. (2011). Swash: An operational public domain code for simulating wave fields and rapidly varied flows in coastal waters. *Coastal Engineering*, 58(10):992–1012. 107